

# Mutations of key cytokinetic abscission mediators cause microcephaly

Jessica Neville Little  
Linden, North Carolina

B.S., North Carolina State University, 2013

A Dissertation presented to the Graduate Faculty of the University of  
Virginia in Candidacy for the Degree of Doctor of Philosophy

Department of Cell Biology

University of Virginia  
May, 2019

Noelle Dwyer, Ph.D. (Dissertation Advisor)

Bettina Winckler, Ph.D.

Ann Sutherland, Ph.D.

Sarah Siegrist, Ph.D.

P. Todd Stukenberg, Ph.D.

## Abstract

The cerebral cortex is our most recently evolved, complex organ. In size and cellular content, the cortex is largely generated before birth. Microcephaly, or the condition of an abnormally small brain, occurs due to both genetic and environmental insults in humans and can be modeled in mice. Genetic causes of microcephaly most often stem from defects in neural stem cell (NSC) divisions or attributes, which prevent these cells from successfully making post-mitotic neurons. Interestingly, germline mutation of cell division genes in mice often impairs brain growth disproportionately to growth of non-neural tissues.

Most described microcephaly mutants have defects in NSC mitotic progression. However, the role of cytokinesis and especially cytokinetic abscission, the final step in the severing of two daughter cells, in cortical development as well as the etiology of microcephaly is less understood. Recently, p53-dependent apoptosis was found to be a common downstream consequence of mitotic defects in NSCs, causative for reduced cell numbers and smaller brain size. Whether p53 also responds to defects in cytokinesis to cause apoptosis in NSCs, or even to regulate cell survival in other cell types, is unclear and controversial.

This thesis work furthers our understanding of normal cortical development through the investigation of two microcephaly mouse mutants with defects in cytokinetic abscission. We show that mutation of the kinesin-6 *Kif20b* and scaffolding protein *Cep55* separately impair cytokinetic abscission in NSCs to impair brain growth. Despite more severe cytokinetic defects observed with acute knockdown of *Cep55* versus knockdown of *Kif20b* in human cells, we find that germline mutation of *Cep55* is remarkably less consequential for embryo development than *Kif20b* loss. However, *Cep55* mutation results in a more severe reduction of brain size and cellular content, similar to a phenotype seen in humans with mutated *Cep55*. Furthermore, we find that microcephaly in both *Kif20b* and *Cep55* mutants occurs partially through p53-dependent apoptosis, as *p53* co-deletion can greatly increase brain size in these mutants. In the *Cep55* mutant, evidence suggests p53 activation occurs in binucleate cells that failed cytokinesis. Interestingly, this apoptosis is specific to neural tissues despite expression of *Cep55* and evidence of cytokinetic defects in non-neural cells. *Kif20b* mutation results in abnormal midbody maturation defects but not failed abscission; yet, p53-dependent apoptosis still occurs.

Taken together, this work elucidates a unique sensitivity of NSCs to activation of p53-dependent apoptotic pathways, and suggests distinct ways that abnormal cytokinetic abscission can lead to activation of p53. We propose that Kif20b and Cep55, two vertebrate-specific proteins, evolved for the successful complex divisions of NSCs needed to create the cellular content necessary for mammalian brain size.

## Acknowledgements

I would first like to thank my research advisor, Noelle Dwyer. I will forever be grateful to her for the opportunity to work in her lab on topics that are so biologically interesting and unique. She has encouraged and inspired me to improve my independent thinking, research, writing, and mentoring skills, while always being available for support and discussions. I am deeply appreciative of the time she has spent working with me on developing and publishing my project.

I would also like to thank the other members of the Dwyer, Lu and Yu labs, my companions through the past four years. Thank you for the help in experiment troubleshooting, reagents, and helping me find things that were usually in plain sight. I am especially grateful to Katrina McNeely and Andre Landin-Malt for advice and discussions both in science and in life, and for so many fun times. To the undergraduates I've worked with through the years – Madison, Gabi, Sara, Adriana, Haley, Mackenzie and Caitlin – I could not have done it without you. Thank you for the opportunity to work with you and watch your scientific enthusiasm grow. I am also incredibly grateful and thankful to the UVA Medical Scientist Training Program and especially my class members and best friends, Maria, Sarb, Ricky, Mark and Jeff.

My committee members, Bettina Winckler, Ann Sutherland, Todd Stukenberg, and Sara Siegrist, have been wonderful sources of encouragement and support. Thank you so much for your help in experiment and publication planning, grant writing and responses to my late-night thought-experiment emails. I am also grateful to many other members of the Cell Biology Department for their constant positive attitudes, helpfulness and amazing examples of how to be a good scientist and person.

Finally, I would like to thank my family. My parents, Thomas and Crissy Neville, have been my role models from the very beginning. I am in constant admiration of their unparalleled work ethics and responses to difficult challenges. They have always offered me uncompromising love and support and I am so grateful. I am also so blessed to have a wonderful relationship with my sisters, Lauren and Emily. Thank you both for your love, hugs, and appropriate checks on my humility at all times. And finally, I want to thank my husband Spencer, who has been so patient, supportive, and helpful throughout this process. Your support has meant the world to me.

## Table of Contents

<i>Abstract</i> .....	<i>ii</i>
<i>Acknowledgements</i> .....	<i>iv</i>
<i>List of Figures and Tables</i> .....	<i>vii</i>
<b>Chapter 1: Introduction</b> .....	<b>1</b>
<b>1.1 Overview</b> .....	<b>1</b>
<b>1.2 Major events in mammalian embryonic cortical development</b> .....	<b>1</b>
A. Cell types and divisions in the cortical epithelium.....	2
B. Regulation of cell proliferation and fate.....	4
C. Post-mitotic neuron polarization.....	7
<b>1.3 Cytokinetic abscission in cell lines and the developing cortex</b> .....	<b>9</b>
A. Mechanisms of abscission and roles of the post-abscission midbody remnant.....	9
B. Consequences of cytokinesis failure .....	11
C. The role of Kif20b in cytokinetic abscission of cultured cells.....	12
D. The role of Cep55 in cytokinetic abscission of cultured cells.....	13
E. Cytokinesis in epithelia and the developing cortex .....	14
<b>1.4 Apoptosis and p53 activation in microcephaly</b> .....	<b>15</b>
A. Microcephaly etiology .....	15
B. Apoptosis and p53 activity in the cortical epithelium .....	16
C. Genetic and environmental causes of microcephaly implicating p53.....	18
D. Pathways of p53 activation following cell division errors.....	27
E. Unresolved questions .....	30
<b>1.5 Research Objectives</b> .....	<b>33</b>
<b>Chapter 2: <i>p53 deletion rescues lethal microcephaly in a mouse mutant with neural stem cell abscission defects</i></b> .....	<b>36</b>
<b>Abstract</b> .....	<b>36</b>
<b>Introduction</b> .....	<b>36</b>
<b>Results</b> .....	<b>39</b>
<b>Discussion</b> .....	<b>46</b>
<b>Methods</b> .....	<b>49</b>
<b>Figures</b> .....	<b>54</b>
<b>Chapter 3: <i>Mutation of the key abscission regulator Cep55 causes microcephaly</i></b> .....	<b>68</b>
<b>Abstract</b> .....	<b>68</b>
<b>Introduction</b> .....	<b>68</b>
<b>Results</b> .....	<b>70</b>
<b>Discussion</b> .....	<b>80</b>
<b>Methods</b> .....	<b>84</b>
<b>Figures</b> .....	<b>90</b>

<b>Chapter 4: p53 inhibition accelerates cortical neuron polarization.....</b>	<b>109</b>
<b>Abstract.....</b>	<b>109</b>
<b>Introduction .....</b>	<b>109</b>
<b>Results .....</b>	<b>111</b>
<b>Discussion .....</b>	<b>116</b>
<b>Methods.....</b>	<b>118</b>
<b>Figures.....</b>	<b>122</b>
<b>Chapter 5: Discussion .....</b>	<b>133</b>
<b>5.1 Overview.....</b>	<b>133</b>
<b>5.2 p53-dependent and -independent pathways in microcephaly etiology of the <i>Kif20b</i> mutant.....</b>	<b>133</b>
<b>5.3 Comparing and contrasting <i>Kif20b</i> and <i>Cep55</i> mutant microcephaly.....</b>	<b>135</b>
Cell line knockdown phenotypes.....	137
Gross phenotypes of mouse mutants .....	138
Cellular phenotypes of mouse mutants .....	139
Levels of p53 increase and apoptosis in mouse mutants.....	139
<b>5.4 Future Directions .....</b>	<b>139</b>
Identifying upstream mediators and downstream effectors of p53 activity in microcephaly mutants .....	140
Examining consequences of apoptosis inhibition in microcephaly mutants.....	144
Investigating the apoptotic process in the cortical epithelium.....	148
Investigating coordination of cytokinetic abscission with multicellular processes in cortical development.....	150
<b>Appendix 1: p53-dependent and -independent consequences of <i>Kif20b</i> loss in NSCs</b>	<b>154</b>
<b>Figures.....</b>	<b>160</b>
<b>Appendix 2: RNA sequencing of <i>Kif20b</i> and <i>Kif20b;p53</i> mutant cortices.....</b>	<b>170</b>
<b>Appendix 3: Postnatal consequences of <i>Cep55</i> loss.....</b>	<b>182</b>
<b>Figures.....</b>	<b>185</b>
<b>Appendix 4: Primary consequences of <i>Cep55</i> loss in NIH 3T3 cells.....</b>	<b>190</b>
<b>Figures.....</b>	<b>192</b>
<b>References .....</b>	<b>197</b>

## List of Figures and Tables

<b>Table 1:</b> Microcephaly mutants implicating p53 .....	19
<b>Table 2:</b> Genes significantly upregulated in p53 mutant compared to wild-type E11.5 cortices (padj < 0.05).....	130
<b>Table 3:</b> Genes significantly downregulated in p53 mutant compared to wild-type E11.5 cortices (padj < 0.05).....	130
<b>Table 4:</b> Genes significantly downregulated in p53 mutant compared to wild-type E11.5 cortices in gene ontology analysis term “axonogenesis”.....	131
<b>Table 5:</b> Genes significantly upregulated in p53 mutant compared to wild-type E11.5 cortices in gene ontology analysis term “axonogenesis”.....	131
<b>Table 6:</b> Genes significantly upregulated in p53 mutant compared to wild-type E11.5 cortices in gene ontology analysis term “neuron projection development”.....	132
<b>Table 7:</b> Comparing and contrasting Kif20b and Cep55 loss in cell lines and mouse mutants .....	136
<b>Table 8:</b> Proposed mouse mutant crosses to identify upstream and downstream-mediators of p53 activation in Kif20b and/or Cep55 mutant microcephaly .....	144
<b>Table 9:</b> Upregulated genes in Kif20b <sup>-/-</sup> ;p53 <sup>+/+</sup> E11.5 cortices compared to wild-type samples (padj < 0.05).....	171
<b>Table 10:</b> Downregulated genes in Kif20b <sup>-/-</sup> ;p53 <sup>+/+</sup> E11.5 cortices compared to wild-type samples (padj < 0.05).....	173
<b>Table 11:</b> Genes Upregulated in Kif20b;p53 mutant E11.5 cortices compared to p53 mutants (Kif20b <sup>+/+</sup> ;p53 <sup>-/-</sup> ) (padj < 0.05).....	177
<b>Table 12:</b> Genes Downregulated in Kif20b;p53 mutant E11.5 cortices compared to p53 mutants (Kif20b <sup>+/+</sup> ;p53 <sup>-/-</sup> ) (padj < 0.05).....	179
<b>Figure 1.</b> Bax deletion partially rescues microcephaly and apoptosis in Kif20b mutant mice. ....	54
<b>Figure 2.</b> p53 deletion rescues microcephaly and apoptosis in Kif20b mutant mice. ....	55
<b>Figure 3.</b> p53 deletion rescues craniofacial defects in Kif20b mutant mice. ....	56
<b>Figure 4.</b> p53 expression is elevated in Kif20b mutant NSCs. ....	57
<b>Figure 5.</b> p53 deletion restores normal production of IPs and neurons in Kif20b mutant cortex. ....	58
<b>Figure 6.</b> p53 deletion rescues postnatal survival but incompletely rescues cortical size at birth in Kif20b mutant mice. ....	59
<b>Figure 7.</b> All neuronal layers are reduced in thickness in double mutant cortices at P0. ....	60
<b>Figure 8.</b> Kif20b loss cell-autonomously causes abscission defects in cortical NSCs. ....	61
<b>Figure 9.</b> Analyses of mitotic and midbody indices in Kif20b mutant NSC cultures. ....	62
<b>Figure 10.</b> DNA damage marker $\gamma$ -H2AX is not increased in Kif20b mutant cortex. ....	63
<b>Figure 11.</b> Apoptotic cells in Kif20b mutant cortices are primarily in the proliferating zones and do not express the neuronal marker TuJ1.....	63
<b>Figure 12.</b> Kif20b loss causes apoptosis in proliferating cortical NSCs.....	64
<b>Figure 13.</b> p53 deletion does not restore normal abscission of Kif20b mutant NSCs.....	66
<b>Figure 14.</b> Cep55 mutation results in microcephaly disproportionate to body size. ....	90
<b>Figure 15.</b> Deletion of exon 6 of Cep55 results in a truncated RNA product and loss of the C terminus.....	91
<b>Figure 16:</b> Cep55 localizes to the midbody at late abscission stages in control but not mutant apical and basal progenitor cells.....	92
<b>Figure 17.</b> Cep55 is expressed in mouse embryonic fibroblasts at late abscission stages. ....	94
<b>Figure 18.</b> Cep55 mutation results in globally reduced brain size and structural defects.....	95

<b>Figure 19.</b> Cep55 mutants have reduced cortical thickness due to reduction of neuronal layers..	96
<b>Figure 20:</b> Cep55 mutant cortices have thinner neuronal layers with decreased proportion of upper layers and decreased density of neurons.....	98
<b>Figure 21:</b> Cep55 mutation results in altered proportions and disorganization of apical and basal progenitors.....	99
<b>Figure 22:</b> Apoptotic cells are specifically increased in Cep55 <sup>-/-</sup> neural tissues.....	100
<b>Figure 23.</b> Cep55 mutation results in defects in both cytokinesis and mitosis. ....	102
<b>Figure 24.</b> Cep55 mutant midbodies have few structural abnormalities. ....	103
<b>Figure 25.</b> Cep55 ensures successful completion of cytokinesis in neural stem cells.....	104
<b>Figure 26.</b> Cep55 mutant MEFs have impaired but not eliminated abscission completion.....	105
<b>Figure 27.</b> p53 nuclear expression is increased in binucleate cortical mutant cells. ....	106
<b>Figure 28.</b> Despite impaired cytokinesis, Cep55 mutant MEFs do not have increased p53 expression or apoptosis. ....	107
<b>Figure 29.</b> p53 mutant cortical neurons polarize more quickly in vitro.....	122
<b>Figure 30.</b> Cell density and apoptosis is not significantly different between cultures, and mitosis is not increased. ....	123
<b>Figure 31.</b> p53 mutant cortical neurons grow longer axons in vitro.....	124
<b>Figure 32.</b> p53 is not necessary for proper cortical neuron minor neurite number or length in vitro.....	125
<b>Figure 33.</b> p53 ensures proper cortical neuron axon and minor neurite width.....	126
<b>Figure 34.</b> p53 ensures proper cortical neuron axon and minor neurite width.....	127
<b>Figure 35.</b> The ratio of acetylated tubulin to tubulin is increased in p53 mutant cortical axons.	128
<b>Figure 36.</b> Polarization and axon outgrowth defects in Kif20b mutants are p53-independent. ...	129
<b>Figure 37:</b> Model for testing microcephaly etiology through p53 inhibition. ....	146
<b>Figure 38.</b> Kif20b;p53 mutant midbodies are wider and longer than control midbodies. ....	160
<b>Figure 39.</b> Midbody maturation is coordinated with NSC apical endfeet morphological changes. ....	161
<b>Figure 40.</b> Kif20b mutants exhibit p53-dependent and p53-independent changes in NSC endfeet morphology. ....	162
<b>Figure 41.</b> Evaluation of DNA damage and Hippo pathways in Kif20b mutants in vitro.....	164
<b>Figure 42.</b> p53 but not Kif20b mutation increases binucleate neuron number in vitro. ....	165
<b>Figure 43.</b> Kif20b mutant NSCs have p53-independent alterations in cell fate.....	167
<b>Figure 44.</b> Kif20b;p53 mutant brains are smaller than controls postnatally.....	169
<b>Figure 45.</b> Cep55 mutants exhibit failure to thrive and pre-weaning lethality.....	185
<b>Figure 46.</b> Cep55 mutants exhibit degeneration of forebrain structures postnatally.....	186
<b>Figure 47.</b> Cep55 mutants have continued apoptosis and p53 activation postnatally and DNA damage prenatally.....	187
<b>Figure 48.</b> Cep55 mutant microcephaly is partially dependent on p53. ....	189
<b>Figure 49.</b> siRNAs to Cep55 decrease Cep55 midbody expression in 3T3 cells.....	192
<b>Figure 50.</b> Cep55 depletion increases midbody-stage cells in 3T3 cultures.....	193
<b>Figure 51.</b> Cep55 depletion decreases 3T3 cell proliferation.....	194
<b>Figure 52.</b> Cep55 depletion in 3T3 cells does not alter apoptosis, p53 expression or mitosis....	196

## Chapter 1: Introduction

### 1.1 Overview

Like all organs in the mammalian body, the cerebral cortex must be built from the basic unit of the cell. The development of the cerebral cortex occurs in great part before the birth of the organism. The major functioning cells of the cortex, neurons, are post-mitotic, and few mechanisms exist to replace them if lost. It is imperative, therefore, that the processes of cortical development are precisely and tightly controlled, in order to produce a cortex of normal size, structure and function.

Divisions of neural stem cells (NSCs) are especially important in producing the correct numbers and types of cortical neurons. We have focused on an aspect of NSC divisions previously overlooked: cytokinetic abscission. The very last step of cell division, abscission takes over an hour to complete, and involves formation of a microtubule-rich structure called the midbody, which mediates the final severing event. In the cortical epithelium, neural stem cells have vastly different parameters and constraints in completing abscission compared to cultured cell lines.

When defects in cortical development do occur, one result can be microcephaly, or a small brain. Recently, the p53-apoptotic signaling axis has been implicated in control of cortical size in mouse mutants with mitotic defects. Whether p53 also responds to defects in cytokinetic abscission in NSCs was previously unaddressed, and in other cell types was unclear. This introduction first reviews the major cellular events in cortical development and our current understanding of cytokinetic abscission in cell lines and in the cortex. Finally, we bring together a recently expanded body of work on errors in NSC divisions resulting in apoptosis and subsequent microcephaly, including our own contributions in connecting defects in NSC cytokinetic abscission to p53-dependent microcephaly.

### 1.2 Major events in mammalian embryonic cortical development

## A. Cell types and divisions in the cortical epithelium

At embryonic day 8 (E8) in mice, neuroepithelial cells (NECs) in a single layer make up the neural tube, the precursor of the central nervous system. At the rostral pole, these cells begin corticogenesis by undergoing symmetric divisions to self-renew and expand the cortical area (Chenn & McConnell, 1995; Rakic, 1995). Around E9.5-10.5 NECs transition into apical progenitor cells, also known as radial glial cells (RGCs). The switch from NECs to RGCs is characterized by a loss of tight junction markers, but retention of adherens junction markers, and gain of astroglial markers (Aaku-Saraste et al., 1996; Manabe et al., 2002; R. & Magdalena, 2003). RGCs are the major neural stem cells that make neurons, predominant before birth in mice, and glia, predominant after birth (Gallo & Deneen, 2014; Malatesta et al., 2000; Noctor et al., 2002). In this thesis, NECs and RGCs will be referred to collectively as neural stem cells (NSCs). NSCs can be characterized by their distinct morphology, with thin cell bodies spanning the entire cortical epithelium even as it expands throughout development. Together, their apical endfeet, connected by adherens junctions, make up the apical membrane of the cortex, in contact with the ventricle. NSC basal processes contact the basal basement membrane at the pial surface, and their nuclei reside in the ventricular zone of the cortex above the ventricle. Additionally, NSCs undergo a specialized cell cycle-coupled movement known as interkinetic nuclear migration. Their nuclei move basally during G1 and S phase, and then move back to the apical surface during G2 to undergo mitosis in a stereotyped manner at the most apical point in the ventricular zone.

NSCs can undergo several types of divisions to produce distinct daughter cell types. At first, NSCs divide symmetrically to increase the pool of NSCs, and later undergo asymmetric and symmetric divisions to create additional NSCs, basal progenitor cells, and post-mitotic neurons (for a review, see Florio & Huttner, 2014). These divisions can be referred to as symmetric proliferative, in which two progenitor daughter cells are made, symmetric differentiative, in which two post-mitotic neurons are made, and asymmetric, in which a progenitor daughter and neuronal daughter are made. An additional fate of daughter cells could be apoptosis, although this is thought to be rare in the case of normal NSC divisions; apoptosis as a consequence of an abnormal division will be discussed in greater detail in this chapter, section 1.4. The precise percentages of types of divisions NSCs undergo is still unclear, due to overlap of markers used to

distinguish cell types, although clonal mosaic analysis is providing greater resolution (P. Gao et al., 2014).

Basal progenitor cells, daughters of apical NSCs, have less proliferative capacity than NSCs. They primarily divide symmetrically to produce two postmitotic neurons (Haubensak et al., 2004; Miyata, 2004; Noctor et al., 2004; Tyler et al., 2015). These cells are distinct morphologically and molecularly from apical NSCs. They have neither apical nor basal attachments, and reside primarily above apical NSCs in the subventricular zone. They are typically identified by their expression of the transcription factor Tbr2 (Sessa et al., 2008). Basal progenitors do not undergo interkinetic migration, dividing instead where they reside in the subventricular zone. It is interesting that despite the many differences in apical and basal progenitor morphology and movements, they can produce similar types of neurons that go on to accomplish similar functions. Thus, it may be that the unique morphology and movements of apical NSCs evolved to rapidly expand the progenitor pool early in development. Finally, mammals have an additional type of progenitor cell termed outer RGCs which lack an apical process but still possess a basal process (Dehay et al., 2015). Interestingly, this population is expanded in primates and humans. This increase in proliferative potential is hypothesized to have led to the expansion of the cortical surface area in mammals with larger brains.

Post-mitotic cortical excitatory pyramidal neurons are born in successive waves throughout cortical development, and eventually make up six separate layers or groups of neurons that have varying protein expression. As neurons are born, they migrate above basal progenitors to comprise the neuronal layer. The birth of both basal progenitors and cortical neurons involves the detachment, or delamination, of these daughter cells from the apical membrane. Interestingly, neuron daughters have been observed to migrate into the cortex using mother apical NSC basal processes as a scaffold until they reach their final location (Miyata et al., 2001).

The neuronal layer is divided into the cortical plate, where the neuronal nuclei reside, and the intermediate zone, where the neuronal axons extend through the cortex to their eventual targets. Interestingly, the first neurons are born before any basal progenitors around embryonic day 11 and migrate above the ventricular zone to comprise a region called the preplate (Haubensak et al., 2004; Miyata et al., 2001). Later, as consecutive layers of neurons are born this layer is split into the upper-most neuronal layer in the cortex, called the marginal zone or layer I, and the lower-

most neuronal layer in the cortex, called the subplate. The marginal zone contains a distinct population of neurons that express Reelin, a molecular cue that guides the subsequently-born neurons to their eventual residence and is necessary for normal neuronal lamination (D'Arcangelo et al., 1997; D'Arcangelo et al., 1995). After the first-born neurons, the next-born neurons migrate above the subplate and form layer VI. The next group of neurons migrates above layer VI and becomes layer V, and so on, with the final group of neurons becoming layer II (Angevine & Sidman, 1961; Rakic, 1972). This process is referred to as the inside-out development of the cortex, where the youngest neurons reside at the top of the cortex and oldest neurons are found in the deeper layers. While this thesis focuses on excitatory neurons that form the cortical plate, there also exist inhibitory interneurons in the cortical epithelium, which are born in the subcortical ganglionic eminences and migrate into the dorsal cortex tangentially (for a review, see Chu & Anderson, 2015).

When cultured *in vitro*, cortical cells still express markers indicating distinct apical progenitor, basal progenitor, and neuronal identities. Strikingly, NSCs cultured *in vitro* recapitulate types of divisions and daughter lineages observed *in vivo* (Gaspard et al., 2008; Qian et al., 1998; Shen et al., 2006). Even when NSCs from different ages of the cortex are co-cultured, they produce the expected lineages based on their developmental age. These data indicate that the types of divisions and fates of daughters produced could be encoded in a cell-autonomous manner. However, more research is needed to further investigate the exact types of daughter cells produced and the timing of cellular divisions *in vitro* versus *in vivo*.

## B. Regulation of cell proliferation and fate

Due to the complex movements and precise balance of symmetric and asymmetric divisions that NSCs must undergo, their divisions are tightly regulated. The complexity of these divisions may be the reason why the loss of many proteins implicated in microcephaly, or the condition of a smaller than normal brain, cause cell division abnormalities *only* in NSCs, while the rest of the body is unaffected (Gilmore & Walsh, 2013). Defects in cell division can lead to a smaller brain through NSC cellular death, arrest, or cell cycle exit, in which an NSC divides prematurely to become a neuron. Many cellular proteins, organelles and behaviors have been proposed to regulate types and fates of NSC divisions. Genetic mouse mutants have been invaluable in our understanding of these processes. Interestingly, there does not exist a mouse mutant in one gene

that completely alters the types of divisions NSCs are able to undergo, indicating that cell fate is likely multifactorial and/or that compensatory mechanisms exist. The following is a brief overview of factors proposed to influence neural stem cell proliferation and fate.

Spindle and cleavage furrow angles. The orientation of mitotic spindles and angle of cleavage furrows has long been proposed to determine cell fate in NSC daughters. This is an attractive hypothesis, as during cell division the cytoplasm, containing many signaling factors and organelles, is segregated (Jongsma et al., 2015). A shift in the angle of cleavage could therefore change how these factors are inherited, as has been seen in other epithelia and in neural cells of other species (Chenn & McConnell, 1995; Rhyu et al., 1994). It was once thought that symmetrical vertical cleavages led to symmetric proliferative daughter fates and an asymmetric cleavage would correlate with an asymmetric division (Kosodo et al., 2004; Véronique Marthiens & French-Constant, 2009). However, subsequent studies have shown that alterations in cleavage angles do not always result in cell fate changes (Konno et al., 2008). Furthermore, the vast majority of divisions are vertical or close to vertical, not perpendicular (Noctor et al., 2008).

Inheritance of the basal process and apical membrane. Unlike most epithelial cells including basal progenitor cells that completely round up during cell division, NSCs retain their basal attachment even during mitosis (Miyata et al., 2001; Noctor et al., 2002). The basal process of NSCs has been proposed to be inherited asymmetrically in an asymmetric division by the cell adopting the NSC fate (Miyata et al., 2001), but has also been observed to split symmetrically (Kosodo et al., 2008). Furthermore, the basal process contains signaling proteins that may directly influence cell fate when inherited (Tsunekawa et al., 2012). Additionally, inheritance of apical junctions may determine whether one or both daughter cells will retain stem cell identity or be capable of migrating away from the ventricular zone to become a basal progenitor or neuron. Mouse mutants with alterations in the inheritance of apical membrane domains in epithelial cells have been suggested to prematurely lose proliferative capacity (Asami et al., 2011; Paolini et al., 2015).

Basal processes and apical membrane domains also contain signaling molecules, which can act as cell fate and polarity cues directly when they are asymmetrically distributed. For example, the Par3 protein complex is normally localized at the apical surface of RGCs, but is dispersed during mitosis and then asymmetrically distributed to progenitor cells (Bultje et al., 2009). PARD3 signals through the Notch and HIPPO signaling pathways to inform cell fate. Interestingly, either

removal or overexpression of PARD3 results in a loss of asymmetric divisions (Bultje et al., 2009). Loss of the PARD3 protein complex during early development results in an expansion of proliferative symmetric divisions at the expense of asymmetric divisions, ultimately resulting in cortical enlargement (W. A. Liu et al., 2018).

Centrosome and midbody inheritance. Cellular organelles that must be segregated from one mother cell to two daughter cells are candidates for cell fate determinants. Asymmetric inheritance of mother and daughter centrosomes has been linked to cell fate outcomes in NSC divisions (Paridaen et al., 2013; Wang et al., 2009). During asymmetric divisions, the mother centrosome is more often inherited by the proliferating daughter cell while the differentiated daughter cell inherits the daughter centrosome (Xiaoqun Wang et al., 2009). Asymmetric inheritance of centrosomes has also been noted in asymmetrically dividing *Drosophila* germline stem cells and neuroblasts (Yamashita & Fuller, 2008).

During cytokinesis, the midbody serves as the last connection between two cells before the final abscission event. In cell lines, abscission can occur on one or both sides of the midbody, resulting in equal or unequal inheritance of this protein-rich organelle. Therefore, the inheritance of the midbody remnant has been proposed as a candidate cell-fate regulator in NSCs (for a review, see Dwyer et al., 2016). Midbody remnants have been proposed to be more often released in association with neurogenic divisions in NSCs (Ettinger et al., 2011). Interestingly, the midbody remnant has also been shown to contain phosphatidylserine, an engulfment signal, which could cause it to be engulfed by daughter cells even after being released (Arai et al., 2015).

Alternatively, phagocytic cells could engulf and degrade the midbody, as has been observed in *C. elegans* (Chai et al., 2012; Ou et al., 2010). Abscission and midbody inheritance mechanisms in NSCs are discussed further in this chapter, section 1.3.

Cell cycle length. The basic phases of the cell cycle in all cells are interphase, or G<sub>0</sub>, G<sub>1</sub>, S, G<sub>2</sub> and M phase. Interestingly, the length of the cell cycle in NSCs more than doubles from embryonic days 11 to 18 in mice. (Takahashi et al., 1995). As this is also the period in which NSCs switch from undergoing primarily symmetric proliferative divisions to asymmetric and symmetric neurogenic divisions, this change in cell cycle length could be significant. The doubling of cell cycle length appears to be due primarily to an increase in G<sub>1</sub> length, although others have proposed a change in S phase length (Arai et al., 2011). In fact, artificial shortening

of G1 length alters modes of divisions, shifting NSCs to more proliferative divisions (Pilaz et al., 2009). Therefore, a longer time in G1 may allow NSCs to prepare for neurogenic divisions, although what cellular events occur during G1 to cause this shift is unclear. In other cell types, G1-delay or arrest leads to increased cell cycle exit, an analogous event to the production of a neuron. On the other hand, the shorter length of G1 and the cell cycle during early proliferative divisions means that cells have less time to successfully divide, which could result in divisions being more susceptible to defects.

In addition to G1, alteration of the length of mitosis has been observed to influence cell fate. Mitotic delay induced by genetic and drug treatments resulted in a shift to increased symmetric neurogenic divisions at the expense of proliferative symmetric divisions (Pilaz et al., 2016). If mitosis extended beyond a certain threshold, the division resulted in cell death through p53-dependent apoptosis. However, mitosis timing did not differ in normal cells undergoing proliferative versus neurogenic divisions, indicating that this mechanism likely does not normally govern cell fate, but can in the case of an abnormal division. Interestingly, faster cytokinetic abscission in the *Kif20b* mouse mutant is similarly suggested to cause a shift from proliferative to symmetric neurogenic divisions (McNeely et al 2019).

### C. Post-mitotic neuron polarization

Once born, post-mitotic neurons must accomplish the task of migrating to their correct location in the cortex, as previously discussed, as well as adapt their morphology in order to perform their eventual functions of receiving and transmitting signals. *In vitro*, although neurons do not migrate to a specified location, they still undergo the process of polarization, first described in hippocampal neuron cultures (Dotti et al., 1988). First, they exhibit actin-rich lamellipodia and filopodial protrusions. Next, they extend multiple microtubule-rich processes, or neurites, of similar lengths. Finally, one of these processes will extend farther than the others and become specified as the axon, adopting a faster rate of growth. Live imaging shows us that the first neurite to extend farthest does not always become the axon, and there is a time of flux where neurites extend back and forth before one eventually “wins” (C G Dotti et al., 1988). Interestingly, experimentally “cutting off” the axon allows another neurite to take its place, indicating the flexibility of this process at early stages (Dotti & Banker, 1987). This system has

also been adapted for study of cortical neurons. Much of what we know about axon specification and outgrowth comes from studies of this *in vitro* system of neuron polarization.

*In vivo*, cortical neurons undergo polarization changes in conjunction with migration. They first adopt a multipolar state in the subventricular zone and intermediate zone where they extend multiple neurites of similar length, similar to stage 2 *in vitro* (Noctor et al., 2004; Tabata & Nakajima, 2018). Next, they specify an axon that extends tangentially through the intermediate zone (Hatanaka & Yamauchi, 2013), followed by the formation of a leading process directed towards the pia (Sakakibara et al., 2014). As the leading process directs the cell upwards, the neuron adopts a bipolar morphology with the axon extended downward. The leading process eventually becomes the apical dendrite and adopts a highly branched morphology. The final morphological shape of most cortical excitatory neurons includes a pyramidal-shaped soma, one thin axon, a thick apical dendrite and other basal dendrites. Interestingly, *in vivo* neurons may inherit apicobasal polarity cues from mother NSCs and receive polarization and migration cues from extracellular sources (Barnes & Polleux, 2009; Evsyukova et al., 2013; Hatanaka et al., 2012). Without these cues, it may be more difficult for neurons to polarize *in vitro*. However, even *in vitro*, plating neurons on various substrates that serve as extracellular cues can speed polarization and outgrowth processes (Esch et al., 1999).

The molecular mechanisms of axon initiation and outgrowth are complex and multifactorial. Cellular polarity cues, such as endogenous N-cadherin gradients and the position of the centrosome, primary cilium and midbody remnant are suggested to predict the site of axon initiation *in vitro* and *in vivo* (Andersen & Halloran, 2012; Baudoin et al., 2012; de Anda et al., 2010; de Anda et al., 2005; Gärtner et al., 2012; Pollarolo et al., 2011). However, because this process is thought to be stochastic, with several neurites having the potential to become the axon, the ability to grow neurites quickly through more stable microtubules could result in one neurite more quickly becoming an axon when it reaches a certain length (Witte & Bradke, 2008). Axon outgrowth requires activation of multiple signal transduction pathways, cytoskeletal remodeling and stabilization of microtubules (for a review, see Barnes & Polleux, 2009). We have found the kinesin-6 family member Kif20b promotes cortical neuron polarization *in vitro* and correct morphology *in vivo* (McNeely et al., 2017), while the transcription factor p53 inhibits cortical neuron polarization and maturation *in vitro* (**Chapter 4**).

### 1.3 Cytokinetic abscission in cell lines and the developing cortex

#### A. Mechanisms of abscission and roles of the post-abscission midbody remnant

Cytokinesis, the final step in cell division, starts in anaphase with the goal of separating the cytoplasmic components of cells following chromosome segregation. This process has been studied primarily in single cells. (For a review, see (Mierzwa & Gerlich, 2014)). First, the cleavage site is specified by signaling from the anaphase spindle to the cell cortex, where RhoA accumulates and directs assembly of an actomyosin-rich contractile ring. Microtubules from the metaphase spindle as well as microtubules assembled de novo form the spindle midzone, which in turn becomes the central spindle. A key regulatory unit of the central spindle is centralspindlin, consisting of the Kinesin-6 family member MKLP1 and MgcRacGAP (Mishima et al., 2002). The contractile ring constricts as the furrow ingresses, compacting central spindle microtubules and proteins into a narrow intercellular bridge. This bridge, also called the midbody, is made of densely packed antiparallel microtubules and is the final connection between cells before abscission. Central spindle proteins relocate to distinct parts of the midbody; in the center, at adjacent sites on the flanks, or in a ring forming an electron-dense center. The midbody is also surrounded by lipids with roles in abscission completion; OCRL phosphatases remodel the actin cytoskeleton and FIP3 positive endosomes form the first narrowing of constriction sites to begin the abscission process. (Dambournet et al., 2011; Schiel et al., 2012).

Abscission requires cleavage of the microtubule bridge as well as membrane severing. Both processes are thought to be mediated by the endosomal sorting complexes required for transport (ESCRT) system, which plays a role in membrane scission in multiple systems including viral budding (Jez G. Carlton & Martin-Serrano, 2007). The key protein directing ESCRT recruitment is Cep55, which recruits ESCRT-I and ALG-2 interacting protein X (ALIX), which act in separate pathways to recruit ESCRT-III proteins (Carlton & Martin-Serrano, 2007; Christ et al., 2016; Hyung et al., 2008; Morita et al., 2007). ESCRT components are at first recruited to the midbody center, but later relocate to the sites of future abscission, called constriction sites (Elia et al., 2011). ESCRT-III assembles helical 17-nanometer-diameter filaments that narrow the midbody at the sites of future abscission (Guizetti et al., 2011). Upon relocation of the final ESCRT component, Vps4, to constriction sites, abscission almost immediately occurs (Elia et al., 2011). The final abscission event couples microtubule disassembly to membrane severing by

ESCRT-III recruitment of the microtubule-depolymerizing enzyme Spastin (Connell et al., 2009; Yang et al., 2008). The ESCRT system is highly conserved, particularly the downstream components; both the ESCRT-III component CHMP4B and VPS4 have orthologs even in archaea (Samson et al., 2008). Cep55, however, is vertebrate-specific.

The timing of abscission, while incompletely understood, is governed at least in part by the mitotic kinases Plk1 and Aurora B. Plk1 must be degraded after mitosis in order for Cep55 to be recruited to the midbody (Bastos & Barr, 2010). Aurora B regulates abscission as a part of the chromosomal passenger complex (CPC), which delays abscission in response to chromatin in the intercellular bridge as well as nuclear pore defects (Chen & Doxsey, 2009; Mackay et al., 2010; Norden et al., 2006; Steigemann et al., 2009). Aurora B phosphorylates the ESCRT-III component CHMP4C to prevent premature abscission and must be inactivated to reverse this inhibition, known as the abscission checkpoint (Capalbo et al., 2012; Jeremy G. Carlton et al., 2012). Interestingly, Aurora B itself is dispensable for abscission; a drug inhibitor applied following cleavage furrowing resulted in faster abscission (Mathieu et al., 2013). Abscission may also be delayed in response to changes in tension, although whether the CPC also responds to this is unknown (Lafaurie-Janvore et al., 2013). In cell lines, abscission has been reported to typically occur within 2 hours after furrowing, but knockdown of proteins involved in abscission can greatly increase time to completion (Florindo et al., 2012; Gromley et al., 2003). Interestingly, cytokinetic abscission occurs in G1, when cells prepare for cell cycle re-entry or exit (Gershony et al., 2014).

Abscission is thought to occur on one or both sides of the midbody in different cell types, resulting in either symmetric release of the midbody remnant or asymmetric retention by one daughter cell (Chun et al., 2013; Crowell et al., 2014). Released midbody remnants can also be engulfed by a daughter cell or another cell type, including phagocytic cells (Chai et al., 2012; Crowell et al., 2014; Fazeli et al., 2016). Midbody remnants, whether acquired through asymmetric abscission or post-abscission engulfment, can be sequestered in autophagosomes and targeted to lysosomes for degradation (Pohl & Jentsch, 2009). There is great interest in how midbody release and subsequent degradation is differentially regulated in various cell types and across development. Furthermore, the possibility of inheritance or release of the midbody indicates that the abscising cell is either acquiring or disposing of an organelle containing over 150 proteins as well as lipids and RNA (Atilla-Gokcumen et al., 2014; Skop et al., 2004) (Ahna

Skop, unpublished data). However, there is disagreement as to how often the midbody is retained or released and how often post-release engulfment occurs in individual cell types and in varying types of divisions. In a comparison of multiple cell lines, midbody release occurred more often in stem cell lines compared to cancer-derived cells, with release increasing in differentiative divisions of stem cells (Ettinger et al., 2011). Another group found that embryonic stem cell lines accumulated midbody remnants. Forced midbody accumulation through inhibition of autophagy led to increased stem-like identity and subsequent tumorigenesis (Kuo et al., 2011). Finally, even released midbody remnants have been shown to bind cell surfaces for several hours, where they could exert signaling roles before being engulfed (Bernabé-Rubio et al., 2016; Crowell et al., 2014).

## B. Consequences of cytokinesis failure

In mammalian cells, cleavage furrowing defects often result in furrow regression, creating a binucleate cell that may merge to form a tetraploid cell (Normand & King, 2010). When cytokinetic defects occur at a later stage after midbody formation, regression of the midbody can occur, or, cells may exhibit long abscission delays and remain connected by persistent intercellular bridges (Gromley et al., 2003; Steigemann et al., 2009). This may also manifest as abnormally long intercellular bridges/midbodies (Florindo et al., 2012; Weiderhold et al., 2016). Cells that fail abscission may continue to cycle, resulting in multicellular syncytia (Gromley et al., 2003). If lagging chromatin is in the intercellular bridge at the time of abscission failure, DNA damage can occur (Christ et al., 2016). Cytokinesis failure at any stage may lead to apoptosis or cell cycle exit. In the case of RhoA deficiency in erythroblasts, cleavage furrowing failure resulted in p53 activation (Konstantinidis et al., 2015).

The consequences of cytokinesis failure in mammalian tissues are less clear, but could theoretically include the above defects seen in cell lines as well as many others specific to the multicellular environment. Consequences may be tissue-dependent, based on the fact that some tissues function normally with binucleate cells, such as the liver (Guidotti et al., 2003; Margall-Ducos et al., 2007), while in others, such as the cerebral cortex, it is a rare occurrence. Intriguingly, germ cells in many species as well as cells in some invertebrate somatic tissues do not complete abscission, instead forming stable intercellular bridges and syncytia (Amini et al., 2014; Lenhart & DiNardo, 2015). However, completion of cytokinesis is necessary in early stage

mouse embryos; mice lacking the furrowing protein MgCRacGAP exhibit pre-implantation lethality (Van de Putte et al., 2001). Interestingly, mouse mutants for other cytokinetic proteins including citron kinase, Kif20b, and Cep55 exhibit severe developmental defects in the central nervous system, suggesting that NSCs may be more sensitive to cytokinetic defects than other cell types (Di Cunto et al., 2000; Janisch et al., 2013; Little & Dwyer, 2018; Sarkisian, Li, Di Cunto et al., 2002) (this thesis, **Chapters 2 and 3**).

### C. The role of Kif20b in cytokinetic abscission of cultured cells

*Kif20b* encodes a plus-end-directed microtubule motor protein in the kinesin-6 family, which have roles in cytokinesis. Unlike the other Kinesin-6 family members, Kif23 (MKLP1) and Kif20a (MKLP2), which have orthologs in invertebrates, Kif20b is vertebrate-specific. Kif20b was first discovered as a mitotic phosphoprotein and has been called Mphosph1, MPP1 or KRMP1 (Kamimoto et al., 2001; Westendorf, 1994). It exhibits a conserved kinesin organization, with a motor domain, central region containing alpha-helical domains and a tail region that binds cargoes. The stalk and tail regions are divergent from the other Kinesin-6 family members.

Kif20b localizes to the central spindle during cytokinetic furrowing and the midbody during abscission in cultured human cells as well as mouse NSCs (Abaza et al., 2003; Janisch et al., 2013; Janisch et al., 2018; Kanehira et al., 2007). Kif20b's important role in cytokinesis has been illustrated by knockdown experiments in dividing human cell lines (Abaza et al., 2003; Kanehira et al., 2007; Liu et al., 2014). In HeLa cells, Kif20b knockdown resulted in delayed cleavage furrowing and misregulated cytokinetic abscission timing (Janisch et al., 2018). Interestingly, no furrow regression or failure of cytokinesis was seen, indicating that Kif20b may be required for ensuring timely, accurate abscission in mammalian cells, but is not absolutely necessary to complete abscission. In addition to timing, Kif20b is necessary for correct midbody width, perhaps due to its microtubule bundling activity. Finally, cell death has been described as a consequence of Kif20b loss, but the degree depends on cell type (Abaza et al., 2003; Janisch et al., 2018; Liu et al., 2014). Kif20b is overexpressed in many human cancers or immortalized human cancer cell lines, where it promotes proliferation and actin-mediated cellular invasion processes (Kanehira et al., 2007; Liu et al., 2014; Lin et al., 2018).

#### D. The role of Cep55 in cytokinetic abscission of cultured cells

Cep55 was first identified from a bioinformatics screen as a putative centrosomal protein, although a subsequent role for Cep55 in the centrosome has not been observed (Fabbro et al., 2005). There is still disagreement on whether Cep55 localizes to or has a role in the centrosome and/or the central spindle. Non-controversial is Cep55's localization to the midbody ring and its importance in cytokinetic abscission of mammalian cells (Bastos & Barr, 2010; Fabbro et al., 2005; Zhao et al., 2006). A scaffolding protein containing coiled-coiled domains, Cep55 is not found in genomes of invertebrates. Cep55 has been reported to associate with microtubules and have microtubule bundling activity *in vitro* (Zhao, 2006).

Knockdown of Cep55 in HeLa cells suggests that Cep55 is required for cytokinesis in cultured mammalian cells: a progressive increase in binucleate cells over time corresponds with a 25-fold increase in cells with 4N DNA content by FACS analysis (Fabbro et al., 2005; Zhao, 2006).

Strikingly, live imaging of Cep55 knockdown HeLa cells in two independent studies showed that the vast majority of cells had abscission delays exceeding 7 hours, which eventually resulted in midbody regression and formation of a binucleate cell (Fabbro et al., 2005; Zhao, 2006).

Importantly, mitosis timing was found to be normal. Cep55 loss has also been reported to result in midbody shape abnormalities including loss of the midbody bulge and loss of typical midbody markers after long abscission delays (Zhao, 2006). Aberrant mitotic spindles were also reported with Cep55 knockdown, however, these were secondary to cytokinesis failure as they were only noted in binucleate cells (Fabbro et al., 2005). Cell death has not been reported as a consequence of Cep55 loss in HeLa cells.

Cep55 is localized to the midbody by and forms a complex with MKLP1 (Zhao, 2006). This recruitment is regulated by Plk1, which phosphorylates Cep55 and prevents its early localization to the midbody center; correctly timed Cep55 localization is necessary for abscission completion (Bastos & Barr, 2010). Once localized, Cep55 recruits the aforementioned ESCRT factors to start the ESCRT cascade (Hyung et al., 2008). From mammalian cell line findings, it would not be expected that vertebrate cells could complete abscission without Cep55. However, Cep55 mutation in humans (thought to be loss of function) have resulted in pre- or peri-natal death of human embryos, but not preimplantation death as would be expected for a protein essential for cytokinesis (Bondeson et al., 2017; Frosk et al., 2017; Rawlins et al., 2019). Thus, it is not clear

whether Cep55 is absolutely required for abscission, or only in some cell types or conditions. We further investigate this question in **Chapter 3**.

#### E. Cytokinesis in epithelia and the developing cortex

Cytokinesis in epithelial tissues as opposed to single cells is a multicellular process, requiring coordination of division with tension induced by surrounding cells, maintenance of apico-basal polarity and formation of new adherens junctions (For a review, see Herszterg et al., 2014). When NSCs undergo cytokinesis in the neuroepithelium, these epithelial factors as well as additional factors specific to the cortex have to be coordinated (Dwyer et al., 2016). NSCs must undergo interkinetic nuclear migration to enter mitosis at the apical membrane. Cleavage furrowing also occurs at the apical membrane; however, furrowing starts basally and proceeds apically, in comparison to the symmetric furrowing seen in single cell cultures. While one study postulated that the basal process of NSCs was split asymmetrically and retained by only one daughter cell, another study observed the basal process to be split symmetrically (Kosodo et al., 2008; Miyata et al., 2001). More work is needed to determine if the basal process is inherited symmetrically or asymmetrically during differing NSC division types and across developmental time. Furrow ingression results in the formation of the midbody at the apical membrane, with its center protruding into the ventricle space after new junctions are made. While we know that midbody severing occurs apically, we do not know how far the nuclei of daughter cells have migrated away basally before abscission occurs. Additionally, NSCs must retain their apicobasal polarity when undergoing abscission, while also allowing neuronal and basal progenitor daughter cells to delaminate and migrate away. How this is coordinated is poorly understood.

NSCs must coordinate cytokinesis with various daughter cell fates, including progenitor or neuron daughters produced through symmetric or asymmetric divisions. As previously discussed, the angle of cleavage was once thought to determine daughter cell fates; a change in cleavage angle could result in differential distribution of cytoplasmic components as well as of the apical membrane itself (Kosodo et al., 2004; Véronique Marthiens & ffrench-Constant, 2009). However, new research shows that cleavage is almost always perpendicular to the apical membrane (Kosodo et al., 2008) and cleavage angles are not always predictive of fate (Konno et al., 2008; Noctor et al., 2008; Postiglione et al., 2011). It is possible that inheritance of apical components could be coordinated at the midbody stage post-furrowing (Paolini et al., 2015).

The symmetry of abscission and fate of the midbody remnant play a role in multiple epithelial processes across species. In *Drosophila*, there is evidence for a role of the midbody in asymmetric cell fate and neuron polarization (Pollarolo et al., 2011; Salzmänn et al., 2013). Strikingly, the midbody remnant specifies the future ventral side of the *C. elegans* embryo and is necessary for dorsoventral axis formation (Singh & Pohl, 2014). In cultured epithelial cells, the midbody is suggested to play a role in ciliogenesis as well as lumen formation (Bernabé-Rubio et al., 2016; Li et al., 2014). It was previously unclear whether cytokinetic abscission in NSCs occurred on one side of the midbody, with asymmetric inheritance, or on both sides, releasing a midbody remnant. Midbody remnants can be detected in the ventricular fluid and in dissociated progenitor cultures (Dubreuil et al., 2007) (McNeely et al., 2019). New data of cytokinetic abscission in apical NSCs indicated that a second abscission occurred at least 60% of the time (McNeely et al., 2019). Therefore, the majority of the time abscission does occur on both sides of the midbody in E11.5 and E13.5 NSCs. Whether asymmetric abscission and/or post-abscission engulfment ever occurs in cortical NSCs is not clear.

Mouse microcephaly mutants with cytokinetic defects offer insight into parameters of cytokinesis important for normal brain size. Citron kinase, Kif20b, Kif20a, Kif14 and Cep55 are proteins involved in cytokinesis that when mutated cause microcephaly in mice and/or humans. These mutations will be discussed in further detail in the next section.

## **1.4 Apoptosis and p53 activation in microcephaly**

### A. Microcephaly etiology

Microcephaly in humans is a clinical finding where the brain at birth is more than 2.5 standard deviations below the mean smaller than control brains, leading to intellectual disability (Duerinckx & Abramowicz, 2018; Faheem et al., 2015) (OMIM 251200). In primary microcephaly, developmental as opposed to degenerative abnormalities are the cause, and classically the brain architecture is normal. Additionally, the number of neurons is typically severely reduced due to a combination of cell death, impaired cell proliferation, and/or changes in symmetric versus asymmetric divisions. Genes implicated in primary microcephaly in humans are involved in many aspects of mitosis including centrosome or centrosomal-related activities,

proper formation and maintenance of the mitotic spindle, chromatin remodeling, and DNA repair. Recently, cytokinetic furrowing has been linked to human microcephaly by the discovery of mutations in citron kinase and Kif14, proteins that localize to the cleavage furrow and midbodies of dividing cells, in humans (Harding et al., 2016; H. Li et al., 2016; Makrythanasis et al., 2018; Moawia et al., 2017). Additionally, cytokinetic abscission has been implicated through human mutations in Cep55 (Bondeson et al., 2017; Frosk et al., 2017). Mouse models of microcephaly give us insight into mechanisms of known human disease and provide candidates for future genetic testing. Analysis of microcephaly mutants importantly elucidates mechanisms of normal cortical development and reveals conserved and differential modes of cell division across embryonic tissues. Forward genetic screens can uncover new genes necessary for brain development (Dwyer et al., 2011). Finally, recent advances in human induced pluripotent stem cell lines and embryoids can be used to discern mechanisms of human-specific disease. Together, these tools have rapidly expanded our understanding of mammalian cortical development.

#### B. Apoptosis and p53 activity in the cortical epithelium

Apoptosis is a conserved mechanism of microcephaly etiology following diverse cellular insults. A process of programmed cell death, apoptosis is necessary during development of many tissues but also occurs in response to cell damage (Arya & White, 2015). While there are other forms of cell death such as necrosis, they seem to be uncommon in normal embryonic development. There are two major pathways of apoptosis, the intrinsic or mitochondrial pathway and the extrinsic or death receptor pathway. The intrinsic pathway is activated by internal cell stressors such as DNA damage, which signals to the mitochondria to activate Bcl-2 family members, including Bax and Bak, to release apoptotic proteins including cytochrome c. (Lindsten et al., 2000; Westphal et al., 2011). Cytochrome c then complexes with apoptotic protease activating factor 1 (APAF1) and procaspase-9, initiating the caspase cascade. The extrinsic pathway of apoptosis is activated by the binding of death receptor ligands such as from the tumor necrosis factor (TNF) family to surface receptors. This forms a complex at the plasma membrane that signals to initiator caspase-8, starting the caspase cascade that converges with the intrinsic pathway at caspase 3, the executioner caspase. Activation of caspase 3 downstream of both pathways results in DNA fragmentation, degradation of cellular proteins, formation of apoptotic bodies and finally uptake by phagocytic cells.

The degree to which programmed cell death occurs in the normal embryonic cortex is surprisingly unclear. Some amount of apoptosis is necessary for normal cortical size. Caspase-9 and caspase-3 knockout mice exhibit cortical overgrowth, but this appears to be due to failure of apoptosis of a region of FGF-8 secreting cells in the anterior neural ridge (Haydar et al., 1999; Kuida et al., 1998; Kulda et al., 1996; Nonomura et al., 2013). When these cells are not eliminated, they continue to secrete FGF-8, signaling to other NSCs to proliferate, causing cortical hyperexpansion. In comparison, very few apoptotic cells are detected in the dorsal-lateral cortical epithelium beginning at embryonic day 10 until birth. However, because apoptotic cells can be quickly eliminated, and alternative modes of apoptosis or cell death can occur that are not caspase-dependent, the amount of naturally-occurring cell death in the cortex may be underreported (Hochreiter-Hufford & Ravichandran, 2013). Recent clonal analysis of basal progenitor fates indicated that more than half of basal progenitor divisions resulted in the asymmetric death of one daughter cell (Mihalas et al., 2016). The discrepancy between this observation and the low number of caspase-3 and TUNEL positive cells in the normal cortex remains to be resolved.

The *Trp53* gene encodes the transcription factor p53 that acts as a tumor suppressor by regulating the cell cycle at multiple points; it is mutated in over 50% of all human cancers (for a review, see Kasthuber & Lowe, 2017). p53 mutation in a variety of tumors confers a poor patient prognosis (Olivier et al., 2010). p53 responds to DNA damage to activate repair, mediates the G1/S and G2/M cell cycle checkpoints, and initiates apoptosis, exclusively through the intrinsic pathway (Knowles & Leitner, 2007). In addition to apoptosis, p53 regulates a vast network of cellular functions, including cellular differentiation, cell cycle arrest or exit, metabolism, proliferation and plasticity. Given its many reported roles, it is surprising that the p53 knockout mouse usually develops normally and is viable (Donehower et al., 1992; Jacks et al., 1994). p53 mutation in *Drosophila* does result in a smaller brain than normal, so additional regulatory mechanisms may exist in the mammalian brain to compensate for loss of p53 activity (Contreras et al., 2018). These could include the vertebrate-specific p53 family members, p63 and p73 (Zhang et al., 2015). However, approximately 10% of p53 mouse mutants develop exencephaly due to lack of normal apoptosis in the central nervous system during neural tube closure (Sah et al., 1995). Additionally, within a few months of birth p53 mutants develop sporadic tumors with high penetrance. Mice heterozygous for p53 also develop tumors, but at a later age (Jacks et al., 1994). Although the p53 mutant phenotype indicates that p53 is not essential for normal development,

other evidence demonstrates that p53 is active during development, ready to respond if a problem should arise (Jain & Barton, 2018). p53 is expressed ubiquitously in developing tissues but declines during terminal differentiation (Schmid et al., 1991). In the cortex, higher expression is seen in proliferating NSCs with lower levels seen in post-mitotic neurons (Van Lookeren Campagne & Gill, 1998).

### C. Genetic and environmental causes of microcephaly implicating p53

A growing body of work indicates that neural stem cells have a unique sensitivity to apoptosis induced by activation of the cell cycle regulator p53. In some mouse microcephaly mutants, widespread p53 activation in the cortex is readily noted by highly elevated nuclear p53 expression; in other mutants p53 expression is only subtly increased, or activation occurs through phosphorylation rather than increased protein levels. Remarkably, inhibition of p53 can fully or partially restore brain size in some microcephaly mutants. Importantly, this is not due to an effect of p53 mutation itself in brain development, as the brains of p53 knockout mice have normal size and structure (Insolera et al., 2014; Little & Dwyer, 2018). The degree of rescue does not always correlate with the amount or degree of p53 activation seen. In some mutants, deleting p53 has resulted in complete or nearly complete rescue of brain size (Insolera et al., 2014; Little & Dwyer, 2019 (**Chapter 2**); Pao et al., 2014), while in others the rescue was more modest (Bianchi et al., 2017; Véronique Marthiens et al., 2013) (this thesis, **Chapter 3**). While less common, in at least one mutant, microcephaly was made worse through p53 deletion (Murga et al., 2009). Regardless of rescue of overall brain size, apoptosis has been rescued in almost all microcephaly mutants tested with p53 inhibition. Therefore, whether brain size is rescued, unchanged or more severe seems to depend on the consequences of cells made “undead” by p53 deletion. The range of these phenotypes is evidence of the diversity of cellular defects that can activate p53. In some cases, these cellular defects are deleterious, while surprisingly, other defects do not appear to result in unfavorable consequences. For a comparison of microcephaly mutants implicating p53, see **Table 1**.

**Table 1: Microcephaly mutants implicating p53**

Model	Cellular observations	Apoptosis and p53 activation	Does p53 deletion rescue?	Observations in double mutants	Hypothesis for p53 activation
Plk4 overexpression with Nestin-Cre (Marthiens et al 2013)	Centrosome amplification; multipolar spindles with failure of clustering resulting in aneuploidy	Apoptosis - yes by CC3 staining from E11.5 and decreased until birth; p53 expression not directly addressed	Rescued apoptosis but only rescued brain size by 12%	Higher incidence of centrosome amplification, multipolar divisions, lagging chromatids and aneuploidy; accumulation of aneuploid cells thought to result in tissue degeneration	Centrosomal amplification resulting in multipolar spindles and aneuploidy
Sas 4 conditional null with Nestin-Cre (Insolera et al 2014)	centrosomes/centrioles and cilia, defects in spindle pole assembly and mitotic prometaphase delay,	Yes by p53 and CC3 antibody staining in the cortex from E12-E15	Yes full rescue of brain size and rescued apoptosis by CC3, but mice still had hydrocephalus	Greatly increased numbers of mislocalized Pax6+ and Tbr2+ cells	Prometaphase delay in mislocalized NSCs
Cep63 T/T (gene trapped) mice (Marjanovic et al 2015)	Defective centrosome maturation and monopolar spindles, mislocalized Sox2+ NSCs, mitotic delay	Yes by p53 and CC3 antibody staining in the cortex at E14.5	Complete rescue of brain size; rescued apoptosis by TUNEL staining; did not rescue fertility in males	Misplaced Sox2+ NSCs	Prometaphase delay in mislocalized NSCs
Magoh+/- (Silver et al 2010; Pilaz et al 2016; Mao et al 2016)	Defects in mitotic spindle formation and orientation; mitotic delay Knock in: Spindle defects with greater vertical divisions; increased mitotic cells in metaphase,	Upregulation of p53 dependent pathways through RNA sequencing; p53+ cells in VZ at E13.5	Complete rescue of apoptosis and partial rescue of brain size	N/A	Mitotic prometaphase delay
Tubb5 conditional knock-in and knock-out with Nestin Cre (Breuss et al 2016)	increased "ectopic DNA elements"; Knock out did	Yes by p53 and CC3 antibody staining in the cortex at E14.5	Rescued apoptosis, brain size not addressed	N/A	Defects in mitosis/mitotic delay
BRCA1 conditional null with Nestin-Cre (Pao et al 2014)	Misoriented pyramidal neurons and abnormal RGC morphology	Yes by p53 and CC3 antibody staining in the cortex at E12.5	Full rescue of cortex size but cerebellum and hippocampus not completely rescued; mice were viable	Subtle layering defects still seen and neurons still misoriented	Unrepaired DNA damage
Nde1-/- mice (Houlihan and Feng 2014)	DNA damage during S phase and lengthened S phase	Apoptosis - yes by CC3 and TUNEL staining from E10.5-12.5; p53 - yes by phosphorylation at Ser18	Full rescue of brain size and apoptosis; mice were viable	S phase still lengthened and reduced BrdU incorporation due to deficient DNA replication	DNA damage during S phase
ATR S/S (severe ATR hypomorph) (Murga et al 2009)	Increased DNA damage and premature aging syndrome	Yes by p53 and CC3 antibody staining in the cortex at E13.5	No; mice were rarely born and those that were had even more accelerated aging, apoptosis was not rescued	Further increase in cells with DNA damage and G2 arrest with p53 inhibition	DNA damage due to replicative stress
Citron kinase-/- (Bianchi et al 2017)	binucleate and tetraploid cells; increased DNA damage in both diploid and tetraploid cells	Increased p53 phosphorylation at Ser-15; increased apoptosis throughout cortical development	Completely rescued apoptosis and partially rescued microcephaly	Double mutants had increased numbers of binucleate/tetraploid cells and still had DNA damage	DNA damage; hypothesized cytokinetic defects were not the cause for p53 activation
Kif20b-/- (Janisch et al 2013; Little and Dwyer 2018)	Late-abscission midbody structural and alignment defects; no binucleates observed	Apoptosis - yes by CC3 staining from E10.5-16.5; p53 - total protein increased by WB and increased nuclear p53 in dissociated NSCs	Completely rescued apoptosis and mostly rescued microcephaly; heterozygote p53 loss equally rescued	Double mutants still had midbody alignment and structural defects	Abscission/midbody maturation defects
Cep55-/- (Little et al unpublished)	Increased numbers of binucleate/tetraploid cells, increased midbody stage cells, increased mitotic basal progenitors	Apoptosis - yes by CC3 staining from E10.5-14.5 and at P0; p53 - yes by p53 staining at E14.5 <i>in vivo</i> ; p53 increased specifically in binucleate cells	Completely rescued apoptosis and partially rescued microcephaly	N/A	Binucleate/tetraploid cells from failed cytokinesis

*Microcephaly caused by centrosome defects*

Centrosomes are the microtubule-organizing centers of the cell, necessary for organization of interphase microtubules, mitotic spindles and cilia and flagella assembly (Conduit et al., 2015). Interestingly, both centrosome loss and amplification cause microcephaly in mice and humans, indicating that despite being ubiquitously expressed, centrosome proteins are especially important for NSC divisions (Faheem et al., 2015). Centrosome amplification is a classic marker of tumorigenesis, allowing cells in some tissues to divide and expand quickly. However, centrosome clustering mechanisms, such as those present in flies and some mammalian cells, are necessary for cells with supernumerary centrosomes to divide without producing aneuploidy (Basto et al., 2008; Marthiens et al., 2012).

*Plk4 overexpression:* In the mouse cortex, centrosome amplification through Plk4 overexpression results in mitotic delay, aneuploidy and subsequent p53-dependent apoptosis and microcephaly (Marthiens et al., 2013). The authors showed that NSCs have inefficient clustering mechanisms, although interestingly, some clustering mechanisms were present and improved during later corticogenesis. Despite rescue of apoptosis, p53 deletion in Plk4 overexpression mutants provided only a very modest increase in brain size, and Plk4OE;p53 mutants subsequently experienced tissue degeneration postnatally, possibly due to a buildup of aneuploid cells.

While Plk4 overexpression has not been discovered as a cause of microcephaly in humans, mutations in STIL, a pericentriolar and centrosome protein, similarly results in centrosome amplification in cell lines and does cause microcephaly in humans (Arquint & Nigg, 2014; Kumar et al., 2008; Papari et al., 2013). We do not yet know whether p53 deletion would be therapeutic in the case of STIL mutation, but a similar result to Plk4OE;p53 mice could be expected.

*Sas4 mutation:* Deletion of Sas-4 (CPAP/CENPJ), a centriole biogenesis protein, results in globally reduced body size in mice and death around mid-gestation (Bazzi & Anderson, 2014). Despite the absence of centrosomes, spindle formation, chromosome segregation, and cell cycle parameters were normal, and DNA damage and aneuploidy were not observed. Instead, p53-dependent apoptosis seemed to result from a specific delay in prometaphase. p53 deletion improved but did not completely rescue embryo size and survival. A conditional forebrain-

specific Sas-4 mutant using *Nestin-Cre* exhibited a similar prometaphase delay in NSCs, widespread p53 activation and apoptosis, and reduced brain size (Insolera et al., 2014). Strikingly, simultaneous removal of p53 completely rescued microcephaly - this is notable in comparison to incompletely rescued embryo size in Sas-4;p53 null mutants. However, analysis of the cortical epithelium showed that apical NSCs in Sas4;p53 mutant cortices were displaced from the ventricle and had randomly oriented mitotic spindles. These data convincingly show that while centrosomes are necessary for apical NSC localization and normal spindle orientation, these parameters are *not required* for correct daughter cell fates and brain size. It is still unclear whether a relationship between NSC mislocalization and mitotic delay exists and whether both factors can lead to p53 activation, or whether these were two independent consequences of centrosome loss.

*Cep63 mutation:* Similarly to Sas-4 mutants, centrosome loss via Cep63 mutation, which causes Seckel syndrome in humans, causes p53-dependent microcephaly through mitotic spindle defects, mitotic delay and mislocalization of apical NSCs (Marjanović et al., 2015). They showed convincingly that p53 activation was not due to double-stranded DNA damage, as ATM and Chk2 co-deletion did not provide any benefit to Cep63 mutants, and few γH2AX puncta were observed in Cep63 mutant cortices. p53 deletion largely rescued brain size in Cep63 mutants; however, Cep63 mutants displayed male-specific infertility due to meiotic recombination errors, which were p53-independent.

#### *Microcephaly caused by other mitotic defects*

*Magoh mutation:* Insights from Sas-4 and Cep63 mouse mutants suggest that impaired centrosome biogenesis ultimately results in microcephaly due to mitotic errors (Insolera et al., 2014; Marjanović et al., 2015). In support of this idea, mutations in non-centrosomal proteins that also result in mitotic defects can similarly produce p53-dependent microcephaly. In fact, a small delay in mitosis of NSCs apart from other defects may be sufficient to activate p53-dependent apoptosis and p53-independent fate changes (Pilaz et al., 2016). Using both the *Magoh*<sup>+/-</sup> microcephaly mutant and drug inhibitors, Pilaz et al. demonstrated that mitotic delay beyond 40 minutes activated p53-dependent apoptosis and p53-independent preferential neurogenic fate of daughter cells. This delay was further shown to be due to a specific delay in prometaphase. Magoh is a component of the exon junction complex that binds mRNA and is necessary for

correct mitotic spindle orientation in NSCs (Silver et al., 2010). Apoptosis and premature neurogenesis were both noted as causes of microcephaly. Notably, conditional deletion of Magoh in NSCs replicated the microcephaly phenotype, but deletion in neurons did not. Careful analysis with live imaging subsequently revealed that spindle misorientation and mitotic delay were separable consequences of Magoh mutation and interestingly, were not correlated. Although no centrosome defects were noted, p53 deletion dramatically rescued microcephaly similar to centrosome biogenesis mutants (Mao et al., 2016). Treatment of NSCs with the drug inhibitors Nocodazole and STLC showed a strikingly similar increase in p53-dependent apoptosis and p53-independent cell fate changes with increasing mitotic delay. These data show that mitotic delay is strongly correlated with p53 activation and apoptosis in NSCs, even apart from spindle or centrosome defects.

*Tubb5 mutation:* Mutations in tubulin-encoding genes can cause a variety of cortical malformations, including lissencephaly and polymicrogyria, and in the case of beta-tubulin isoform TUBB5, microcephaly in mice and humans (Breuss et al., 2012; Breuss et al., 2017; Ngo et al., 2014). A conditional knock-in and knock-out mutation in TUBB5, which is expressed in both NSCs and neurons, exhibits a similar phenotype of severe microcephaly as seen in human patients (Breuss et al., 2012; Breuss et al., 2017). In the knockout mouse, mitotic spindle orientation was normal but mitotic progression was still impaired, with formation of multipolar spindles, ectopic DNA elements and aneuploidy. Widespread apoptosis was found to be p53-dependent. Upper-layer neurons were more severely reduced than deep-layer neurons, reflecting possible premature cell cycle exit of progenitors reducing the progenitor pool. Whether p53 deletion rescued microcephaly was not addressed; we would be interested to see whether a near-complete rescue is seen as in other mouse mutants with mitotic delay (Insolera et al., 2014; Mao et al., 2016) or if the presence of aneuploidy results in more severe defects as seen with centrosome gain (Marthiens et al., 2013).

#### *Microcephaly caused by DNA damage*

*Brca1 mutation:* The DNA damage pathway is the best-described pathway for p53 activation in the mouse cortex. A conditional mutant in BRCA1, a known tumor suppressor whose loss leads to DNA damage, exhibits microcephaly (Pao et al., 2014). Despite its known role in breast cancer, BRCA1 is highly expressed in the developing neuroepithelium. The cortex is thinned due

to complete loss of upper-layer neurons; additionally, pyramidal neurons are misoriented. p53 activation and apoptosis were widespread throughout the cortical epithelium. Moreover, p53 deletion completely rescued microcephaly and perinatal lethality in BRCA1 mutants. However, subtle layering defects and neuron misorientation still occurred. Excitingly, co-deletion of the DNA double-strand break sensor ATM, shown to activate p53 in cell lines, with BRCA1 also completely rescued microcephaly as well as all other observed defects. This is notable in comparison to Cep63 mutants, which did not exhibit rescue with deletion of ATM (Marjanović et al., 2015). Thus, differential pathways for p53 activation in the cortex do exist and can be separated.

*Nde1 mutation:* The *Nde1* mouse mutant provides further evidence for a DNA-damage mediated pathway for p53 activation in the cortex (Houlihan & Feng, 2014). Nde1 functions as a multifunctional scaffold protein and binds with Lis1; mutations in both proteins can cause microlissencephaly in humans. Loss of Nde1 in mice resulted in prolonged S phase, DNA replication errors, severe DNA damage as evidence by widespread  $\gamma$ H2AX+ puncta, p53 activation and apoptosis. p53 activity was noted specifically through increased phospho-p53 at site Ser18, a site specific for ATM/ATR kinases. This culminates in a specific loss of upper layer neurons (Feng & Walsh, 2004). The requirement for Nde1 in NSC divisions is strikingly specific to a window of time in cortical development around E12-13; the peak of  $\gamma$ H2AX+ puncta and apoptosis were noted at this time and were decreased before and afterwards. Although mitotic spindle defects were observed, the authors postulated that this was secondary to S phase defects. Interestingly, simultaneous deletion of p53 rescued apoptosis but did not rescue genomic defects. It is quite surprising, given the severity of DNA damage observed, that p53 deletion was able to fully rescue *Nde1*<sup>-/-</sup> microcephaly, but is consistent with the rescue seen in the case of *Brcal* mutation. It would be interesting to know whether ATM deletion can similarly rescue *Nde1*<sup>-/-</sup> microcephaly.

*Atr mutation:* In contrast to the above examples, another DNA-damage mediated microcephaly mutant exhibits microcephaly unable to be rescued by p53 deletion. Mutation of ATR, an upstream activator of p53, causes a build-up of replicative stress and single-stranded DNA breaks in proliferating cells during development, resulting in dwarfism and microcephaly in mice (Murga et al., 2009). It is notable that ATR is required for normal development as compared to its partner ATM, which is dispensable for normal development but responds to double-stranded

DNA breaks to activate p53 in abnormal mutants such as the BRCA1 mutant described above (Pao et al., 2014). Postnatally, ATR-deficient mice exhibited severe premature aging (Murga et al., 2009). Surprisingly, although  $\gamma$ H2AX+ puncta, p53 activation and apoptosis were seen in embryonic ATR mutant tissues, p53 deletion was unable to rescue dwarfism and premature aging phenotypes. Instead, double mutant embryos rarely survived past birth, and  $\gamma$ H2AX+ puncta and apoptosis were elevated in double mutant cortices. The inability of p53 deletion to rescue microcephaly in the ATR mutant suggests that single-stranded breaks are more deleterious for development than double-stranded breaks. It would be very interesting to know the p53-independent mechanism of apoptosis in ATR;p53 double mutant embryos.

Citron kinase mutation: Interestingly, DNA damage has been implicated as a cause of microcephaly in the Citron Kinase (CK) mutant, which is known for its role in cytokinesis. CK is an important regulator of cleavage furrowing and localizes to the central spindle. Mouse mutants in CK exhibit microcephaly, characterized by a notable increase in binucleate and tetraploid cells in the cortex resulting from cytokinesis failure (Di Cunto et al., 2000; Sarkisian et al., 2018). Apoptosis and p53 activation are also increased in CK<sup>-/-</sup> cortices. However, in addition to its primary role in cytokinesis, recent evidence has emerged for a role of CK in DNA repair (Bianchi et al., 2017). NSCs in CK mutant cortices exhibit increased levels of  $\gamma$ H2AX+ and 53BP1+ puncta and increased total  $\gamma$ H2AX protein. Notably, DNA damage is seen in both diploid and tetraploid cells, so is not simply a consequence of cytokinesis failure. p53 deletion completely rescues apoptosis and partially rescues microcephaly in CK mice. Increased numbers of tetraploid cells are seen in double mutant cortices compared to CK mutant cortices, suggesting that an increased proportion of dying cells are tetraploid. However, DNA damage is noted in double mutant cortices as well and is therefore also an upstream consequence of CK loss. More work is needed to determine whether cytokinesis failure and DNA damage are completely separate consequences of CK mutation and whether either, or both, lead to p53 activation. This would be relevant to our understanding of the human microcephaly disease caused by CK loss (Harding et al., 2016; H. Li et al., 2016). Interestingly, RNA sequencing analysis showed a profile of cell cycle exit genes were upregulated in double mutant cortices. The incomplete rescue of CK mutant brains could be because premature cell cycle exit occurs in a p53-independent manner due to unresolved cytokinetic or DNA repair defects.

### *Microcephaly caused by cytokinesis defects*

The goals of chromosome separation and cytoplasm separation in cell division are unique, and therefore the processes of mitosis and cytokinesis are distinctly regulated. In the last section, we gave an example of a mutant in citron kinase with defects in cytokinesis resulting in binucleate and tetraploid cells, with some indication that this may contribute to p53 activation (Bianchi et al., 2017). Citron kinase regulates the first step of cytokinesis, or cleavage furrowing. However, the second phase of cytokinesis, cytokinetic abscission, is regulated separately and takes much longer, on the order of hours instead of minutes. Abscission is the process of severing the last connection between two daughter cells, termed the intercellular bridge or midbody, resulting in release of the midbody or inheritance by one of the daughter cells. Cytokinetic abscission proteins have recently been implicated in human microcephaly through mutations of *Cep55* (Bondeson et al., 2017; Frosk et al., 2017).

*Cep55 mutation:* In **Chapter 3** and **Appendix 3** of this thesis, I show that *Cep55* mutation in mice replicates the human phenotype of neurodevelopmental defects including a smaller brain. Interestingly, despite germline mutation of *Cep55*, the brain is more severely affected than the rest of the body. Similarly to CK mutant mice, greatly increased numbers of binucleate cells are observed in *Cep55* mutant brains and in cortical cultures. Increased midbody, or cytokinetic abscission stage, NSCs are observed *in vivo*. While the apical mitotic index is normal, increased mitotic basal progenitors are seen, indicating a possible secondary defect of mitotic delay in basal progenitors. Widespread p53 activation and apoptosis are also observed in *Cep55* mutant cortices, but interestingly, not in *Cep55* mutant cultured MEFS or in other non-neural embryonic tissues. Strikingly, the greatest p53 activation was seen in binucleate cells. p53 deletion completely rescued apoptosis but only partially rescued microcephaly. Data from this mutant suggest that a p53-dependent apoptotic response to binucleate cells could exist in the cortex. This could explain why other tissues such as the liver have a higher tolerance for binucleate cells than the cortex, in which they are rarely seen. More work is needed to determine whether p53 is activated directly by cells that fail cytokinesis or whether errors in the next S phase or mitosis could be the direct cause.

*Kif20b mutation:* Cytokinetic abscission defects may not always result in furrow regression, but instead incomplete abscission or abscission that completes with errors. The *Kif20b*<sup>-/-</sup><sup>magoo</sup> model

of microcephaly, discovered through an ENU screen for defective cortical development, is an example (Dwyer et al., 2011). Kif20b protein localizes to the central spindle during cytokinetic furrowing and the midbody during abscission specifically in dividing NSCs. Mutant mice exhibit perinatal lethality, dying before or soon after birth, and have a smaller forebrain (Janisch et al., 2013). Abnormalities in parameters of cytokinesis, including the number, shape and alignment of midbodies, are seen in *Kif20b*<sup>-/-</sup> cortex (Janisch et al., 2013; Janisch & Dwyer, 2016). Apoptosis is also increased, although not to as high of levels as seen in other mouse mutants.

It was surprising, then, that not only homozygous but also heterozygous deletion of p53 could completely rescue apoptosis and greatly improve brain size in *Kif20b* mutant mice (Little & Dwyer, 2018, this thesis, **Chapter 2**). Remarkably, perinatal lethality was rescued, with *Kif20b* mutant; *p53* heterozygote mice living normal lifespans. Notably, neither DNA damage, increased mitotic cells, mislocalization of NSCs nor binucleate cells were observed in *Kif20b* mutant and *Kif20b;p53* double mutant cortices, strongly suggesting that the mechanism for p53 activation in the *Kif20b* mutant is unique. Midbody misalignment as well as midbody shape defects were not rescued in *Kif20b;p53* double mutants, indicating that they may lead to p53 activation or be independent consequences of Kif20b loss. p53 activation was not as obviously increased in the *Kif20b* mutant compared to other mouse mutants, but a small increase in nuclear p53 was noted at the midbody stage. Subsequent analysis has indicated that *Kif20b* mutants undergo abscission faster than control cells (McNeely et al., 2019). More work is needed to determine the molecular pathway that could signal from abscission defects to activate p53 in the *Kif20b* mutant cortex.

#### *Microcephaly through external insults*

Exciting new research indicates that p53 can be activated in NSCs due to external insults as well as genetic defects. Environmental factors, such as Zika virus infection during pregnancy, are more common causes of microcephaly in humans than genetic defects (Abuelo, 2007). Zika virus crosses the placenta and has a tropism for NSCs, causing proliferation defects and apoptosis in cultured human NSCs (H. Tang et al., 2016), human cerebral organoids (Dang et al., 2016; Garcez et al., 2016; Qian et al., 2016) and mouse models (Li et al., 2016). However, it is still unclear why Zika virus causes such damage to the CNS, as it can and does infect other cell types. One possibility is that the molecular response to Zika virus infection is more robust in NSCs. In support of this idea, p53 activation was shown to be a consequence of infection in NSCs, and the

cause of apoptosis (Ghouzzi et al., 2016). However, p53 activation is not necessarily a response to all viral infection, as CMV infection did not show a transcription profile similar to Zika infection. DNA damage was noted in Zika infected NSCs, but it was not clear whether it was the cause or a consequence of p53 activation. Interestingly, Zika virus infection in NSCs was recently suggested to impair cytokinesis completion through viral protease cleavage of Septin-2 (Li et al., 2019). A detailed analysis of cell cycle parameters in Zika infected NSCs would enable further comparison with other microcephaly mutants. Furthermore, it would be informative to investigate the consequences of Zika virus infection of NSCs for brain growth in the setting of p53 inhibition.

In addition to infectious causes, nutrient deficiencies are a cause of neurodevelopmental defects in humans. Zinc is a necessary nutrient for mammalian neural tube closure in both humans and mice. This was recently shown to be through direct regulation of p53 activity (Li et al 2018). Zinc is necessary for the interaction between p53 and the zinc-dependent E3 ubiquitin ligase Mdm2, which ubiquitylates p53 in order to negatively regulate its activity. Without zinc, p53 was disinhibited and activated apoptosis. Use of the p53 inhibitor pifithrin-alpha was sufficient to restore p53 activity to normal levels and allow neural tube closure in zinc-deficient embryos. These data show another pathway for p53 activation through the removal of its inhibitor.

#### D. Pathways of p53 activation following cell division errors

Wild-type p53 possesses DNA binding domains and acts as a transcription factor, suppressing growth in cell culture (Kasthuber & Lowe, 2017). The total pool of active p53 in cells is regulated in several ways. Its ubiquitin ligase, MDM2, facilitates its degradation in order to keep its expression at low levels in normal cells. p53 can be stabilized through phosphorylation, blocking MDM2 from degrading it, or by inhibition of MDM2 itself. Increased transcription of p53 and translocation to the nucleus are also modes of p53 activation. Although p53 controls transcription of many target genes, two large groups have been identified: those that inhibit cell cycle progression, including p21 which binds and inhibits cyclin-dependent kinases, and those that promote apoptosis, including p53 upregulated modulator of apoptosis (PUMA) and BH domain proteins Bak and Bax. How the decision to arrest or undergo apoptosis is made is poorly understood, but does seem to depend on cell-type.

Intriguingly, recent studies indicate that cultured cells carry “memories” of mitogens and stress signals into daughter cells after division, influencing the decision of whether to re-enter or exit the next cell cycle (Yang et al., 2017). These memories are specifically transduced through p53 protein levels that directly dictate p21 levels as well as cyclin D1 mRNA. These data have broad implications for studies of mouse mutants, in which numerous divisions have occurred by the time of analysis. Therefore, a combination of acute knockdown and total knockout studies are necessary to differentiate primary and secondary effects. Importantly, for the cortical development field, these data also suggest that small defects in cell division could be magnified in subsequent divisions as the memory of the original division is retained.

A large scale CRISPR/Cas-9 knockout analysis in cancerous and non-cancerous human cell lines revealed that various cellular defects can activate p53 through distinct molecular pathways (McKinley & Cheeseman, 2017). Interestingly, the p53 status of individual cell lines, whether wild-type as in h-TERT-RPE1 cells or mutated as in HeLa cells, was able to account for the severity of cellular defects seen with knockout of the same protein. In cell lines with intact p53, cell cycle exit or arrest, which was p21-dependent, eliminated abnormal cells, whereas in HeLa cells they continued to divide and accumulate. Notably, p53 deletion itself accelerated the rate of proliferation of RPE1 cells and resulted in a shift in cell cycle parameters on flow cytometry. McKinley et al found three groups of cellular defects resulting in p53- and p21-dependent cell cycle arrest, and an accumulation of defects upon simultaneous removal of p53 or p21: centrosome duplication, DNA damage repair, and cytokinesis furrowing/cleavage failure. These remarkably parallel the categories of cellular defects shown to activate p53 to cause microcephaly, as discussed so far. Furthermore, McKinley et al. found that spindle assembly checkpoint defects did not result in cell cycle arrest, suggesting that p53 activation is not necessarily a response to all cellular defects. We will briefly review the molecular understanding of the main pathways proposed for p53 activation that have been validated in cell lines below.

#### *p53 activation following DNA damage*

The DNA damage pathway has been long-described to activate p53 to cause cell cycle arrest and apoptosis (Kastan et al., 1991; Williams & Schumacher, 2016). The DNA damage response is transduced through activation of either ATM or ATR kinases, which phosphorylate effector kinases Chk1 and Chk2 (Maréchal & Zou, 2013). ATM/Chk2 is activated in response to double-

stranded DNA breaks, while ATR/Chk1 is activated in response to single-strand breaks. ATM marks sites of DNA damage within minutes of the insult by phosphorylation of the histone variant H2AX. While phosphorylation of H2AX, or  $\gamma$ H2AX, is often used as an indicator of DNA damage in cells, it is important to note that this is only a marker for double-stranded breaks, not single-strand breaks and other types of damage. Along with many other targets, ATM and ATR also directly phosphorylate to activate p53. In less severe forms of damage, p53 halts the cell cycle just long enough for DNA repair machinery to resolve defects, and the cell cycle continues (Reinhardt & Schumacher, 2012). This cell cycle arrest, which can occur during G1/S, intra-S and G2/M checkpoints, is mediated through the downstream p53 target p21. If damage is more extensive, cell cycle exit or apoptosis may occur, preventing damaged DNA from being passed on to daughter cells.

#### *P53 activation following mitotic defects*

In the case of centrosome loss or extended mitotic duration, 53BP1 and USP28 proteins mediate p53 activation and G1 arrest, in hTERT-RPE1 cells. Interestingly, these proteins are not activated in response to cytokinesis failure or DNA damage (Lambrus et al., 2016; Meitinger et al., 2016). Inhibition of 53BP1 rescues p53-dependent cell cycle arrest in cells with knockdown of the Plk4 inhibitor Centrinone, which have fewer than normal centrosome numbers and mitotic delay. However, 53BP1 inhibition does not rescue p53-dependent cell cycle arrest in cells with defects in cytokinesis, DNA replication or kinetochore maintenance, due to knockdown of PRC1, ORC1 and KNL1, respectively (McKinley & Cheeseman, 2017). Taken together, these data indicate that the p53-dependent response to centrosome defects and mitotic delay is *separate* from the DNA damage and cytokinetic pathways. In support of this idea, another study found that aneuploidy itself does not activate p53, but does so only secondarily through mitotic delay caused through chromosome segregation defects (Santaguida et al., 2017). However, more work is needed to determine how alterations in mitotic timing are transduced to 53BP1 and USP28 activation at the molecular level.

#### *P53 activation following cytokinesis defects*

Cytokinesis failure may result in p53 activation through multiple avenues as there can be distinct consequences of cytokinetic defects. Failure to complete cleavage furrowing may result in

regression to form a binucleate cell. This has been shown to result in p53 activation in the case of RhoA depletion, a key factor in furrowing (Konstantinidis et al., 2015). Binucleate cells have been seen to arrest in the next G1 in a p53 dependent manner, but what triggers p53 is unclear (Stukenberg, 2004). The hypothesis that mammalian cells have a “tetraploidy checkpoint” that arrests binucleate cells in G1 has been suggested, but has been controversial, as it is not observed in all cell types (Uetake & Sluder, 2004; Wong & Stearns, 2005). Recently, the hippo tumor suppressor pathway was shown to mediate p53 activation in tetraploid cells, via sensing of cell shape changes; this pathway was shown to be distinct from the DNA damage pathway (Ganem et al., 2014). The role of the Hippo pathway in response to binucleates was further validated to occur upon PRC1 knockdown (McKinley & Cheeseman, 2017).

The consequences of abscission defects are less understood, but in addition to midbody regression may include inability to complete abscission resulting in persistent intercellular bridges and/or syncytia, midbody structural defects and abnormal abscission timing. Changes in abscission timing can result in apoptosis through the caspase cascade (Joshi et al., 2011). Chromatin that is not cleared from the midbody or intercellular bridge can result in DNA damage, which activates p53 through the aforementioned ATM/ATR pathway (Giunta et al., 2010). Additionally, DNA damage activates the Aurora B abscission “checkpoint” (Steigemann et al., 2009) which communicates with the ESCRT pathway to delay abscission until chromatin is cleared (Carlton et al., 2012). The abscission checkpoint has also been proposed to be activated by tension, or defects in nuclear pore reassembly during cytokinesis (Lafaurie-Janvore et al., 2013; Mackay et al., 2010). However, no link between the abscission checkpoint and p53 activation has been identified.

#### E. Unresolved questions

This is an exciting time in the field of cortical development. The cell and developmental biology techniques used over the past half-century have given us unprecedented insight into the temporal events of corticogenesis. More recently, we have begun to gain an understanding of molecular control of cortical development with genetic and sequencing techniques. The discovery of p53 as a molecular linchpin in the etiology of microcephaly is a powerful example of the ability of genetic techniques to reveal fundamental processes. We now understand that a rare event in

normal cortical development, p53-dependent apoptosis, is a driving factor for the onset of neurodevelopmental disease. However, many fundamental questions remain to be answered.

It is apparent from the literature thus far reviewed that p53 signaling is a widespread factor for the development of microcephaly in multiple models with various cellular defects. However, it still remains to be answered whether there are forms of microcephaly not dependent on p53. In particular, some microcephaly mutants have been proposed to have cell fate changes as their underlying cause rather than cell death (Geng et al., 2018; Pulvers et al., 2010). It would be informative to know whether p53 deletion is able to provide any rescue to microcephaly in these mutants. It may be that low levels of apoptosis, when occurring at early time points in development, are still consequential for brain size, as seen in the *Kif20b* mutant (Little & Dwyer, 2019). Furthermore, it is possible that p53 signaling could also influence cell fate decisions in the cortex, as has been proposed (Tedeschi & Di Giovanni, 2009). In the case of mitotic delay and abscission defects, fate changes have been proposed to be p53-independent (Pilaz et al., 2016) (McNeely et al 2019). However, given p53's role in cell cycle exit decisions in other cell types, it is likely that p53-dependent forms of cell cycle exit also exist in NSCs (Kastenhuber & Lowe, 2017).

Additionally, it remains to be adequately answered what other forms of p53-independent apoptosis and other types of cell death beyond apoptosis contribute to normal cortical development as well as the onset of microcephaly. We described one example of p53-independent apoptosis in a mouse mutant with single-stranded DNA breaks due to ATM deletion (Murga et al., 2009), but few other examples have been noted. It would be informative to know the mechanism of degeneration noted upon p53 deletion in mouse mutants with supernumerary centrosomes, which must be p53-independent (Marthiens et al., 2013).

An outstanding issue for the field is identification of molecular pathways activating p53 in NSCs and/or neurons. It is still unclear how molecularly distinct the p53 activation mechanisms are in the microcephaly mutants thus far described. One strategy to take in addressing this would be to test the previously described pathways found for activation of p53 in cell lines in NSCs, whether cultured or *in vivo*. The DNA damage pathway is the only molecular pathway for p53 activation that has been shown definitively to act in the cortex (Houlihan & Feng, 2014; Pao et al., 2014). It may still be worthwhile to evaluate the DNA damage pathway in microcephaly mutants that did

not have elevated  $\gamma$ H2AX<sup>+</sup> cells, as other forms of DNA damage can occur and even subtle damage can result in downstream consequences. Additionally, the USP28-53BP1 signaling pathway, shown to respond to mitotic delay in cell lines (Lambrus et al., 2016; Meitinger et al., 2016), could be tested in centrosome mutants and mutants with other mitotic defects for a causative role. It is not clear whether mutants with reduced and supernumerary numbers of centrosomes activate p53 through separate pathways, or simply have different cellular consequences with p53 co-deletion. Finally, the Hippo pathway could be tested for p53 activation in cytokinesis mutants (Ganem et al., 2014).

In addition to simultaneous deletion of p53, crosses of microcephaly mutants to other proteins upstream or downstream of p53 could be informative. For example, co-deletion of ATM, an upstream regulator of p53 in the DNA damage pathway, was found to rescue microcephaly in a mutant with DNA damage defects (Pao et al., 2014) but not in one with centrosome defects (Marjanović et al., 2015). A cross to the USP28 mouse mutant, which develops normally, would be informative in testing for microcephaly rescue in mutants with mitotic delay (Knobel et al., 2014). In the Kif20b mutant, co-deletion of Bax, a downstream effector of p53-dependent apoptosis, partially rescued apoptosis and microcephaly (Little & Dwyer, 2019). It would be interesting to see whether downstream factors such as p21, known to control cell cycle exit, and Puma, known to regulate p53-dependent apoptosis, could also rescue apoptosis and/or microcephaly in mutants implicating p53. p21 and Puma knockout mice develop normally, similarly to p53 mutants (Jeffers et al., 2003; Martín-Caballero et al., 2001). Additional analyses into the mechanism of p53 activation in NSCs is also needed. Phosphorylation has been seen in the case of DNA damage mutants, but whether p53 is also regulated by stabilization or change in localization in mutants with other defects has not been addressed

Finally, a key question that remains virtually unaddressed by the cortical development field is how whole-body knockouts of microcephaly proteins often affect brain size much more than body or other organ size. If the mutated genes are ubiquitously expressed, then differential requirements for proteins in epithelial tissues versus other tissue types, or downstream molecular effectors such as the p53 signaling axis, may be the cause. Baseline levels of p53 expression and the degree of p53 response to cell cycle defects does vary between cell types (Kastenhuber & Lowe, 2017). Additionally, a consequence of p53 loss in cell lines appears to be more often cell-cycle arrest or exit instead of apoptosis. How differential responses to p53 activation including

cell cycle arrest, exit and/or apoptosis is determined is not understood. Further analysis of other cell types besides NSCs, *in vitro* and ideally *in vivo*, in both epithelial and non-epithelial tissues, is warranted in microcephaly mutants.

## 1.5 Research Objectives

Investigations into mechanisms of normal cortical development have in the past focused primarily on regulation of cell identity and daughter cell fate. More recently, efforts to understand abnormal cortical development through genetic mouse mutants, in some cases modeling human disease, were expanded. Through this work we now understand that cell death is as often, if not more so, a cause of microcephaly as are cell fate changes. Because apoptosis does not often occur in the normal cortical epithelium, it is primarily through disease mutants that we have gained an understanding of the apoptotic pathways that normally lie dormant in the cortex, waiting for a defect to occur. With cell death identified as a common mechanism for smaller brain phenotypes, our attention has turned to identifying the underlying cellular and molecular defects that can activate these pathways, and how. Mitotic failure in neural stem cells has been described as a cellular pathway that can lead to p53 activation, apoptosis, and ultimately a smaller brain. Whether cytokinetic defects, and especially defects in cytokinetic abscission, result in microcephaly through distinct or similar mechanisms was not previously known.

*Broadly, the goal of this thesis was to determine if p53 activation and/or apoptosis occurred in response to cytokinetic abscission defects in NSCs in the cortex to cause microcephaly. To this end, we induced cytokinetic abscission defects in NSCs through two mouse mutants for proteins involved in completion of abscission.*

In **Chapter 2**, we first investigated the role of apoptosis in *Kif20b* mutant microcephaly. The *Kif20b* mutant is a unique microcephaly mutant, with defects observed only in the late stages of cytokinesis. Apoptosis in the cortices of *Kif20b* mutant mice was previously described (Janisch et al., 2013) but was noted at low levels compared to some other reported microcephaly mutants. Our goals were to: determine the contribution of apoptosis versus other causes to the microcephaly in the *Kif20b* mutant, evaluate the benefits and consequences of apoptosis inhibition for *Kif20b* mutant cells, individually, and *Kif20b* mutant mice, on a larger scale, and determine whether cytokinetic defects induced by *Kif20b* loss led to p53 activation and/or

apoptosis. We set out to accomplish these goals by crossing the *Kif20b* mutant to the *p53* mouse mutant. Excitingly, heterozygous and homozygous *p53* deletion not only rescued apoptosis in the *Kif20b* mutant, but largely rescued cortical size. Moreover, *p53* deletion allowed *Kif20b* mutants, which normally die around birth, to live normal life spans. However, there was still a component of brain size not rescued by *p53* deletion. Additional studies supported a role for *Kif20b* in neuron outgrowth and maintenance of proliferative divisions that was p53-independent (See **Chapter 4** and **Appendix 1**).

In **Chapter 3**, we investigated whether mutation of another cytokinetic abscission protein could also result in p53-dependent apoptosis and microcephaly. We chose to study the result of *Cep55* mutation in mouse cortical development, as mutation of this protein was previously shown to cause a neurodevelopmental disease incompatible with life in humans. We were excited to find that *Cep55* mutation in mice replicated the human phenotype, causing a severe microcephaly, but only a mild reduction in overall body size. Interestingly, we found that *Cep55* mutants did not have a defect in midbody thinning as seen in the *Kif20b* mutant, but had an increased number of cells at the midbody stage, and a substantial increase in binucleate cells presumably resulting from cytokinesis failure. p53<sup>+</sup> cells and apoptosis were widespread throughout the cortical epithelium, and dissociated progenitors showed greatly increased p53 expression in binucleate cells. *p53* deletion completely rescued apoptosis in the cortex and partially rescued brain size, though not to as great a degree as the *Kif20b* mutant.

As a tangential benefit to this thesis work, we were also able to evaluate the role of p53 in cortical development. **Chapter 4** shows our unexpected finding of a role for p53 in neuron polarization and maturation. p53 mutant neurons polarized more quickly *in vitro*, with faster specification of the axon and subsequent axon outgrowth. A role for p53 in neuron maturation was also supported by RNA sequencing of p53 mutant cortices, shown in **Appendix 2**. Finally, **Appendix 1** provides further evidence that p53 may normally act to eliminate binucleate cells, as increased numbers of binucleate cells are observed in p53 mutant cortical cultures.

Our findings support the existence of a p53-dependent apoptotic response pathway to cytokinetic abscission defects in NSCs. Unexpectedly, however, we found evidence for two separate pathways that lead from impaired cytokinetic abscission to p53 activation. Mutation of *Kif20b* results in defective midbody maturation which is not rescued by *p53* deletion, and increased

nuclear p53 at the midbody stage in *Kif20b* mutant cells, suggesting a novel midbody-mediated pathway for p53 activation. In contrast, mutation of *Cep55* causes a more severe block to abscission and results in failure to complete cytokinesis in a percentage of cortical cells. While the binucleate cell state has been previously suggested to activate p53 in cell lines, we show here for the first time that binucleate cells accumulate high levels of p53 in NSCs. The many cellular defects observed in *Cep55* mutants may mean that multiple pathways lead to p53 activation, resulting in apoptosis and microcephaly. Together, these two mutants elucidate how more subtle and severe abscission defects can lead to p53 activation in separate ways, but with ultimately similar consequences.

## Chapter 2: *p53* deletion rescues lethal microcephaly in a mouse mutant with neural stem cell abscission defects

*Adapted from:*

Little, J. N., & Dwyer, N. D. (2019). *p53* deletion rescues lethal microcephaly in a mouse model with neural stem cell abscission defects. *Human Molecular Genetics*. 28(3), 434–447. <https://doi.org/10.1093/hmg/ddy350>

### **Abstract**

Building a cerebral cortex of the proper size involves balancing rates and timing of neural stem cell (NSC) proliferation, neurogenesis and cell death. The cellular mechanisms connecting genetic mutations to brain malformation phenotypes are still poorly understood. Microcephaly may result when NSC divisions are too slow, produce neurons too early or undergo apoptosis but the relative contributions of these cellular mechanisms to various types of microcephaly are not understood. We previously showed that mouse mutants in *Kif20b* (formerly called *Mphosph1*, *Mpp1* or *KRMP1*) have small cortices that show elevated apoptosis and defects in maturation of NSC midbodies, which mediate cytokinetic abscission. Here we test the contribution of intrinsic NSC apoptosis to brain size reduction in this lethal microcephaly model. By making double mutants with the pro-apoptotic genes *Bax* and *Trp53* (*p53*), we find that *p53*-dependent apoptosis of cortical NSCs accounts for most of the microcephaly, but that there is a significant apoptosis-independent contribution as well. Remarkably, heterozygous *p53* deletion is sufficient to fully rescue survival of the *Kif20b* mutant into adulthood. In addition, the NSC midbody maturation defects are not rescued by *p53* deletion, showing that they are either upstream of *p53* activation, or in a parallel pathway. Accumulation of *p53* in the nucleus of mutant NSCs at midbody stage suggests the possibility of a novel midbody-mediated pathway for *p53* activation. This work elucidates both NSC apoptosis and abscission mechanisms that could underlie human microcephaly or other brain malformations.

### **Introduction**

Human genetics is increasingly successful at linking specific gene mutations to congenital brain malformations and other neurodevelopmental disorders. However, the cellular mechanisms

connecting genetic mutations to brain phenotypes are still poorly understood. There are 17 human primary microcephaly genes identified, and there are many syndromes that feature microcephaly [(Duerinckx & Abramowicz, 2018); Online Mendelian Inheritance in Man (OMIM) database]. Thus, it is a heterogeneous disorder. Known microcephaly genes encode proteins with diverse molecular functions, but many are involved in cell division.

Cell division genes may be prominent in brain malformations like microcephaly because cortical neural stem cell (NSC) divisions have several unusual features (Dwyer et al., 2016). NSCs are tall, thin cells that reside in the pseudostratified epithelium of the cortex, with their apical endfeet forming the ventricular surface, and their basal processes stretching to the basal lamina beneath the meninges. Their nuclei undergo interkinetic nuclear migration during the cell cycle, moving basally for S phase (DNA Synthesis phase) and to the apical membrane for Mphase (Mitosis phase) and cytokinesis. In addition, NSC divisions can produce symmetric or asymmetric daughter fates, giving rise to more NSCs, neurons, intermediate progenitors (IPs) and glia during corticogenesis. These stem cells must produce the right types and numbers of daughter cells within specific windows of time. With all these complex demands, the developing cortex is particularly vulnerable to insults to cell division.

We previously identified a mouse model of microcephaly that is recessive, perinatal lethal and relatively severe, with a brain about half as thick as normal during late gestation. It carries a recessive loss-of-function mutation in the kinesin microtubule motor gene *Kif20b* that causes a splicing error, frameshift and reduction of the protein to undetectable levels.

These *Kif20b*<sup>magoo</sup> mutant brains do not display NSC mitotic arrest or abnormal cleavage angles, which have been noted in other microcephaly mutants. Instead, *Kif20b* mutant brains display defects in cytokinetic abscission (Dwyer et al., 2011; Janisch et al., 2013). Abscission is the process of severing the connection between mother and daughter cell, taking an hour or more after telophase (Mierzwa & Gerlich, 2014). The cleavage furrow compacts the central spindle microtubules into the midbody, which mediates abscission by recruiting proteins to remodel and ‘cut’ the cytoskeleton and membrane. We showed that Kif20b protein localizes to the central spindle and midbody in human cell lines and mouse NSCs (Janisch et al., 2013; Janisch et al., 2018). Furthermore, Kif20b appears to facilitate changes in midbody microtubule structure as the midbody ‘matures’ during the abscission process, and ensures timely abscission in cell lines. Suggesting that it may accelerate cell division, *Kif20b* is elevated in some cancers (Kanehira et al., 2007; Liu et al., 2014; W.-F. et al., 2018). Interestingly, *Kif20b* evolved with the vertebrate

lineage, so its subtle role in abscission may be important for growing bigger, more complex nervous systems.

In addition to abnormal midbodies, *Kif20b<sup>magoo</sup>* mutants (called *Kif20b* mutant or *Kif20b<sup>m/m</sup>* hereafter) also display increased apoptosis in the embryonic cortex from embryonic day (E)10.5–16.5 (Janisch et al., 2013). However, it was unclear whether the relatively small amount of detectable apoptosis observed could account for the severity of the microcephaly. Apoptosis appears to be relatively low in the healthy embryonic neocortex. Prevention of apoptosis by knockout of caspase-9 or caspase-3 does cause cortical overgrowth, but this appears to be because of failure of apoptosis of a small cluster of FGF8-secreting cells that is normally eliminated around E10.5, rather than failure of widespread programmed cell death (Haydar et al., 1999; Kuida et al., 1998; Kulda et al., 1996; Nonomura et al., 2013). Elevated apoptosis is seen in some mouse models of brain malformations (Chen et al., 2014; Insolera et al., 2014; Marjanović et al., 2015; Marthiens et al., 2013; Stottmann et al., 2013; Vonberg et al., 2016; Yingling et al., 2008). The intrinsic or stress-induced apoptotic pathway can be triggered by environmental stresses or genetic insults, such as particular mutations (Arya & White, 2015). Bax and p53 (gene *Trp53*) are expressed in embryonic brain and appear to respond to damage. In response to apoptotic stimuli, Bax, a multi-BH domain-containing member of the BCL2 family, can form pores across the outer mitochondrial membrane, thereby releasing cytochrome c that can activate the caspase cascade. p53, a tumor suppressor mutated in many human cancers, is an upstream activator of Bax (Kasthuber & Lowe, 2017). Mouse knockouts of *Bax* and *p53* have normal brain development with surprisingly few low penetrance defects (Insolera et al., 2014; Jacks et al., 1994; Knudson et al., 1995).

Here, we set out to determine the relative contributions of apoptosis and abscission dysregulation to the microcephaly of the *Kif20b* mutant and to understand the relationship between these phenotypes. To do this, we crossed genetic mutants of the intrinsic apoptosis pathway to *Kif20b* mutant mice and asked whether the apoptosis, microcephaly and abscission defects in *Kif20b* mutants were rescued, unaffected or potentially worsened. To our surprise, we found that *p53* deletion prevented apoptosis and rescued brain size and structure to a remarkable degree. A partial apoptosis inhibition by *Bax* deletion correlated with a lesser extent of brain size rescue. Surprisingly, deletion of even one allele of *p53* is able to completely block the apoptosis and lethality in *Kif20b* mutants. However, *Kif20b; p53* double mutant brains are still smaller than controls at birth, suggesting that *Kif20b* regulates cortical development through additional p53-

independent mechanisms, perhaps by ensuring timely abscission. Indeed, *p53* deletion does not rescue the defects in midbody structure seen in *Kif20b* mutant NSCs, and additional midbody defects are revealed when *p53* is deleted. Our data provide the first evidence that abscission defects may cause *p53* accumulation in NSCs or any cell type, through a yet-to-be identified pathway. Finally, our work informs apoptosis inhibition as a potential way to ameliorate the severity of microcephaly caused by genetic, viral or environmental insults.

## Results

### *The intrinsic apoptotic pathway is the key driver of microcephaly in Kif20b mutant mice*

To test whether the intrinsic apoptotic pathway mediates the elevated apoptosis and microcephaly in the *Kif20b* mutant cortex, we utilized genetic crosses to mutants in two key genes in this pathway, *Bax* and *p53* (*Trp53*). Importantly, homozygous deletion mutants in *Bax* or *p53* develop properly with normal size cortices (Insolera et al., 2014; Jacks et al., 1994; Knudson et al., 1995). Due to the low number of true wild-type  $^{+/+}$  mice (1/16) produced from double heterozygote crosses, we elected to use double heterozygotes (*Kif20b* $^{+/m}$ ; *Bax* $^{+/-}$  and *Kif20b* $^{+/m}$ ; *p53* $^{+/-}$ ) as controls in order to compare to single and double mutant littermates. First, we produced *Kif20b*; *Bax* double mutants. *Bax*, together with its partner *Bak*, increases the permeability of the mitochondrial membrane, increasing cytochrome c release (Westphal et al., 2011). We examined double mutant brains at age E14.5, when apoptosis is elevated in *Kif20b* mutants, and the cortical plate (cp) has started to form. Interestingly, embryos carrying homozygous mutations in both *Bax* and *Kif20b* showed a partial block of the elevated apoptosis, as marked by cleaved caspase-3 (CC3), and a partial rescue of cortical thickness (Fig. 1A–J). Heterozygous deletion of *Bax* showed a trend for mild rescue, but this result did not reach statistical significance. Craniofacial defects observed in *Kif20b* mutants were not rescued by heterozygous or homozygous *Bax* mutation (data not shown). These data suggest that apoptosis and microcephaly are correlated, but that additional proteins are required for the full apoptotic response to *Kif20b* loss. For example, *Bak* is a partner of *Bax* and is partially redundant (Lindsten et al., 2000).

The tumor suppressor *p53* is upstream of *Bax*/*Bak* in the intrinsic apoptotic pathway. Therefore, we tested whether *p53* deletion could fully block the apoptosis in *Kif20b* mutants by crossing to the *Trp53* mutant (Jacks et al., 1994). Strikingly, apoptosis and cortical thickness of

E14.5 *Kif20b*<sup>m/m</sup> embryos are both fully rescued by either heterozygous or homozygous deletion of *p53* (Fig. 2A–J). Thus, two functional *p53* genes are required to produce the apoptosis and microcephaly triggered by *Kif20b* loss. Furthermore, *p53* is required for the craniofacial defects of *Kif20b*<sup>m/m</sup> embryos: either heterozygous or homozygous *p53* deletion significantly ameliorates the small eye and snout phenotypes (Fig. 3). *p53* protein appears to be elevated in *Kif20b* mutant cortices, as immunoblots of E12.5 cortical lysates show *p53* band intensity increased 50% in *Kif20b*<sup>m/m</sup> samples, normalized to the NSC protein beta-catenin (Fig. 4A-B). This increase was not detectable by immunohistochemistry on cortical sections (data not shown). However, immunostaining for *p53* on dissociated NSC cultures shows an increase in the median nuclear-to-cytoplasmic ratio (N:C ratio) of *p53* in *Kif20b* mutant NSCs (Nestin positive), but not in neurons or other cell types (Nestin negative) (Fig. 4C-F). Together, these data show that *p53* accumulates in the nucleus of NSCs when *Kif20b* is lost, and *p53* function is required for the excess apoptosis and microcephaly in this mutant. Moreover, the partial and full rescues of microcephaly by *Bax* and *p53* deletion show that the amount of apoptosis and the severity of microcephaly are strongly correlated, suggesting that apoptosis is the key cellular mechanism driving microcephaly in *Kif20b* mutant mice.

#### *p53* deletion restores growth of neuronal and subventricular layers in embryonic *Kif20b* mutant cortex

We previously showed that the reduced cortical thickness of *Kif20b* mutants is because of thinner neuronal layers and fewer IPs (Janisch et al., 2013). To determine if *p53* deletion could rescue cortical neurogenesis and structure as well as thickness, we labeled *Kif20b* single mutant and *Kif20b*; *p53* double mutant E14.5 cortical sections for Pax6, Tuj1 and Tbr2, to label NSCs, neurons and IPs, respectively. In *Kif20b*<sup>m/m</sup> single mutant brains, as expected, the neuronal layer (nascent cp) is thin, and the axonal layer (intermediate zone, iz) is barely detected (Fig. 5A and B). As a proportion of total cortical thickness, the ventricular zone (vz) is increased, and IPs are reduced (Fig. 5D and E). Remarkably, double mutant *Kif20b*<sup>m/m</sup>; *p53*<sup>-/-</sup> embryos have cortices that appear to have normal organization, with cortical plates and intermediate zones indistinguishable from controls (Fig. 5C and G). Additionally, *Kif20b*<sup>m/m</sup>; *p53*<sup>-/-</sup> embryos display normal vz thickness and IP generation (Fig. 5F, H and I). Therefore, blocking apoptosis by *p53* deletion in the cortices of *Kif20b*<sup>m/m</sup> brains increased cortical thickness by improving production or survival of neurons and IPs. Furthermore, the neurons and IPs in double mutant brains appear to migrate normally and create a normal-appearing structure.

*p53 deletion rescues postnatal survival but not full cortical size of Kif20b mutant mice at birth*

In addition to reduced brain size, *Kif20b* mutant mice exhibit perinatal lethality. Remarkably, while no *Kif20b<sup>m/m</sup>* mutant mice with wild-type *p53* status survive the day of birth (postnatal day 0, P0), *Kif20b<sup>m/m</sup>* mice with heterozygous or homozygous *p53* deletion survive postnatally at expected Mendelian ratios (Fig. 6A). Even more surprising, most *Kif20b<sup>m/m</sup>; p53<sup>+/-</sup>* mice and *Kif20b<sup>m/m</sup>; p53<sup>-/-</sup>* mice live to adulthood and are fertile. Some *Kif20b<sup>m/m</sup>; p53<sup>+/-</sup>* mice (~15%) still have visible craniofacial defects including a small eye or short snout, and ~5% have hydrocephalus, but the majority have normal facial structure. Double homozygotes (*Kif20b<sup>m/m</sup>; p53<sup>-/-</sup>*) have even fewer craniofacial defects, but die prematurely at ~3–4 months of age due to spontaneous tumors, as do *p53<sup>-/-</sup>* single mutants (Jacks et al., 1994).

The postnatal survival of *Kif20b; p53* double mutant mice enabled us to investigate the requirement of *Kif20b* for corticogenesis without the confounding factor of excess apoptosis. Interestingly, in contrast to the full rescue of cortical thickness seen at E14.5 in *Kif20b<sup>m/m</sup>; p53<sup>-/-</sup>* brains, at P0 they show a 5% decrease in cortical length and a 15–20% reduction in total cortical thickness compared to heterozygous controls (Fig. 6B–F). This is not due to *p53* mutation, as *Kif20b<sup>+/-</sup>; p53<sup>-/-</sup>* mice had normal cortical length and thickness, in agreement with previous studies [Fig. 6B, C and F; (Insolera et al., 2014)]. The reduction in thickness in *Kif20b; p53* double mutants is in the cortical plate and intermediate zone, but not the vz and subventricular zone (svz) (Fig. 6G). To determine whether superficial or deep layers of the cortical plate were reduced in the double mutant, we labeled sections with *Cux1* for layers II–IV, *Ctip2* for layers V–VI and *Tbr1* for layer VI. We saw reduced thickness of all layers, with the most significant decrease in layer VI (Fig. 7A–D). Further analysis of layer VI showed that there was a loss in the absolute number of *Tbr1*<sup>+</sup> cells, and that these cells were more densely packed (Fig. 7E–H). These data indicate that despite the dramatic improvements in cortical growth and postnatal survival afforded by blocking p53-dependent apoptosis, a deficit remains in neurogenesis of all cortical plate layers. Thus, while elevated apoptosis largely accounts for the microcephaly of the *Kif20b* mutant, proper cortical growth requires a *Kif20b* function that cannot be compensated by deleting p53 and preventing apoptosis.

*Kif20b is required cell autonomously for midbody maturation of cortical NSCs*

Previously we showed that *Kif20b* is expressed in germinal zones of the embryonic brain, and that Kif20b protein localizes to midbodies of dividing embryonic cortical NSCs at the ventricular surface (Janisch et al., 2013). We further showed that *Kif20b* mutants have abnormalities in NSC midbodies; they tend to be wider and less aligned to the apical membrane. These phenotypes could be due to a cell-autonomous requirement for Kif20b during abscission or due to non-cell autonomous effects through cell–cell interactions at the apical membrane junctions, because cytokinesis in epithelia is a multicellular process (Herszterg et al., 2014). To further probe Kif20b’s function in embryonic NSC division, we used dissociated cortical cell cultures.

Midbodies at various stages of maturation can be detected with tubulin and Aurora Kinase B (AurKB) staining by their characteristic shapes (Fig. 8A–C). Early-stage midbodies are wide (Fig. 8A), but become thinner as the midbody matures (Guizetti et al., 2011). At late stages, microtubule constriction sites (abscission sites) are detectable on one or both sides of the midbody center [Fig. 8B and C, arrows; (5)]. We found in human cell lines that Kif20b is recruited to early stage midbodies, and at late stages accumulates around the constriction sites (Janisch et al., 2018). Interestingly, *Kif20b<sup>m/m</sup>* NSC cultures have an increased frequency of wide midbodies (Fig. 8D), and fewer midbodies with at least one constriction site (Fig. 8E). These analyses show that *Kif20b* is required for normal NSC midbody maturation, and that this requirement is cell autonomous.

Some other mouse models of microcephaly show increased mitotic index in the cortex, because of NSC mitosis delay or arrest (Chen et al., 2014; Insolera et al., 2014; Marjanović et al., 2015; Marthiens et al., 2013; Vonberg et al., 2016). We showed previously that the *Kif20b* mutant cortex does not have increased mitotic index (Janisch et al., 2013), but here we use the dissociated cortical cell cultures to address this possibility with higher cellular resolution. We assayed whether *Kif20b* mutant NSCs spent more time in mitosis or abscission than control NSCs by determining the mitotic and midbody index in cultures. Surprisingly, among cycling NSCs (Ki67+) in *Kif20b* mutant cultures, both the mitotic index and midbody index were not increased but were actually slightly reduced (Fig. 9B). This could suggest that *Kif20b* mutant NSCs undergo mitosis and abscission more rapidly than control cells, or that more are undergoing apoptosis. To analyze relative durations of cell division phases, we categorized mitotic and midbody stage NSCs into sub-stages by phospho-histone H3 (PH3) and AurKB appearance (Fig. 9A, C). Among mutant NSCs at some stage of cell division, the percentages in prophase or prometa/metaphase were not different, but the percentage in anaphase/early telophase was

slightly increased in *Kif20b* mutant cultures. These data are consistent with our previous results that early steps of mitosis are not disrupted in *Kif20b*-depleted cells, but that cytokinesis is affected, with a small delay in furrow ingression (Janisch et al., 2018).

Since we observed cell-autonomous defects in midbody maturation (Fig. 8A–E) as well as increased nuclear p53 in *Kif20b* mutant NSCs (Fig. 4E), we next tested whether these findings were correlated. Analyzing p53 immunostaining in midbody stage cells of control and *Kif20b* mutant NSC cultures, we noted higher N:C ratios of p53 signal in *Kif20b* mutant cells (Fig. 8F–H). All observed control and mutant cells in M phase (35 control and 21 mutant), as determined by chromatin appearance, did not have chromatin-associated p53. Furthermore, testing for a correlation between p53 N:C ratios and midbody width uncovered a significant negative correlation between these measurements in *Kif20b* mutant but not control cells. Thinner midbodies (which normally indicates a later stage of abscission) were more likely to have higher N:C p53 ratios (Fig. 8I–J). While these levels of nuclear p53 accumulation in the midbody stage cells were not as high as in some interphase *Kif20b* mutant NSCs (Fig. 4D and E), these data nevertheless suggest that a subset of *Kif20b* mutant NSCs have elevated nuclear p53 during abscission. This is notable, since total p53 is reported to normally be low during mitosis and the following G1, but may rise in G1 under stress conditions (Yang et al., 2017). Whether midbody maturation defects could lead to p53 accumulation in the nucleus, or conversely whether p53 accumulation can lead to midbody defects, is unknown. DNA damage is known to activate p53 through a defined pathway, but we did not detect any increase in DNA damage in *Kif20b* mutant NSCs over controls (Fig. 10), suggesting that a different pathway causes nuclear p53 accumulation in *Kif20b* mutant NSCs.

#### *Kif20b* loss activates apoptosis cell autonomously in proliferating cortical NSCs

An attractive hypothesis is that defective midbody maturation of dividing NSCs in *Kif20b* mutants causes p53 to accumulate in some NSCs, starting in abscission and continuing afterward, eventually activating the intrinsic pathway of apoptosis. Supporting the idea that apoptosis predominantly occurs in NSCs in *Kif20b* mutant brains, we previously observed that the greatest-fold increase in apoptosis over control levels was seen at E10.5, when the cortex consists only of NSCs, as IPs and neurons have not yet been produced; the relative increase in apoptosis declined through E16.5 (Janisch et al., 2013). At E14.5 in *Kif20b<sup>m/m</sup>; p53<sup>+/+</sup>* mutant samples, 74% of apoptotic cells are found in the proliferative zones and 67% do not express neuronal tubulin

(Fig. 11). However, these *in vivo* analyses do not distinguish whether apoptosis is triggered cell autonomously or by cell–cell interactions, and whether it is associated with cell division. Therefore, we used dissociated NSC cultures to distinguish these possibilities. Indeed, in cultures of *Kif20b* mutant cells after 1 day *in vitro*, apoptotic cells are increased more than 2-fold over controls (Fig. 12A–C, arrows, CC3+ cells), suggesting that apoptosis is triggered cell autonomously. In cultures from *Kif20b*; *p53* double mutant mice, the rate of apoptosis is similar to controls, showing that the elevated apoptosis in isolated *Kif20b*<sup>m/m</sup> NSCs is also p53-dependent (Fig. 12D). Furthermore, neurons (TuJ1+) do not display increased apoptosis, while NSCs (Nestin+) do, and cycling NSCs (Ki67+) show a more pronounced increase (Fig. 12E–F).

Next, we wanted to ask whether NSC apoptosis was associated with cell division. Apoptotic cells with midbodies or mitotic spindles were not observed, perhaps because by the time CC3 is high and apoptotic chromatin changes are detectable, the microtubules of spindles and midbodies were already degraded. Therefore, we added Bromodeoxyuridine (BrdU) to the NSC cultures to test whether apoptosis was associated with proliferation. Indeed, when BrdU, which incorporates into DNA during replication, was present in NSC cultures during the 24-hour culture period, we found that apoptosis was specifically increased in BrdU+ but not BrdU– cells of *Kif20b* mutant cultures, suggesting that apoptosis occurred in cells that went through S phase (and presumably mitosis and cytokinesis) in the dish (Fig. 12G and H). To further refine the time interval between S phase and apoptosis, we added BrdU after 12 h *in vitro* before fixing at 24 h. Again, we found that the percentage of BrdU+ cells that were apoptotic was significantly higher in *Kif20b* mutant cultures than in control cultures (Fig. 12H). By contrast, when BrdU was added only 2 h before fixation, to label cells currently in S phase, no apoptotic cells were BrdU+ (0/36 control and 0/98 mutant). Given that S phase, G2, M phase and cytokinesis combined take about 7 h to complete in NSCs at E12 (Pancarci et al., 2010), these data are consistent with apoptosis occurring following cell division. Together, these data show that loss of *Kif20b* causes cell-intrinsic, p53-dependent apoptosis, primarily in proliferative NSCs.

#### *p53 deletion does not rescue impaired abscission in Kif20b mutant mice*

The preceding data show that in *Kif20b* mutant brains, the NSC apoptosis and microcephaly are downstream of p53 activation. However, another important question is whether the midbody defects seen in *Kif20b* mutant NSCs, indicating an abnormal abscission process, are upstream or downstream of p53 activation. The correlation of increased p53 N:C ratios with midbody width

in *Kif20b* mutant NSCs suggest that defects or delays in midbody maturation could cause p53 accumulation. Alternatively, these midbody defects could be a consequence of p53 activation, since p53 can regulate many genes and processes. To distinguish these possibilities, we tested whether abnormal midbody phenotypes observed in *Kif20b* mutant NSCs are rescued by *p53* deletion. First, we analyzed NSC midbody index in the dissociated cultures. As *Kif20b<sup>m/m</sup>* NSCs *in vitro* are less frequently observed at the midbody stage (Fig. 9B), and we hypothesized this is due to NSC arrest or apoptosis, we predicted the midbody index phenotype would be rescued by *p53* deletion. In fact, the midbody index of *Kif20b<sup>m/m</sup>; p53<sup>-/-</sup>* NSCs is not decreased, but instead is significantly increased above controls (Fig. 13A and B). This is consistent with the notion that some *Kif20b<sup>m/m</sup>* midbody-stage NSCs die, and further suggests that if these cells are prevented from dying, they take longer to complete abscission than control cells. Next, we analyzed NSC midbody structure in dissociated cultures. Similar to *Kif20b<sup>m/m</sup>* midbodies, *Kif20b<sup>m/m</sup>; p53<sup>-/-</sup>* midbodies are significantly wider than controls *in vitro* (data not shown), and fewer of them have constriction sites (Fig. 13C, compare with Fig. 8E). Thus, unlike apoptosis, the midbody width and constriction site phenotypes are not p53-dependent.

We next analyzed *Kif20b<sup>m/m</sup>; p53<sup>-/-</sup>* double mutant midbodies *in vivo* in E13.5 cortices. Cytokinesis is more complex in the cortical neuroepithelium than *in vitro*. NSC nuclei must migrate to the apical membrane to undergo mitosis and cytokinesis. During cytokinesis, the cleavage furrow ingresses asymmetrically from the basal side of the cell, forming the midbody at the apical membrane (Kosodo et al., 2008). To visualize NSC midbodies *en face*, we immunostained cortical slab whole-mounts for AurKB and the apical junction marker zona occludens-1 (ZO-1), and imaged the apical/ventricular surfaces (Fig. 13D). Similar to *in vitro* NSCs, some midbodies are short and wide, and others are long and thin, since midbodies narrow as they mature (see examples at Fig. 13E). In *Kif20b<sup>m/m</sup>* cortices, midbodies have a shifted width distribution with an increased median width compared to controls [Fig. 13F, white bars; (Janisch & Dwyer, 2016)]. Interestingly, we find that the *Kif20b<sup>m/m</sup>; p53<sup>-/-</sup>* double mutant cortices have a strikingly similar midbody width distribution as *Kif20b* single mutants, with the same median (Fig. 13F, gray bars). Thus, this midbody maturation phenotype (width) *in vivo* is not rescued by *p53* deletion. But surprisingly, we find that midbody lengths, which are similar in controls and *Kif20b<sup>m/m</sup>* single mutants, are significantly longer in *Kif20b<sup>m/m</sup>; p53<sup>-/-</sup>* double mutants than in either *Kif20b<sup>m/m</sup>* single mutants or controls (Fig. 13G). Exceptionally long

midbodies were observed after delayed abscission in cell lines that are resistant to apoptosis (Gromley et al., 2003; Weiderhold et al., 2016). Thus, *Kif20b* mutant NSCs may have delayed abscission, which can manifest as longer midbodies only if apoptosis is prevented. An additional midbody phenotype we observe *in vivo* in *Kif20b* mutant cortices is that ~30% of NSC midbodies are not aligned parallel to the apical membrane, compared to ~15% in control brains [(Janisch et al., 2013); Fig. 13H]. The cause of this phenotype is unclear, but we used the *Kif20b; p53* double mutants to test whether it is p53-dependent, perhaps because of the apoptotic process in dividing or neighboring cells. Interestingly, *p53* deletion did not prevent the misalignment phenotype, showing that it is not because of p53 activation or apoptosis (Fig. 13H). Taken together, these midbody analyses support the hypothesis that defective midbody maturation and alignment are primary consequences of *Kif20b* loss rather than secondary consequences of p53 activation. Further, the additional midbody phenotypes detected in *Kif20b; p53* double mutant NSCs, namely increased midbody index and midbody length, suggest that some symptoms of midbody maturation defects from *Kif20b* loss are normally precluded in single mutants by p53 activation and apoptosis.

## Discussion

Here we have tested the contribution of the intrinsic apoptosis pathway to the reduced cortex size in a lethal microcephaly model, the *Kif20b* mouse mutant. We have shown that apoptosis of cortical NSCs accounts for most of the microcephaly, but that there is a significant apoptosis-independent contribution as well. Furthermore, we showed that the excess apoptosis is cell autonomous, partially dependent on Bax and fully dependent on p53. Remarkably, heterozygous *p53* deletion is sufficient to fully suppress the lethality of the *Kif20b* mutant, and rescues the brain size equally as well as homozygous *p53* deletion. Importantly, we demonstrated that the NSC midbody maturation defects are not rescued by *p53* deletion, which indicates that they are not caused by p53 activation, but may be upstream of p53. Thus, this work potentially identifies a novel midbody-initiated pathway for p53 activation, and suggests that at least some types of microcephaly, although severe, could be greatly ameliorated by inhibiting apoptosis.

The genetic and cellular experiments herein support the following working model for the etiology of microcephaly in the *Kif20b* mutant (Fig. 13I). Loss of *Kif20b* causes midbody maturation defects in some *Kif20b* mutant NSCs, leading to nuclear p53 accumulation by an unknown molecular pathway that could be distinct from the DNA damage pathway (black dashed line).

Elevated levels of p53 then trigger the apoptotic cascade including Bax and other effectors. Apoptosis in proliferating NSCs depletes the NSC pool, thereby reducing the number of neuron and IP daughters produced, resulting in a small brain. It also remains plausible that *Kif20b* loss causes p53 activation and midbody defects through two separate pathways, and that p53 could be activated due to a different cellular defect (gray dashed line). We favor the former model for three reasons. First, we found the apoptosis is associated with markers of proliferation (Nestin, Ki67 and BrdU incorporation). Second, the increased nuclear accumulation of p53 in *Kif20b* mutant NSCs at midbody but not mitotic stage and in thinner (late stage) midbodies indicates an acute change in p53 levels or localization at this stage of division. Third, the new midbody defects that appear in *Kif20b*; *p53* double mutants, namely increased midbody index and longer midbodies, suggest that *Kif20b* loss would cause abscission delay if it were not precluded by p53-dependent apoptosis. In either case, the *Kif20b* mutant is a tool to elucidate a potentially novel pathway to p53 activation, one that appears very sensitive in cortical NCSs.

There is likely some stochasticity to the apoptotic process, as not all *Kif20b<sup>m/m</sup>* NSCs have midbody defects, and only a small percentage undergo apoptosis (Janisch et al., 2013); this work). It may be that apoptosis is only triggered if midbody maturation (and hence abscission) is delayed beyond a certain threshold. This would be analogous to a previous study in developing cortex showing that apoptosis likelihood increases if prophase is delayed past a threshold (Pilaz et al., 2016). Though both of these types of cell division delay trigger apoptosis through p53, the molecular 'error sensor' upstream of p53 is likely distinct, since midbody maturation takes place well after telophase, in the next G1 phase (Gershony et al., 2014). In fact, how defects in early steps of mitosis signal to trigger p53 activation is only beginning to be elucidated, primarily in immortalized cell lines that are apoptosis-resistant (Lambrus et al., 2016; McKinley & Cheeseman, 2017; Meitinger et al., 2016). The idea that abscission delay or 'stress' could activate p53 has not been previously addressed. More work is needed to determine whether and how a midbody error sensor could directly or indirectly cause p53 accumulation in NSCs or other cell types.

### *p53 activates apoptosis in NSCs following diverse cellular defects*

Our work furthers the evidence that p53 responds to multiple intrinsic cellular defects to acutely regulate NSC survival. For eventual treatment of human microcephalies caused by genetic mutations or viruses, it is important to determine which types of microcephaly or which

phenotypes might be treatable by inhibiting apoptosis. Zika virus infection activates p53-dependent apoptosis in human NSCs (Ghouzzi et al., 2016). Some other microcephalic mouse mutants, with impaired DNA replication, mitosis or cleavage furrowing have implicated p53 in apoptosis and reduced brain size (Bianchi et al., 2017; Houlihan & Feng, 2014; Insolera et al., 2014; Marjanović et al., 2015; Marthiens et al., 2013; Murga et al., 2009). Interestingly, inhibition of p53 in these mutants was sometimes able to increase cortical thickness, but in other cases worsened brain phenotypes (Mao et al., 2016; Marthiens et al., 2013; Murga et al., 2009). By contrast, *Kif20b<sup>m/m</sup>* embryonic brain structure and postnatal survival were well-rescued by even heterozygous deletion of *p53*. Heterozygous *p53* deletion has not been reported to rescue other microcephaly mouse mutants. In the *Brca1* mutant, dwarfism but not microcephaly was rescued by heterozygous *p53* deletion (Xu et al., 2001). Thus, the *Kif20b* microcephaly model is more severe in reduction of brain size compared to some other models, but it is also more easily rescuable by p53 inhibition. As a key cell cycle regulator, it is also possible that p53 activation in the *Kif20b* mutant reduces brain size by other mechanisms in addition to apoptosis, such as by causing NSC cell cycle exit. Future work will continue to investigate such possibilities.

*A p53-independent consequence of Kif20b loss accounts for the remaining cortical size deficit at birth*

The deficit in cortical thickness in *Kif20b; p53* double mutant mice at birth indicates that even without the excess apoptosis, *Kif20b* mutant NSCs and neurons cannot create a brain of normal size and structure. This could be due to abnormal abscission causing some other problem in *Kif20b* mutant NSCs, or due to postmitotic roles of Kif20b, or both. The midbody maturation defects that are more frequent in *Kif20b* mutant brains could affect whether abscission is completed on both sides of the midbody or only on one side, resulting in either midbody release into the ventricle, or midbody inheritance by one daughter cell. They could also impair daughter cell severing from the mother cell and delamination from the apical membrane in the case of neuronal daughters. The significance of the midbody misalignment increase is not clear, but here we showed that it is not caused by p53 activation or apoptosis. It is possible that Kif20b may help anchor or stabilize midbodies at the apical membrane via cell adhesion junctions until abscission is complete. Much more work is needed to understand how cytokinetic abscission mechanisms are coordinated with cell fate decisions and maintenance of neuroepithelial structure.

The reduced thickness of neuronal layers at P0 indicates a role for Kif20b in the production of neurons at all developmental timepoints. However, the most dramatic reduction was seen in layer VI neurons, which were fewer in number but also more densely packed. This may indicate that Kif20b plays a more important role in earlier stages of neurogenesis, and/or in postmitotic neurons for neurite outgrowth. We previously showed that *Kif20b* mutant embryonic cortical neurons in culture display a polarization defect and abnormalities in neurite growth and branching. Thus, the increased density of layer VI cells at birth may be due to reduced neuropil. A key function of Kif20b is to enable tight microtubule packing: Kif20b has microtubule crosslinking activity *in vitro*, and in *Kif20b* mutant neurons, wider neurites and gaps in microtubule bundles were noted (Abaza et al., 2003; McNeely et al., 2017). Therefore, Kif20b may help to organize microtubules in both NSC midbodies and neuronal axons.

### *Elucidating the heterogeneous mechanisms of brain malformations requires many genetic models and culture systems*

Defects in cytokinetic abscission mechanisms could underlie a range of poorly understood microcephalies and related brain malformations. For example, human genetic studies in two different families showed that a very severe prenatal lethal microcephaly/anencephaly is caused by mutations in the gene encoding the key abscission protein Cep55 [(Bondeson et al., 2017; Frosk et al., 2017); OMIM Ref #236500]. Cep55 depletion in cell lines causes more severe midbody structural defects and abscission delay than Kif20b depletion does (Zhao, 2006). Patients with *Kif20b* loss-of-function mutations have not yet been identified, so it remains to be seen whether the severity of single-cell abscission phenotypes correlates with the severity of brain malformation. Cell lines such as HeLa cells can model some abscission defects, for example midbody maturation, but not others, such as midbody positioning at the apical membrane, p53 activation or apoptosis. Our studies of the *Kif20b* mouse model provide human geneticists with a candidate gene and cellular markers for syndromes involving peri- or prenatal lethality, microcephaly, craniofacial defects or microphthalmia. Comparing mouse models for abscission genes with other microcephalic mice as well as human phenotypes will help us understand the heterogeneous etiologies of and potential diagnosis and treatments for these devastating conditions.

## **Methods**

### *Mice*

Mouse colonies were maintained in accordance with NIH guidelines and policies approved by the IACUC. Embryos were harvested by cesarean section, and the morning of the vaginal plug was considered E0.5. Littermate embryos served as controls for all experiments. The Kif20b magoo allele, as previously described (K. M. Janisch et al., 2013) is maintained on both C57BL/6 and FVB/N backgrounds, and 50/50% mixed background embryos are used for experiments. Trp53tm1Tyj mice on C57BL/6 background were obtained from The Jackson Laboratory [(Jacks et al., 1994); JAX stock #002101]. Mixed BL6/FVB/N background Baxtm1Sjk mice were a gift from Christopher Deppmann [(Knudson et al., 1995); JAX stock #002994]. Sex of embryonic mice were not noted as sex was not a relevant biological variable for these experiments. The specific ages of embryonic mice used is noted in figure legends for each experiment.

#### *Cortical cell cultures*

Cells were dissociated from E12.5 cortices following a protocol adapted from Sally Temple's laboratory (Qian et al., 1998). The Worthington Papain Dissociation Kit was used to dissociate cells (Worthington Biochemical Corporation, Lakewood, NJ, Cat # LK003150). Cells were cultured in DMEM with Na-Pyruvate, L-Glutamine, B-27, N2, N-acetyl-cysteine and basic fibroblast growth factor. After 24 h, cells were fixed by adding an equal volume of room temperature 8% PFA (paraformaldehyde) for 5 min to cell media, followed by removal of media and addition of  $-20^{\circ}$  cold methanol for 5 min. For BrdU experiments, BrdU was added to culture media at a final concentration of 10  $\mu$ m.

#### *Apical slab preparation*

Apical slabs were prepared as previously described (Janisch & Dwyer, 2016). The meninges and skull were removed to expose the brain in E13.5 embryos, followed by fixation with 2% PFA for 20 min. Next, apical slabs were made by pinching off cortices, flipping so that the apical surface was upright, and trimming to flatten the slab. Slabs were fixed for another 2 min with 2% PFA followed by blocking with 5% normal goat serum (NGS) for 1 h. Primary antibodies were applied for 1 h at room temperature and then moved to  $4^{\circ}$  overnight. The next day, after 3 times, 10-minute PBS (phosphate-buffered saline) washes, secondary antibodies and DAPI were applied at

a concentration of 1:200 for 30 minutes. After two more 10-minute PBS washes, slabs were coverslipped with VectaShield fluorescent mounting medium (Vector Laboratories Inc., H-1000) and imaged. z-stack depth was 8–20  $\mu\text{m}$  and step size was 0.5  $\mu\text{m}$ . Midbodies were considered misaligned if the two halves of the midbody were not in the same z-plane or within two adjacent z-planes.

### *Immunoblotting*

Brain lysates were prepared with RIPA lysis buffer (150 mM NaCl, 1% NP40, 0.5% sodium deoxycholate, 0.1% SDS, 50 mM Tris-HCl pH 8) with protease and phosphatase inhibitors. Protein concentration in lysates was determined by bicinchoninic acid (BCA) assay, and 60  $\mu\text{g}$  total protein was loaded per lane on 4–20 gradient% polyacrylamide gels. Proteins were transferred by electroblotting onto a 0.2  $\mu\text{m}$  PVDF membrane overnight at 30 mA. Membranes were blocked in 150 mM NaCl, 100 mM Tris-HCl pH 7.5 and 0.5% Tween 20 (TBST) with 5% dried milk (blocking buffer) for 1 hour. Primary antibodies were incubated with the membrane overnight at 4 °C. After three washes, LI-COR IRDye 800 CW goat anti-rabbit IgG and 680 RD goat anti-mouse secondary antibodies were applied (1:10000) in blocking buffer for 1 hour at room temperature. After washing with TBST for 5 minutes, 3 times, immune complexes were visualized using a LI-COR western blot imager.

### *Immunostaining*

To collect cryosections for IHC, age E14.5 and P0 brains were removed from heads and fixed for 6 and 24 hours, respectively, in 4% PFA, followed by immersion in 30% sucrose in PBS overnight. Next, whole brains were embedded in OTC (Tissue-Tek, 4583) and cryosections were cut at 20  $\mu\text{m}$  thickness and collected on Superfrost Plus slides (Fisher Scientific, 12–550-15). Frozen sections were stored at –80 degrees. Prior to immunostaining, cryosections were warmed to room temperature, then if antigen retrieval was needed, immersed in 10 mM citrate buffer at 95 degrees for 20 minutes. After cooling, sections were blocked in 2% NGS for 1 hour, followed by incubation with primary antibodies overnight at 4 °C. The next day, after PBS washes sections were incubated with AlexaFluor secondary antibodies at 1:200 and DAPI at 1:100 for 30 min followed by PBS washes and coverslipping with VectaShield fluorescent mounting medium. For IF on coverslips of dissociated cortical progenitors, a similar protocol was used but with primary

antibodies applied for 3 h at room temperature. Antigen retrieval was not used in dissociated progenitors except in the case of BrdU; coverslips were immersed in 0.07M NaOH pH 13 for 2 min before permeabilization. Coverslips were mounted on Superfrost Plus slides with Fluoro-Gel (Electron Microscopy Sciences, Hatfield, PA, 17985–10).

### *Antibodies*

Antibodies used in this analysis were rabbit polyclonal anti-human CC3 (Cell-Signaling 9661S, 1:250), mouse monoclonal anti-rat beta-III-tubulin (Tuj1) (BioLegend, San Diego, CA, 801201, 1:500), rat monoclonal anti-mouse Tbr2 (eBioscience (Thermo Fisher Scientific), Waltham, MA 14–4875, 1:200), rabbit polyclonal anti-mouse Pax6 (BioLegend PRB-278P, 1:200), mouse monoclonal anti-rat Aurora B kinase (BD Biosciences 611082, 1:300), rabbit polyclonal anti-human alpha-tubulin (Thermo Scientific RB-9281-P0, 1:300), rat monoclonal alpha-tubulin (Novus Biologicals NB600–506, 1:300), rabbit monoclonal anti-human PH3 (Cell Signaling 3458, 1:200), chicken polyclonal anti-mouse Nestin (Aves Labs NES, 1:600), rat monoclonal anti-human Ki67 (eBioscience 14–5698, 1:100), mouse monoclonal anti-human p53 (MilliporeSigma, Burlington, MA, 05–224, 1:250), rabbit polyclonal anti-mouse p53 (Leica Biosystems, Wetzlar, Germany, NCL-L-p53-CM5p, 1:500), mouse monoclonal anti-human phospho-Histone H2A.X (Ser139) (Millipore 05–636 1:500), rabbit polyclonal anti-mouse Cux1 (Santa Cruz Biotechnology, Inc., Dallas, TX, (M-122) sc-13024, 1:100), rat monoclonal anti-human Ctip2 (Abcam 18465, 1:400), rabbit polyclonal anti-mouse Tbr1 (Abcam, Cambridge, MA 31940, 1:200), mouse monoclonal anti-BrdU (BD Biosciences, San Jose, CA Clone B44, 20 µl/50 µl block), rabbit polyclonal anti-human Beta-Catenin (MilliporeSigma, Burlington, MA, SAB4500545 1:1000), and polyclonal rabbit anti Zo-1 (rabbit, Invitrogen (Thermo Fisher Scientific) 61–7300, 1:50). All antibodies were validated for the application used in multiple previous publications.

### *Imaging and statistical analysis*

Images in Figures 1F–I, 2F–I and 3A–F were taken on an Olympus Confocal Fluoview FV1000. Images in Figures 5A–E, 6, 7A and [S2–6](#) were collected on either a Zeiss Axio ImagerZ1 microscope with AxioCam MRm or a Zeiss AxioObserver fluorescent widefield inverted scope microscope. Images in Figures 5F–J and 7D–J were taken on an inverted DeltaVision with

TrueLight deconvolution microscope with softWoRx Suite 5.5 image acquisition software (Applied Precision (GE Healthcare), Issaquah, WA). A Leica MZ16F microscope with DFC300FX camera was used for images in Figures 1A–E, 2A–E and 4. Control and mutant fluorescence images were collected with the same exposure times and on the same day. All image analysis was performed in ImageJ/Fuji and any changes to brightness and contrast were applied uniformly across images. Statistical analyses were performed using Excel (Microsoft) or GraphPad PRISM software. The sample sizes were pre-determined based on our lab's previous experience with cortical development analyses and others' published results. After obtaining pilot data, power analyses were performed if necessary to determine if the number of samples obtained was high enough for the effect size seen. NSC cultures that were unhealthy were not imaged and analyzed, but no other data was excluded from the analysis. No randomization or blinding was used as no experimental manipulation was applied other than genetic knockouts. Genotyping was performed after collection of embryos to determine genetic status. Statistical tests used are specified in each figure legend. For each sample set a statistical test of normality was performed using GraphPad PRISM software. Parametric tests were used when sample sets had a normal distribution and non-parametric tests were used when sample sets did not have a normal distribution. Variance was calculated and was typically similar between groups. N's listed in figure legends indicate the number of coverslips, brains and litters collected for each experiment. For each brain, at least three sections were imaged, and for each coverslip, at least 5, 20× pictures or 10, 40× pictures were analyzed.

## Figures

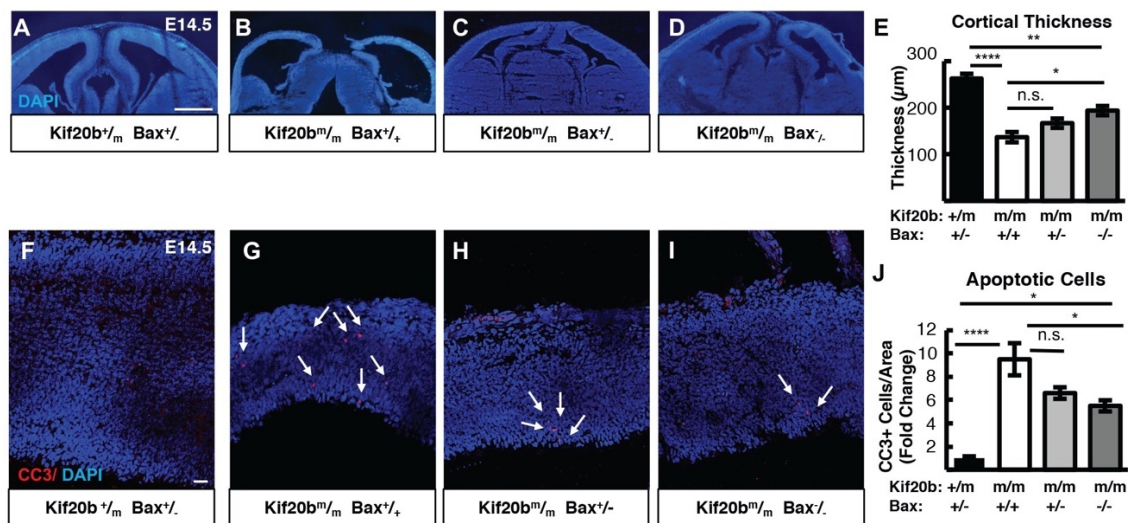


**Figure 1.** *Bax* deletion partially rescues microcephaly and apoptosis in *Kif20b* mutant mice.

**A-E.** Representative E14.5 cortical sections and plotted mean of cortical thicknesses show the severe reduction in *Kif20b* mutants is partly restored in *Kif20b*; *Bax* double mutants.

**F-J.** CC3 staining in E14.5 cortices show the increased apoptosis in *Kif20b* mutants is partially reduced in *Kif20b*; *Bax* double mutants. Arrows denote apoptotic cells.

For (E, J),  $n = 5$  *Kif20b*<sup>+/-</sup>; *Bax*<sup>+/-</sup>, 4 *Kif20b*<sup>m/m</sup>; *Bax*<sup>+/+</sup>, 4 *Kif20b*<sup>m/m</sup>; *Bax*<sup>+/-</sup>, 5 *Kif20b*<sup>m/m</sup>; *Bax*<sup>-/-</sup> mice, from a total of 8 litters. \* $P < 0.05$ , \*\* $P < 0.01$ , \*\*\* $P < 0.001$ , \*\*\*\* $P < 0.0001$ , n.s. not significant, one-way ANOVA. Error bars are  $\pm$  s.e.m. Scale bars: A: 500  $\mu$ m; E: 20  $\mu$ m.

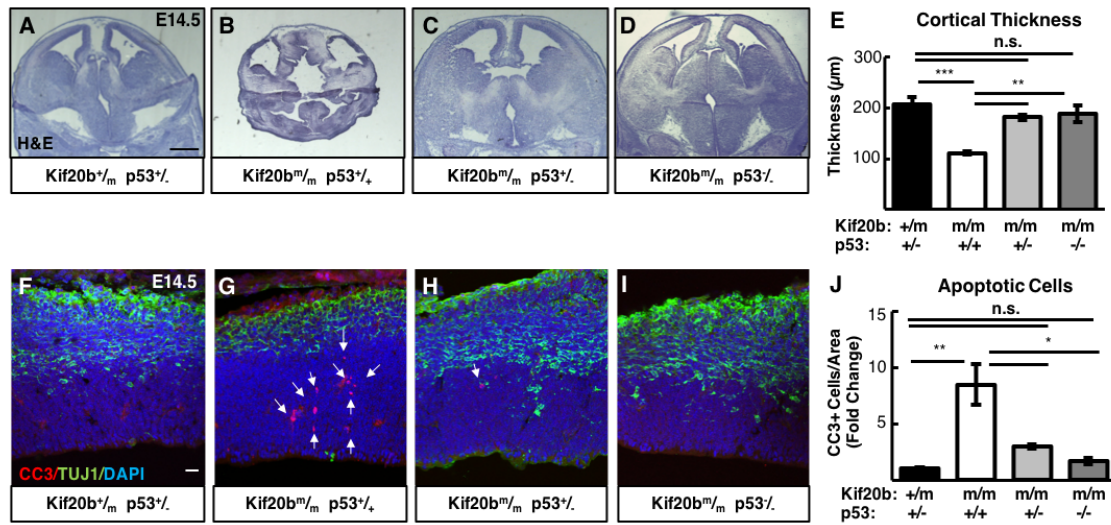


**Figure 2.** *p53* deletion rescues microcephaly and apoptosis in *Kif20b* mutant mice.

A-E. E14.5 cortical sections and plotted mean cortical thicknesses show the severe reduction in *Kif20b* mutants is fully rescued by heterozygous or homozygous *p53* deletion.  $n = 6$  *Kif20b*<sup>+/*m*</sup>; *p53*<sup>+/*-*</sup>, 3 *Kif20b*<sup>m/*m*</sup>; *p53*<sup>+/*+*</sup>, 4 *Kif20b*<sup>m/*m*</sup>; *p53*<sup>+/*-*</sup>, 4 *Kif20b*<sup>m/*m*</sup>; *p53*<sup>-/*-*</sup> mice, from a total of 7 litters. F-J. CC3 staining shows apoptosis in *Kif20b* mutants returns to control levels by heterozygous or homozygous *p53* deletion. Arrows denote apoptotic cells.  $n = 3$  *Kif20b*<sup>+/*m*</sup>; *p53*<sup>+/*-*</sup>, *Kif20b*<sup>m/*m*</sup>; *p53*<sup>+/*+*</sup>, *Kif20b*<sup>m/*m*</sup>; *p53*<sup>+/*-*</sup>, *Kif20b*<sup>m/*m*</sup>; *p53*<sup>-/*-*</sup> mice, from a total of 6 litters. \* $P < 0.05$ , \*\* $P < 0.01$ , \*\*\* $P < 0.001$ , n.s., not significant, one-way ANOVA. Error bars are +/- s.e.m. Scale bars: A: 500 µm; F: 20 µm.

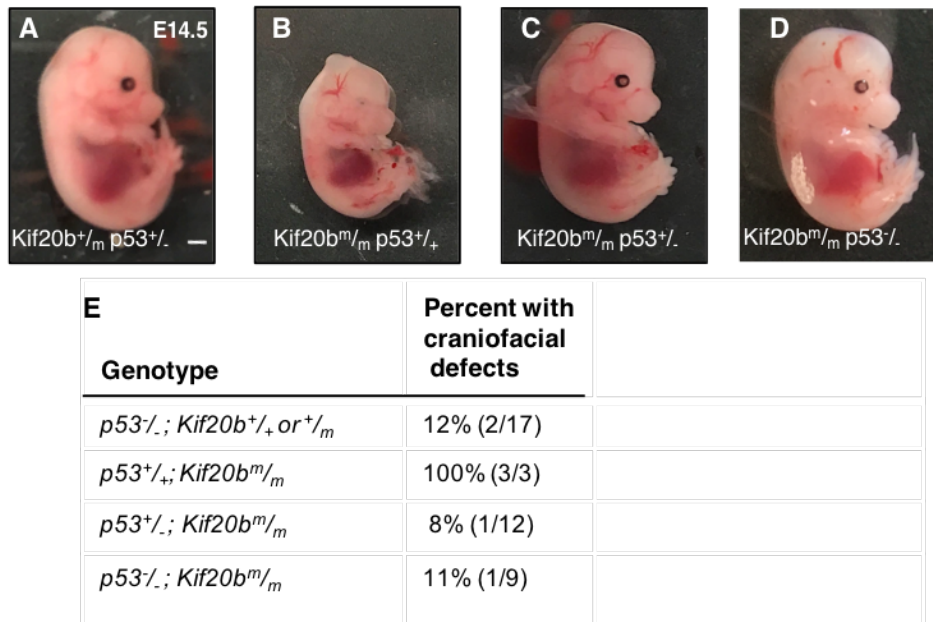


**Figure 3.** *p53* deletion rescues craniofacial defects in *Kif20b* mutant mice.

**A-D.** Representative E14.5 embryos of the indicated genotypes.

**E.** Quantification of rescue of E14.5 craniofacial defects including shortened snout, underdeveloped eyes, and/or brain malformations of the indicated genotypes.

Scale bar (A): 1 mm.

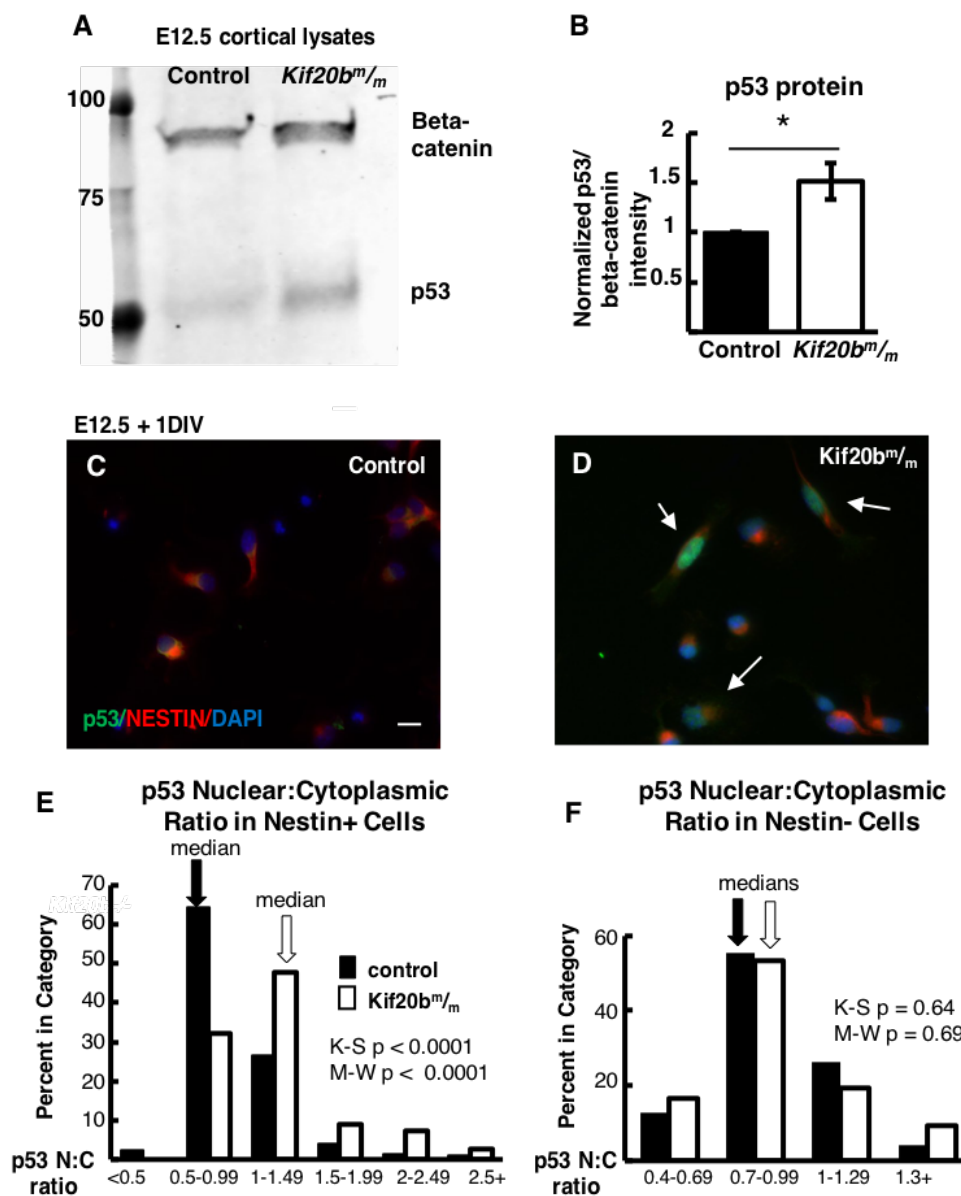


**Figure 4.** p53 expression is elevated in *Kif20b* mutant NSCs.

**A.** Immunoblot from E12.5 control and *Kif20b<sup>m/m</sup>* cortical lysates shows bands for p53 (53 kDa) and beta-catenin (95 kDa) as a loading control.

**B.** p53 band intensity, normalized to beta-catenin bands, is increased by 50% in *Kif20b<sup>m/m</sup>* samples. n= 4 blots from 4 embryos each.

**C, D.** Representative images of control (C) and *Kif20b<sup>m/m</sup>* (D) E12.5 dissociated cortical cultures fixed after 24 hrs *in vitro*, and immunostained for p53 (green) and Nestin (red) to mark NSCs. Scale bar: 10  $\mu$ m. Arrows in D denote *Kif20b<sup>m/m</sup>* NSCs with high p53 N:C ratios.

**E.** The distribution and median p53 nuclear: cytoplasmic ratios is significantly altered in *Kif20b* mutant NSCs (Nestin+) compared to control, with a higher median N:C ratio.

**F.** The distribution and median of p53 N:C ratios is not altered in *Kif20b* mutant Nestin- cells compared to control. n for E, F= 3 coverslips for each genotype, from 2 E12.5 brains each.

Control denotes a combination of *Kif20b<sup>+/+</sup>* and *Kif20b<sup>+/-</sup>* embryos.

\* p  $\leq$  0.05, paired ratio t-test (B), Kolmogorov-Smirnov and Mann-Whitney tests (E, F).

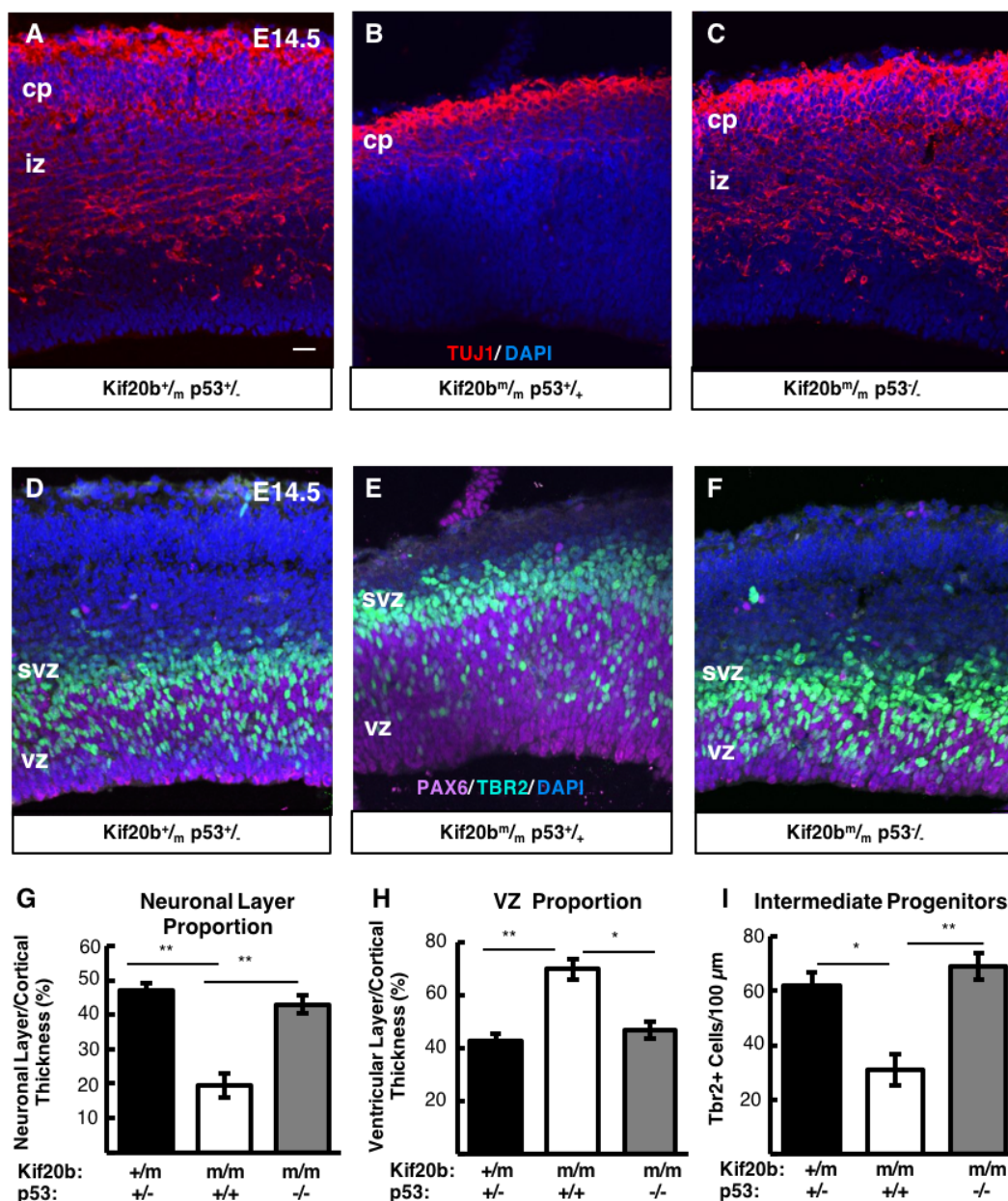


**Figure 5.** *p53* deletion restores normal production of IPs and neurons in *Kif20b* mutant cortex. A-C. E14.5 cortical sections labeled with neuronal-specific tubulin (Tuj1, red) show the decreased neuronal layer thickness in *Kif20b* mutants is rescued in *Kif20b*; *p53* double mutants. cp, cortical plate; iz, intermediate zone. D-F. E14.5 cortices labeled with Pax6 (NSCs, magenta) and Tbr2 (IPs, green) show the altered layer proportions in *Kif20b* mutant are rescued by *p53* deletion. Svz, subventricular zone; vz, ventricular zone. G. The mean neuronal layer proportional thickness is halved in *Kif20b* mutants but rescued by *p53* co-deletion. H. The proper NSC layer (Pax6<sup>+</sup>) proportionality is restored by *p53* co-deletion. I. The density of Tbr2<sup>+</sup> IPs is reduced in *Kif20b* mutants, but rescued in *Kif20b*; *p53* double mutants. *n* = 3 each *Kif20b*<sup>+/*m*</sup>; *p53*<sup>+/*-*</sup>, *Kif20b*<sup>*m/m*</sup>; *p53*<sup>+/*+*</sup>, *Kif20b*<sup>*m/m*</sup>; *p53*<sup>-/*-*</sup> mice for Tuj1 and Pax6 layer thickness. *n* = 6 *Kif20b*<sup>+/*m*</sup>; *p53*<sup>+/*-*</sup>, 3 *Kif20b*<sup>*m/m*</sup>; *p53*<sup>+/*+*</sup>, 4 *Kif20b*<sup>*m/m*</sup>; *p53*<sup>-/*-*</sup> mice for Tbr2<sup>+</sup> cell counts, from a total of 6 litters. \**P* < 0.05, \*\**P* < 0.01, one-way ANOVA. Error bars are  $\pm$  s.e.m. Scale bars: 20  $\mu$ m.

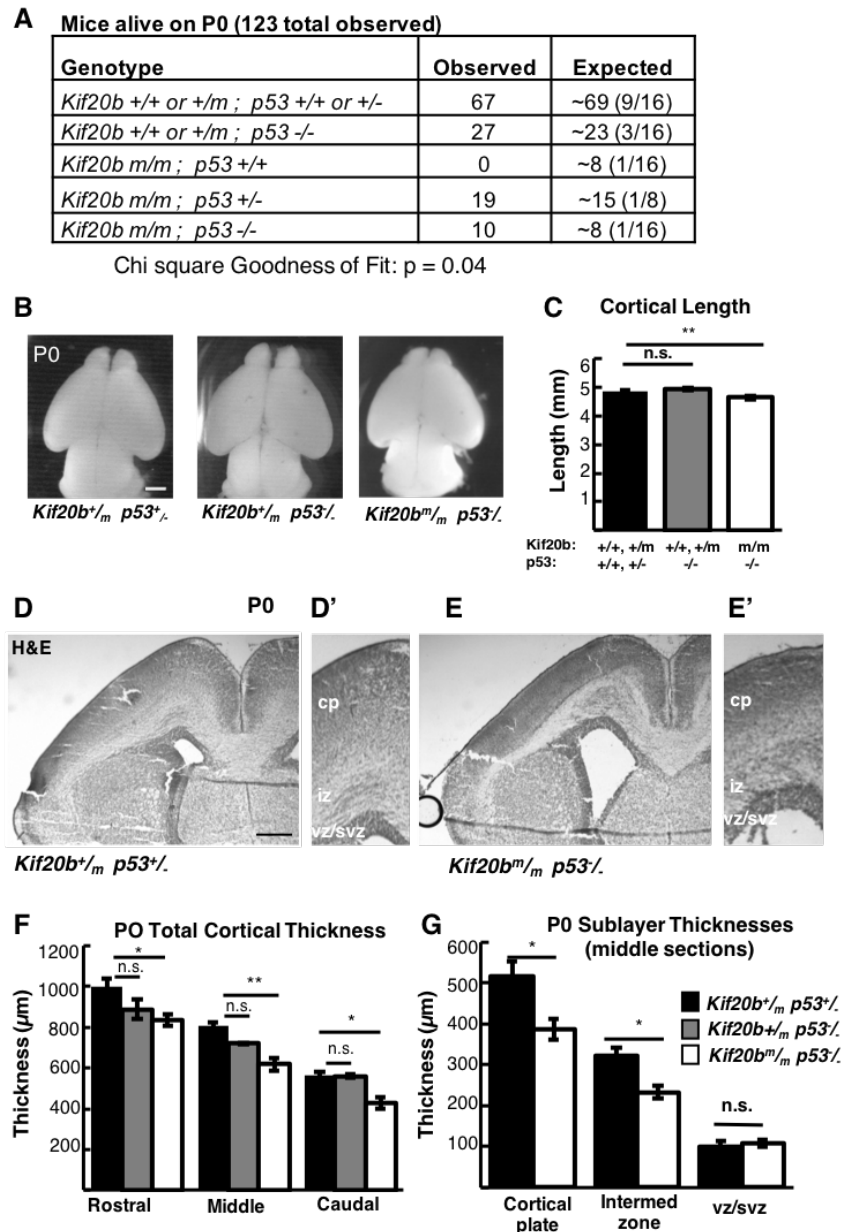


**Figure 6.** *p53* deletion rescues postnatal survival but incompletely rescues cortical size at birth in *Kif20b* mutant mice.

**A.** *Kif20b*<sup>m/m</sup>; *p53*<sup>+/+</sup> mice do not survive at birth at expected Mendelian ratios, but *Kif20b*<sup>m/m</sup>; *p53*<sup>+/-</sup> and *Kif20b*<sup>m/m</sup>; *p53*<sup>-/-</sup> mice survive at comparable levels to controls. **B, C.** The average cortical length of *Kif20b*<sup>m/m</sup>; *p53*<sup>-/-</sup> mice is slightly decreased compared to controls at P0.  $n = 54$  *Kif20b*<sup>+/+</sup> or *+/-* *p53*<sup>+/+</sup> or *+/-* mice, 22 *Kif20b*<sup>+/+</sup> or *+/-* *p53*<sup>-/-</sup> and 5 *Kif20b*<sup>m/m</sup>; *p53*<sup>-/-</sup> mice. **D, E.** Coronal sections from P0 rostral forebrains stained with hematoxylin and eosin show reduced cortical thickness and enlarged ventricles of double mutants. **F.** Cortical thickness in *Kif20b*<sup>m/m</sup>; *p53*<sup>-/-</sup> mice is reduced 15–20% compared with *Kif20b*<sup>+/m</sup>; *p53*<sup>+/-</sup> controls in rostral, middle and caudal sections at P0. **G.** cp and iz show reduced thickness, but not vz/svz layers. For F and G,  $n = 6$  *Kif20b*<sup>+/m</sup>; *p53*<sup>+/-</sup>, 3 *Kif20b*<sup>+/m</sup>; *p53*<sup>-/-</sup> and 6 *Kif20b*<sup>m/m</sup>; *p53*<sup>-/-</sup> brains. \* $P < 0.05$ , \*\* $P < 0.01$ , n.s. not significant, one-way ANOVA (C, F) and Student's *t*-test (G). Error bars are  $\pm$  s.e.m. Scale bars: B: 1 mm; D: 200  $\mu\text{m}$ ; D': 100  $\mu\text{m}$ .

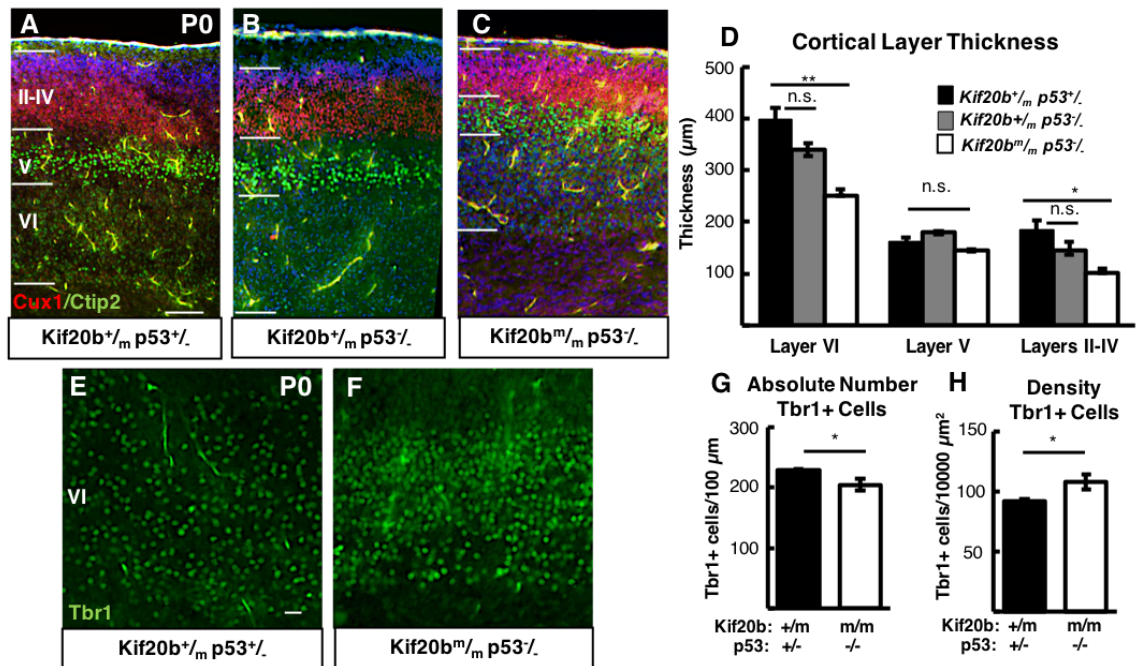


**Figure 7.** All neuronal layers are reduced in thickness in double mutant cortices at P0.

**A-C.** Representative images of P0 coronal cortical sections labeled with Cux1 for layers II-IV and Ctip2 for layer V (bright) and layer VI (faint) show that both upper and deep neuronal layers of *Kif20b*; *p53* double mutants are thinner. Note that autofluorescence in blood vessels appears as yellow linear segments. Scale bar (A): 100 µm.

**D.** Layer VI and layers II-IV are significantly reduced in *Kif20b*<sup>*m*/m</sup>; *p53*<sup>-/-</sup> cortex compared to *Kif20b*<sup>+/m</sup>; *p53*<sup>+/-</sup> control. n = 3-4 sections from 4 brains for each genotype

**E, F.** Representative images of P0 coronal cortical sections labeled with Tbr1 for layer VI show reduced layer thickness and increased density of Tbr1+ cells in *Kif20b*<sup>*m*/m</sup>; *p53*<sup>-/-</sup> cortex compared to *Kif20b*<sup>+/m</sup>; *p53*<sup>+/-</sup> control.

**G.** The number of Tbr1+ cells per 100 µm length of ventricle is reduced in *Kif20b*<sup>*m*/m</sup>; *p53*<sup>-/-</sup> cortex compared to *Kif20b*<sup>+/m</sup>; *p53*<sup>+/-</sup> control.

**H.** The density of Tbr1+ cells per area is increased in *Kif20b*<sup>*m*/m</sup>; *p53*<sup>-/-</sup> cortex compared to *Kif20b*<sup>+/m</sup>; *p53*<sup>+/-</sup> control. n for G, H= 3-4 sections from 3 brains for each genotype.

\*p < 0.05, \*\* p < 0.01, n.s., not significant; one-way ANOVA (D), Student's t-test (G, H).

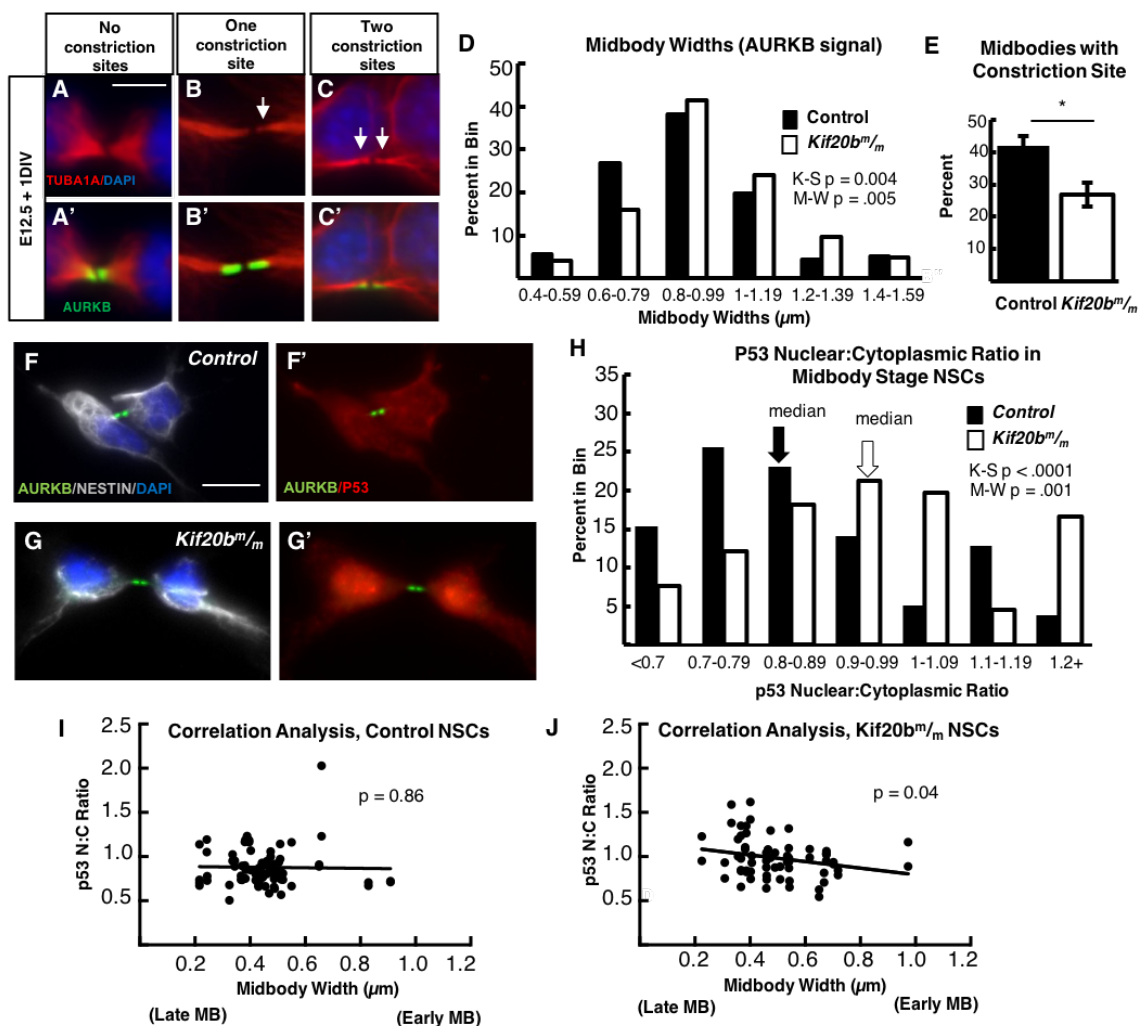


**Figure 8.** *Kif20b* loss cell-autonomously causes abscission defects in cortical NSCs.

A-C. Dissociated E12.5 NSC midbodies MBs at 24 h in culture labeled with alpha-tubulin (red) and AurKB (green). Early-stage MBs are wider with no constriction sites (A); late-stage MBs are thinner and have one (B) or two (C) constriction sites (arrows). **D.** *Kif20b<sup>m/m</sup>* MBs (white bars) have a significantly shifted width distribution, with more wide MBs compared to controls (black bars). (Medians: Control, 0.89  $\mu\text{m}$ ; Mutant, 0.96  $\mu\text{m}$ ). **E.** The mean percentage of MBs with at least one constriction site (detected by tubulin) is significantly reduced in *Kif20b* mutant cultures. \* $P < 0.05$ , Student's *t*-test; *n* for D, E = 141 control, 125 mutant MBs; 6 coverslips and 3 embryos each, 3 litters. **F-G.** Representative images of p53 localization in control (F, F') and *Kif20b* mutant (G, G') NSCs show that p53 signal in the nucleus is increased in *Kif20b<sup>m/m</sup>* NSCs compared to control NSCs. Cells labeled with AurKB (green) to detect MBs, and 4'-6-diamidino-2-phenylindole (DAPI; blue) and Nestin (white) to differentiate NSC nucleus and cytoplasm, respectively. **H.** *Kif20b<sup>m/m</sup>* NSCs at the MB stage have a significantly shifted distribution of nuclear: cytoplasmic ratios of p53, with a higher median N:C ratio. (Medians: Control, 0.83; Mutant, 0.95). K-S, Kolmogorov–Smirnov and M-W, Mann–Whitney tests. **I-J.** Correlation analysis of p53 N:C ratio versus MB widths shows that MB width is significantly negatively correlated with increasing p53 N:C ratio in *Kif20b<sup>m/m</sup>* NSCs, but not controls. Mutant NSCs with thinner MBs (predicted to be late stage) are more likely to have higher p53 N:C ratios. *P*-values are for Pearson's correlation test. *n* for F–J = 78 control and 66 *Kif20b<sup>m/m</sup>* MB stage NSCs from 2 control and 2 mutant coverslips and embryos. Control denotes a combination of *Kif20b<sup>+/+</sup>* and *Kif20b<sup>+/m</sup>* embryos. Error bars are  $\pm$  s.e.m. All cultures from E12.5 cortices and fixed after 24 h. Scale bar in A: 5  $\mu\text{m}$ ; F: 10  $\mu\text{m}$ .

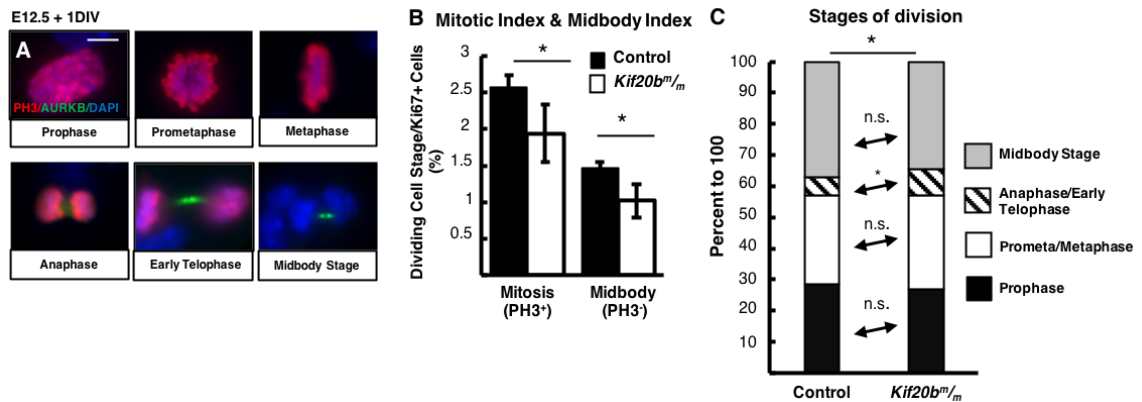


**Figure 9.** Analyses of mitotic and midbody indices in *Kif20b* mutant NSC cultures.

**A.** Examples of E12.5 dissociated cortical NSCs at stages of mitosis and cytokinesis, labeled with PH3 (red) and AurkB (green).

**B.** The mean percentages ( $\pm$  s.e.m.) of cycling NSCs (Ki67+) in mitosis or midbody stage are slightly reduced in *Kif20b*<sup>m/m</sup> cultures.

**C.** Categorizing the dividing NSCs from B, there is a small increase of *Kif20b*<sup>m/m</sup> NSCs in anaphase/early telophase.

Control denotes a combination of *Kif20b*<sup>+/+</sup> and *Kif20b*<sup>+/m</sup> embryos. For B and C,  $n = 3$  coverslips from 3 embryos each, with 1499 control and 1421 *Kif20b*<sup>m/m</sup> Ki67+ cells. \*  $p \leq 0.05$ , Student's *t*-test for (B), Chi Square and Fisher's exact test for (C). All cultures dissociated from E12.5 cortices and fixed after 24 hours. Scale bar, 5  $\mu$ m.

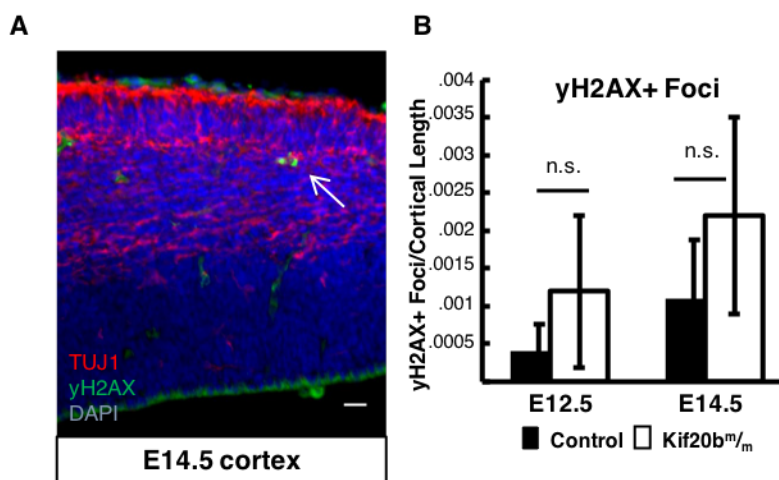


**Figure 10.** DNA damage marker  $\gamma$ -H2AX is not increased in *Kif20b* mutant cortex.

**A.** Example image of control E14.5 cortex labeled with gamma-Histone-H2AX (yH2AX, green), Tuj1 (red, neuronal marker) and DAPI. Arrow denotes a yH2AX+ cell in the neuronal layer. Scale bar: 20  $\mu$ m.

**B.** No difference in the number of yH2AX+ cells per ventricle length was noted in *Kif20b*<sup>m/m</sup> cortex at E12.5 or E14.5 compared to control. A positive control section with greatly increased DNA damage was used to verify the IHC method worked.

Control denotes a combination of *Kif20b*<sup>+/+</sup> and *Kif20b*<sup>+/m</sup> embryos. n = 3-4 sections from 3 embryos of each genotype. n.s. = not significant, Student's t-test.

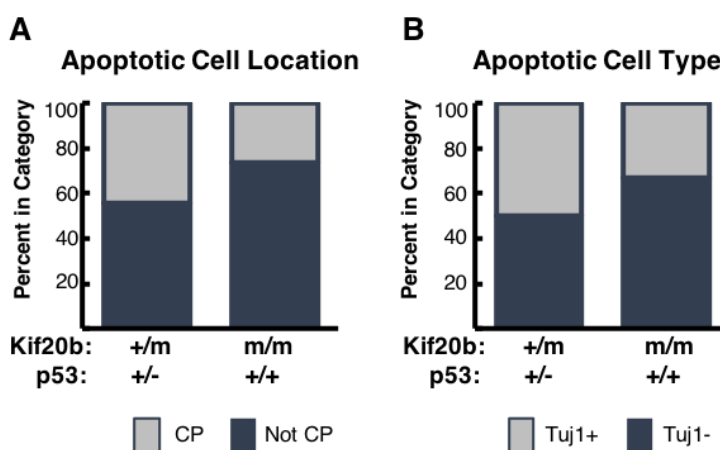


**Figure 11.** Apoptotic cells in *Kif20b* mutant cortices are primarily in the proliferating zones and do not express the neuronal marker TuJ1.

**A.** Using images of control and *Kif20b* mutant E14.5 cortical sections collected for Figure 2, the locations of apoptotic (CC3+) cells were categorized as within the cortical plate (CP) or proliferating zones (not CP). 74% of *Kif20b*<sup>m/m</sup>; *p53*<sup>+/+</sup> apoptotic cells were located in the proliferating zones (not CP) and 25% were located in the cortical plate, compared to 56 and 44%, respectively, in *Kif20b*<sup>+/m</sup>; *p53*<sup>+/-</sup> controls.

**B.** Apoptotic (CC3+) cells were further classified according to their type by labeling with Tuj1 (beta-III-tubulin) for neurons. 67% of apoptotic cells were Tuj1- and 33% were Tuj1+ in the *Kif20b* single mutant (*Kif20b*<sup>m/m</sup>; *p53*<sup>+/+</sup>), compared to 50% and 50%, respectively, in *Kif20b*<sup>+/m</sup>; *p53*<sup>+/-</sup> controls.

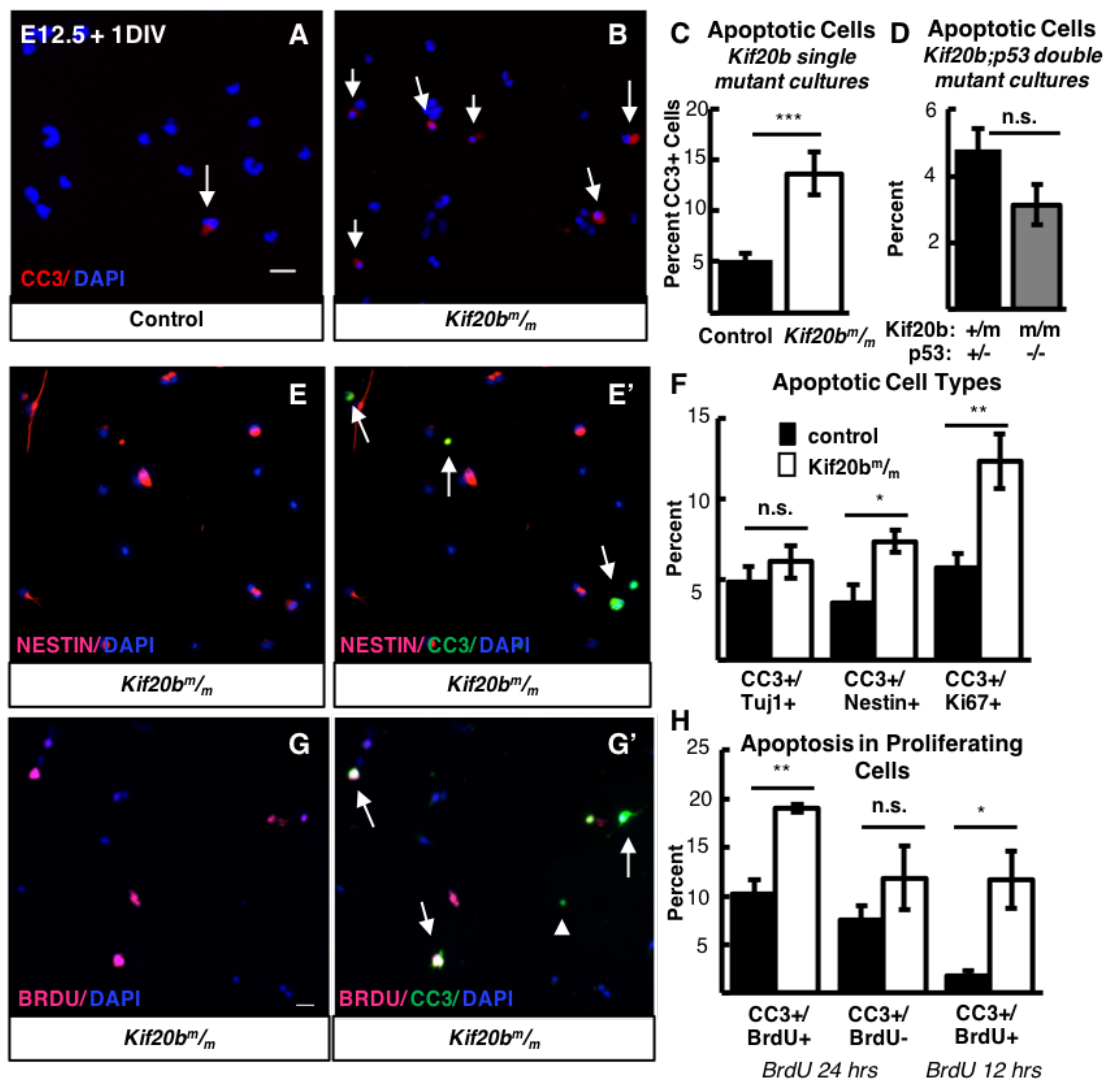


**Figure 12.** *Kif20b* loss causes apoptosis in proliferating cortical NSCs.  
(continued on next page)

**Figure 12.** *Kif20b* loss causes apoptosis in proliferating cortical NSCs.

**A, B.** Representative fields of control (left) and *Kif20b*<sup>m/m</sup> (right) dissociated cortical cultures labeled with CC3 (red, arrows) for apoptotic cells. **C.** The mean percentage of apoptotic cells in *Kif20b*<sup>m/m</sup> cortical cultures is increased (>2-fold) above controls.  $n = 13$  control, 11 mutant coverslips; 8 and 7 brains, 7 litters. **D.** Apoptosis is not increased in *Kif20b*; *p53* double mutant cultures.  $n = 4$  *Kif20b*<sup>+/-</sup>; *p53*<sup>+/-</sup>, 3 *Kif20b*<sup>m/m</sup>; *p53*<sup>-/-</sup> coverslips; 3 and 2 embryos, 2 litters. **E.** Representative fields labeled with Nestin (NSCs, pink) (E,E') and CC3 (green) (E'). Arrows in E' indicate cells co-positive for Nestin and CC3. **F.** The percent of apoptotic neurons (CC3+/Tuj1) is not increased in *Kif20b* mutant cultures, but the percent of apoptotic NSCs and proliferating NSCs (CC3+/Nestin+; CC3+/Ki67+) are significantly increased. Tuj1/CC3 analysis:  $n = 7$  control, 6 mutant coverslips; 4 and 3 brains, 4 litters. Nestin/CC3 analysis:  $n = 7$  control, mutant coverslips; 4 brains each, 3 litters. Ki67/CC3 analysis:  $n = 6$  control, 5 mutant coverslips; 3 brains each, 3 litters. **G.** Representative fields labeled with BrdU (cells that incorporated BrdU, pink, G, G') and CC3 (green, G'). Arrows in G' indicate cells co-positive for BrdU/CC3, and arrowhead indicates a cell negative for BrdU but positive for CC3. **H.** Apoptosis is associated with proliferation in *Kif20b* mutant NSCs. Significantly more BrdU<sup>+</sup> cells are apoptotic (CC3<sup>+</sup>) in *Kif20b* mutant cultures than control cultures, but BrdU<sup>-</sup> cells show no increase in apoptosis, when BrdU was in the bath for the 24 h culture period. When BrdU is given for the last 12 h before fixing at 24 h, the percent of apoptotic BrdU<sup>+</sup> cells are also increased in *Kif20b* mutant cultures compared to control. For 24 h experiment,  $n = 3$  control and mutant coverslips from 3 embryos and 2 litters. For 12 h experiment,  $n = 4$  control and mutant coverslips from 3 embryos and 2 litters. Control denotes a combination of *Kif20b*<sup>+/+</sup> and *Kif20b*<sup>+/-</sup> embryos. \* $P < 0.05$ , \*\* $P < 0.01$ , \*\*\* $P < 0.001$ , Student's *t*-test. Error bars are +/- s.e.m. All cultures from E12.5 cortices and fixed after 24 h. Scale bars in A, E, H: 20  $\mu$ m.

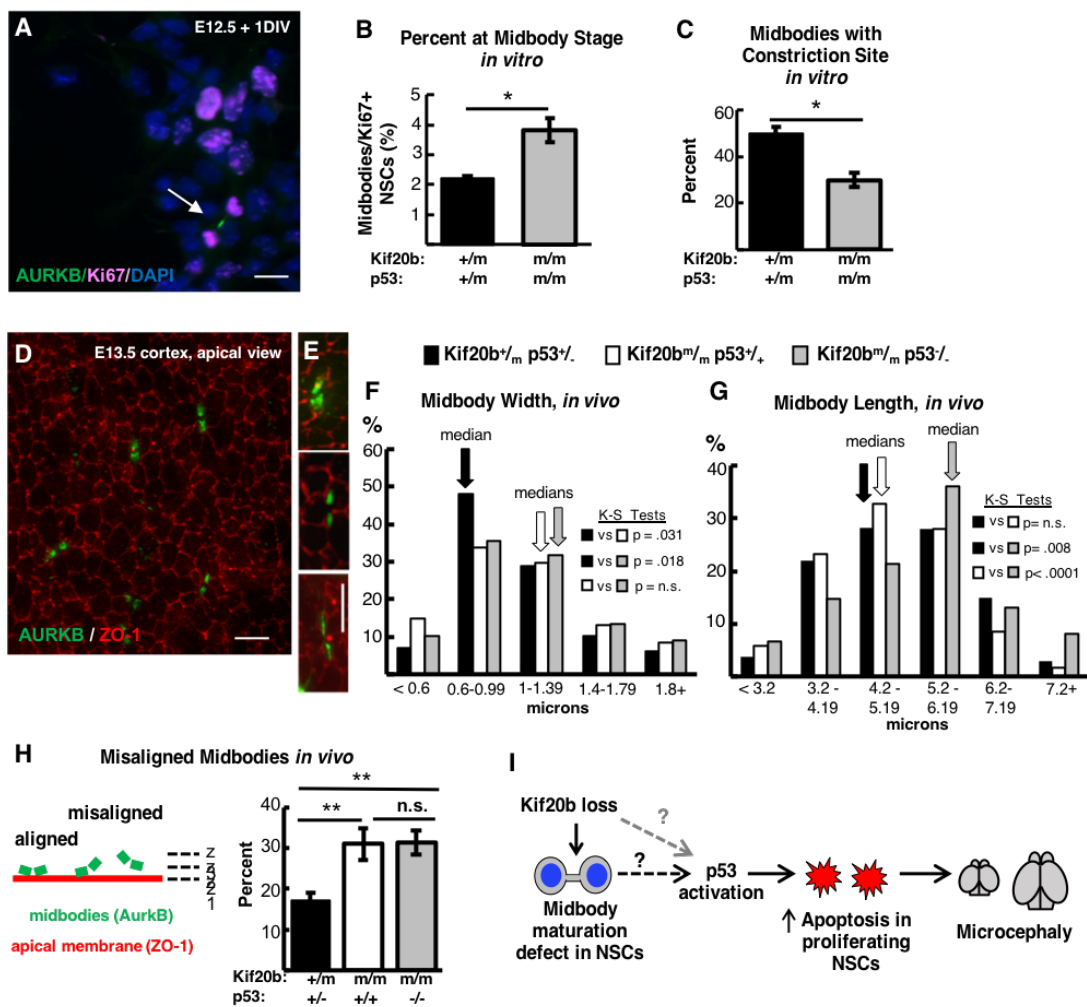


**Figure 13.** *p53* deletion does not restore normal abscission of *Kif20b* mutant NSCs.  
(continued on next page)

**Figure 13.** *p53* deletion does not restore normal abscission of *Kif20b* mutant NSCs.

**A.** Representative image of E12.5 dissociated cortical cells, labeled with AurKB for MBs (green, arrow) and Ki67 for proliferating NSCs (pink). **B.** The mean percent MB stage proliferating NSCs is significantly increased in *Kif20b*/m; *p53*<sup>-/-</sup> cultures. *n* = 4 *Kif20b*<sup>+/-</sup>; *p53*<sup>+/-</sup>, 3 *Kif20b*/m; *p53*<sup>-/-</sup> coverslips; 3 embryos each, 2 litters. **C.** Of the NSCs at MB stage, the percent with a constriction site is significantly reduced in *Kif20b*; *p53* double mutant cultures. *n* = 111 *Kif20b*<sup>+/-</sup>; *p53*<sup>+/-</sup>, 101 *Kif20b*/m; *p53*<sup>-/-</sup>-MBs; 3 embryos each, 2 litters. For comparison to *Kif20b*/m; *p53*<sup>+/-</sup> single mutant cultures, see Fig. 5E. **D.** Representative image of E13.5 cortical slab, apical surface, labeled with ZO-1 (red, apical junctions) and AurKB (green, MBs). **E.** NSC MBs range from short and wide (top) to long and thin (bottom). **F.** The median MB width is similarly increased in *Kif20b* single and *Kif20b*; *p53* double mutant cortices compared to controls. Median widths (μm) = 0.92 in *Kif20b*<sup>+/-</sup>; *p53*<sup>+/-</sup>, 1.0 in *Kif20b*/m; *p53*<sup>+/-</sup>, 1.02 in *Kif20b*/m; *p53*<sup>-/-</sup> cortices. **G.** The median MB length is similar in *Kif20b* mutant and control cortices, but is significantly increased in *Kif20b*/m; *p53*<sup>-/-</sup> cortices. Median lengths (μm) = 4.82 in *Kif20b*/m; *p53*<sup>+/-</sup>, 5.11 in *Kif20b*<sup>+/-</sup>; *p53*<sup>+/-</sup>, 5.43 in *Kif20b*/m; *p53*<sup>-/-</sup> cortices. *n* for (F, G) = 346 *Kif20b*<sup>+/-</sup>; *p53*<sup>+/-</sup>, 189 *Kif20b*/m; *p53*<sup>+/-</sup> and 299 *Kif20b*/m; *p53*<sup>-/-</sup> MBs; 8, 5 and 7 cortical hemisphere slabs; 6, 4 and 5 embryos, 8 litters. **H.** Left, Schematic of aligned and misaligned MBs of NSCs *in vivo* relative to the apical membrane. Right, the percent misaligned MBs is doubled in both *Kif20b*/m; *p53*<sup>+/-</sup> and *Kif20b*/m; *p53*<sup>-/-</sup> cortices compared to controls. *n* = 8 *Kif20b*<sup>+/-</sup>; *p53*<sup>+/-</sup>, 7 *Kif20b*/m; *p53*<sup>+/-</sup>, 7 *Kif20b*/m; *p53*<sup>-/-</sup> cortical slabs from 6, 4, and 6 embryos, respectively, 8 litters. **I.** Working model for the etiology of *Kif20b* microcephaly (see text also). *p53* is required for NSC apoptosis and microcephaly caused by *Kif20b* loss but is not required for the MB defects. Thus, the MB maturation defect in the *Kif20b* mutant cells could signal to induce *p53* accumulation through an unknown pathway (dashed black arrow with question mark). Alternatively, another cellular defect caused by *Kif20b* loss could induce *p53* accumulation through a non-MB mediated pathway (dashed gray arrow with question mark). A–C are E12.5 cortical cultures fixed at 24 h. \**P* < 0.05, \*\**P* < 0.01, Student's *t*-test for (B, C); K.S. test for (F, G); one-way ANOVA for (H). Error bars are +/- s.e.m. Scale bars, 10 μm.

## Chapter 3: Mutation of the key abscission regulator *Cep55* causes microcephaly

### **Abstract**

Building a cerebral cortex of the proper size involves balancing rates and timing of neural stem cell (NSC) proliferation, neurogenesis, and cell death. The cortex appears to be particularly susceptible to developmental defects. Genetic and environmental insults often disproportionately impair brain growth in comparison to other tissues, resulting in microcephaly. Mutations of the cytokinetic abscission regulator, *Cep55*, cause a neurodevelopmental syndrome in humans that is incompatible with life. *Cep55* is thought to be essential for vertebrate abscission completion, as the recruiter of ESCRT factors in mammalian cells. In order to elucidate the role of *Cep55* in vertebrate cytokinetic abscission and mammalian embryogenesis, we investigated a mouse mutant for *Cep55*. Here, we show for the first time that mutation of *Cep55* causes microcephaly in mice disproportionate to reduced body size, corroborating the human phenotype. Surprisingly, ESCRT recruitment is impaired but not eliminated without *Cep55*. Furthermore, we observe cytokinetic defects in both neural and non-neural cells, including high levels of binucleate cells. However, we observe p53 activation and apoptosis only in neural cell types. Therefore, we find that differential p53-dependent responses to cytokinesis failure contribute to tissue-specific phenotypes.

### **Introduction**

Proper growth of the cerebral cortex requires coordination of numerous cellular processes within strict developmental time constraints. Genetic and environmental insults often disproportionately impair brain development compared to the growth of other tissues. However, why the mammalian brain is uniquely sensitive to developmental insults remains unclear. Important insights have come from investigation of human microcephalies and microcephalic mouse mutants, in which the brain is smaller than other body tissues. Genes implicated in microcephaly are almost all involved in processes of cell division; mitosis and DNA replication especially are vulnerable to insults (Duerinckx & Abramowicz, 2018). Cytokinesis, apart from mitosis, has been implicated in the etiology of microcephaly (Bondeson et al., 2017; Di Cunto et al., 2000; Frosk et al., 2017; Janisch et al., 2013; H. Li et al., 2016; Little & Dwyer, 2018; Makrythanasis et al., 2018; Moawia

et al., 2017). Many microcephalic mutants also have in common activation of p53-dependent signaling pathways (Bianchi et al., 2017; Insolera et al., 2014; Little & Dwyer, 2019; Pao et al., 2014). Evidence suggests that p53-dependent responses are tissue and cell-type specific (Kasthuber & Lowe, 2017), but whether this contributes to disparate tissue phenotypes in microcephaly mutants has not been addressed.

We previously showed that mutation of the kinesin-6 family member *Kif20b* disrupted normal cytokinetic abscission in mice, but did not alter mitosis ((Janisch et al., 2013; Little & Dwyer, 2018); McNeely et al 2019). Cytokinesis takes longer to complete than mitosis, and consists of two main events, cleavage furrowing and abscission (Mierzwa & Gerlich, 2014). Beginning in anaphase following chromosome segregation, central spindle proteins induce cleavage furrowing. The ingressing furrow compacts the central spindle proteins into a structure called the midbody within the intercellular bridge. Finally, midbody proteins mediate the final abscission event, in which the midbody is cleaved to separate the two daughter cells, either on one or both sides. The abscission process involves membrane severing using the ESCRT system and microtubule disassembly (Connell et al., 2009; Guizetti et al., 2011).

Because cytokinesis has been studied primarily in single cell models and invertebrate epithelia, less is known about how it is differentially regulated in vertebrate epithelia and in the cortex specifically. Neural stem cells (NSCs) are polarized, with apical and basal processes spanning the entire cortical epithelium. NSC nuclei migrate to the apical membrane to undergo mitosis and cytokinesis, and the cleavage furrow ingresses asymmetrically from the basal process, forming the midbody at the apical-most point. The cytokinetic process must also be coordinated with NSC daughter cell fates. Early in development, NSCs undergo primarily proliferative divisions to increase the progenitor pool, but later undergo progressively more neurogenic divisions to produce neuron daughters that detach and migrate into the cortical plate (Bizzotto & Francis, 2015; Dwyer et al., 2016).

*Kif20b* mutant NSCs display abnormal midbody structure, faster abscission timing, and p53-dependent apoptosis ((Little & Dwyer, 2019); McNeely et al 2019). However, *Kif20b* mutant NSCs were always observed to complete abscission (McNeely et al 2019). In order to further investigate cytokinetic abscission processes during cortical development, we sought to more significantly impair abscission completion in NSCs. Recently, mutation of the vertebrate-specific

*Cep55*, a key regulator of abscission that recruits ESCRTs to accomplish membrane severing (Carlton et al., 2008; Carlton & Martin-Serrano, 2007; Hyung et al., 2008; Morita et al., 2007), was discovered as a cause of microcephaly in humans (Bondeson et al., 2017; Frosk et al., 2017; Rawlins et al., 2019). In cell lines, *Cep55* knockdown almost completely eliminates abscission completion (Fabbro et al., 2005; Zhao, 2006). Thus, we sought to inhibit *Cep55* function during mouse embryogenesis and elucidate developmental consequences.

Here, we show that *Cep55* mutation in mice corroborates the human microcephaly phenotype, including disproportionate reduction of brain size. Although consistent with the human phenotype, it is highly surprising that mammalian cells are capable of completing abscission without functional *Cep55*. Surprisingly, our data indicate that ESCRT recruitment is impaired, but not eliminated in *Cep55* mutant midbodies, consistent with the ability of some cells lacking *Cep55* to actually complete abscission. Interestingly, we found highly increased numbers of apoptotic cells in *Cep55* mutant neural but not non-neural tissues, resulting in decreased neurogenesis and impaired brain growth. Further analysis indicated that p53 activation occurred preferentially in binucleate NSCs and neurons, but not in non-neural cells. Therefore, we propose that impaired abscission completion in *Cep55* mutant cells is especially consequential for brain development due to differential activation of p53-dependent responses.

## Results

### ***Cep55* mutation results in microcephaly disproportionate to body size.**

Given *Cep55* protein's essential role in cell division, we were surprised to discover that *Cep55* mutants were born at expected Mendelian ratios, but exhibited failure to thrive and died before weaning (data not shown). This is consistent, however, with predicted loss of *Cep55* function in human fetuses not precluding survival until birth (Rawlins et al., 2019). *Cep55* mouse mutants appeared phenotypically normal at birth except for a noticeably flatter head shape, and, when measured, 10% reduction in body length (Fig. 14 A-B). Strikingly, *Cep55* mutants exhibited an approximately 50% reduction in cortical area and 30% reduction in cortical length on postnatal day 0 (P0) (Figure 14 C, D, G). A ratio of cortical length to body length revealed that cortical size was much more severely affected than body size (Fig. 14 H).

Next, we wanted to identify when *Cep55* mutant brain growth was impaired. Cortical growth begins at embryonic day 10 with symmetric divisions of apical progenitor cells to increase the progenitor pool, and over time, progressively more neuron-producing divisions. By birth, the majority of neurons of the mouse embryo have been produced, and glia-genesis has begun. Interestingly, we found that *Cep55* mutants exhibited a similar reduction in brain size compared to controls at E14.5 as was seen at P0 (Fig. 14 E-F, G). Thus, the primary mechanisms driving reduction in brain size occur prior to E14.5. At age E12.5, *Cep55* mutants have significantly decreased cortical length, but the reduction is only 8% compared to controls (Fig. 14 G). Thus, we conclude that *Cep55* mutation in mice impairs brain development significantly more so than body development, and that the greatest reduction in cortical growth coincides with the onset of neurogenesis around E12.5.

***Cep55* localizes to the midbody at late abscission stages in control but not mutant apical and basal progenitor cells.**

The mutation of *Cep55* used in this analysis, which was generated by the Toronto Centre for Genomics for the Canadian Mouse Mutant Repository via CRISPR/Cas9, is expected to produce a 600 base-pair deletion of exon 6. The total murine *Cep55* sequence consist of 9 exons (Fig. 15A) and 462 amino acids (AA). *Cep55* protein sequence consists of an N terminus, two coiled-coil regions (CC1 and CC2) surrounding the ESCRT- and Alix- binding region (EABR), and a C-terminus (Fig. 15B). *Cep55* is recruited to the midbody by MKLP1 via binding at the C-terminus. Plk1 also binds to *Cep55* at the C-terminus (S436) to prevent premature recruitment to the midbody. *Cep55* recruits ESCRT-I and Alix through the EABR. We verified the correct mutation in our mutants with DNA sequencing (data not shown). This deletion results in the expected 311 bp deletion in the RNA product (Fig. 15C,D). RNA is still produced in the *Cep55* mutant, but we noted that less *Cep55* mutant RNA is made in heterozygotes than wild-type transcript, indicating that *Cep55* mutant RNA is produced less efficiently. This deletion is predicted to result in a frameshift starting at AA226, resulting in a premature stop codon at AA238. We verified the full-length protein is not produced in *Cep55* mutant samples with an antibody to the C-terminus (Fig. 15E).

We next investigated *Cep55* expression patterns. *Cep55* is vertebrate-specific, and *Cep55* RNA is expressed in the murine cerebral cortex at E14.5 and P0, at higher levels in progenitor

populations than in neurons (Loo et al., 2019). *Cep55* is also expressed in zygote-blastocyst stage embryos (Gao et al., 2017), as well as in all sequenced adult murine tissues at 6-weeks of age (Li et al., 2017). RNA *in situ* analysis showed that *Cep55* RNA is expressed in proliferative zones of the cortex at E14.5, but is not detectable in neuronal layers. Low level expression in other tissues is observed (GenePaint, MH1690, <http://www.GenePaint.org>); (Visel, 2003). In evaluation of protein expression we found that as expected, *Cep55* is expressed in dividing NSCs (Fig. 16A-E). *Cep55* localization is specific to cell division stage; no specific expression was found in metaphase (Fig. 16A), anaphase (Fig. 16B) or early midbody-stage cells (Fig. 16C). However, late midbody stage cells with thinner midbodies showed a ring of *Cep55* localized to the center of the midbody between opposing Aurora-B positive flanks (Fig 16D). *Cep55* was also found highly expressed in released midbody remnants (Fig. 16E). Mutated *Cep55* did not localize to the midbody in NSCs and was not noted in mutant midbody remnants (Fig. 16A-E, right images). Using antibodies to the C-terminus and to the entire protein sequence, we found a significant reduction in *Cep55* fluorescence at the center of the midbody, but not in the nucleus, in *Cep55* mutant samples (Fig. 16F). In addition to apical progenitor cells expressing Nestin, we found *Cep55* had a similar localization pattern in basal progenitors expressing Tbr2 (Fig. 16G). Notably, we did not see any co-localization of *Cep55* with pericentrin, a centrosome marker (Fig. 16H).

To investigate whether *Cep55* was expressed in cells of non-neural tissues, we dissociated mouse embryonic fibroblasts from E14.5 control and *Cep55* mutant embryo bodies. We noted the same expression pattern in MEFs as in apical progenitor cells, with localization only to late-stage midbodies (Fig. 17A-B). Furthermore, midbody localization was lost in *Cep55* mutant MEFs (Fig. 17C). Therefore, our evidence suggests that phenotypic differences observed in *Cep55* mutant brain versus body size are not simply due to differences in expression.

### **Reduced cortical size in *Cep55* mutants is due to reduced neuron number.**

Broadly, microcephaly can occur due to reduced cell proliferation, cell death, cell fate changes, and/or impaired post-mitotic neuron outgrowth. Furthermore, microcephalic brains can have reduced brain size with preservation or disruption of brain structure. To elucidate these possibilities, we first visualized *Cep55* mutant brain structures at P0 with hematoxylin and eosin (H&E) to label nuclei and axons, respectively. We noted a reduction in size of all brain structures, including the cortex, hippocampus and cerebellum (Fig. 18A-E). Midline defects, including

impaired axon crossing to contralateral cortical hemispheres, were evident in coronal sections (Fig 18C). Ventricles were enlarged laterally, providing a possible explanation for the caudal-lateral thinning we saw in whole brains (Fig. 14C, Fig. 18D). We decided to first focus on the reduction in *Cep55* mutant cerebral cortex size, as we reasoned that common mechanisms likely led to the reduction of all brain structures.

Cortical thickness is reduced in *Cep55* mutants at P0 and E14.5 in rostral, middle and caudal sections, but most dramatically caudally (Fig. 19A-C, E-G). At P0, this was not due to a reduction in the thickness of the ventricular zone (vz) or subventricular zone (svz), where neural stem cells reside. Instead the cortical plate (cp), where post-mitotic neuronal nuclei reside, and the intermediate zone (iz) where they extend axons, was significantly reduced in thickness (Fig. 19D). During corticogenesis, waves of neurons are born over developmental time, and neuronal sisters migrate together into the cortex. Later-born neurons migrate above earlier-born neurons, forming an inside-out lamination pattern. We labeled control and *Cep55* mutant P0 sagittal sections with *Ctip2*, to identify neuronal layers V and VI, and *Satb2*, to identify neuronal layers II-IV. *Cep55* mutant cortical layers were ordered similarly to controls, with *Satb2* positive upper layers above *Ctip2* positive lower layers (Fig. 20A-B). However, all neuronal layers were reduced in thickness (Fig. 20C). Interestingly, lower neuronal layers V-VI took up a slightly greater proportion of the total cp in *Cep55* mutants, while upper neuronal layers II-IV comprised a reduced proportion (Fig. 20D). This could be because of early production of neurons and/or early death of progenitors, either of which would deplete the progenitor pool available to produce the later-born upper layer neurons. Thus, we conclude that reduced cortical thickness in *Cep55* mutants is due to reduced thickness of neuronal layers.

During post-mitotic neuron development, neurons extend processes which add to the growth of the cp, and also increase the space between neuronal nuclei. To determine whether reduced thickness of the neuronal layer was due to reduced neuron content and/or increased density of neurons, which would signify a defect in post-mitotic neuron outgrowth, we analyzed the number and density of cells in layer VI. We noted that the absolute number of cells in layer VI was significantly reduced in *Cep55* mutants (Fig. 20E). Surprisingly, the density of layer VI cells was also significantly reduced compared to controls (Fig. 20F). Therefore, the neuronal cell content in *Cep55* mutants is even further reduced than the reduction of cortical thickness implies. We

conclude that reduced cortical thickness in *Cep55* mutants is due to a reduced number of neurons in the cp.

### ***Cep55* mutants have disorganized embryonic cortical structure.**

Because *Cep55* mutant brains were already dramatically reduced in size at E14.5, we focused further analysis on early embryonic cortical development. To determine whether the reduction in the cp seen at P0 was evident at E14.5, we analyzed cortical layering with H&E. *Cep55* mutant vz and svz thickness was not altered, but cp and iz thicknesses were reduced (Fig. 19H). However, the marginal zone, comprising first-born neurons, was significantly thicker in *Cep55* mutants at E14.5, possibly due to increased neurogenesis at early developmental timepoints (Fig. 19H). To further investigate the structure of neuronal layers, we labeled E14.5 sections with neuronal tubulin (Tubb3) (Fig. 21A). We observed loss of a clear distinction between the cp and iz. However, we did not observe impaired neuronal migration to the cp/iz. As observed with H&E, the neuronal layer proportion of the cortical thickness was reduced in *Cep55* mutants, while non-neuronal layer proportions were increased (Fig. 21B).

The neurons of the cp are produced by divisions of apical and basal progenitor cells. Apical progenitors divide symmetrically or asymmetrically to produce additional apical and basal progenitor cells as well as neurons. Basal progenitors typically divide symmetrically to produce two neurons. To determine whether the organization and numbers of apical and basal progenitors in *Cep55* mutant cortices was altered, we labeled E14.5 sections with antibodies to Pax6 and Tbr2, respectively (Fig. 21C). We observed a slight decrease in the number of apical progenitors per cortical length while the number of basal progenitors was maintained in *Cep55* mutants (Fig. 21D). This suggests a premature production of basal progenitors from apical progenitor divisions. Notably, apical and basal progenitor positioning appeared more disorganized than controls, with a small but significant number of apical progenitor nuclei mislocalized basally (arrows, Fig. 21C, right and D). Finally, we observed that *Cep55* mutant apical and basal progenitor nuclei were slightly larger than control nuclei, and that there was increased “dead space” that was not filled by nuclei in *Cep55* mutant cortices. (Fig. 21C, right).

### **Apoptotic cells are specifically increased in *Cep55* mutant neural tissues.**

Reduced neurogenesis in *Cep55* mutants could be due to a defect in production of neurons and/or increased progenitor or neuron death. The increased space between neuronal nuclei and overall disorganization of neuronal layers led us to hypothesize that some neurons may be dying, and were thereafter removed. To address this, we labeled E14.5 sections with antibodies to cleaved-caspase 3, a marker of apoptosis. We saw a striking increase in apoptotic cells throughout the cortical epithelium (Fig. 22A,B). Apoptosis was most increased in the proliferative zones, but was also increased in the cp. This is consistent with widespread apoptosis in multiple cortical cell types. Since brain size was already significantly decreased at E14.5, we looked earlier to see if apoptosis was similarly increased. Apoptosis was dramatically increased in *Cep55* mutant cortical epithelium at E12.5 as well as at E10.5, before the onset of neurogenesis (Fig. 22C, E). Therefore, we conclude that apoptosis of both NSCs and neurons contributes to impaired cortical growth. NSCs and neurons may die due to the same or disparate cellular and molecular pathways.

As apoptosis appeared to be a major driver for *Cep55* mutant microcephaly, we wondered whether a lack of apoptosis could explain the less severe body size phenotype. Alternatively, apoptosis did occur in these tissues, but proliferation increased to compensate. To address this question, we labeled E12.5 whole-head coronal sections with CC3. Interestingly, apoptosis was observed throughout neural tissues (Fig. 22C) but was not seen in the rest of the head region, including, notably, the retina (Fig. 22D). At E10.5, we noted apoptosis throughout the central nervous system, including in the forebrain (Fig. 22E) as well as the midbrain (Fig. 22F), hindbrain (Fig. 22G), and interestingly, the spinal cord (Fig. 22H). However, we noted a lack of apoptosis throughout the rest of the embryo, including in the heart precursor (Fig. 22I) and the forelimb (Fig. 22J). Therefore, we propose the exciting possibility that a differential apoptotic response occurs in response to *Cep55* loss in distinct tissues. As this does not appear to be simply due to differences in expression, the interesting question arises as to whether apoptosis is itself differentially regulated in distinct cell types, and/or whether it is the cellular consequences of *Cep55* loss that differ.

### ***Cep55* mutation results in defects in both cytokinesis and mitosis.**

Based on the specific localization of *Cep55* to late-stage NSC midbodies, as well as the literature evidence of a requirement for *Cep55* in completion of cytokinetic abscission, we hypothesized

that apoptosis in *Cep55* mutants was due to impaired abscission completion. However, the growth of the brain as well as normal body size of *Cep55* mutants strongly suggest that abscission is completing in most cells. While abscission defects are thought to be the cause of at least one other microcephaly mutant that lacks *Kif20b* (Janisch et al., 2013; Little & Dwyer, 2018), mitotic defects are observed in many other microcephaly mutants.

To investigate mitosis and abscission processes in *Cep55* mutants, we made cortical slabs at E14.5 to visualize the apical membrane. We first noticed a significant decrease in the number of apical endfeet per cortical area (Fig. 23A-C). *Cep55* mutant endfeet are more variable in size, with many larger endfeet. This could be secondary to apoptosis and/or formation of binucleate cells. The number of mitotic cells per endfeet can be used to estimate the duration of time a cell spends in mitosis, while the number of midbodies per endfeet can be used to estimate the amount of time a cell spends completing abscission. The number of mitotic cells per apical endfeet was not altered in *Cep55* mutants, but the number of midbodies per endfeet was increased by approximately 25% (Fig. 23D,E). During the time between cleavage furrowing completion and abscission, midbodies become thinner, before forming constriction sites, the site of eventual abscission completion (Guizetti et al., 2011). We did not note any significant difference in midbody width in *Cep55* mutant NSCs using Aurora B labeling (Fig. 24B). However, *Cep55* mutant midbodies were significantly shorter (Fig. 24A). Therefore, these data suggest that *Cep55* mutant E14.5 apical NSCs may spend a normal amount of time in mitosis, but are delayed in completing abscission and have some defects in midbody structure.

To investigate mitosis in further detail, we also looked at mitotic cells in cross-sections, co-labeled with Pax6 and Tbr2 (Fig 23F). We observed a trend for increased numbers of mitotic cells in *Cep55* mutant cortical sections (Fig. 23G). The number of mitotic cells at the apical membrane was not significantly altered, consistent with our analysis in apical slabs (Fig. 23D,G). However, the number of basally-located mitotic cells was significantly increased (Fig. 23G). This increase in basally located mitotic cells was not due to an increase in mitotic apical progenitors, but an increase in mitotic basal progenitors (Fig. 23H). Therefore, these data suggest that mitotic duration in apical progenitors may be normal, but may be delayed in basal progenitors. As basal progenitors are produced from apical progenitors, we hypothesize that mitotic delay in basal progenitors may be a secondary consequence of abscission defects in apical progenitors. However, we cannot rule out a primary role of *Cep55* in mitosis of basal progenitors.

### **Cep55 mutant cortices exhibit increased numbers of binucleate cells.**

In addition to abscission delay, abscission failure and midbody regression resulting in binucleate cells was a common outcome of *Cep55* knockdown in cultured cells (Fabbro et al., 2005; Zhao, 2006). To investigate whether regression was occurring in cortical cells, we analyzed DNA content with flow cytometric analysis of E15.5 cortices (Fig. 25A-G). First, we used propidium iodide to analyze DNA content in all cortical cells. We noted a dramatic shift in the DNA content of *Cep55* mutant cells, including a 37% reduction in cells with 2N DNA content and 15-fold increase in cells with 4N DNA content (Fig. 25A-C). Interestingly, there was a slight increase in cells with DNA content between 2N and 4N as well (Fig. 25C). An increase in cells with 4N DNA content could come from either an arrest after DNA replication in G2 or mitosis before cytokinesis, or failed cytokinesis resulting in regression and formation of a binucleate and/or tetraploid cell. To further investigate these two possibilities, we used Ki67 and DAPI co-labeling to differentiate cycling (Ki67+) from non-cycling (Ki67- cells). Interestingly, we observed an increased 4N DNA peak in both cycling (Fig. 24D-E) and non-cycling *Cep55* mutant cells (Fig. 25F-G). In controls, there was no 4N DNA peak in non-cycling cells. The increased 4N DNA content in *Cep55* mutant cycling cells could come from either of our aforementioned possibilities. However, the increased 4N DNA content in non-cycling cells strongly suggests the presence of binucleate or tetraploid neurons in *Cep55* mutant cortices. Additionally, these data also suggest that the larger apical and basal progenitor nuclei seen in *Cep55* mutant cortices (Fig. 21C) could be due to tetraploid DNA content.

To investigate the possible existence of binucleate cells in more detail, we dissociated cortical cells from control and *Cep55* mutant E14.5 cortices and cultured them for 24 hrs. This allows the separation of individual cells for easier visualization of cellular structure. We used Phalloidin to identify the Actin network of individual cells, combined with Nestin to label NSCs. This allowed us to differentiate cells with one or two nuclei within one cytoplasm. We observed greatly increased numbers of binucleate cells, including binucleate progenitors (Nestin+) and binucleate neurons (Nestin-) (Fig 25H-J), confirming our hypothesis. Our data corroborate that *Cep55* enables successful completion of cytokinesis in NSCs, and is consistent with the finding of binucleate neurons in human tissues of fetuses with *Cep55* mutation (Frosk et al., 2017).

### **Abscission is impaired but not eliminated without Cep55.**

While our data supports a role for Cep55 in completion of cytokinetic abscission, *Cep55* mutants still exhibit brain and body growth over time and the majority of cells in *Cep55* mutants were not found to be binucleate. It is surprising that cells lacking Cep55 can complete abscission at all. Cep55 has been shown to be necessary to recruit ESCRTs in human cells, which mediate the final severing event (J. G. Carlton et al., 2008; Jez G. Carlton & Martin-Serrano, 2007; Hyung et al., 2008; Morita et al., 2007). It has been proposed that cells may be able to complete abscission through tension-mediated forces in the absence of ESCRTs (Gupta et al., 2018). We wondered whether *Cep55* mutant cells were completing abscission without ESCRT recruitment, or whether ESCRT recruitment was occurring without Cep55, possibly through compensation by another cytokinesis protein. To address this, we analyzed ESCRT recruitment and cytokinesis completion in MEFs, which exhibit Cep55 expression at late-stage midbodies that is absent in mutants (Fig. 17). Cep55 recruits ESCRTs through two parallel pathways, one beginning with recruitment of ESCRT-I/TSG101, and one beginning with recruitment of Alix. Interestingly, we found that both Alix and TSG101 were capable of being recruited to *Cep55* mutant midbodies (Fig. 26A-B). However, recruitment of both of these proteins was significantly decreased (Fig. 26C,D). Downstream of both pathways, Chmp2a is recruited to the midbody (Christ et al., 2016). We found a trend for decreased recruitment of Chmp2a (Fig. 26E). Therefore, our data indicates that Cep55 does ensure timely ESCRT recruitment, but is not absolutely required for their recruitment.

Cep55 was previously suggested to ensure normal formation of the midbody ring, seen as a dark zone with alpha-tubulin or Aurora b labeling (Zhao, 2006). We did not find a difference in the presence of a dark zone in *Cep55* mutant MEFs (Fig. 24C), or in midbody length (Fig. 24D) but did find that *Cep55* mutant MEF midbodies were thinner with alpha-tubulin labeling (Fig. 24E). This suggests *Cep55* mutant MEFs may be delayed in completing abscission at late stages. Furthermore, we found no significant difference in the number of midbodies with constriction sites, the site of eventual abscission (Fig. 26F). However, there were decreased numbers of midbodies with constriction sites that also had ESCRT localization in *Cep55* mutant MEFs (Fig. 26G). Even in control MEFs, most cells with constriction sites did not have ESCRT localization, supporting the idea that constriction sites are initially formed by endosomes rather than ESCRTS (Schiel et al., 2012).

We next sought to determine whether decreased ESCRT recruitment in *Cep55* mutant MEFs had any consequence for completion of abscission in these cells. Although *Cep55* was expressed in MEFs in a similar distribution as seen in NSCs, we did not observe apoptosis in *Cep55* mutant embryonic body tissues as we did in neural tissues, and body size was near normal at birth. We observed a significant increase in binucleate cells in *Cep55* mutant MEF cultures, although the increase was not as dramatic as seen in NSC cultures (Fig. 26H,I). Therefore, we find that *Cep55* does ensure successful completion of cytokinesis in MEFs.

**p53 nuclear expression is increased in binucleate neural but not non-neural *Cep55* mutant cells.**

We previously showed that microcephaly in an abscission mutant was driven largely through p53-dependent apoptosis (Little & Dwyer, 2019). Furthermore, p53 has been shown to activate apoptosis in response to mitotic defects and DNA damage (McKinley & Cheeseman, 2017). However, apoptosis due to loss of *Cep55* in a zebrafish model was proposed to be p53-independent (Jeffery et al., 2015). To determine whether p53 activation occurred in *Cep55* mutant cortices, we labeled E14.5 cortical sections with antibodies to p53. Indeed, while virtually no cells with bright nuclear p53 expression were observed in control sections, greatly increased numbers of p53+ cells were seen in *Cep55* mutant sections (Fig. 27A-B). We noticed these cells throughout the cortex, but especially increased towards the apical membrane in proliferating zones. To further delineate in which *Cep55* mutant cells p53 expression occurred, we used dissociated cortical cultures. We observed a 5-fold increase in the number of cells with twice the expression of p53 in the nucleus as the cytoplasm, or a nuclear:cytoplasmic (N:C) ratio of 2 or greater (Fig. 27C-E). Interestingly, just as we observed apoptosis in both progenitor and neurons, this increase in nuclear p53 expression occurred in both cell types. While cytokinetic defects would occur only in dividing NSCs, we reasoned that a failed cytokinesis event could result in the formation of either a binucleate or tetraploid progenitor cell or neuron. Indeed, we found increased numbers of binucleate progenitors and neurons in *Cep55* mutant cultures (Fig 25J). Therefore, we wondered if binucleation/tetraploidy could be a cause of p53 activation and apoptosis in progenitor cells and neurons. In support of this theory, a tetraploidy pathway for p53 activation has been proposed to act separately of mitotic or DNA damage defects (Ganem et al., 2014; McKinley & Cheeseman, 2017). To investigate this possibility, we co-labeled cells with

Nestin, Phalloidin and p53. We observed an increased nuclear:cytoplasmic ratio of p53 expression in *Cep55* mutant binucleate progenitors and neurons separately from mononucleate cells (Fig. 27F). Furthermore, we found that very few mononucleate progenitors or neurons in *Cep55* mutant cultures had p53 N:C ratios  $> 2$ , while more than 50% of binucleate progenitors and 20% of binucleate neurons did (Fig. 27G). Therefore, our data supports the existence of a p53-dependent pathway for elimination of binucleate cells in the cortex. Whether the binucleate state directly activates p53, or does so through secondary consequences of binucleation, awaits further analysis.

While we had observed cytokinetic defects in *Cep55* mutant MEFs including binucleate cells, we did not observe apoptosis in *Cep55* mutant embryonic body tissues. Similarly, we did not observe increased apoptosis in *Cep55* mutant MEF cultures (Fig. 28C). We wondered whether mutant MEFs did not display apoptosis due to lack of a p53-dependent response system to failed cytokinesis. Indeed, we did not observe a difference in the N:C ratio of p53 expression in mutant MEFs (Fig. 28A,B,D). Furthermore, binucleate mutant MEFs did not have any difference in p53 expression compared to mononucleate cells (Fig. 28E). These data suggest the possibility that the p53-dependent apoptotic response system is regulated differently in various cell types, contributing to tissue-level phenotypic differences observed in germline mutants.

## Discussion

Here for the first time we investigate the essentiality of the vertebrate-specific cytokinetic abscission regulator *Cep55* for embryonic development. Surprisingly, we find that *Cep55* is not essential for mammalian cell division, but is necessary for proper brain growth. Furthermore, our data suggest that despite being expressed in diverse cell types, *Cep55* is most important for divisions of NSCs to enable growth of brain tissues. We find that *Cep55* is expressed in the midbodies of both neural and non-neural embryonic cells (Fig. 28F). Loss of *Cep55* results in impaired ESCRT recruitment and indications of abscission delay. While abscission does complete in most cells, at least some fail abscission resulting in regression and the formation of a binucleate cell. Cytokinesis failure likely impairs further cell division in all cell types, but interestingly appears to result in increased p53 expression and apoptosis only in neural cells. This cell death impairs growth of brain tissues. Therefore, we propose that differential p53-dependent

responses in neural versus non-neural cells may explain phenotypic differences in *Cep55* mutant tissues, and potentially in other microcephaly mutants.

The phenotypes we observed in *Cep55* mutant mice are reminiscent of human disease caused by *Cep55* mutation. First, despite the reported essential role of Cep55 in cell division, various mutations of *Cep55* in humans thought to result in non-functional proteins did not eliminate embryo formation (Bondeson et al., 2017; Frosk et al., 2017; Rawlins et al., 2019). Cytokinesis is not dispensable for development; mutations in cytokinetic furrowing protein mgcRacGAP result in pre-implantation lethality in mice (Van de Putte et al., 2001). Therefore, cytokinesis must be able to complete in the majority of cells without Cep55. However, *Cep55* mutation in humans is more severe than in mice, as most human embryos died before birth while *Cep55* mutants were collected at normal ratios at birth, but died before weaning. Similar to the human disease, *Cep55* mutation in mice impaired brain development significantly more so than development of other tissues, and enlarged ventricles were observed. Furthermore, we observed binucleate neurons as were found in *Cep55*-mutated human tissues (Frosk et al., 2017). However, we did not observe any gross kidney abnormalities, digit webbing or other facial abnormalities as were seen in humans.

Our results illustrate the importance of comparing germline mutation to acute knockdown in determining the necessity of a protein for cell division. Knockdown studies have elucidated a requirement for Cep55 in direct binding and recruitment of proteins in parallel arms of the ESCRT pathway, ALIX and Tsg101, which eventually lead to ESCRT-III and Vps4 recruitment and membrane severing (Carlton et al., 2008; Carlton & Martin-Serrano, 2007; Hyung et al., 2008; Morita et al., 2007). Cep55 is recruited to the midbody by Centralspindlin/MKLP1 (Zhao, 2006). Plk1 phosphorylates Cep55 and inhibits its premature recruitment to late-stage midbodies; inhibition of Plk1-mediated phosphorylation shows that Cep55 is capable of localizing to the central spindle and early-stage midbodies, but normally does not (Bastos & Barr, 2010). *Cep55* knockdown in HeLa cells results in normal midbody formation, but severe abscission delay culminating most often in regression of the midbody and formation of a binucleate cell (Fabbro et al., 2005; Zhao, 2006). We find that Cep55 does ensure proper recruitment of ESCRT factors, but is not absolutely required for their recruitment. Notably, Cep55 is not found in invertebrates. Interestingly, abscission in *C. elegans* is accomplished without Cep55 but still uses the ESCRT system (Green et al., 2013). It is thought that the MKLP1/centralspindlin complex, which recruits

Cep55 in vertebrate cells, may directly bind and recruit ESCRTs in invertebrates. However, this remains to be fully demonstrated. We speculate that MKLP1 may partially compensate for Cep55 loss in mammalian cells.

Many of our observed phenotypes are likely downstream consequences of failed abscission in Cep55 mutant NSCs. A careful analysis of *Cep55* knockdown in human cell lines indicated that mitosis was not impaired by Cep55 loss in mononucleate cells, but was delayed as a consequence of binucleation from failed cytokinesis (Fabbro et al., 2005). Binucleate cells endure errors in chromosome segregation in the next mitosis, resulting in mitotic delay, aneuploidy, and DNA damage (Storchova & Kuffer, 2008). Therefore, mitotic delay in *Cep55* mutant basal progenitors may be a consequence of failed cytokinesis. Mitotic delay and DNA damage have been separately implicated in p53 activation in addition to the binucleate state itself (Meitinger et al., 2016). It is likely that multiple pathways result in p53 activation and apoptosis in *Cep55* mutants. Furthermore, the apoptotic process itself may exert secondary defects on cortical structure. It is poorly understood how apoptotic cells are eliminated from the cortical epithelium, whether by extrusion from the apical membrane and/or phagocytosis by other cell types, as has been observed in other cell and tissue types (Poon et al., 2014). The disorganization of *Cep55* mutant cortical structure may be secondary to apoptosis, or to impaired abscission completion. It will likely be helpful to compare phenotypes of acute Cep55 loss to germline mutation in neural cells. Additionally, inhibition of p53 would allow p53-dependent and -independent effects to be differentiated.

More work is needed to determine how consequences of cytokinesis failure differ in epithelia and NSCs compared to cultured cell lines. While binucleate cells have been observed in the cortices of murine citron kinase mutants (Di Cunto et al., 2000; Sarkisian et al., 2018), as citron kinase is necessary for proper cleavage furrowing, Cep55 is thought to act at a later stage of abscission, after the midbody is formed. In the cortex, nuclei begin to migrate away during abscission. Furthermore, abscission occurs in the next G1 phase (Gershony et al., 2014). In *Kif20b* mutants, we did not observe an increase in binucleate cells compared to controls (Janisch et al., 2013; Little & Dwyer, 2018). More investigation is needed to elucidate how pre- or post-midbody formation regression occurs in the cortex.

While some amount of cytokinesis completion is necessary for mammalian embryo formation, there is interesting variation in the regulation of cytokinesis and abscission completion across species and tissues. Some mammalian tissues, such as the liver and heart, have binucleate cells normally, while they are rarely found in the cortex and in cortical cells (Guidotti et al., 2003; Paradis et al., 2014). Furthermore, syncytia development occurs due to incomplete cytokinesis during germ cell cyst formation in male invertebrates and vertebrates (Greenbaum et al., 2011). Up to 650 interconnected cells have been observed (Ren & Russell, 1991). In male testes, this is thought to be regulated by binding of Tex14 to Cep55, inhibiting ESCRT recruitment (Iwamori et al., 2010; Kim et al., 2015). Furthermore, Cep55 overexpression results in male-specific infertility in mice (Sinha et al., 2018). It would be interesting to determine whether incomplete abscission can still occur in *Cep55* mutant testes. Evidence for differential regulation of cytokinesis suggests a differential tolerance for binucleate cells and incomplete abscission across species and tissues. Our data suggests that the p53-apoptotic response system may have evolved to eliminate cells that failed cytokinesis from the cortical epithelium.

p53-dependent apoptosis has now been implicated in several etiologies of microcephaly due to genetic defects (Bianchi et al., 2017; Houlihan & Feng, 2014; Insolera et al., 2014; Marjanović et al., 2015; Véronique Marthiens et al., 2013; Pao et al., 2014). Interestingly, p53 activity was also observed to occur in response to Zika virus infection in NSCs (Ghouzzi et al., 2016). Zika virus is capable of infecting other cell types, but primarily impairs brain growth. It is possible that highly sensitive p53-responses in NSCs and neurons could contribute to the discrepancy in brain growth. The question remains as to why p53-dependent responses are extra-sensitive to defects in cell division in cortical tissues. With the inability to regenerate cells if defects occur due to terminal cell cycle exit in neurons and the tight developmental time window for brain development, it is possible that evolution currently values elimination of abnormal cortical cells over survival and accumulation of further defects.

We noted some indications that premature cell cycle exit may contribute to microcephaly in the *Cep55* mutant, including a thicker marginal zone and increased numbers of basal progenitors. In addition to expression in late-stage midbodies, Cep55 can be observed in NSC midbody remnants. Asymmetric versus symmetric abscission, resulting in either inheritance of the midbody by one cell or release of a remnant, has been suggested to have downstream consequences for cell polarity and fate (Dionne et al., 2015; Dwyer et al., 2016). Furthermore,

even released midbody remnants can bind to cell receptors and be internalized, possibly exerting functions or simply being degraded. Midbody remnants are observed in cortical NSC cultures and on the apical membrane of the cortex (McNeely et al 2019). Therefore, it is possible that *Cep55* loss could shift the balance of inheritance or release of the midbody, or alter functions of midbody remnants when inherited. These changes could have long-ranging consequences for cell-cell signaling and cell fate, and deserve further investigation.

In conclusion, we present an exciting analysis of the role of the key abscission regulator *Cep55* during embryonic development. We find that *Cep55* is not absolutely essential for cytokinesis completion, as previously thought. We show that *Cep55* is expressed in both murine neural and non-neural cells, and prevents formation of binucleate cells in both cell types. However, we only observed p53 activation and apoptosis in neural tissues, suggesting a tissue-specific differential response to cytokinesis failure that could explain the severity of the *Cep55* mutant brain phenotype. Our data present many intriguing questions for further investigation concerning the role of *Cep55* in cytokinetic abscission, and the regulation of abscission and response to abscission failure during mammalian embryogenesis.

## **Methods**

### *Mice*

Mouse colonies were maintained in accordance with NIH guidelines and policies approved by the IACUC. Embryos were harvested by cesarean section, and the morning of the vaginal plug was considered E0.5. Littermate embryos served as controls for all experiments. The *Cep55* allele was obtained from the Canadian Mouse Mutant Repository (strain C57BL/6NCep55<em1(IMPC)Tcp>, and is maintained on C57BL/6 and 50/50% C57BL/6 and FVB/N background embryos, which were used for experiments. Sex of embryonic mice were not noted as sex was not a relevant biological variable for these experiments. The specific ages of embryonic mice used is noted in figure legends for each experiment.

### *Cortical cell cultures*

Cells were dissociated from E14.5 cortices following a protocol adapted from Sally Temple's laboratory (Qian et al., 1998). The Worthington Papain Dissociation Kit was used to dissociate cells (Worthington Biochemical Corporation, Lakewood, NJ, Cat # LK003150). Cells were cultured in DMEM with Na-Pyruvate, L-Glutamine, B-27, N2, N-acetyl-cysteine and basic fibroblast growth factor. After 24 h, cells were fixed by adding an equal volume of room temperature 8% PFA (paraformaldehyde) for 5 min to cell media, followed by removal of media and addition of  $-20^{\circ}$  cold methanol for 5 min.

#### *Mouse embryonic fibroblast (MEF) cultures*

Embryos from timed pregnant females were collected at E14.5. Embryos were decapitated, organs were removed from bodies, and resulting tissue was titrated with a 1 ml pipette and incubated in 1ml of 0.25% trypsin-EDTA for 25min at  $37^{\circ}\text{C}$ . The tissue was further triturated and tubes were spun at 1000 rpm for 5 min and the medium was aspirated off. The pellet was resuspended in DMEM/20% FBS with pen/strep added. The resulting cells from each embryo were plated in two 10 cm plates in DMEM/10% FBS. The next day, media was replaced. When confluent, cells were trypsinized and plated on fibronectin-coated coverslips, grown overnight, and fixed with 4% paraformaldehyde (PFA) for 10 minutes or cold methanol for 10 minutes at 24 or 48 hrs.

#### *Apical slab preparation*

Apical slabs were prepared as previously described (Janisch & Dwyer, 2016). The meninges and skull were removed to expose the brain in E13.5 embryos, followed by fixation with 2% PFA for 20 min. Next, apical slabs were made by pinching off cortices, flipping so that the apical surface was upright, and trimming to flatten the slab. Slabs were fixed for another 2 min with 2% PFA followed by blocking with 5% normal goat serum (NGS) for 1 h. Primary antibodies were applied for 1 h at room temperature and then moved to  $4^{\circ}$  overnight. The next day, after 3 times, 10-minute PBS (phosphate-buffered saline) washes, secondary antibodies and DAPI were applied at a concentration of 1:200 for 30 minutes. After two more 10-minute PBS washes, slabs were coverslipped with VectaShield fluorescent mounting medium (Vector Laboratories Inc., H-1000) and imaged. z-stack depth was 8–20  $\mu\text{m}$  and step size was 0.5  $\mu\text{m}$ . Midbodies were considered

misaligned if the two halves of the midbody were not in the same z-plane or within two adjacent z-planes.

### *Sequencing and RT-PCR*

Sequencing of lysed tail samples from Cep55 wildtype, heterozygote and mutant mice was performed by Eurofins Genomics. RT-PCR was performed with RNA extracted from E14.5 cortices. RNA extraction of the harvested cells was done using the PureLink™ RNA Mini Kit from life technologies according to the manufacturer's handbook. RNA content in the samples was determined with a nano-drop spectrometer at 260 nm. 100 ng RNA were used in the reactions with the Invitrogen superscript III one-step RT-PCR kit. The PCR products were run on 3% ultrapure agarose with ethidium bromide at 95 V for 1 h. Gels were visualized on a UV light box.

Primers: AAGCCAGTACACTCCACCTG  
GAATGGCTGCTCTGTGATGG

### *Immunostaining and H&E Staining*

To collect cryosections for IHC, age E12.5, E14.5 and P0 brains were removed from heads and fixed for 4, 6 and 24 hours, respectively, in 4% PFA, followed by immersion in 30% sucrose in PBS overnight. Whole E10.5 embryos were fixed overnight. Next, whole brains or embryos were embedded in OTC (Tissue-Tek, 4583) and cryosections were cut at 20 µm thickness and collected on Superfrost Plus slides (Fisher Scientific, 12–550-15). Frozen sections were stored at –80 degrees. Prior to immunostaining, cryosections were warmed to room temperature, then if antigen retrieval was needed, immersed in 10 mM citrate buffer at 95 degrees for 20 minutes. After cooling, sections were blocked in 2% NGS for 1 hour, followed by incubation with primary antibodies overnight at 4 ° C. The next day, after PBS washes sections were incubated with AlexaFluor secondary antibodies at 1:200 and DAPI at 1:100 for 30 min followed by PBS washes and coverslipping with VectaShield fluorescent mounting medium. For IF on coverslips of dissociated cortical progenitors, a similar protocol was used but with primary antibodies applied for 3 h at room temperature. Antigen retrieval was not used in dissociated progenitors except in the case of Tbr2 immunostaining; coverslips were immersed in 0.07M NaOH pH 13 for 2 min

before permeabilization. Coverslips were mounted on Superfrost Plus slides with Fluoro-Gel (Electron Microscopy Sciences, Hatfield, PA, 17985–10).

H&E staining was performed on cortical sections from paraffin-embedded brains by the UVA Research Histology Core.

### *Antibodies*

Antibodies used in this analysis were mouse polyclonal anti-human Cep55 (Abnova H00055165-B01P), mouse monoclonal anti-mouse Cep55 (Santa Cruz, sc-377018), rabbit polyclonal anti-human CC3 (Cell-Signaling 9661S, 1:250), rat monoclonal anti-mouse Tbr2 (eBioscience (Thermo Fisher Scientific), Waltham, MA 14–4875, 1:200), rabbit polyclonal anti-mouse Pax6 (BioLegend PRB-278P, 1:200), mouse monoclonal anti-rat Aurora B kinase (BD Biosciences 611082, 1:300), rabbit monoclonal anti-human Aurora B kinase (Abcam ab2254), rat monoclonal alpha-tubulin (Novus Biologicals NB600–506, 1:300), rabbit monoclonal anti-human PH3 (Cell Signaling 3458, 1:200), chicken polyclonal anti-mouse Nestin (Aves Labs NES, 1:600), rat monoclonal anti-human Ki67 (eBioscience 14–5698, 1:100), rabbit polyclonal anti-mouse p53 (Leica Biosystems, Wetzlar, Germany, NCL-L-p53-CM5p, 1:500), rat monoclonal anti-human Ctip2 (Abcam 18465, 1:400), rabbit polyclonal anti-mouse Tbr1 (Abcam, Cambridge, MA 31940, 1:200), rabbit monoclonal Satb2 (Abcam, ab92446), rabbit polyclonal pericentrin (BioLegend 92371), mouse monoclonal Tubb3 (Tuj1) (BioLegend 801201), mouse monoclonal phospho-histone H3 (Ser10) (Cell Signaling 9706), Phalloidin Oregon Green (Invitrogen 07466), chicken polyclonal anti-human alpha-tubulin (Abcam, ab89984), mouse monoclonal Alix (Santa Cruz, SC-53538), mouse monoclonal Tsg101 (Santa Cruz, SC-7964), rabbit polyclonal CHMP2A (Proteintech 10477-1-AP), rat monoclonal Zo-1 (DSHB, R26.4DC) and polyclonal rabbit anti Zo-1 (rabbit, Invitrogen (Thermo Fisher Scientific) 61–7300, 1:50). All antibodies were validated for the application used in multiple previous publications.

### *Flow Cytometry*

Cells from E15.5 brains were dissociated using the Papain Dissociation Kit (Worthington Biochemical Corporation). Single-cell suspensions were obtained by filtering through a 40 µm filter (BD Falcon Cell Strainer, blue nylon mesh, catalog #352340). For propidium iodide (PI)

staining, cells were resuspended in 500  $\mu$ l PBS and added to 4.5 ml ice-cold 70% ethanol for at least 2 hours. Samples were stored at 4°C. Fixed cells were rinsed in PBS and resuspended in 1 ml solution containing 100  $\mu$ g/ml RNase A, 0.1% Triton X-100 and 50  $\mu$ g/ml PI, and incubated at room temperature for 30 minutes in the dark. For Ki-67 and DAPI analysis, single-cell suspensions of E15.5 brains ( $n=3$  pairs of *Cep55* mutants and littermate controls) were fixed in 1.5% PFA for 15 minutes on ice. Cells were then washed twice with FACS buffer (2% BSA, 1 mM EDTA, 0.01% sodium azide, PBS) and permeabilized in 0.1% Triton X-100 in PBS for 30 minutes on ice. Cells were washed twice in FACS buffer and  $2 \times 10^6$  cells were incubated in 100  $\mu$ l FACS buffer with 1  $\mu$ g/ml DAPI and 2  $\mu$ l anti-Ki-67 antibody (monoclonal rat anti-Ki-67 Alexa Fluor 647, clone SolA15, eBioscience). Following three washes with FACS buffer, fluorescence was measured using a FACSCanto II flow cytometer (Becton Dickinson). At least 20,000 events were collected per sample. Data were analyzed using FlowJo software (TreeStar).

### *Imaging and statistical analysis*

Images in Figures 16E-H, 20, 22, 26, 27 and 28 were collected on either a Zeiss Axio ImagerZ1 microscope with AxioCam MRm or a Zeiss AxioObserver fluorescent widefield inverted scope microscope. Images in Figures 16I-J, 17, 21, 22 and 25H-I were taken on an inverted DeltaVision with TrueLight deconvolution microscope with softWoRx Suite 5.5 image acquisition software (Applied Precision (GE Healthcare), Issaquah, WA). A Leica MZ16F microscope with DFC300FX camera was used for images in Figures 14, 18, and 19. Control and mutant fluorescence images were collected with the same exposure times and on the same day. All image analysis was performed in ImageJ/Fuji and any changes to brightness and contrast were applied uniformly across images. Statistical analyses were performed using Excel (Microsoft) or GraphPad PRISM software. The sample sizes were pre-determined based on our lab's previous experience with cortical development analyses and others' published results. After obtaining pilot data, power analyses were performed if necessary to determine if the number of samples obtained was high enough for the effect size seen. NSC cultures that were unhealthy were not imaged and analyzed, but no other data was excluded from the analysis. No randomization or blinding was used as no experimental manipulation was applied other than genetic knockouts. Genotyping was performed after collection of embryos to determine genetic status. Statistical tests used are specified in each figure legend. For each sample set a statistical test of normality was performed using GraphPad PRISM software. Parametric tests were used when sample sets had a normal

distribution and non-parametric tests were used when sample sets did not have a normal distribution. Variance was calculated and was typically similar between groups. N's listed in figure legends indicate the number of coverslips, brains and litters collected for each experiment. For each brain, at least three sections were imaged, and for each coverslip, at least 5, 20× pictures or 10, 40× pictures were analyzed.

## Figures

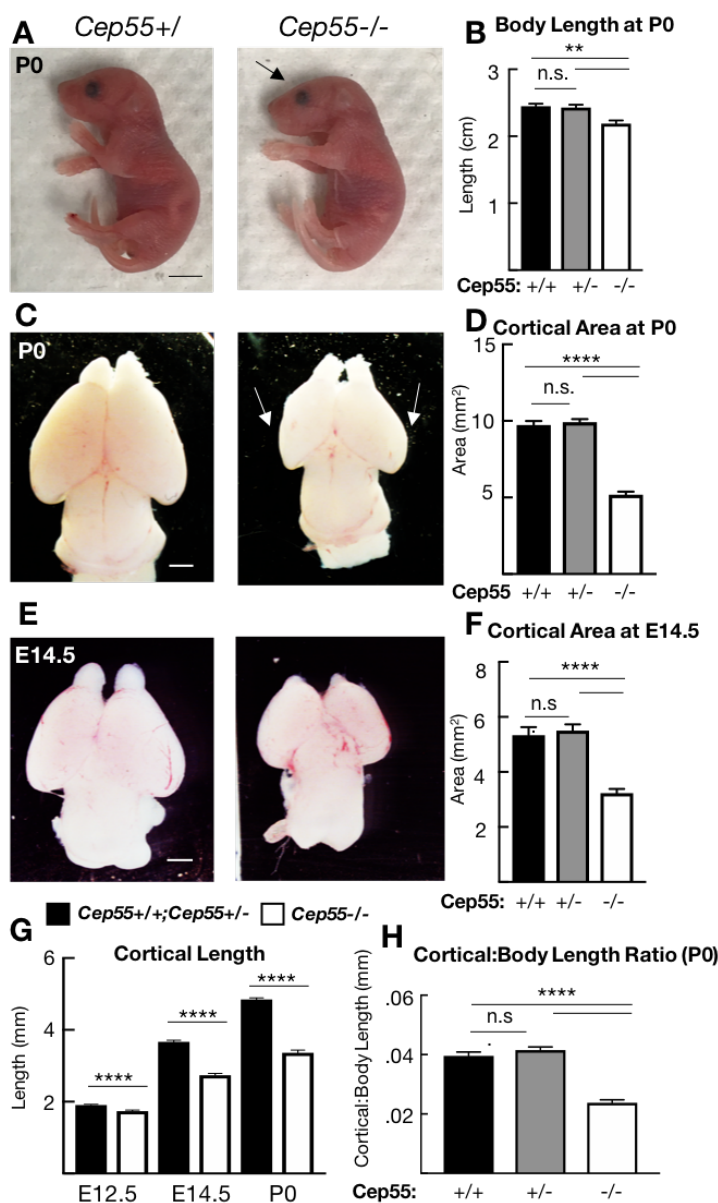


**Figure 14.** *Cep55* mutation results in microcephaly disproportionate to body size.

**A-B.** *Cep55* mutant mice have 10% shorter body length and a flatter head (arrow) but otherwise appear morphologically normal compared to wild-type and heterozygote controls at the day of birth (P0). **C-D.** Cortical area is reduced by approximately 50% in *Cep55* mutants compared to wild-type and heterozygote controls at P0. *Cep55* mutant cortices exhibit caudal thinning (arrows). **E-F.** Cortical area in *Cep55* mutants is reduced by 40% compared to controls at embryonic day (E)14.5, similarly as to P0. **G.** *Cep55* mutants have significantly reduced cortical length compared to controls as early as E12.5 (9% reduced), but a greater reduction at E14.5 (26% reduced) and P0 (29% reduced). **H.** The ratio of the cortical length to the body length of *Cep55* mutants at P0 is reduced by 40% compared to wild-type and heterozygote controls. N for P0 (A-D, G, H) = 7 *Cep55*<sup>+/+</sup>, 14 *Cep55*<sup>+/-</sup> and 8 *Cep55*<sup>-/-</sup> mice; N for E14.5 (E-F, G) = 5 *Cep55*<sup>+/+</sup>, 13 *Cep55*<sup>+/-</sup> and 10 *Cep55*<sup>-/-</sup> mice, and N for E12.5 (G) = 17 *Cep55*<sup>+/+</sup>;+/- and 9 *Cep55*<sup>-/-</sup> mice. Scale bars: A: 5 mm; C and E: 1 mm; \*\*  $p < 0.01$ ; \*\*\*\*  $p < 0.0001$ . B,D,F and H: one-way ANOVA; G: t-test.

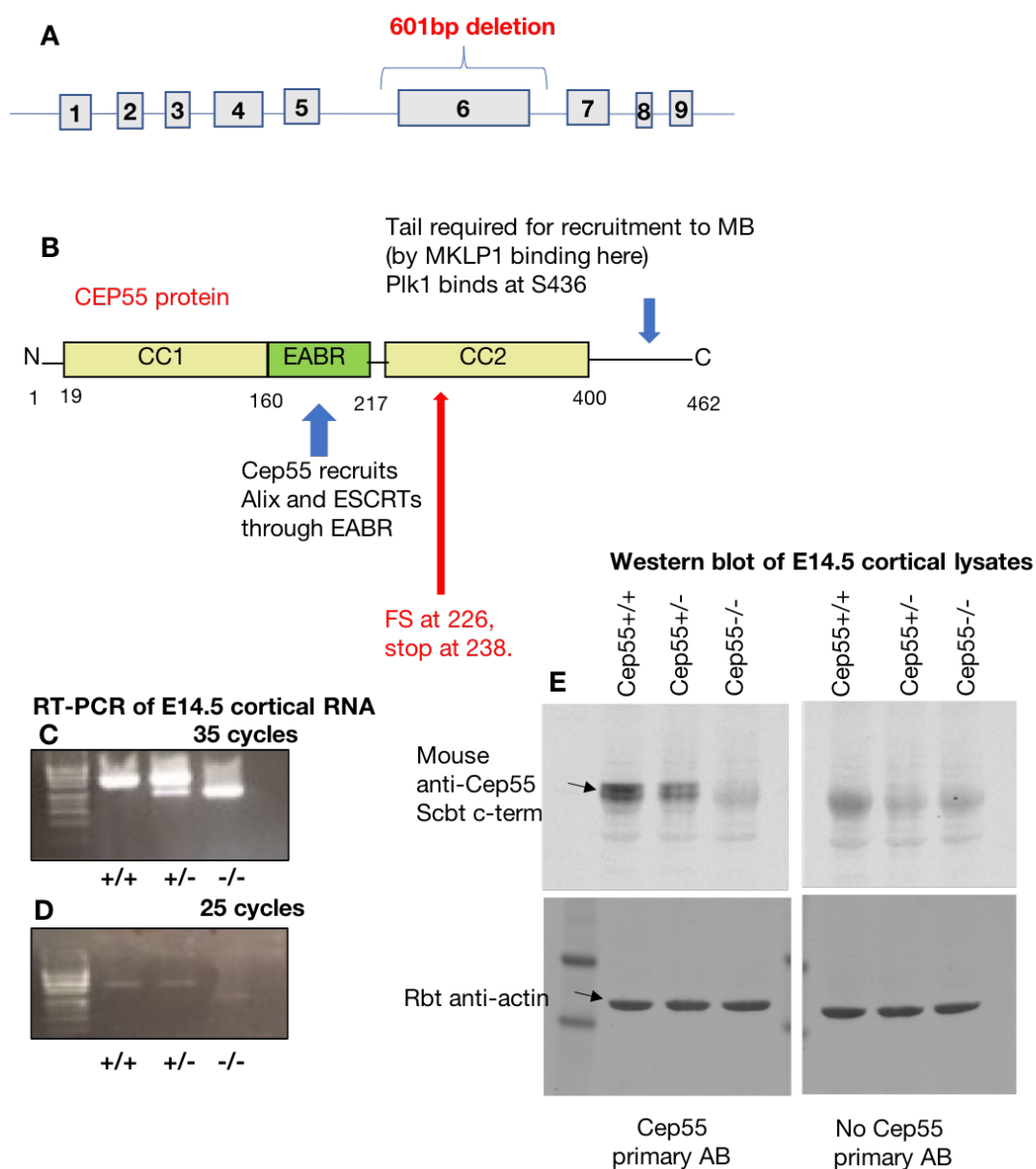


**Figure 15.** Deletion of exon 6 of *Cep55* results in a truncated RNA product and loss of the C terminus.

**A.** *Cep55* sequence consists of 9 exons. The mutation reported here is a 601 base-pair deletion surrounding exon 6. **B.** *Cep55* protein sequence consists of an N terminus, two coiled-coil regions (CC1 and CC2) surrounding the ESCRT- and Alix- binding region (EABR), and a C-terminus. *Cep55* is recruited to the midbody by MKLP1 via binding at the C-terminus. Plk1 also binds to *Cep55* at the C-terminus (S436) to prevent premature recruitment to the midbody. *Cep55* recruits ESCRT-I and Alix through the EABR. The total murine sequence is 462 amino acids. The deletion of *Cep55* reported here is expected to result in a frameshift (FS) at amino acid (AA) 226 and a premature stop codon at AA 238. **C-D.** RT-PCR of RNA extracted from E14.5 cortical samples confirmed the expected 794 bp product was present in wild-type and heterozygote samples and the expected 483 bp product was present in heterozygote and mutant samples at both 35 (C) and 25 (D) cycles. **E.** Western blots of E14.5 cortical lysates show the expected *Cep55* protein product as a doublet at approximately 55 kDa in wild-type and heterozygote samples, but not in mutant samples. An antibody to Actin was used as a loading control.

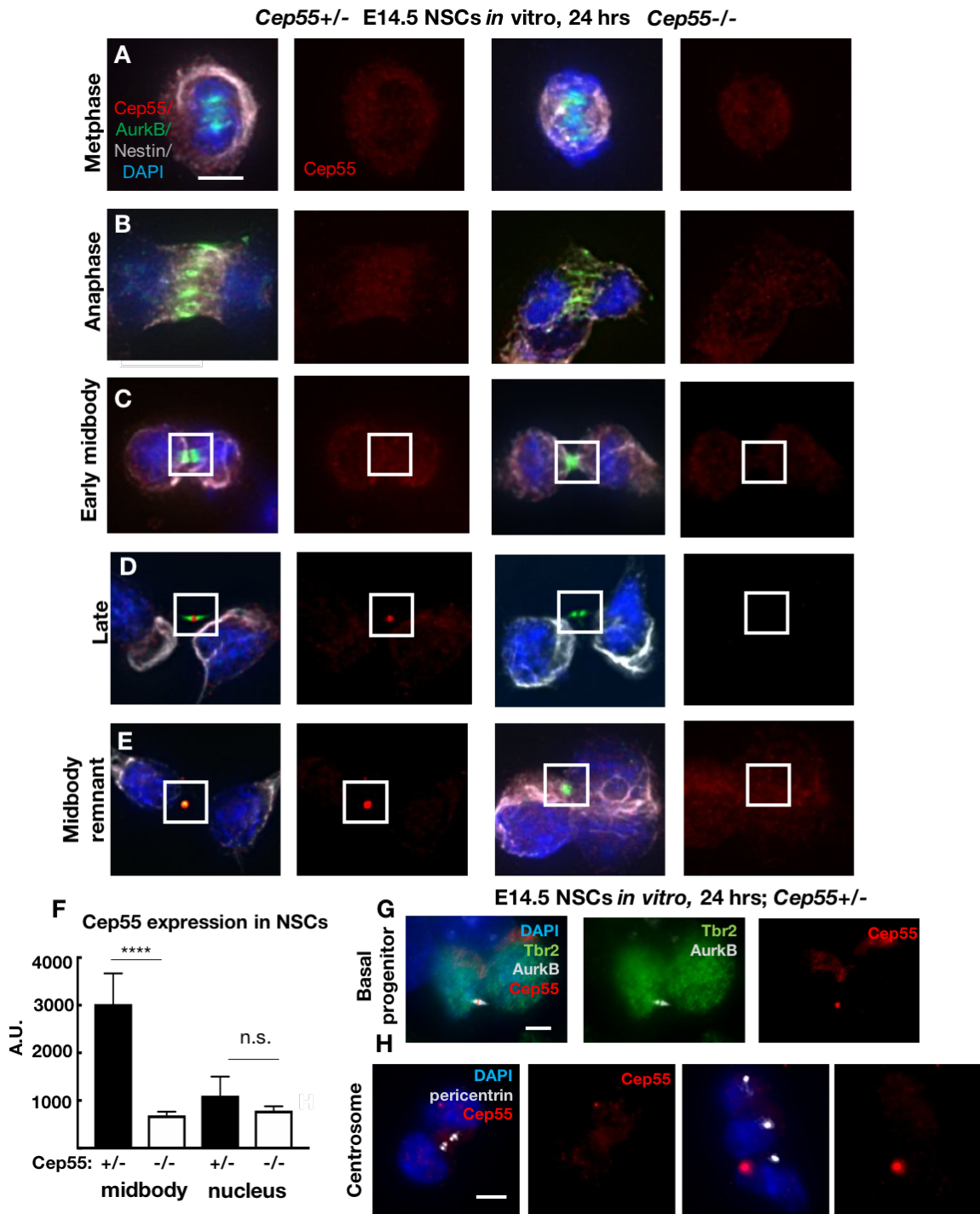


**Figure 16:** Cep55 localizes to the midbody at late abscission stages in control but not mutant apical and basal progenitor cells.  
(continued on next page)

**Figure 16.** Cep55 localizes to the midbody at late abscission stages in control but not mutant apical and basal progenitor cells.

**A-E.** E14.5 neural stem cell (NSC) cultures fixed at 24 hrs are labeled with Cep55 (red), Aurora kinase B for spindles and midbodies (green), Nestin for apical NSCs (grey) and DAPI. Cep55 does not localize to spindles or centrosomes in metaphase (A), anaphase (B), or early midbody stage (C) NSCs. (D-E) Cep55 localizes in a ring to the center of the midbody at late stages in control but not mutant NSCs. (E) Cep55 is detected in midbody remnants in control but not mutant NSCs. **F.** Quantification of Cep55 expression in control and mutant NSCs at midbody center and in the nucleus with an antibody to the C-terminus. **G.** Cep55 (red) is expressed in late-stage midbodies (Aurb+, grey) of basal progenitors marked with Tbr2 (green). **H.** Cep55 (red) does not colocalize with pericentrin (grey), a marker for centrosomes, in NSCs. Scale bar: A, 5  $\mu\text{m}$ ; G,H 4  $\mu\text{m}$ .

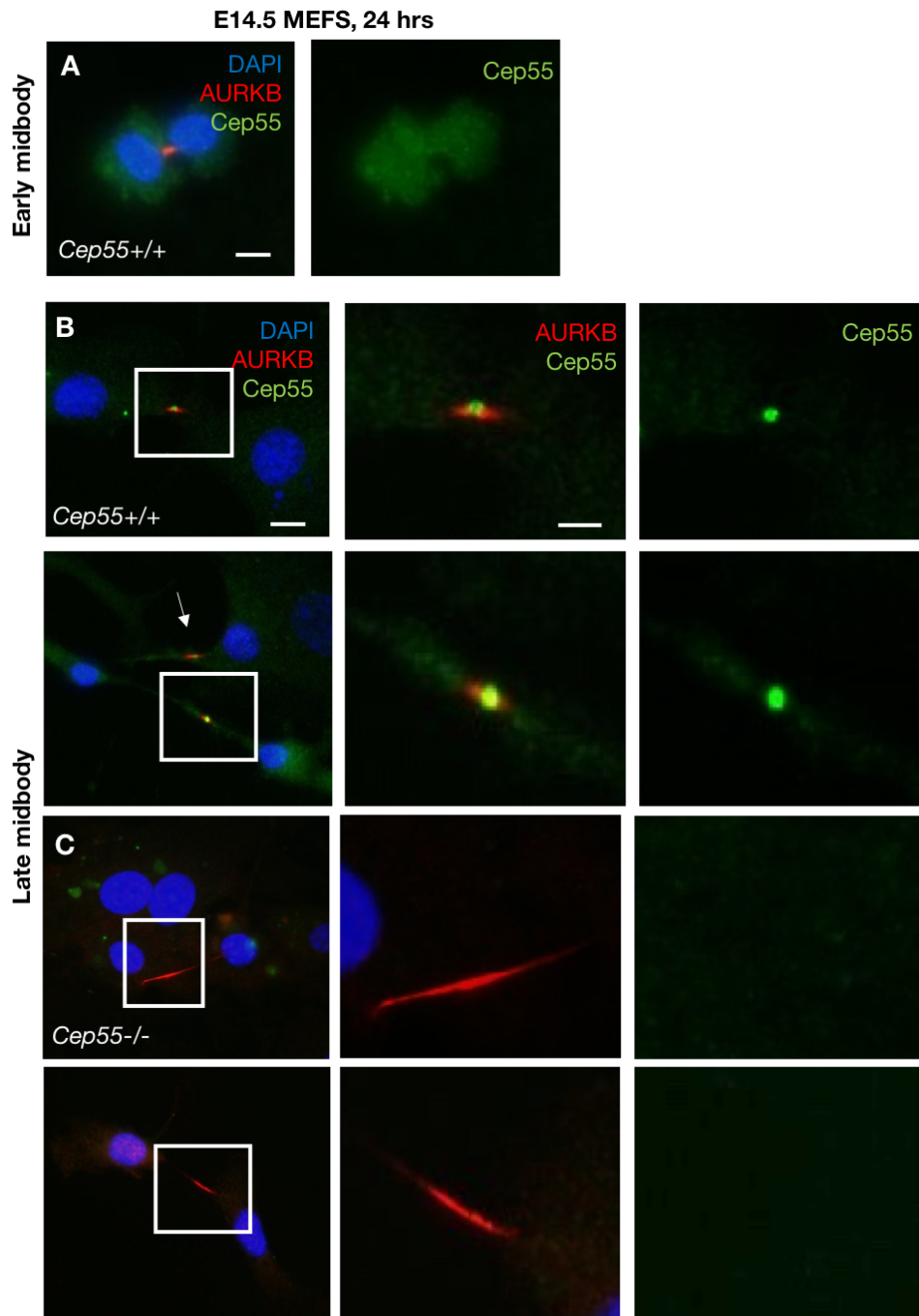


**Figure 17.** Cep55 is expressed in mouse embryonic fibroblasts at late abscission stages.

A-C. Mouse embryonic fibroblasts (MEFs) from control and Cep55 mutant embryos fixed at 24 hrs are labeled with Aurora B kinase to identify midbodies (red), Cep55 (green) and Dapi. Cep55<sup>+/+</sup> MEFs show a similar pattern of Cep55 expression as do apical and basal neural progenitor cells (See Figure 2): early-stage midbodies do not show specific Cep55 localization (A), but late-stage midbodies show Cep55 localized to the center of Aurora B+ midbody flanks (insets and arrow) (B). Cep55 localization to the midbody does not occur in mutant MEFs (C). Scale bars: B, 10  $\mu$ m; inset, 5  $\mu$ m.

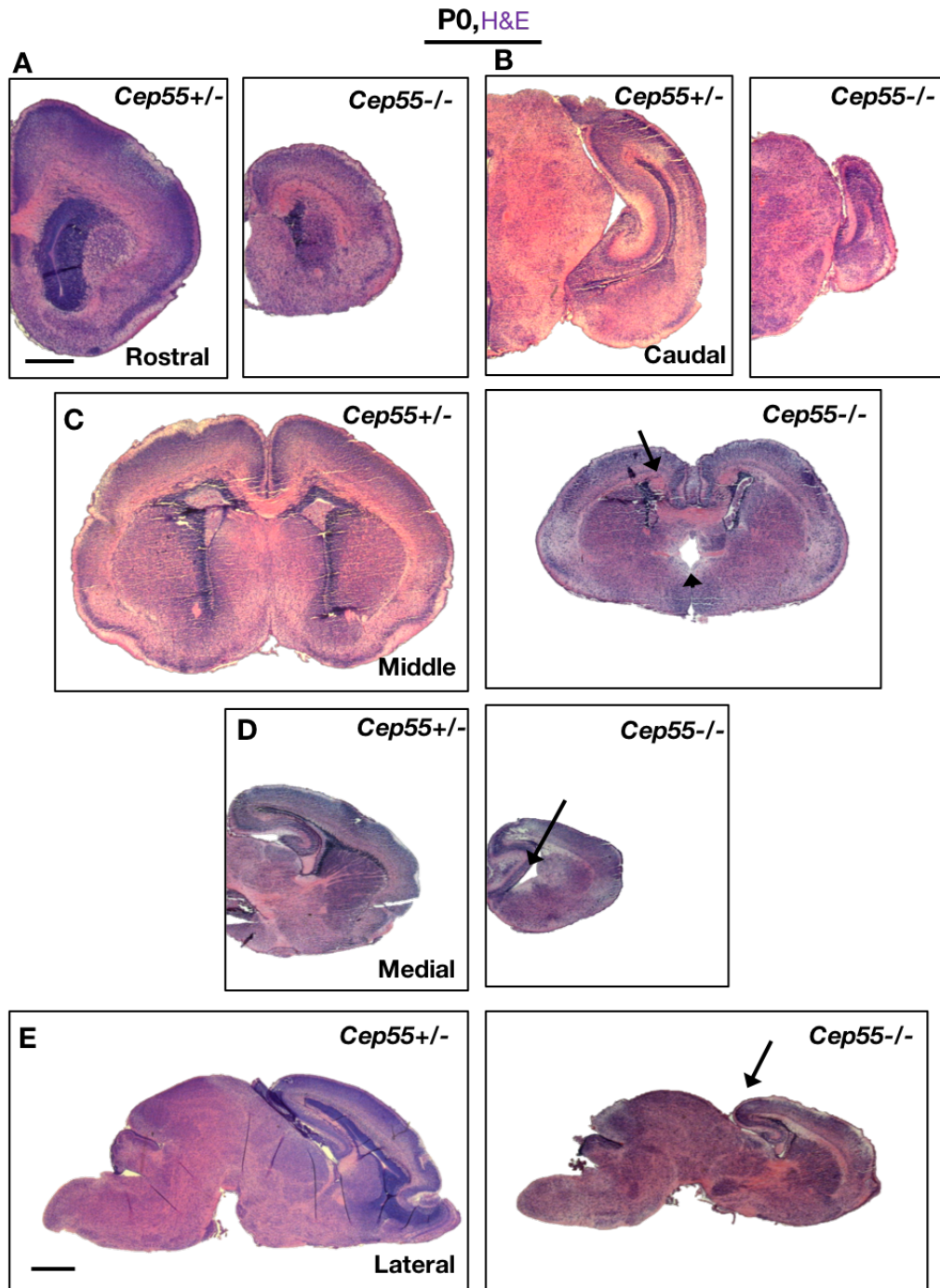


**Figure 18.** *Cep55* mutation results in globally reduced brain size and structural defects. **A-C.** *Cep55+/-* and *Cep55-/-* coronal sections are stained with hematoxylin and eosin (H&E) at birth (P0). Brain size is notably reduced in *Cep55* mutants at rostral, middle and caudal levels. Decreased cellularity is noted in the cortical epithelium of *Cep55* mutants. Proboscis bundles (**C**, right, arrow) and midline defects (**C**, right, arrowhead) are also observed. **D-E.** *Cep55+/-* and *-/-* sagittal sections are stained with hematoxylin and eosin (H&E). *Cep55* mutants have enlarged ventricles laterally (**D**, right, arrow) and a shorter cortex (**E**, right, arrow). N = at least 3 *Cep55+/-*, *+/-* and *-/-* mice for both coronal and sagittal sections. Scale bars: 500  $\mu$ m.

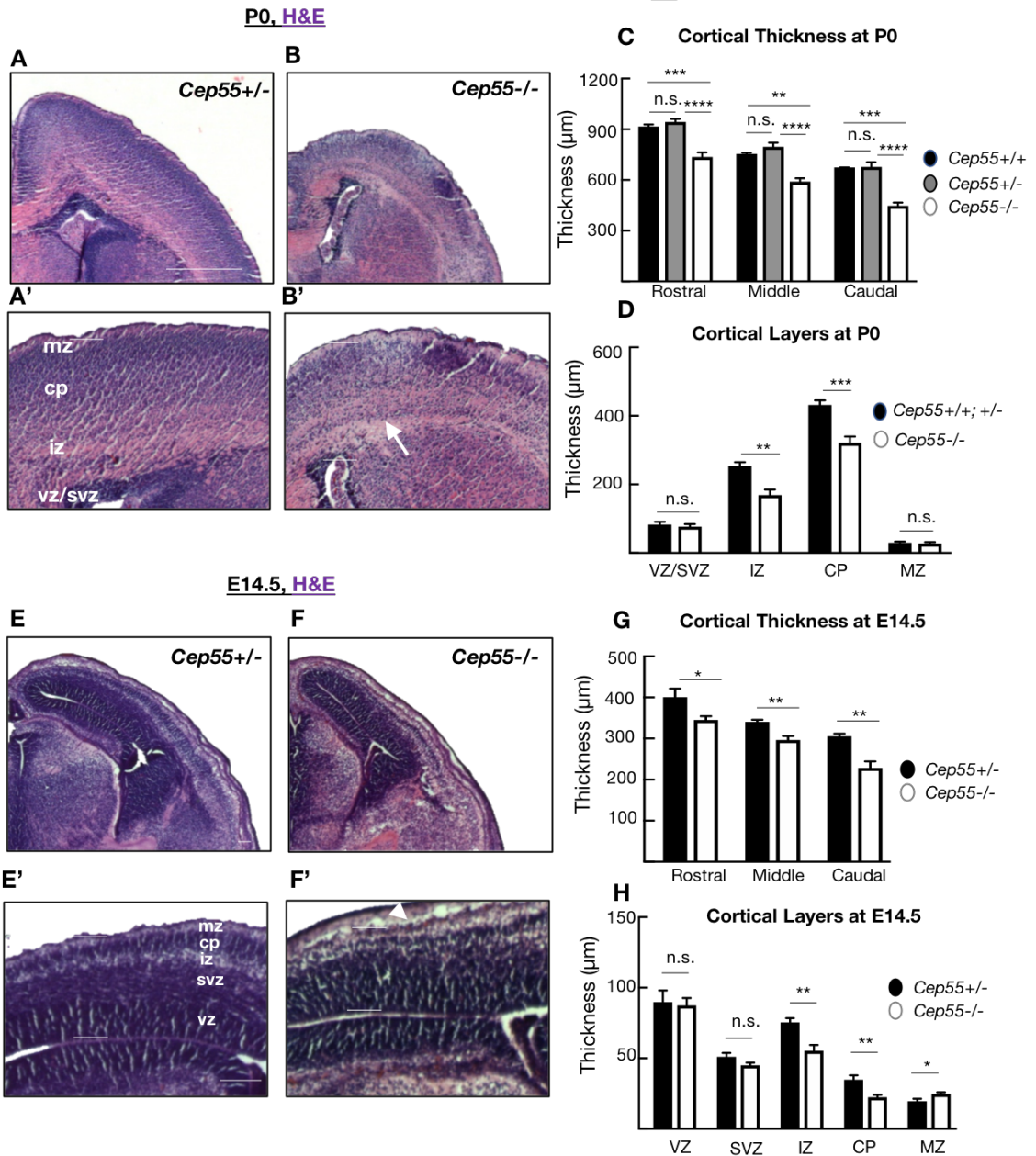


**Figure 19.** *Cep55* mutants have reduced cortical thickness due to reduction of neuronal layers. (continued on next page)

**Figure 19.** *Cep55* mutants have reduced cortical thickness due to reduction of neuronal layers.

**A-B.** Representative images of P0 *Cep55*<sup>+/-</sup> and *-/-* coronal, middle sections stained with H&E. (A',B'). The cortical thickness was measured between the marginal zone (mz) and ventricular zone/subventricular zone (vz/svz). *Cep55* mutants have reduced cellular density in neuronal layers (B', arrow). **C.** The cortical thickness in *Cep55* mutants is reduced in rostral (by 18%), middle (by 18%) and caudal (by 32%) sections compared to wild-type and heterozygote controls. **D.** The VZ/SVZ and MZ thickness are unaltered in *Cep55* mutants at P0, but the intermediate zone (IZ) and cortical plate (CP) are reduced by approximately 30%. **E-F.** Representative images of E14.5 *Cep55*<sup>+/-</sup> and *-/-* coronal, middle sections stained with H&E. (E',F'). The cortical thickness was measured between the vz and mz. *Cep55* mutants have a more prominent mz (arrowhead) **G.** The cortical thickness in *Cep55* mutants is reduced in rostral (14%), middle (12%) and caudal (25%) sections compared to wild-type and heterozygote controls. **H.** At E14.5, the vz and svz thickness in *Cep55* mutants are unaffected, but the iz and cp are approximately 30% thinner than controls. However, the mz is 20% thicker in *Cep55* mutants compared to controls. N for P0 (A-D) = 3 *Cep55*<sup>+/+</sup>, 5 *Cep55*<sup>+/-</sup> and 5 *Cep55*<sup>-/-</sup> mice; N for E14.5 (E-H) = 6 *Cep55*<sup>+/-</sup> and 5 *Cep55*<sup>-/-</sup> mice. Scale bars: A: 0.5 mm; C and E: 100  $\mu$ m; \* p < 0.05; \*\* p < 0.01; \*\*\* p < 0.001; \*\*\*\* p < 0.0001. C: one-way ANOVA; D, G and H: t-test.

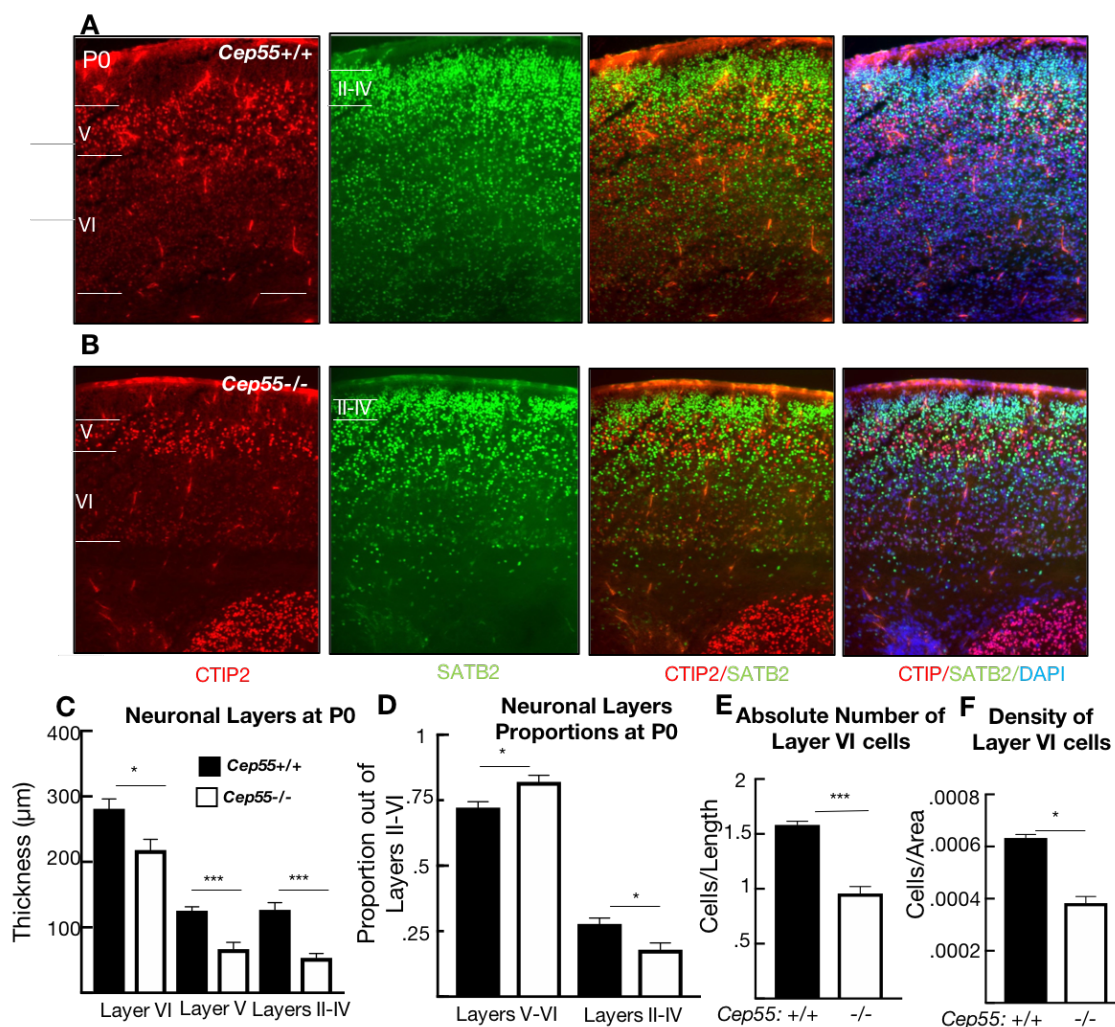


**Figure 20:** *Cep55* mutant cortices have thinner neuronal layers with decreased proportion of upper layers and decreased density of neurons.

**A-B.** Cortical layer order is not noticeably altered in *Cep55* mutants. Representative images of P0 *Cep55*<sup>+/+</sup> and *-/-* sagittal sections labeled with antibodies to *Ctip2*, marking layers VI (faint staining) and V (bright staining) and *Satb2*, marking layers II-IV. **C.** All neuronal layers are thinner in *Cep55* mutant cortices at P0; layer VI is decreased by 22%, layer V by 44% and layers II-IV by 59%. **D.** Layers V-VI take up a higher proportion and layers II-IV take up a decreased proportion of the cortical plate in *Cep55* mutants compared to wild-type controls. **E.** The absolute number of layer VI cells (nuclei/length of cortex) is reduced by 40% in *Cep55*<sup>-/-</sup> cortices. **F.** *Cep55*<sup>-/-</sup> layer VI neurons are 25% less dense than wild-type cells (nuclei/area). N for (C,D) = 5 *Cep55*<sup>+/+</sup> and 4 *Cep55*<sup>-/-</sup> mice; for (E,F) = 3 *Cep55*<sup>+/+</sup> and 3 *Cep55*<sup>-/-</sup> mice. Scale bar: A: 100  $\mu$ m. \*  $p < 0.05$ ; \*\*\*  $p < 0.001$ . C-F: t-test.

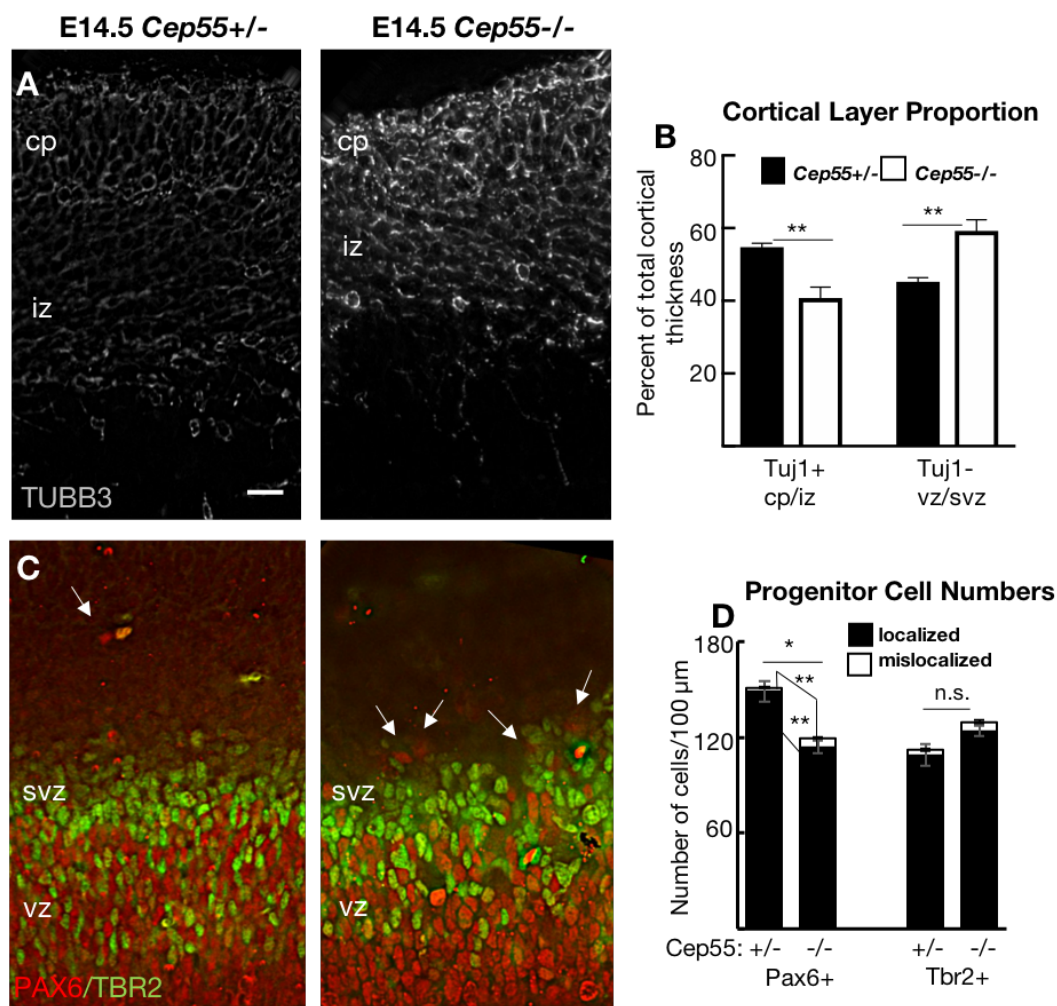


**Figure 21:** *Cep55* mutation results in altered proportions and disorganization of apical and basal progenitors.

**A-B.** The cortical epithelium in *Cep55* mutants at E14.5 (A, right) appears more disorganized than heterozygote controls (A, left). While most neurons (Tubb3<sup>+</sup>, gray, left and middle) have migrated to the basal cortex, the distinction between the cortical plate and the intermediate zone is less clear, and the cortical plate is disorganized with open spaces. **B.** At E14.5, the cortical plate and intermediate zone take up a decreased proportion of the cortex in *Cep55* mutants, while the ventricular and subventricular zones comprise an increased proportion. **C.** Apical and basal progenitor cell nuclei (Pax6<sup>+</sup>, red and Tbr2<sup>+</sup>, green respectively) are more disorganized in *Cep55* mutants (right) with more apical progenitor nuclei located basally (arrows). **D.** There are decreased numbers of Pax6<sup>+</sup> apical progenitors in *Cep55* mutant cortices per cortical length. The numbers of localized apical progenitors are decreased but the numbers of mislocalized apical progenitors are increased. There is no difference in the number of Tbr2<sup>+</sup> basal progenitors, whether localized or mislocalized, in *Cep55* mutant cortices. cp: cortical plate; iz: intermediate zone; svz: subventricular zone; vz: ventricular zone. N = 4 *Cep55*<sup>+/-</sup> and 4 *Cep55*<sup>-/-</sup> brains. Scale bar: (A): 20 μm. n.s.; not significant, \* p < 0.05; \*\* p < 0.01; \*\*\* p < 0.001

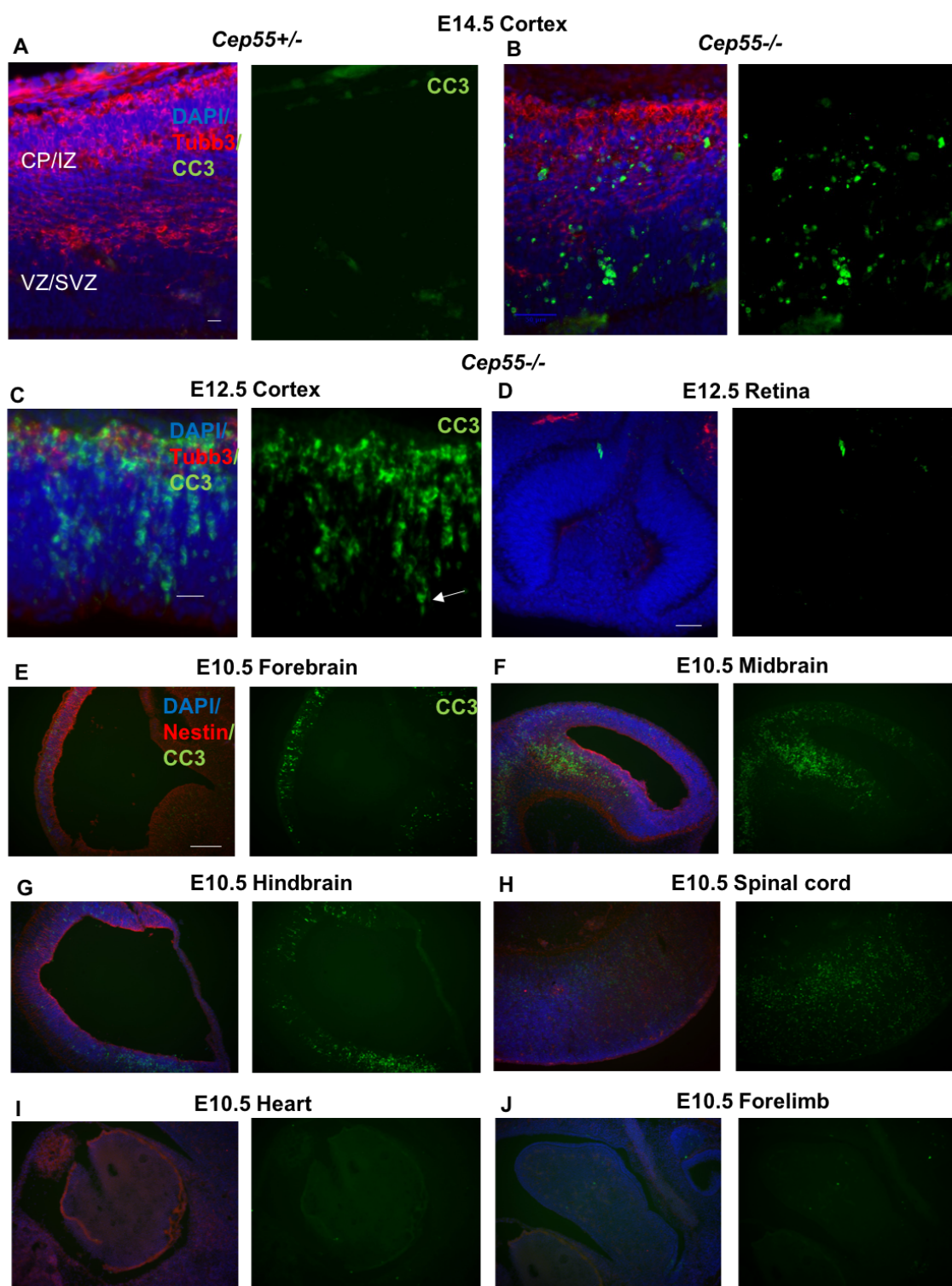


**Figure 22:** Apoptotic cells are specifically increased in *Cep55*<sup>-/-</sup> neural tissues.  
(continued on next page)

**Figure 22.** Apoptotic cells are specifically increased in *Cep55*<sup>-/-</sup> neural tissues.

**A-B.** We noted highly increased numbers of apoptotic cells (cleaved-caspase 3 (CC3) positive, green) throughout the cortical epithelium in E14.5 *Cep55* mutant cortices, while they were rarely observed in controls. Apoptotic cells were observed throughout the cortical plate and intermediate zone (Tubb3 positive, red) but were most increased in the ventricular zone (Tubb3<sup>-</sup>). **C.** At E12.5, even higher numbers of apoptotic cells were observed in the cortex of *Cep55* mutants than at E14.5, both in the thin Tuj1<sup>+</sup> neuronal layer and in the ventricular zone. Apoptotic cells appeared less pin-point than at E14.5, including some with processes reminiscent of radial glial cells (arrow). **D.** In contrast to the cortical epithelium, few apoptotic cells were observed in the retina of E12.5 *Cep55* mutants **E-J.** At E10.5, neurogenesis has not yet begun and apical progenitor cells divide symmetrically to produce more NSCs. At this age, apoptosis is highly increased in the forebrain of *Cep55* mutants (Nestin positive, red) (E). Apoptosis is not specific to the forebrain, as highly increased numbers of CC3 positive cells are also observed in the midbrain (F), hindbrain (G) and spinal cord (H). However, apoptosis is not observed in non-neural (Nestin<sup>-</sup>) tissues, such as the heart (I) and forelimb (J). N = 3 control and *Cep55* mutant brains (E12.5-E14.5) and embryos (E10.5) at each age. Scale bars: (A): 20  $\mu$ m (C): 20  $\mu$ m, (D): 40  $\mu$ m, (E): 200  $\mu$ m.

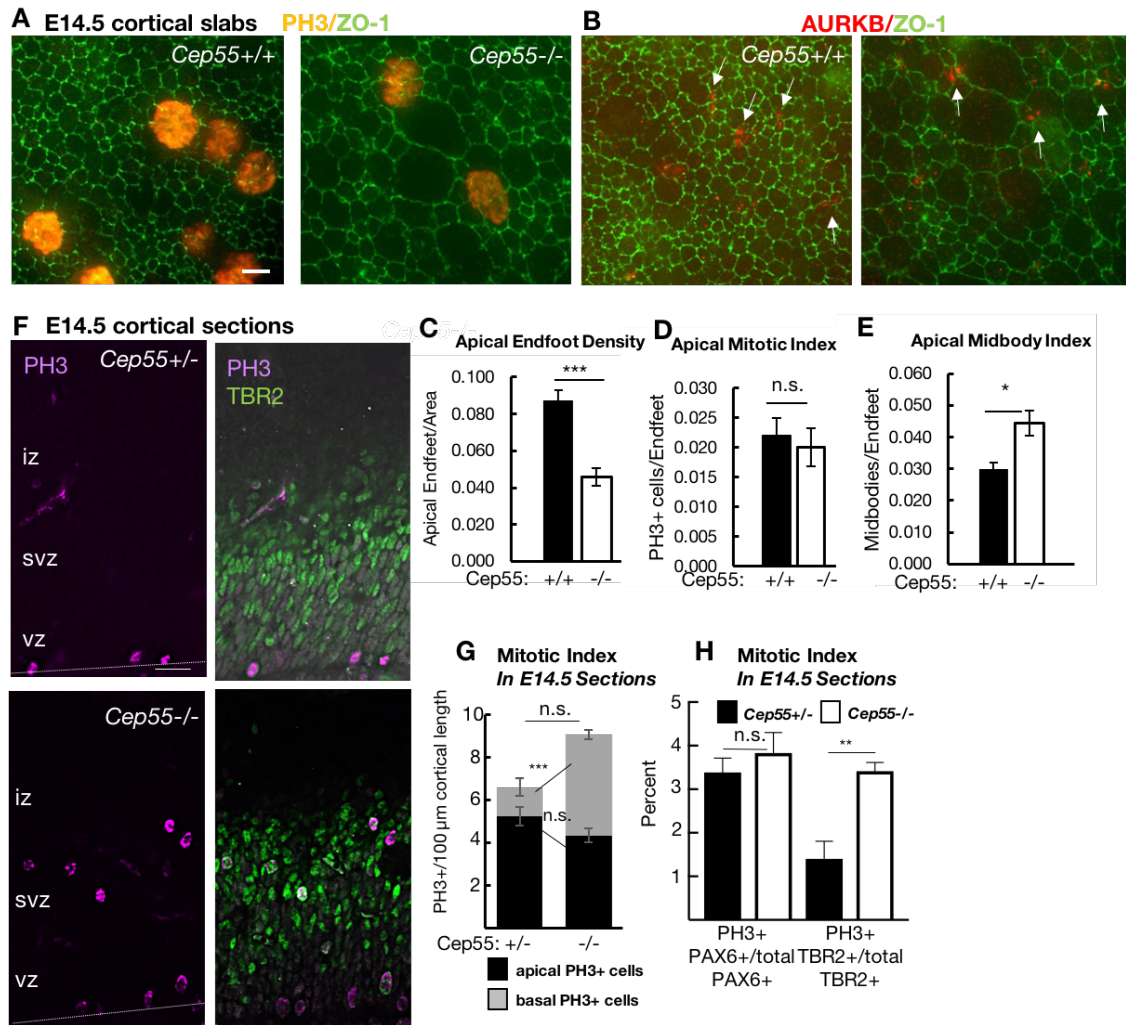
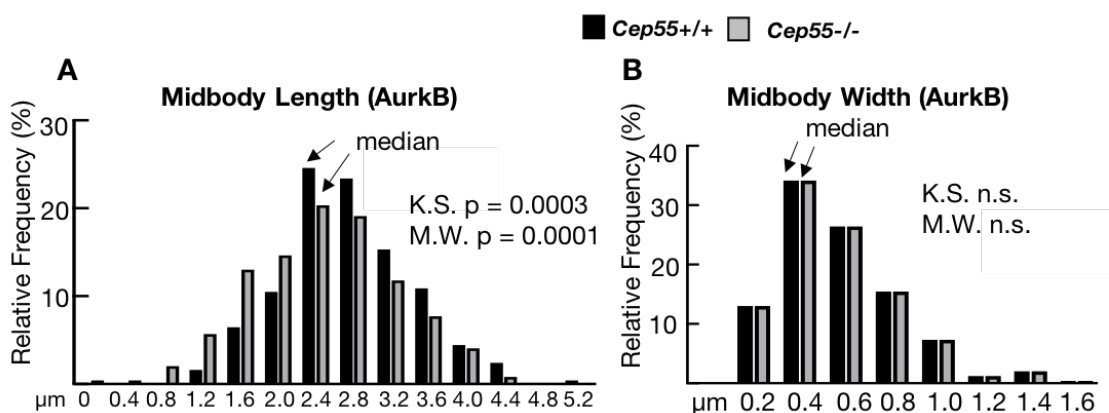


**Figure 23.** *Cep55* mutation results in defects in both cytokinesis and mitosis.

**A-B.** E14.5 cortical slabs were immunostained for Zona-occluden-1 (Zo-1, apical junctions), PH3 (mitotic cells), and AuroraB (midbodies). **C.** There is a significant decrease in the number of endfeet in the *Cep55* mutant. N= 6 slabs, 6 brains wild type, 7 slabs, 6 brains *Cep55* mutant **D.** There is no change in the number of mitotic cells per endfoot, **E.** but there is an increase in midbodies per endfeet suggesting defects in cytokinesis. N for D = 4 slabs, 4 brains wildtype and 5 slabs, 6 brains *Cep55* mutant. N for E = 5 slabs, 5 brains wild type and 5 slabs, 5 brains *Cep55* mutant. **F.** E14.5 *Cep55* mutant cortices show a normal number of mitotic cells (PH3+, magenta) at the apical membrane but an increased number of mitotic cells basally, the majority of which co-label with the basal progenitor marker *Tbr2* (green). **G.** The mitotic index (number of mitotic cells per cortical length) is not significantly increased in *Cep55* mutant E14.5 sections compared to heterozygote controls. Further analysis indicates that the apical mitotic index (mitotic cells at the apical membrane/cortical length) is normal, but the basal mitotic index (mitotic cells away from the apical membrane) is significantly increased. **H.** Co-labeling of mitotic cells with an apical progenitor marker (*Pax6*) and basal progenitor marker (*Tbr2*) shows that the mitotic index in apical progenitors is normal but in basal progenitors is significantly increased in *Cep55* mutants compared to heterozygote controls. N for (G,H) = 4 *Cep55*+/- and 4 *Cep55*-/- brains. Scale bars: A: 2  $\mu$ m; F: 20  $\mu$ m; n.s., not significant, \*  $p < 0.05$ ; \*\*  $p < 0.01$ ; \*\*\*  $p < 0.001$ . C-E, G-H: t-test.

### E14.5 NSC midbodies in cortical slabs



### E14.5 MEFs, 24 hrs

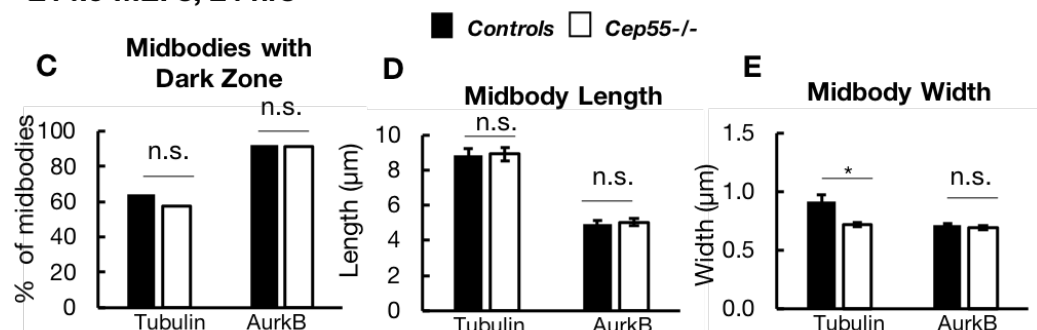


**Figure 24.** *Cep55* mutant midbodies have few structural abnormalities.

**A-B.** NSC midbodies in E14.5 *Cep55* mutant cortical slabs are shorter (A), but have normal width (B). Length and width determined by Aurora kinase B (AurkB) immunolabeling. Medians: A: *Cep55*<sup>+/+</sup> 2.71; *Cep55*<sup>-/-</sup> 2.48 µm. B: both 0.51 µm. For images, see Figure 6. **C.** Midbodies in E14.5 *Cep55* mutant mouse embryonic fibroblast (MEF) cells cultured for 24 hrs have a detectable dark zone (defined as absence of immunostaining) in a similar percentage of midbodies as control cells. **D-E.** Midbodies in E14.5 *Cep55* mutant mouse embryonic fibroblast (MEF) cells cultured for 24 hrs have normal length (D), but are thinner as determined by alpha-tubulin immunolabeling (E). For images, see Figure 8. N for (A-B) = 248 control and 246 mutant midbodies; for (C) = 402 control and 366 mutant midbodies; for (D-E) = 280 control and 202 mutant midbodies. n.s., not significant, \*  $p < 0.05$ . K.S., Kolmogorov-Smirnov test; M.W., Mann-Whitney test. C-E, t-test.

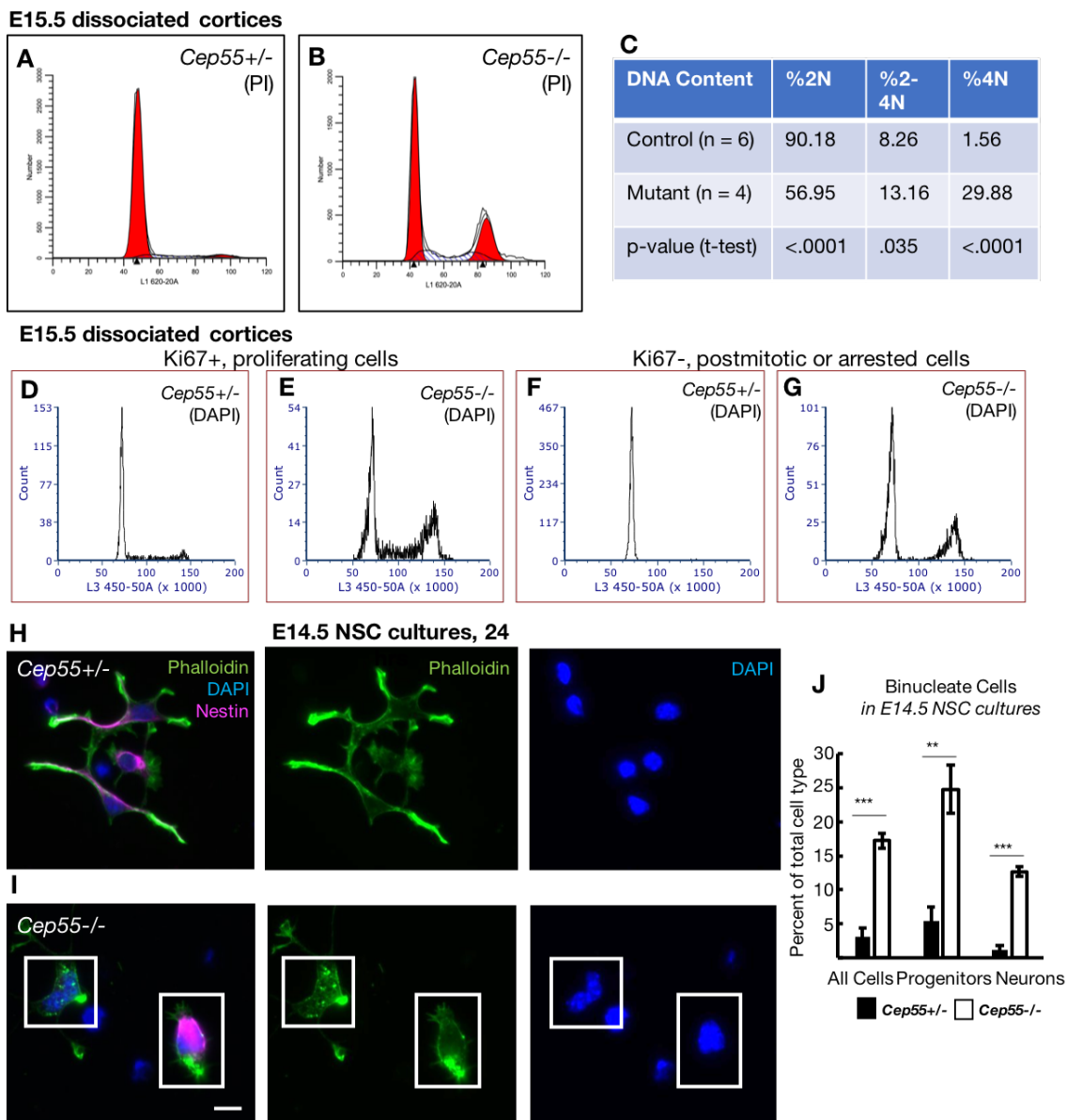


**Figure 25.** *Cep55* ensures successful completion of cytokinesis in neural stem cells.

**A-C.** Flow cytometric analysis of E15.5 control and *Cep55*<sup>-/-</sup> cortices using propidium iodide (PI) to analyze cell cycle parameters indicates a 15-fold increase in cells with tetraploid (4N) DNA content. The number of cells with 2N DNA content is reduced by approximately half. There is also a small but significant increase in cells with DNA content in-between 2 and 4N. **D-G.** Flow cytometric analysis of E15.5 control and *Cep55*<sup>-/-</sup> cortices using antibodies to Dapi and Ki67, a marker of proliferating cells, again shows an increase in cells with tetraploid DNA content in *Cep55* mutants. Notably, this increase of tetraploid cells is seen in both the Ki67<sup>+</sup> (D,E) and Ki67<sup>-</sup> (F,G) cell populations. **H-J.** Increased numbers of binucleate (defined as having two Dapi<sup>+</sup> nuclei with one cytoplasm, identified with Phalloidin labeling of actin structure) cells are seen in *Cep55* mutant NSC cultures dissociated from E14.5 brains at 24 hrs. There are increased numbers of both binucleate progenitors (Nestin<sup>+</sup>) and neurons (Nestin<sup>-</sup>). N (A-C) = 6 *Cep55*<sup>+/+; +/-</sup> and 4 *Cep55*<sup>-/-</sup> dissociated cortices; (D-G) = 5 *Cep55*<sup>+/+; +/-</sup> and 5 *Cep55*<sup>-/-</sup> dissociated cortices; (H-J) = 4 *Cep55*<sup>+/+; +/-</sup> and 4 *Cep55*<sup>-/-</sup> coverslips from 2 embryos each. n.s.; \*\*  $p < 0.01$ ; \*\*\*  $p < 0.001$ . Scale bar: I, 10  $\mu\text{m}$ .

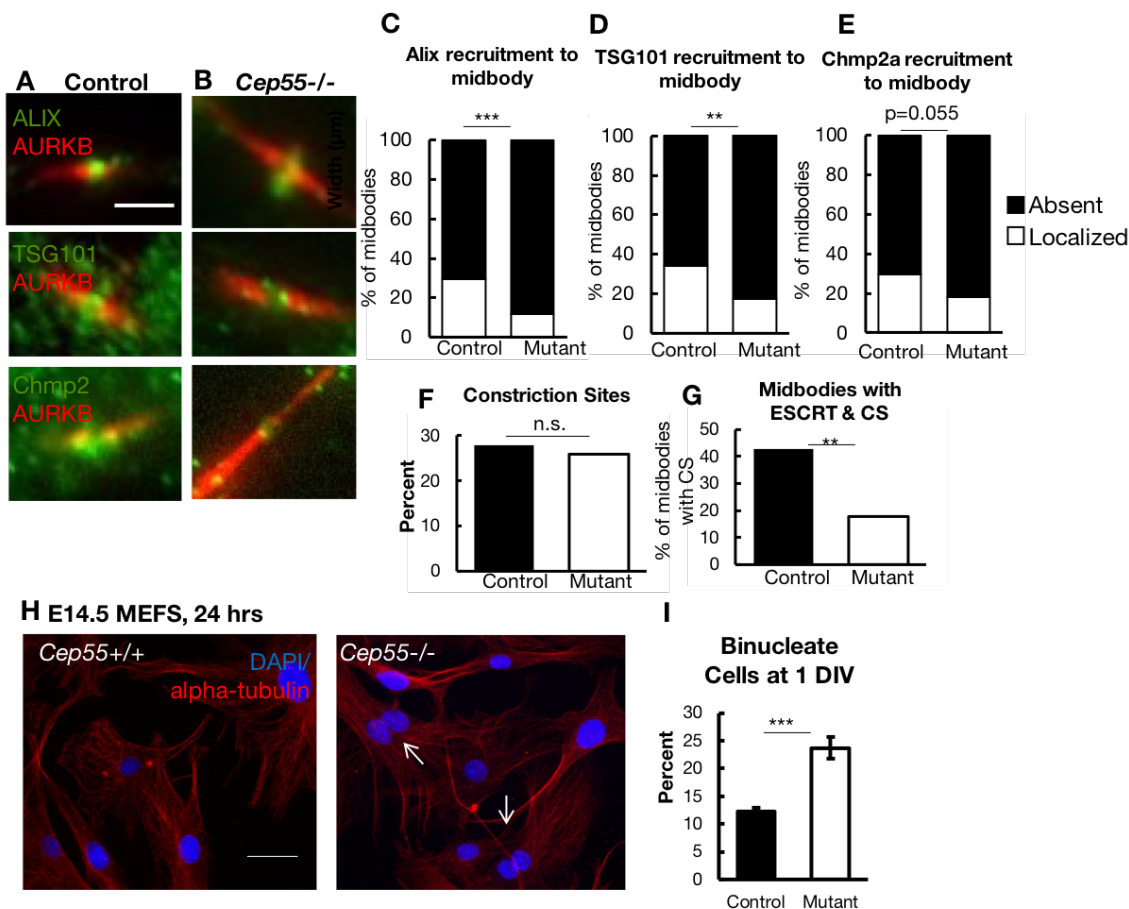


**Figure 26.** *Cep55* mutant MEFs have impaired but not eliminated abscission completion. **A.** Immunofluorescent labeling of AurorB (midbody) and ESCRT components Alix, TSG101, and Chmp2a on E14.5 mouse embryonic fibroblasts. **B.** Alix, TSG101, and Chmp2a are recruited to the midbody in the absence of *Cep55*. **C-E.** Quantification reveals a significant decrease in the percentage of midbodies with ESCRTs in *Cep55* mutant MEFs. Alix: control n=153 *Cep55* mutant n= 129 (4 animals, 4 coverslips, 3 experiments) ; Tsg101: control n= 141 *Cep55* mutant n= 132 (4 animals, 4 coverslips, 3 experiments); Chmp2a: control n=108 *Cep55* mutant n= 105 (3 animals, 3 coverslips, 3 experiments) **F.** *Cep55* mutant MEFs had a similar number of constriction sites as control MEFs. N= 402 control, 355 *Cep55* mutant ( 5 animals, 11 coverslips, 3 experiments) **G.** The number of midbodies with an ESCRT and a constriction site (CS) out of the number of midbodies with a CS is decreased in the *Cep55* mutant. N (midbodies with constriction sites) = 110 control, 95 *Cep55* mutant, (5 animals, 11 coverslips, 3 experiments) **H-I.** *Cep55* mutant mouse embryonic fibroblasts (MEFs) from E14.5 embryos have a two-fold increase in binucleate cells after 24 hours of culture. Binucleate cells were defined as having two Dapi<sup>+</sup> nuclei within one alpha-tubulin<sup>+</sup> cell body. N=5 *Cep55*<sup>+/+</sup> and 5 *Cep55*<sup>-/-</sup> coverslips from 3 embryos each. Scale bars: A: 2  $\mu$ m; H: 20  $\mu$ m. n.s., not significant, \* p < 0.05; \*\* p < 0.01; \*\*\* p < 0.001; \*\*\*\* p < 0.0001. C-G: Fisher's exact test; I: t-test. MEFs were passaged 1-2 times before the time points indicated.

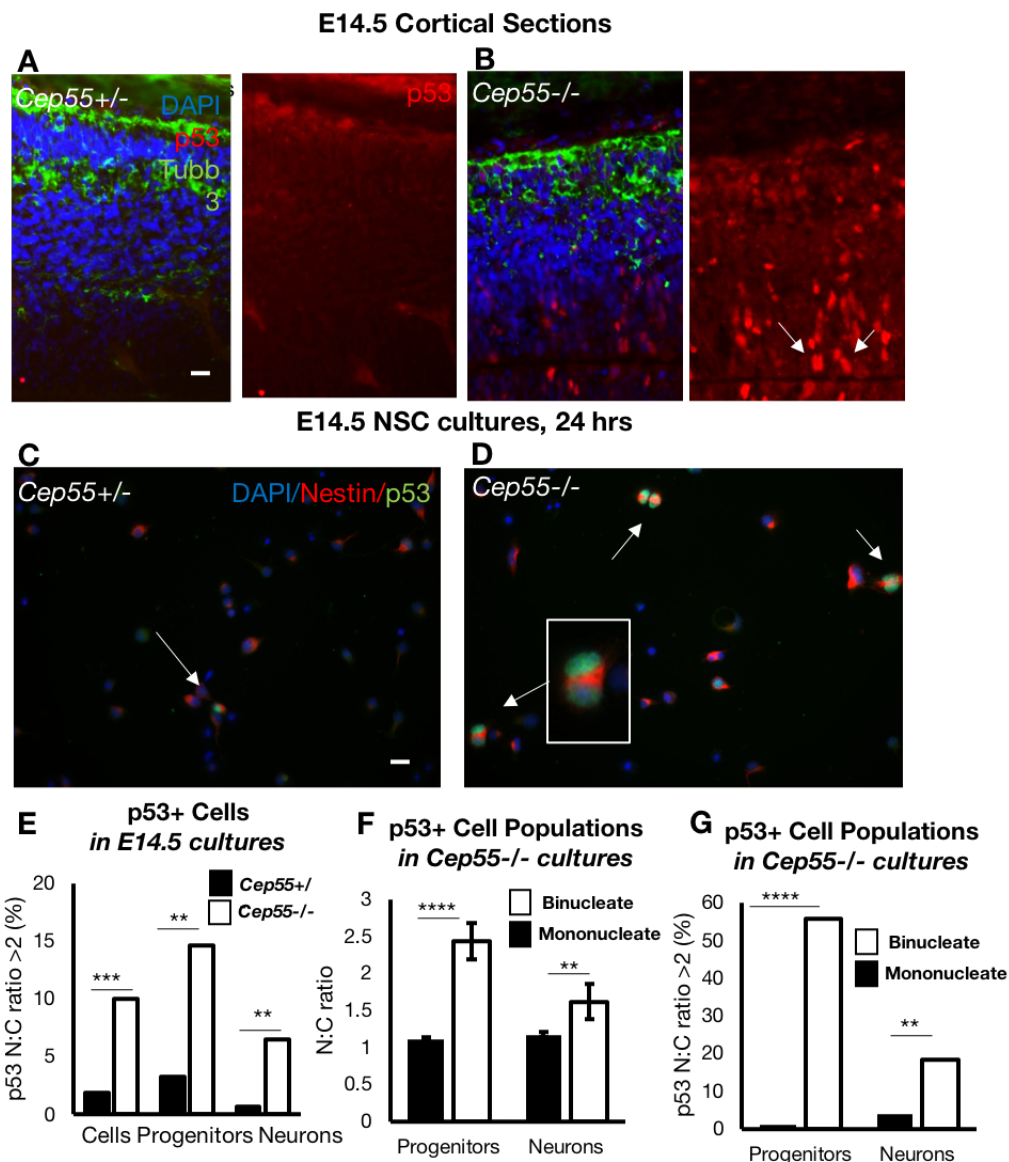


**Figure 27.** p53 nuclear expression is increased in binucleate cortical mutant cells.

**A-B.** While in control cortices cells with high nuclear p53 expression are rarely seen, they are greatly increased in Cep55 mutant E14.5 cortices (p53, red). The nuclei sometimes appear paired (arrows). p53+ cells are more often found in the ventricular zone than neuronal layers (marked by Tubb3, green). **C-E.** Cep55 mutant NSC cultures have approximately a 3-fold increase in the number of cells with a p53 nuclear:cytoplasmic ratio of >2 (labeled with antibodies to p53, green). While these cells can sometimes be detected in control cultures, they are more often seen as single nuclei (C, arrow), while in Cep55 mutant cultures they are usually observed as paired nuclei (D, arrows). The p53 N:C ratio is increased in both Cep55 mutant progenitors (Nestin+, red) and neurons (Nestin- red). **F.** In Cep55 mutant cultures, the p53 N:C ratio is significantly higher in binucleate progenitors and neurons compared to mononucleate cells. **G.** More than 50% of binucleate progenitors in Cep55 mutant cultures have a p53 N:C ratio > 2 compared to only 1% of mononucleate cells. Approximately 20% of binucleate neurons have a p53 N:C ratio of >2 compared to 2% of mononucleate cells. Thus, increased p53 expression in Cep55 mutant cultures is specifically found in binucleate cells. N (A-B) = 3 Cep55+/+; +/- and 3 Cep55-/- brains; (E-G) = 4 Cep55+/+; +/- and 4 Cep55-/- coverslips from 2 embryos each. Scale bars: A, C 20  $\mu$ m. n.s., \*\* p < 0.01; \*\*\* p < 0.001; \*\*\*\* p < 0.0001.

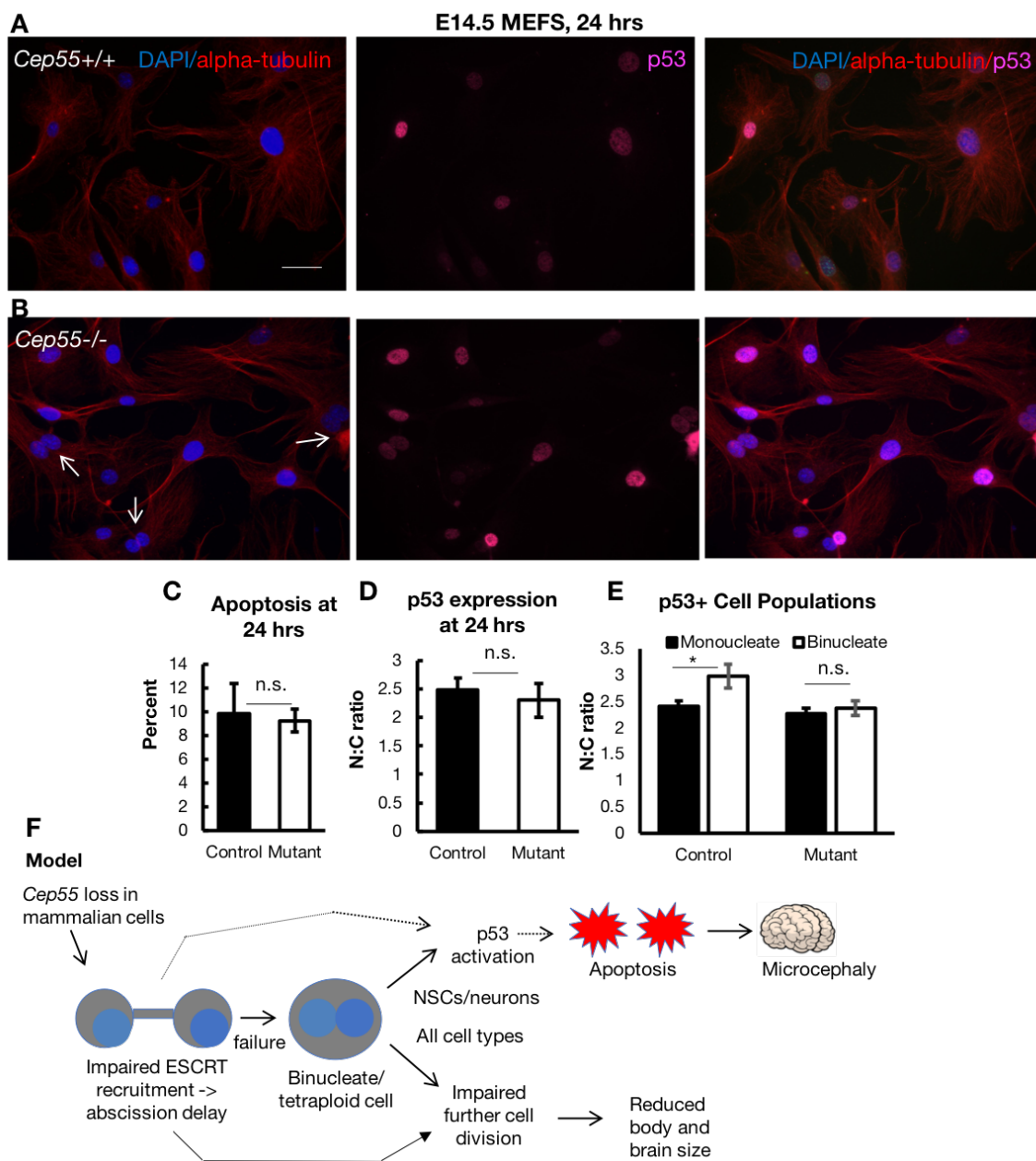


**Figure 28.** Despite impaired cytokinesis, *Cep55* mutant MEFs do not have increased p53 expression or apoptosis. (continued on next page)

**Figure 28.** Despite impaired cytokinesis, Cep55 mutant embryonic fibroblasts do not have increased p53 expression or apoptosis.

**A-E.** Cep55 mutant mouse embryonic fibroblast cultures (MEFs) have increased numbers of binucleate cells (see Figure 7). (C) However there is no difference in the number of apoptotic cells (CC3+) compared to controls after 24 hrs of culture. (D) Furthermore, there was no difference in the nuclear:cytoplasmic ratio of p53 expression (p53, pink, middle and right images) in Cep55 mutant MEFs compared to controls. (E) Unlike Cep55 mutant NSCs and neurons, binucleate Cep55 mutant MEFs had no difference in p53 expression compared to mononucleate cells. **F.** Our data is consistent with the reported role for Cep55 in cytokinetic abscission, but suggests it may not be absolutely required for abscission as has been proposed. Cep55 mutant cells have impaired ESCRT recruitment and indications of abscission delay. Interestingly, cells lacking Cep55 localization to the midbody are capable of completing abscission. However, at least some Cep55 mutant cells fail to complete cytokinesis resulting in increased binucleate, and possibly tetraploid cells. While abscission defects and binucleate cells are observed in both Cep55 mutant neural cell types and MEFs, p53 activation and apoptosis are only noted in neural tissues. Thus, we propose that a differential apoptotic response to cytokinesis failure may occur in specific cell types. This model provides an explanation for the increased severity of Cep55 mutant brain phenotypes in comparison to other tissues. Further work is needed to determine whether p53 activation and apoptosis are a direct or indirect consequence of cytokinesis failure in NSCs and neurons. N: (C) = 3 control and 3 Cep55<sup>-/-</sup> coverslips from 3 embryos each; (D) = 195 control and 232 mutant cells from 3 control and Cep55<sup>-/-</sup> coverslips and embryos each; (E) = 153 mononucleate and 25 binucleate control cells and 158 mononucleate and 68 binucleate mutant cells from 3 coverslips and 3 embryos each. Scale bar: A, 20  $\mu$ m. n.s., not significant; \* p < 0.05. MEFs were passaged 1-2 times before the time points indicated.

## Chapter 4: *p53* inhibition accelerates cortical neuron polarization

### Abstract

*p53* is a known regulator of multiple facets of cell behavior, including the maturation of several cell types. However, the role of *p53*, if any, in cortical neuron growth and maturation is unclear. Here, we use a *p53* knockout mouse to investigate the role of *p53* in the normal development of cortical neurons. We find that *p53* deletion accelerates cortical neuron polarization *in vitro*, compelling neurons to more rapidly transition out of a multipolar state, extend their axons and become polarized. We additionally show that *p53* mutant neurons have more mature morphological characteristics, including longer and thinner axons, thinner minor neurites, shorter filopodia, and increased expression of acetylated tubulin. Bulk RNA sequencing data of embryonic *p53* mutant cortices confirms significant changes in genes related to axonogenesis. We previously discovered that *p53* deletion partially rescues microcephaly in a kinesin-6 (*Kif20b*) mutant. *Kif20b* mutants have impaired neuron polarization and axon outgrowth. Interestingly, we find that polarization defects in *Kif20b* mutant neurons are *p53*-independent. Thus, we conclude that *p53* and *Kif20b* function independently with opposing roles in neuron outgrowth.

### Introduction

The transcription factor *Trp53* has diverse roles in various cell types, including in cellular division, survival, differentiation, morphology and movement. It is well known for its role as a tumor suppressor, as the most commonly mutated protein in human cancer (Kasthuber & Lowe, 2017). However, the varied and numerous reported roles of *p53* have also led to confusion over its fundamental functions. It has been reported to paradoxically promote and inhibit stemness, differentiation, proliferation and cell cycle exit. In post-mitotic neurons, there is evidence of a role for *p53* in both the promotion and inhibition of neuronal differentiation and maturation; therefore, its function, if any, is unclear (Di Giovanni et al., 2006; Di Giovanni & Rathore, 2012; Ferreira & Kosik, 1996; Qin et al., 2009).

The *p53* knockout mouse provides valuable insight into the essential roles of the protein. Surprisingly, mice lacking *p53* usually develop normally with no noticeable differences in body or brain size or morphology (Donehower et al., 1992). However, approximately 10% of *p53* mutants develop exencephaly due to lack of normal apoptosis in the central nervous system during neural tube closure (Sah et al., 1995). Additionally, within a few months of birth *p53*

mutants develop sporadic tumors with high penetrance. Mice heterozygous for *p53* also develop tumors, but at a later age (Jacks et al., 1994). Although the *p53* mutant phenotype indicates that *p53* is not essential for normal development, other evidence demonstrates that *p53* is active during development, ready to respond if a problem should arise (Jain & Barton, 2018). Several mouse mutants with microcephaly and/or dwarfism have shown remarkable rescue of brain and/or body size by crossing to the *p53* mutant to inhibit *p53* activity (Insolera et al., 2014; Little & Dwyer, 2019; Pao et al., 2014). This seems to be primarily through inhibition of *p53*-dependent apoptosis, demonstrating *p53*'s essential role in activating cell death pathways in abnormal cells. Recently, we found *p53* to be essential in the etiology of microcephaly in a kinesin-6 mutant that has defects in cytokinetic abscission (Little & Dwyer, 2019). Strikingly, even heterozygous loss of *p53* completely rescued apoptosis and significantly ameliorated the *Kif20b* mutant small brain phenotype. However, *Kif20b;p53* double mutant brains were still smaller than controls at birth, indicating that additional *p53*- independent functions of *Kif20b* contributed to microcephaly.

In order to understand *p53*'s critical role in microcephaly etiology, it is necessary to establish the normal role of *p53* in cortical development. Conflicting reports indicating a role for *p53* in both promoting and inhibiting cortical neuron maturation make it an open question whether *p53* mutant cortical neurons polarize and mature normally. To address this, we cultured cortical neurons from wild-type and mutant *p53* littermate controls *in vitro* and evaluated polarization and morphology using an established assay (Barnes & Polleux, 2009; C G Dotti et al., 1988). We hypothesized that *p53* mutant neurons would polarize and mature normally, given the preserved brain size and structure of *p53* mutants. Surprisingly, we found instead that *p53* mutant cortical neurons have accelerated polarization and maturation *in vitro*. Interestingly, this is not simply due to a role for *p53* in cortical neuron survival.

Having established the consequence of *p53* mutation on cortical neuron differentiation in our *in vitro* assay, we next evaluated the role of *p53* in *Kif20b* mutant neuron morphology. Previously, we showed that *Kif20b* has a cell-autonomous role in promoting cortical neuron polarization and maturation, with neurons from the *Kif20b* mutant being less polarized and mature (McNeely et al., 2017). Given our finding that *p53* functions in neurons to decelerate polarization, we hypothesized *Kif20b* mutant neuron morphology defects were a consequence of *p53* activation. Instead, we found that *Kif20b;p53* mutant neurons still have reduced polarization and less mature neuron morphology compared to neurons from *p53* mutants. Together, these data indicate that

p53 normally inhibits too-fast cortical neuron differentiation *in vitro*, and that p53 and Kif20b have opposing, independent roles in this process.

## Results

### Loss of p53 accelerates cortical neuron polarization *in vitro*

We first tested whether p53 function is required for normal polarization of isolated cortical neurons *in vitro*. When embryonic cortical pyramidal neurons are dissociated and cultured, they re-establish polarity and progress through defined stages (Dotti et al., 1988). Neurons first begin round in structure (Stage 1) and then shift to multipolar cells by extending undifferentiated neurites of equal length (Stage 2). Finally, a single neurite rapidly elongates to become the axon, resulting in polarization (Stage 3). We began by examining cortical neuron cultures from control and *p53* mutant brains at E14.5 after two days *in vitro* (DIV) (Fig.29A). We observed that after two DIV, approximately 20 percent of neurons were polarized (stage 3, with one neurite at least twice as long as the next longest neurite) in control cultures. Interestingly, we found a 27 percent increase in polarized and 21 percent decrease in multipolar (stage 2) neurons in *p53* mutant cultures, suggesting that p53 typically functions to inhibit the progression from stage 2 into stage 3 (Fig. 29C).

To investigate the time-frame within which *p53* mutant neuron polarization was accelerated, we evaluated whether neuron polarization abnormalities were detectable at an earlier time point. We examined cortical neurons cultures fixed after just one DIV (Fig. 29A). Interestingly, we found more than a 2-fold increase in polarized neurons in mutant cultures compared to control at one DIV (Fig. 29B). In control cultures, approximately half as many neurons were polarized at one DIV as were at two DIV. In mutant cultures, however, there were only 17 percent fewer polarized neurons at one DIV compared to two (Fig. 29B,C). Because the percentage of polarized neurons in mutant cultures after one DIV was much higher than that of the control cultures, and because mutant neurons experienced a smaller increase in polarized neurons from one DIV to two DIV, we can conclude that *p53* deletion accelerates the process of neuron polarization primarily within the first 24 hours of plating. This suggests that typically, p53 functions to inhibit or slow early polarization. We hypothesized that accelerated neuron polarization might be secondary to roles of p53 in cell survival, given its known role as an apoptosis activator. Surprisingly, we found no

difference in apoptosis, neuronal cell density and cell identity in *p53* mutant cultures, and no increase in proliferation (Fig. 30). Thus, it is more likely that *p53*'s role in neuron outgrowth is cell autonomous.

### ***p53* mutant polarized neurons have longer axons and thinner processes**

We next investigated whether *p53* has functions in neuron morphology in addition to neuron polarization. We hypothesized that accelerated polarization in mutant neurons might result in more mature neuron characteristics. As neurons mature, they specify an axon which continues to extend; this extension has also been associated with a decrease in axon width and axon branching. Additionally, minor neurites extend as well, although this occurs on a different time-scale than axon extension (Dotti et al., 1988). Consistent with our hypothesis, *p53* mutant neurons have significantly longer axons at 2 DIV (Fig. 31A-C). However, there were no differences in the length of *p53* mutant minor neurites and the average number of minor neurites per cell (Fig. 32A-C). Furthermore, *p53* mutant axons did not show any significant differences in the number or length of axon branches compared to controls after two DIV (Fig. 31A, D). While *p53* mutation did not affect axon branching, the total axon length, calculated by adding axon length to branch length, in the *p53* mutant neurons was still significantly increased, supporting the robust nature of the longer-axon phenotype (Fig 31E).

Because *p53* deletion accelerates neuron polarization within the first 24 hrs of plating, we also investigated axon length at one DIV. While the axon length of both control and mutant neurons was reduced compared to two DIV, mutant axons were still approximately 15% longer than control axons (Fig. 31A). The rate of axon extension between 24 and 48 hrs was not significantly different in *p53* mutants compared to controls, indicating that increased axon extension in *p53* mutants primarily occurs in the first 24 hrs. This observation provides further evidence that *p53* functions to slow neuronal maturation primarily by targeting axon outgrowth, interestingly not affecting the length or abundance of minor neurites or axon branches.

Next, we tested whether the strengthened polarity characteristics of *p53* mutant neurons altered axon and minor neurite width. In mature pyramidal neurons, the axon is long and thin, while dendrites are shorter, wider, and more tapered. Therefore, we measured the widths of axons and minor neurites at given distances from the cell body, using neuronal (beta-III) tubulin staining

(Fig. 33). Surprisingly, in culture, both the axons and minor neurites of *p53* mutant neurons were significantly thinner than controls (Fig. 33A-D). At 5 and 10 microns from the soma, mutant axons were approximately 30 percent thinner than controls and mutant minor neurites were approximately 25 percent thinner. Because axon and minor neurite width decreases with tighter microtubule packing, it is possible that *p53* typically promotes wider neurites by inhibiting such tight packing. Together, these analyses demonstrate that *p53* is required for multiple aspects of cortical neuron polarization and maturation.

### ***p53* mutant cortical neurons have shorter axonal filopodia**

Normal axon growth is defined by multiple subprocesses. Axons, axon branches, and minor neurites can all be tipped by growth cones, an actin-rich motile cap thought to be important in directing axon elongation (Lowery & Vactor, 2009). Filopodia, long, thin extensions with a dense actin core, extend out from the periphery of the growth cone. Microtubules also play an integral role in axon growth and form major dynamic frameworks in the shaft of the axon. Both stable microtubules in the axon and actin bundles in the growth cone are thought to be signs of axon growth. Furthermore, larger axonal growth cones are associated with the initiation of axon outgrowth (Bradke & Dotti, 1997).

Hippocampal neurons over-expressing *p53* possess larger axonal growth cones and longer branched filopodia (Qin et al., 2009). Thus, we wanted to examine the effect of *p53* deletion on axonal growth cone and filopodia morphology in polarized cortical neurons. Surprisingly, we found that there was no significant difference between control and *p53* mutant growth cone areas (Fig. 34D). *p53* mutant growth cones also did not differ significantly in the number of filopodia per growth cone (Fig. 34B). However, consistent with previous findings, *p53* mutant filopodia were significantly shorter than control axonal filopodia (Fig. 34C).

### ***p53* mutant cortical neurons have increased acetylated tubulin**

Microtubule stability in the axon is characteristic of polarized neurons, and higher levels of acetylation have been shown to correlate with increased microtubule stability. Moreover, in polarized neurons, higher proportions of acetylated microtubules are found in the axonal shaft compared to the shafts of minor neurites (Witte & Bradke, 2008). Likewise, we found higher

proportions of acetylated tubulin in the axon of *p53* mutant polarized neurons (Fig. 35). We subsequently segregated neurons into categories determined by axon length and discovered significantly increased acetylation across all axon lengths. However, mutant axons longer than 100 $\mu$ m showed even higher proportions of acetylation compared to shorter axons. Together, these analyses provide evidence that *p53* deletion promotes neuronal maturity, characterized by longer, more acetylated axons and shorter filopodia.

### **Promotion of cortical neuron maturation by *Kif20b* function is *p53*-independent**

We previously showed that loss of the Kinesin-6 family member *Kif20b* in mice results in microcephaly due to defects in cell division as well as neuronal maturation defects (Dwyer et al., 2011; Janisch et al., 2013; McNeely et al., 2017). Moreover, we found that microcephaly in the *Kif20b* mutant is primarily due to *p53*-dependent apoptosis, as *p53* deletion largely rescues apoptosis and brain size (Little & Dwyer, 2019). Interestingly, heterozygote and homozygous deletion of *p53* equally rescue apoptosis and brain size. Because data reported here indicate that *p53* normally inhibits cortical neuron polarization, we hypothesized that *p53* activation in the *Kif20b* mutant could be the cause of polarization defects. To address this, we cultured neurons from *Kif20b;p53* wildtype, *Kif20b* mutant *p53* heterozygote, *Kif20b* wildtype *p53* mutant and *Kif20b;p53* mutant cortices. Despite having rescued apoptosis and brain size, we found that neurons cultured from *Kif20b* mutant *p53* heterozygote cortices replicated our previous findings from *Kif20b* mutant *p53* wild-type cortices, specifically fewer polarized neurons and shorter axons compared to wild-type controls (Figure 36A-B). This demonstrates that neuron morphology defects in the *Kif20b* mutant are not simply secondary to apoptosis or smaller brain size. We also noted that *Kif20b;p53* mutant neurons were similar to wild-type neurons in both polarization status and axon length. However, if neuron morphology defects in the *Kif20b* mutant were *p53*-dependent, *Kif20b;p53* mutant neurons should be similar to *p53* mutant neurons. Instead, *Kif20b;p53* mutant neurons exhibited significantly decreased polarization and axon length compared to *p53* mutant neurons (Figure 36A-B). Therefore, we conclude that neuron maturation defects in the *Kif20b* mutant are *p53*-independent. *p53* deletion can rescue neuron polarization and axon length in the *Kif20b* mutant to wild-type levels only because of the independent role of *p53* in accelerating these parameters.

### ***p53* but not *Kif20b* mutant cortices have global changes in expression of neuronal maturation genes**

As p53 functions molecularly as a transcription factor, we hypothesized that p53's role in inhibiting neuronal maturation could be multi-factorial. To investigate this possibility, we performed bulk mRNA sequencing of wild-type and *p53* mutant cortices at embryonic day 11, the start of neurogenesis. While our *in vitro* analyses were performed from embryonic day 14 neurons, they were allowed to repolarize in culture, and we noticed the most dramatic p53-dependent effects in the first 24 hours. Therefore, we chose E11 as an early time point in the polarization of first-born neurons.

At a significance level of  $p_{adj} < \text{or} = 0.05$ , we found 8 significantly upregulated genes and 15 significantly downregulated genes in *p53* mutant samples. Upregulated genes include the previously validated targets *Fam49a* and *Xaf1* (Table 2). Related to neuronal development, we saw upregulation of calcium channel genes *Stac* and *Cabp1*, and of the synaptic vesicle modulator *Cplx2*. Downregulated genes included *Trp53*, as expected, as well as several extracellular matrix genes (*Krt5*, *Fbn1*, *Hmcn1*) and other previously validated p53 targets (*Eda2r*, *Ccng1*) (Table 3). Our sequencing results support a role for p53 in post-mitotic neuron maturation. Axonogenesis was a significantly enriched gene ontology analysis (GOA) term, comprising both up- and down-regulated genes (Tables 4-5). While GOA of all significantly downregulated genes in the *p53* mutant showed enrichment for a diverse array of developmental processes (data not shown), we were surprised to find that GOA of significantly upregulated genes showed only enrichment for terms specific to neuronal maturation (Table 6). Distal axon, glutamatergic synapse, postsynapse, synaptic membrane, cell body, somatodendritic compartment and synaptic vesicle membrane were significantly enriched cellular compartments, and neuron projection development, modulation of chemical synaptic transmission, vesicle-mediated transport in a synapse, and protein transport within a lipid bilayer were significantly enriched biological processes. Some up- and down-regulated targets of p53 involved in neuronal maturation have been previously validated, notably *Unc5b*, a repulsive guidance cue (Tanikawa et al., 2003).

Contrary to the *p53* mutant, the *Kif20b* mutant and *Kif20b;p53* double mutant did not show significant GO enrichment of neuronal maturation terms (data not shown). This was expected, as *Kif20b*'s role as a kinesin is likely to be post-transcriptional, in microtubule bundling and

transport of axonal proteins. Taken together, this sequencing data supports the existence of a p53-dependent transcriptional program that serves to downregulate neuronal maturation genes, and a post-transcriptional role for Kif20b in proper neuron structure.

## Discussion

Here we report a definitive role for p53 in inhibition of the early stages of cortical neuron polarization and axon morphology *in vitro*. While p53 has been previously implicated in this process, results were conflicting and made it unclear whether p53 deletion would result in accelerated, decelerated or normal neuron development in our *in vitro* model. Thus, our establishment that *p53* mutation in cortical neurons promotes early steps of their polarization and morphological maturation is essential in moving the field forward. Our finding that *p53* mutant neurons polarize more quickly *in vitro* is consistent with previous work in hippocampal neuron cultures that indicated *p53* mutant neurons have accelerated polarization (Ferreira & Kosik, 1996). However, it disagrees with studies of *p53* knockdown resulting in inhibition of axon outgrowth (Di Giovanni et al., 2006; Di Giovanni & Rathore, 2012; Qin et al., 2009). It is likely that tissue- and cell-type specific temporal and regional variation accounts for at least some of these discrepancies. p53 activates differential apoptotic and cell-cycle arrest programs in divergent tissue types (Kasthuber & Lowe, 2017). Furthermore, acute knockdown of p53 could manifest distinct effects from germline knockout. In support of this idea, opposing gene expression changes are observed with acute versus long-term knockdown of p53 protein (Couture et al., 2013).

A reasonable hypothesis would be that neuron morphology changes are secondary to a role for p53 in the health and survival of neurons in culture. However, we found no difference in apoptosis or neuron density in p53 wildtype versus mutant cultures. It is still possible that apart from outright cell death, neurons in *p53* mutant cultures could have health advantages compared to wildtype cultures. Nevertheless, the specific effects of *p53* mutation on axon width and acetylated tubulin levels in axons are suggestive of a cell-autonomous role for p53 in axon morphology. Thinner axons with more acetylated tubulin are consistent with more stable, tightly bound microtubules. p53 can bind microtubules in the cytoplasm and is transported to the nucleus by dynein upon DNA damage or microtubule instability events (P. Giannakakou et al., 2002; Paraskevi Giannakakou et al., 2000). Even when nuclear localization is blocked, p53 can exert

functions in the cytoplasm of neurons (Qin et al., 2009). However, as p53 does not have microtubule bundling activity, axon morphology effects are more likely to be secondary to increased expression or stabilization of proteins in neuronal axons or growth cones which promote these processes.

To begin to investigate which proteins could mediate neuron morphology changes in *p53* mutant neurons, we performed bulk RNA sequencing of *p53* mutant cortices. Interestingly, axonogenesis was a significantly enriched gene family. Consistent with previous reports that p53-dependent transcriptional targets include axon-guidance molecules, we found that repulsive axon guidance cues, including *Unc5b*, were globally downregulated (Arakawa, 2005). Given the many reported roles of p53 in developmental processes, we were surprised that GOA of upregulated genes in *p53* mutant cortices showed only terms specific to post-mitotic neuronal processes. While we sequenced only the cortex, some upregulated genes are known to promote cellular outgrowth in other cell types as well. This suggests that p53 normally inhibits a transcriptional program of genes related to cellular outgrowth, consistent with its reported role in prevention of tumor metastasis. An alternative explanation for enrichment of neuronal maturation specific terms could be that p53 mutation results in premature neuronal fate of daughter cells produced from neural stem cell divisions. However, neurogenesis-related genes were not upregulated in our data set; rather, upregulated genes were involved in secondary processes of neuronal maturation. Furthermore, premature neurogenesis would ultimately result in reduced brain size as NSCs are prematurely depleted, which is not seen in the *p53* mutant (Insolera et al., 2014; Little & Dwyer, 2019). Accelerated polarization and neuron outgrowth would not necessarily impact final brain size; therefore, our data is consistent with the *p53* mutant brain phenotype.

Finally, we used our *in vitro* model system to establish the role of p53 in *Kif20b* mutant neuron morphology defects. We found that deleting p53 could rescue *Kif20b* mutant polarization and axon length to wild-type levels. However, *Kif20b;p53* mutant neurons were still significantly less polarized and exhibited shorter axons than *p53* mutant neurons. Therefore, rescue of *Kif20b;p53* mutant neuronal defects was due to the opposing consequence of p53 deletion in promoting neuron maturation. These data highlight the importance of using a *p53* mutant control when investigating p53-dependent effects. It further establishes that *Kif20b* mutant neuron morphology defects are not secondary to p53 activation. *In vivo*, we found that *p53* deletion completely rescued *Kif20b* mutant brain size at E14, but by P0, brain size in double mutants was smaller than

double-heterozygote and *p53* mutant controls. It is possible that neuronal maturation defects in *Kif20b* mutants could have been partially masked by *p53* co-deletion at early ages due to the independent and opposite role of *p53* in this process. However, by later ages the *p53*-independent role of *Kif20b* in neuron outgrowth may be unmasked and contribute to smaller brain size. In support of this idea, we observed that neurons in *Kif20b;p53* mutant cortices were more dense than double heterozygote or *p53* mutant controls, perhaps due to reduced neuropil.

Taken together, our data indicate that post-mitotic polarization and maturation of cortical neurons *in vitro* is complex and multi-factorial, sensitive to the loss of proteins involved in diverse functions. This includes the transcriptional regulator *p53* and the Kinesin-6 family member *Kif20b*, which act through independent mechanisms to inhibit and promote neuronal maturation, respectively. This and previous work suggest these proteins are involved in these processes *in vivo*. Functions of these proteins in post-mitotic neurons could extend beyond initial polarization events; notably, while as a tumor suppressor *p53* function is often lost in tumor progression, increased expression of *Kif20b* has been observed in several forms of cancer. Therefore, loss of *p53* suppression of and enhancement of *Kif20b* promotion of cellular outgrowth processes could similarly promote tumor metastasis.

## Methods

### Cell Culture

To prepare for neuron culturing, first, 18 mm round coverslips were washed twice every 10 min with double-distilled, UV-irradiated water and treated in nitric acid overnight. The coverslips were washed 3 additional times with double-distilled water and then placed in an oven at 160°C overnight to dry and sterilize. Once cool, each coverslip was treated with 200  $\mu$ L poly-L-lysine (PLL) solution (1  $\mu$ g/mL in borate buffer and subsequently incubated overnight at 37 °C. The next day, the coverslips were washed twice with double-distilled water after 3 quick rinses, and the neuron plating media was applied (.5 mL-1 mL). The neuron plating media was previous filter-sterilized and consists of 500 mL Minimum Essential Medium (MEM) with glutamine, 5 mL Penicillin/Streptomycin, 15 mL 20% glucose, 5 mL Sodium Pyruvate, and 10% Fetal Bovine Serum. Pregnant females were sacrificed at E14.5 and placed into cold HBSS mix (500 mL Hank's Balanced Salt Solution (HBSS) with 5 mL HEPES and 5 mL Penicillin/Streptomycin).

Next, pieces of cortex were collected with forceps and placed into a tube filled with a 0.05% trypsin solution. The tube was then placed in a 37 °C water bath for 15 min. The resulting neuron pellets were washed 3 times every 5 minutes with HBSS mix. After washing, the pellets were treated with neuron plating medium during trituration. Appropriate volumes of the resulting solution of dissociated neurons and neuron plating medium were pipetted onto PLL-coated coverslips such that cell density measured 50,000 cells/mL. After 3 hours, the Neuron Plating Medium was changed to Neurobasal and B27 (NB27). For experiments looking at neuron stage, axon morphology and minor neurite morphology, neurons were fixed both 24 hours and 48 hours following initial plating. These coverslips were then fixed in 4% Paraformaldehyde (PFA) for 10 minutes. Experiments investigating filopodia and growth cone morphology were fixed in 2% PFA for 10 minutes and then in 2% PFA with 30% sucrose for 10 minutes. Finally, for experiments measuring acetylated tubulin intensity, neurons were fixed in 4% PFA for 1 minute. The PFA was then removed and replaced with MeOH, and the coverslip was placed in the freezer for 4 minutes. Finally, all coverslips from all experiments were washed 3 times in Phosphate Buffer Saline (PBS) for 10 minutes kept at 4°C until immunofluorescent staining.

### **Immunocytochemistry**

After the neurons were dissociated, plated and fixed, the coverslips were incubated for an hour at room temperature in a blocking buffer (0.1% Triton-X, 2% Normal Goat Serum in PBS) and then for 3 hours in the appropriate primary antibody solution (primary antibody diluted in blocking buffer). Following primary incubation, coverslips were washed 3 times for 10 minutes in PBS and then incubated for 30 minutes at room temperature with appropriate secondary antibody (1:200 dilution) in the dark. Next, DAPI was applied for 10 minutes at room temperature in the dark (1:100 dilution). Finally, the coverslips were washed for 10 minutes three times in PBS and mounted onto glass slides using Fluoromount.

### **Antibodies**

Primary antibodies used were a rabbit or mouse monoclonal antibody against neuron-specific beta-III tubulin (Tuj1) at a dilution of 1:500 in blocking buffer (Biolegend 801201, Abcam ab52623), a F-actin probe conjugated to green fluorescent Oregon Green 488 dye (Phalloidin) at a dilution of 1:50 (Invitrogen, O7466), a mouse monoclonal antibody for acetylated tubulin (SIGMA, T-6793) at 1:800, and a rabbit polyclonal antibody for p53 (Leica Biosystems, NCL-L-

p53-CM5p) at 1:500. Species-specific secondary antibodies were conjugated to Alexa fluorophores (Invitrogen) at a dilution of 1:200 in blocking buffer.

### **Image Acquisition and Analysis**

All fluorescent images were taken on a Carl Zeiss widefield epi-fluorescence microscope via AxioVision camera and software. To quantify neuron stage, low-magnification images were acquired at 20x. For experiments measuring axon length, axon branching, acetylated tubulin, filopodia and growth cone morphology and minor neurite length, images were acquired at 40x. Finally, for experiments looking at axon and minor neurite width, higher-magnification images were acquired at 100x. Image analysis was completed using ImageJ software for all measurements except acetylated-tubulin intensity, which was traced along the axon using Zeiss Zen 2 lite imaging software profile tool. We used the NeuronJ software plugin to trace and measure the length and width of axons, axon branches, minor neurites, in addition to the length of filopodia and area of the growth cone. Axon branches were only counted if they were larger than or equal to 5  $\mu\text{m}$ . Neurite lengths were measured from the base of the process at the soma to the tip of the Tuj1 stain. The axons of Stage 3 neurons were measured at 5  $\mu\text{m}$ , 10  $\mu\text{m}$ , and 25  $\mu\text{m}$  from the edge of the soma, and the minor neurites of Stage 3 neurons were measured at 0  $\mu\text{m}$ , 5  $\mu\text{m}$ , and 10  $\mu\text{m}$  from the edge of the soma.

### **Polarity Stage Analysis**

Neurons were labeled Stage 1 if they extended broad lamellipodia with no clear, coalesced neurites. In Stage 2 neurons, all neurites were of similar length. A neuron was considered “polarized” or Stage 3 if one neurite was at least 30  $\mu\text{m}$  in length and at least twice as long as the next neurite. Neuronal protrusions were considered to be neurites or neurite branches if they had significant microtubule invasion.

### **Measuring Growth Cones and Filopodia**

To measure growth cone area, we began tracing at the base of intense phalloidin-stained actin at the axon neck and then continued tracing lamellipodia edges (the base of the filopodium and where the filopodium becomes uniform in width). Actin protrusions extending out of lamellipodia at the growth cone were considered to be filopodia. These extensions generally had brighter

phalloidin staining than neighboring lamellipodia edges. To measure filopodia length, we traced from the filopodia tip to its base where edges became lamellae.

### **Measuring Acetylated Tubulin Intensity**

Images of Acetylated Tubulin immunostaining were captured using a Carl Zeiss widefield epifluorescence microscope, using AxioVision camera and software. All images were acquired at a 40x oil objective and a constant 100-millisecond exposure time for acetylated tubulin and a 400-millisecond exposure time for beta-III tubulin (Tuj1). Zeiss Zen 2 lite imaging software profile tool was used to measure the intensity of both acetylated tubulin and beta-III tubulin down the axon from the soma to the growth cone. Excel was used to compare individual cells line scans as well as create averages across genotypes for comparison, including specifically the ratio of acetylated tubulin to beta-III tubulin.

### **RNA Sequencing**

Only cortices were collected for RNA extraction, but at this age it was not possible to separate meninges from cortical tissue, so meningeal cells were present in the analysis. Embryos were dissected from pregnant mothers and place. In PBS on ice. Tails were collected for genotyping, the primitive skull was removed, and cortices were quickly dissected out. Cortices were placed into 1.5 ml Eppendorf tubes and immediately submerged in dry ice with an ethanol bath. Flash-frozen cortices were placed in a -80 freezer for storage. RNA was extracted from frozen samples using the Qiagen RNeasy Mini kit (Cat# 74104). RNA concentration and quality were assessed using a NanoDrop. Further quality analysis was done at the UVA sequencing core with Agilent analysis; all samples were of high quality. Library preparation and sequencing was performed by the core. 3 samples of each genotype were analyzed for a total of 12 samples. Statistical analysis was done using DeSeq software with further gene ontology analysis obtained using Panther Gene Ontology software. For gene ontology analysis, we varied the statistically significant threshold used (from  $\text{padj} < 0.05$  to  $\text{p} < 0.05$ ) as needed in order to include enough genes to observe trends.

## Figures

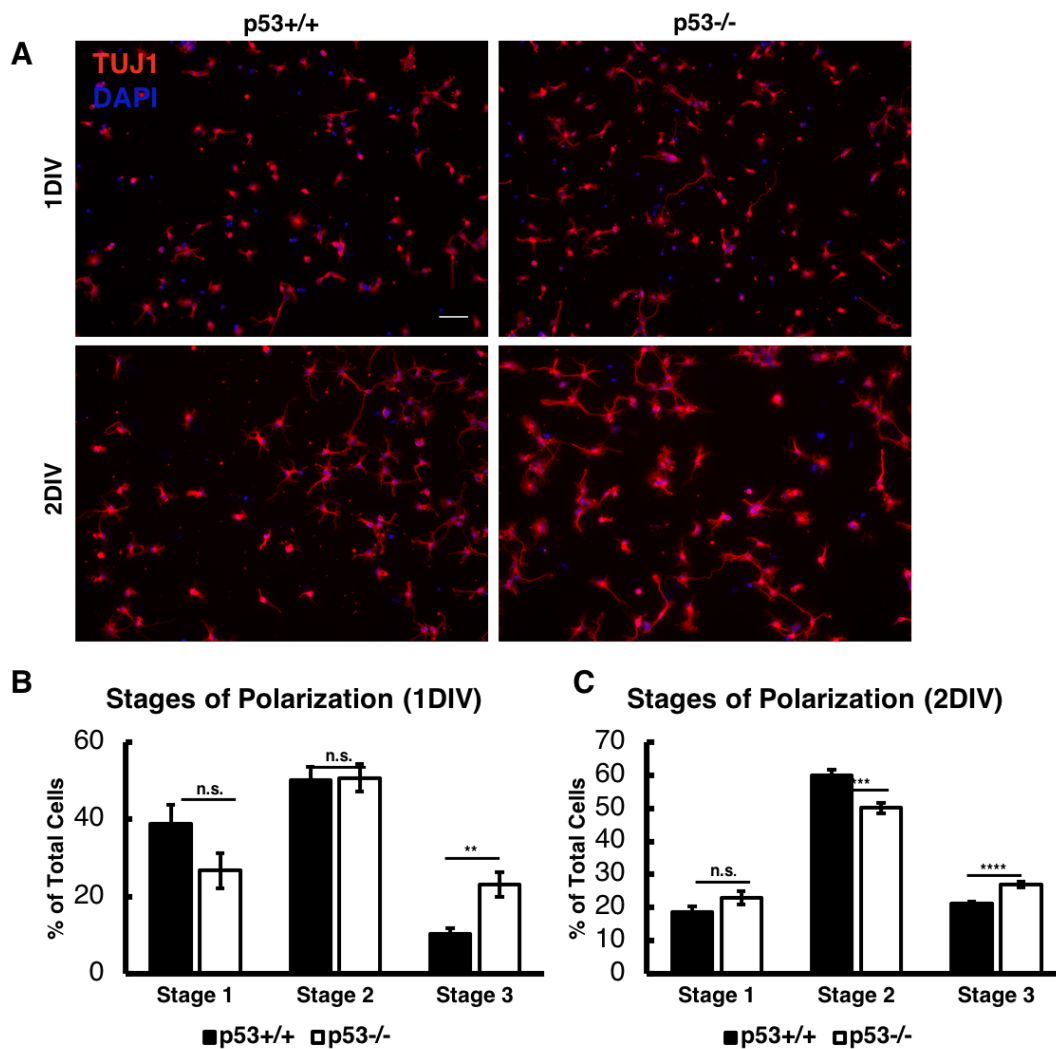


**Figure 29.** *p53* mutant cortical neurons polarize more quickly *in vitro*.

**A**, Representative images of E14.5 cortical cells cultured for 1 day in vitro and 2 days in vitro (DIV) respectively, immunostained for neuronal marker beta-III-tubulin (Tuj1, red) and nuclei (DAPI, blue). Scale bar, 50  $\mu$ m. **B**, The average percentage ( $\pm$ s.e.m.) of neurons at each stage in cultures from control wildtype *p53* (+/+), black bars) or mutant *p53* (-/-, white bars) cortices after 1DIV. Mutant cultures have more polarized neurons (stage 3).  $n = 7$  control (+/+) and 7 mutant (-/-) coverslips from 3 independent experiments with 1962 total control and 1540 mutant cells scored. **C**, After 2DIV, *p53* mutant neurons have less multipolar neurons and are still more likely to be polarized compared to controls.  $n = 6$  control (+/+),  $n = 6$  mutant (-/-) coverslips from 3 independent experiments; 1551 control, 2340 mutant neurons.

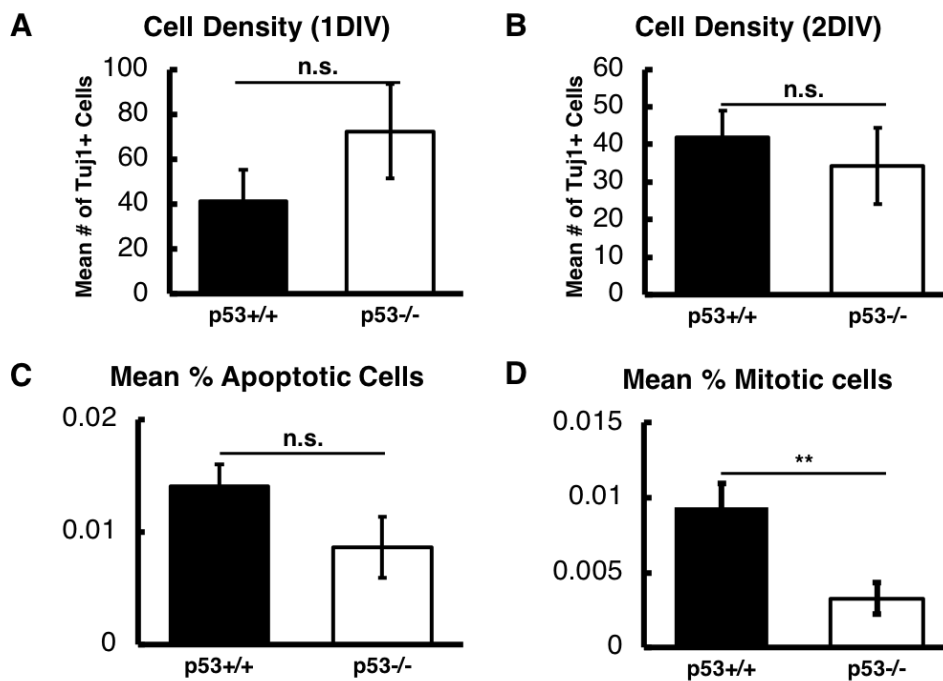


**Figure 30.** Cell density and apoptosis is not significantly different between cultures, and mitosis is not increased.

**A**, The average number ( $\pm$ s.e.m.) of *tuj1*+ positive cells from control wild type p53 (+/+), black bars) and mutant p53 (-/-, white bars) neuron cultures for 1 day in vitro. There is no significant difference in the number of cells positive for *tuj1* between control and mutant cultures.  $n = 7$  control (+/+) and 7 mutant (-/-) coverslips from 3 independent experiments with 1962 total control and 1540 mutant cells scored. **B**, The average number ( $\pm$ s.e.m.) of *tuj1*+ positive cells from control wild type p53 (+/+, black bars) and mutant p53 (-/-, white bars) neuron cultures for 2 days in vitro. There is no significant difference in the number of cells positive for *tuj1* between control and mutant cultures.  $n = 6$  control (+/+),  $n = 6$  mutant (-/-) coverslips from 3 independent experiments; 1551 control, 2340 mutant neurons.

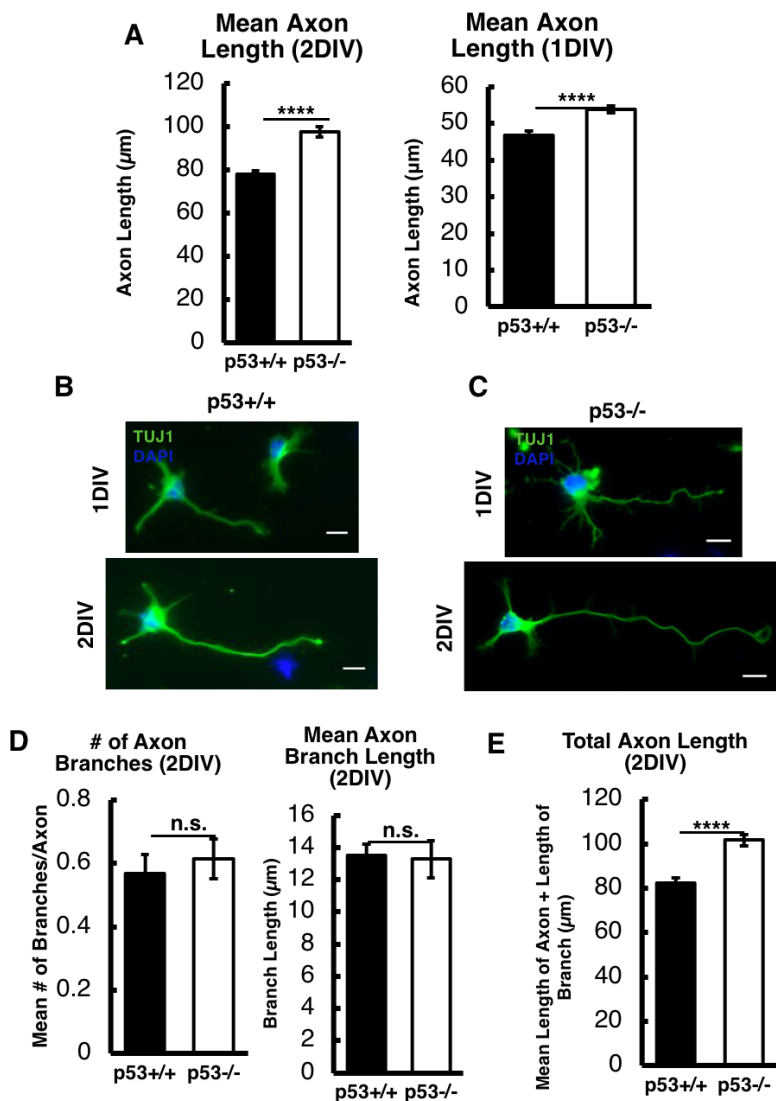


**Figure 31.** *p53* mutant cortical neurons grow longer axons *in vitro*.

**A**, The average length ( $\pm$ s.e.m.) of axons from control wild type *p53* (+/+, black bars) and mutant *p53* (-/-, white bars) neuron cultures either for 1 day *in vitro* or 2 days *in vitro* (DIV) respectively. Mutant cultures show longer axons at both time points.  $n=6$  control (+/+) and  $n=6$  mutant (-/-) coverslips from 3 independent experiments with 225 total control and 400 total mutant axons measured at 1DIV.  $n=7$  control (+/+) and 7 mutant (-/-) coverslips from 3 independent experiments with 272 total control and 234 total mutant axons measured at 2DIV. **B**, Representative images of E14.5 cortical neurons cultured for 1DIV, immunostained for neuronal marker beta-III-tubulin (Tuj1, red) and nuclei (DAPI, blue). Scale bars, 10  $\mu\text{m}$ . **C**, Representative images of E14.5 cortical neurons cultured for 2DIV, immunostained for neuronal marker beta-III-tubulin (Tuj1, green) and nuclei (DAPI, blue). Scale bars, 10  $\mu\text{m}$ . **D**, The average number of axon branches reported per axon measured and the average length of each branch after 2DIV. We see that *p53* deletion has no effect on either the number or the length of axon branches present.  $n=7$  control (+/+) and 7 mutant (-/-) coverslips from 3 independent experiments with 261 total control and 231 total mutant neurons scored and 100 control and 70 mutant axon branches measured. **E**, The average total axon length calculated by adding each neuron's axon length to the length of any axon branches present after 2DIV.  $n=7$  control (+/+) and 7 mutant (-/-) coverslips from 3 independent experiments with 272 total control and 234 total mutant neurons measured.

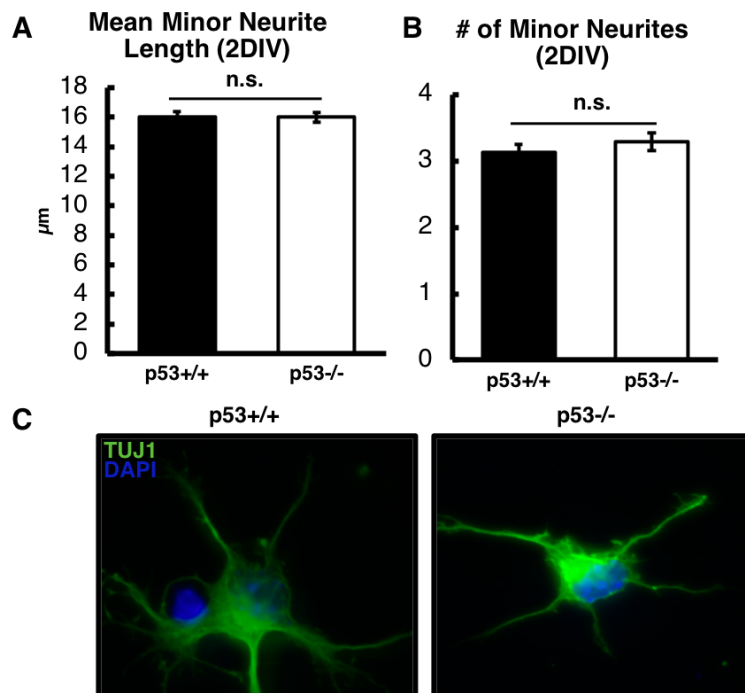


**Figure 32.** p53 is not necessary for proper cortical neuron minor neurite number or length *in vitro*.

**A**, The average number ( $\pm$ s.e.m.) of minor neurites per neuron from control wild type p53 (+/+, black bars) and mutant p53 (-/-, white bars) neuron cultures after 2 days in vitro (DIV). Control and mutant cultures show no significant difference in the number of minor neurites,  $p = 0.37$ .  $n = 7$  control (+/+) and 7 mutant (-/-) coverslips from 3 independent experiments with 272 total control and 234 total mutant neurons scored.

**B**, The average length of minor neurites after 2 days in vitro (DIV). Minor neurite length is not significantly different between the two groups,  $p = .93$ .  $n = 7$  control (+/+) and 7 mutant (-/-) coverslips from 3 independent experiments with 605 total control and 527 total mutant neurons measured.

**C**, Representative images of E14.5 cortical cell minor neurites cultured for 2DIV respectively, immunostained for neuronal marker beta-III-tubulin (Tuj1, green) and nuclei (DAPI, blue).

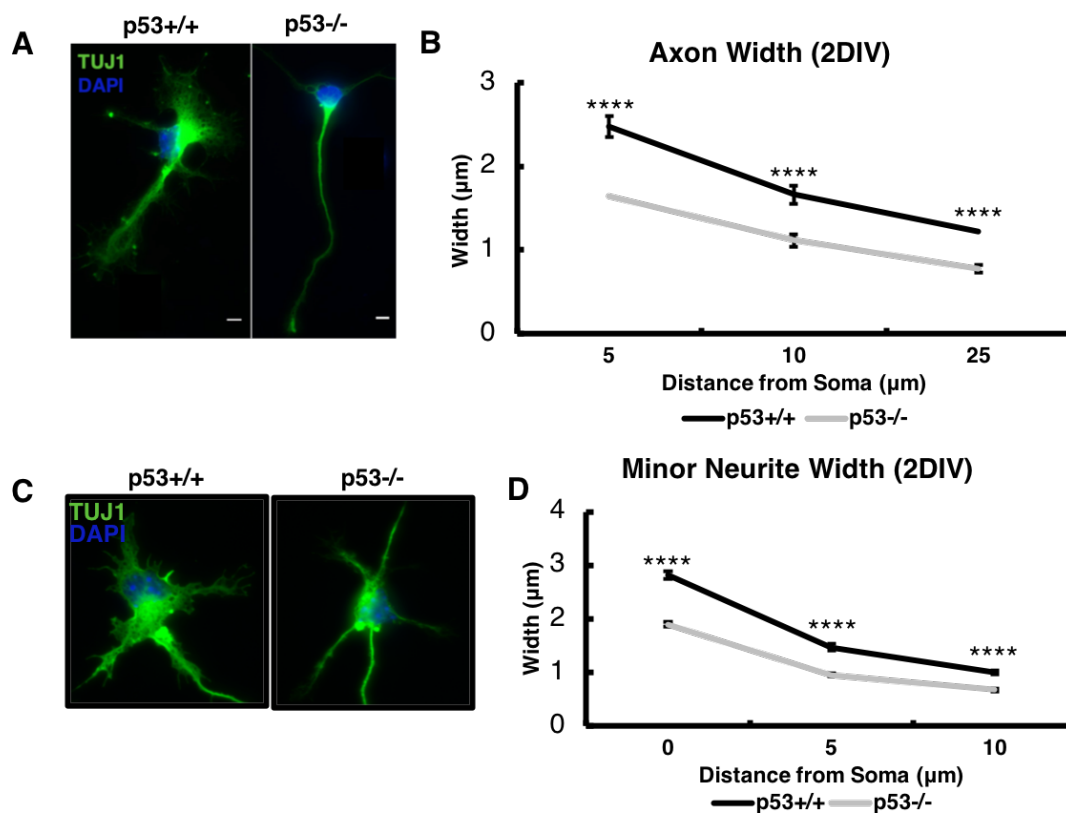


**Figure 33.** p53 ensures proper cortical neuron axon and minor neurite width.

**A**, Representative images of E14.5 cortical neurons, showing differences in axon width, cultured for 2DIV respectively, immunostained for neuronal marker beta-III-tubulin (Tuj1, green) and nuclei (DAPI, blue). Scale bars, 5 μm. **B**, Average axon width (±s.e.m.) at 5μm, 10μm, and 25μm from the soma from control wild type p53 (+/+), black bars) and mutant p53 (-/-, white bars) neuron cultures at 2 days in vitro (DIV). Control axons are wider than mutant neurons at all distances measured. n = 6 control (+/+) and 6 mutant (-/-) coverslips from 3 independent experiments with 144 total control and 136 total mutant neurons scored. **C**, Representative images of E14.5 cortical neurons, showing differences in minor neurite width width, cultured for 2DIV respectively, immunostained for neuronal marker beta-III-tubulin (Tuj1, green) and nuclei (DAPI, blue). Scale bars, 5 μm. **D**, Average axon width (±s.e.m.) at 0μm, 5μm, and 10μm from the soma from control wild type p53 (+/+), black bars) and mutant p53 (-/-, white bars) neuron cultures at 2 days in vitro (DIV). Control minor neurites are wider than mutant minor neurites at all distances measured. n = 6 control (+/+) and 6 mutant (-/-) coverslips from 3 independent experiments with 311 total control and 324 total mutant neurons scored.

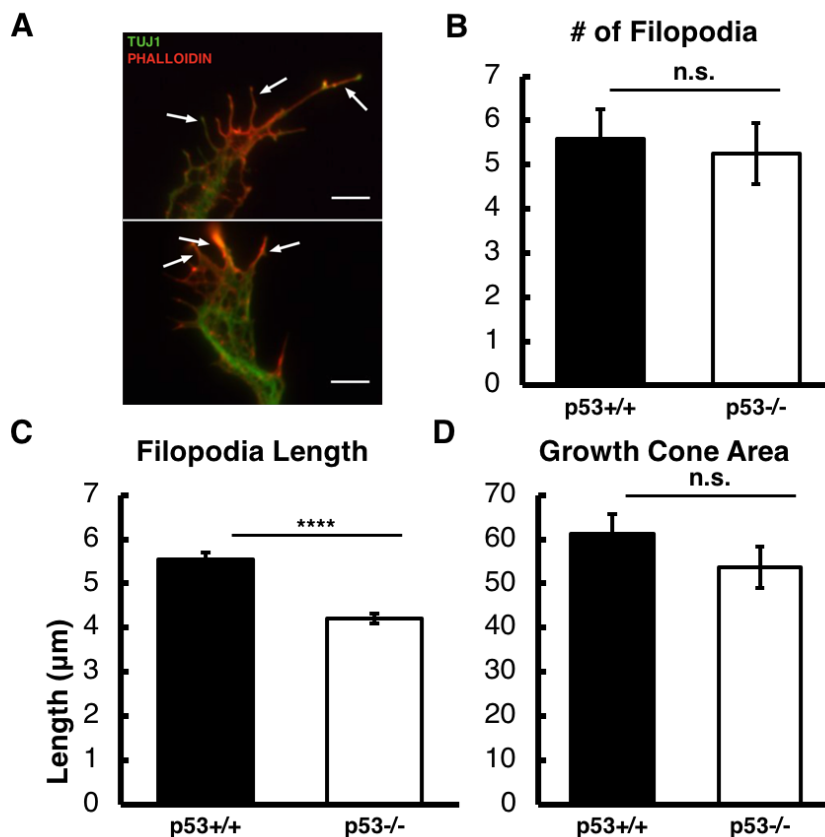


**Figure 34.** p53 ensures proper cortical neuron axon and minor neurite width.

**A**, Representative images of E14.5 cortical neurons, showing the axonal growth cone and filopodia (the 3 longest filopodia for each genotype are marked by white arrows), cultured for 2DIV respectively, immunostained for neuronal marker beta-III-tubulin (Tuj1, green) and actin (phalloidin, red). Scale bars, 5  $\mu$ m. **B**, Average number of filopodia ( $\pm$ s.e.m.) per axon from control wild type p53 (+/+, black bars) and mutant p53 (-/-, white bars) neuron cultures at 2DIV. There is no significant difference in the number of filopodia between groups.  $p = .59$ .  $n = 4$  control (+/+) and 4 mutant (-/-) coverslips from 2 independent experiments with 43 total control and 47 total mutant neurons scored. **C**, Average axonal filopodia length from control wild type p53 (+/+, black bars) and mutant p53 (-/-, white bars) neuron cultures at 2DIV. Mutant filopodia are significantly shorter than the controls.  $n = 4$  control (+/+) and 4 mutant (-/-) coverslips from 2 independent experiments with 226 total control and 226 total mutant filopodia measured. **D**, Average axonal growth cone area from control wild type p53 (+/+, black bars) and mutant p53 (-/-, white bars) neuron cultures at 2DIV. Growth cone area is not significantly different between both groups.  $p = .97$ .  $n = 4$  control (+/+) and 4 mutant (-/-) coverslips from 2 independent experiments with 53 total control and 57 total mutant growth cones measured.

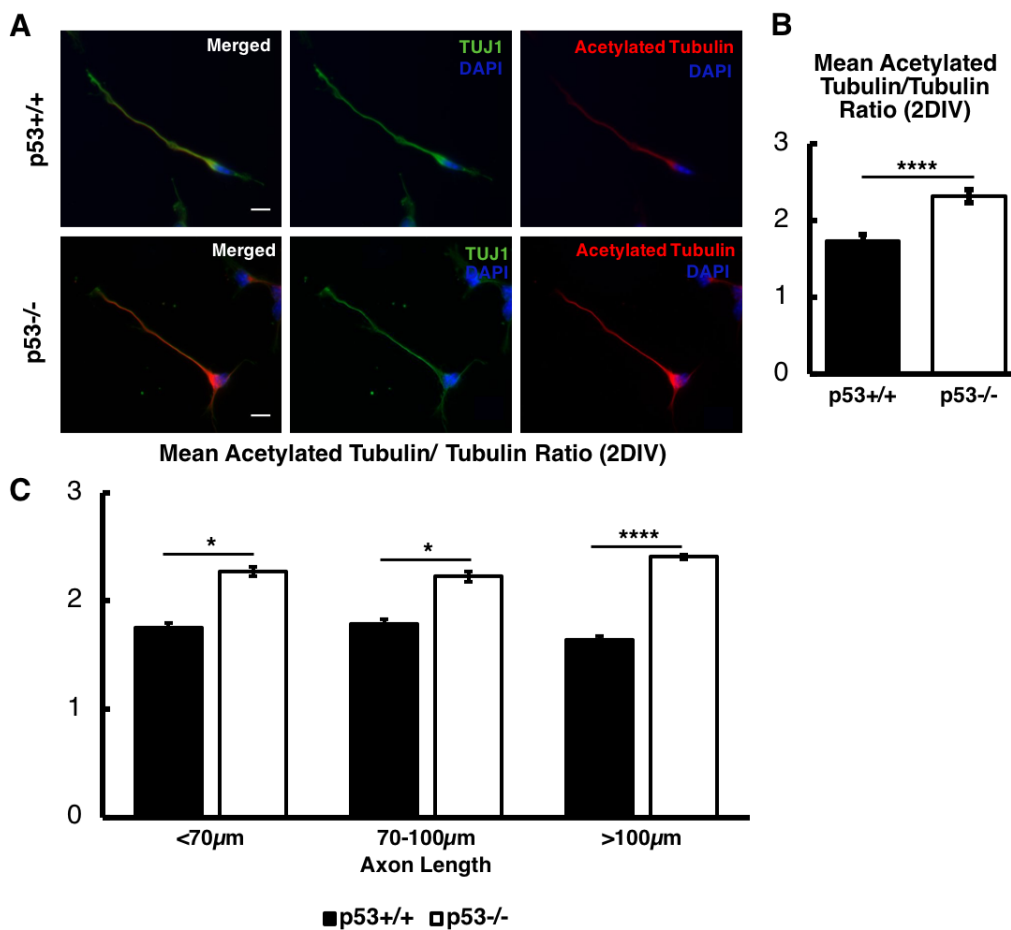


**Figure 35.** The ratio of acetylated tubulin to tubulin is increased in *p53* mutant cortical axons. **A**, Representative images of E14.5 cortical neurons, showing increased acetylated tubulin (red, right) in mutant neurons. Neurons are also immunostained for nuclei (DAPI, blue) and beta-III tubulin (Tuj1, green, center). **B**, The average ratio of acetylated tubulin intensity to tubulin intensity ( $\pm$ s.e.m.) along the axon from control wild type *p53* (+/+, black bars) and mutant *p53* (-/-, white bars) neuron cultures after 2DIV. We see significantly higher proportions of acetylated tubulin in neurons without functional *p53*.  $n = 5$  control (+/+) and 5 mutant (-/-) coverslips from 3 independent experiments with 144 total control and 147 total mutant axons scored. **C**, The average ratio of acetylated tubulin intensity to tubulin intensity binned by length. We see that the significantly higher proportions of acetylated tubulin occur in mutant axons over 100 $\mu$ m in length.  $n = 3$  control (+/+) and 3 mutant (-/-) coverslips from 2 independent experiments with 92 total control and 88 total mutant axons scored.

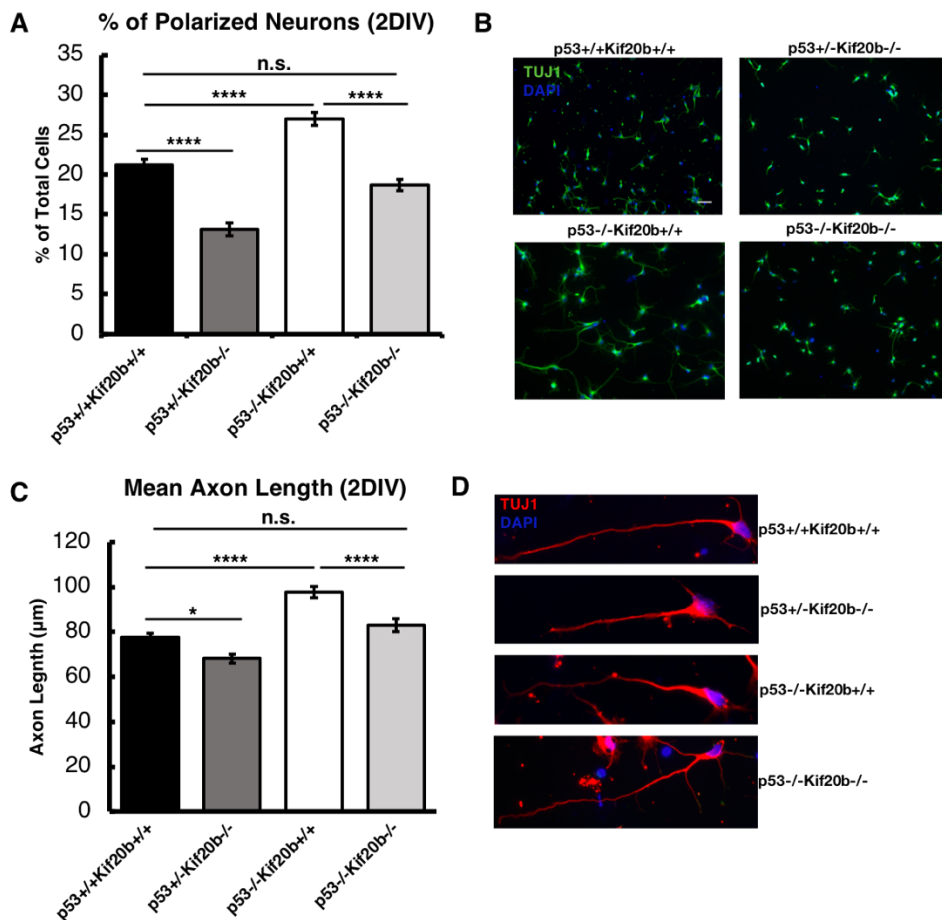


**Figure 36.** Polarization and axon outgrowth defects in Kif20b mutants are p53-independent. **A**, The average percentage ( $\pm$ s.e.m.) of neurons at each stage in cultures from control 53<sup>+/+</sup>-Kif20b<sup>+/+</sup> (black bars), p53<sup>+/+</sup>-Kif20b<sup>-/-</sup> (dark grey bars), mutant p53<sup>-/-</sup>-Kif20b<sup>+/+</sup> (white bars), and double mutant (p53<sup>-/-</sup>-Kif20b<sup>-/-</sup>, light grey bars) cortices after 2DIV. p53 Mutant cultures have more polarized neurons (stage 3) than both double mutant and control. p53<sup>+/+</sup>-Kif20b<sup>-/-</sup> cultures show significantly decreased percentages of polarized neurons compared to all other genotypes. n = 7 p53<sup>+/+</sup>-Kif20b<sup>+/+</sup>, 5 p53<sup>+/+</sup>-Kif20b<sup>-/-</sup>, 7 p53<sup>-/-</sup>-Kif20b<sup>+/+</sup>, and 7 p53<sup>-/-</sup>-Kif20b<sup>-/-</sup> coverslips from 3 independent experiments with 1962 p53<sup>+/+</sup>-Kif20b<sup>+/+</sup>, 2803 p53<sup>+/+</sup>-Kif20b<sup>-/-</sup>, 1540 p53<sup>-/-</sup>-Kif20b<sup>+/+</sup>, and 3807 p53<sup>-/-</sup>-Kif20b<sup>-/-</sup> cells scored. **B**, Representative images of E14.5 cortical cells cultured for 2 days in vitro (DIV), immunostained for neuronal marker beta-III-tubulin (Tuj1, green) and nuclei (DAPI, blue). Scale bar, 50  $\mu$ m. **C**, The average length ( $\pm$ s.e.m.) of axons from control p53<sup>+/+</sup>-Kif20b<sup>+/+</sup> (black bars p53<sup>+/+</sup>-Kif20b<sup>-/-</sup> (dark grey bars), mutant p53<sup>-/-</sup>-Kif20b<sup>+/+</sup> (white bars), and double mutant (p53<sup>-/-</sup>-Kif20b<sup>-/-</sup>, light grey bars) cortices after 2DIV. p53 Mutant neurons extend longer axons than double mutant and control. p53<sup>+/+</sup>-Kif20b<sup>-/-</sup> neurons show significantly shorter axons compared to all other genotypes. n=6 control (+/) and n=6 mutant (-/-) coverslips from 3 independent experiments with 225 total control and 400 total mutant axons measured at 1DIV. n = 7 p53<sup>+/+</sup>-Kif20b<sup>+/+</sup>, 5 p53<sup>+/+</sup>-Kif20b<sup>-/-</sup>, 7 p53<sup>-/-</sup>-Kif20b<sup>+/+</sup>, and 7 p53<sup>-/-</sup>-Kif20b<sup>-/-</sup> coverslips from 3 independent experiments with 272 p53<sup>+/+</sup>-Kif20b<sup>+/+</sup>, 612 p53<sup>+/+</sup>-Kif20b<sup>-/-</sup>, 234 p53<sup>-/-</sup>-Kif20b<sup>+/+</sup>, and 980 p53<sup>-/-</sup>-Kif20b<sup>-/-</sup> cells scored. **D**, Representative images of E14.5 cortical neurons cultured for 2DIV, immunostained for neuronal marker beta-III-tubulin (Tuj1, red) and nuclei (DAPI, blue).

**Table 2:** Genes significantly upregulated in *p53* mutant compared to wild-type E11.5 cortices ( $\text{padj} < 0.05$ ).

Gene	Log2foldchange	Fold change	P value	Padj value
Fam49a	0.52	1.43	5.82E-06	0.011
Maf1	0.25	1.19	7.52E-06	0.011
Xaf1	3.73	13.3	7.69E-06	0.011
Abr	0.55	1.46	1.27E-05	0.017
Stac	2.27	4.81	2.18E-05	0.026
Cabp1	1.38	2.6	5.75E-05	0.047
Mkm1	0.32	1.25	6.5E-05	0.05
Cplx2	0.65	1.57	7.51E-05	0.052

**Table 3:** Genes significantly downregulated in *p53* mutant compared to wild-type E11.5 cortices ( $\text{padj} < 0.05$ ).

Gene	Log2foldchange	Foldchange	P value	Padj value
Trp53	-1.32	-2.5	2.47E-23	3.59E-19
Krt5	-8.9	-496.84	2.92E-06	0.011
Alx1	-3.61	-12.22	2.93E-06	0.011
Fbn1	-0.88	-1.84	4.55E-06	0.011
Man2b2	-0.39	-1.31	4.74E-06	0.011
Zbed6	-0.46	-1.37	4.87E-06	0.011
Eda2r	-1.84	-3.59	6.92E-06	0.011
En1	-5.61	-48.71	3.06E-05	0.034
Hmcn1	-1.67	-3.18	3.37E-05	0.035
Unc5b	-0.53	-1.44	5.41E-05	0.047
Gylt1b	-0.84	-1.78	5.65E-05	0.047
Igsf10	-0.51	-1.42	5.8E-05	0.047
B230120H23	-0.62	-1.53	8.02E-05	0.052
Prkg1	-0.61	-1.53	8.02E-05	0.053
Ccng1	-0.97	-1.96	8.55E-05	0.054

**Table 4:** Genes significantly downregulated in p53 mutant compared to wild-type E11.5 cortices in gene ontology analysis term “axonogenesis”.

Gene	Log2foldchange	Fold change	P value	Padj value
Unc5b	-0.52	-1.44	5.41E-05	0.047
Alcam	-.93	-1.91	0.00035	0.12
Slit3	-1.33	-2.51	0.00036	0.12
ErbB2	-0.36	-1.28	0.0014	0.19
Epha7	-0.42	-1.34	0.0019	0.20
Itga4	-0.84	-1.79	0.0020	0.20
Lama2	-1.16	-2.23	0.012	0.36
Wnt7b	-0.33	-1.25	0.013	0.36
Vegfa	-0.34	-1.26	0.014	0.36

**Table 5:** Genes significantly upregulated in p53 mutant compared to wild-type E11.5 cortices in gene ontology analysis term “axonogenesis”.

Gene	Log2foldchange	Fold change	P value	Padj value
Pitpna	0.15	1.11	0.0053	0.28
Ndn	0.44	1.35	0.0064	0.3
Plxna4	0.68	1.60	0.0082	0.33
Gap43	0.48	1.40	0.009	0.33
Prdm8	1.21	2.32	0.011	0.34
Evl	0.2	1.15	0.011	0.35
Uchl1	0.33	1.26	0.011	0.35
Mapt	0.76	1.69	0.014	0.36
Ntng2	0.61	1.53	0.014	0.36
Stmn1	0.33	1.26	0.014	0.36

**Table 6:** Genes significantly upregulated in *p53* mutant compared to wild-type E11.5 cortices in gene ontology analysis term “neuron projection development”.

Gene	Log2foldchange	Foldchange	P value	Padj value
Nrep	0.35	1.27	0.0011	0.18
Cd24a	0.34	1.27	0.0015	0.19
Hdgfrp3	0.25	1.19	0.0026	0.22
Trappc4	0.18	1.13	0.0027	0.23
Rab11a	0.17	1.13	0.003	0.24
Lingo1	0.75	1.68	0.0034	0.25
Ugt8a	0.45	1.36	0.004	0.26
Arf4	0.14	1.10	0.0044	0.27
Prdm12	0.79	1.73	0.0049	0.27
Tshr	1.36	2.56	0.0053	0.28
Pitpna	0.15	1.11	0.0053	0.28
Ndn	0.44	1.35	0.0064	0.30
Plxna4	0.68	1.60	0.0082	0.33
Gap43	0.48	1.39	0.0090	0.33
Stmn2	0.62	1.53	0.0095	0.33
Prdm8	1.21	2.32	0.011	0.34
Evl	0.20	1.15	0.011	0.35
Uchl1	0.33	1.26	0.011	0.35
Hdac2	0.15	1.11	0.013	0.36
Mapt	0.76	1.69	0.014	0.36
Ntng2	0.61	1.53	0.014	0.36
Stmn1	0.33	1.26	0.014	0.36
Stmn3	0.46	1.38	0.014	0.36
Gpm6a	0.57	1.48	0.014	0.36

## Chapter 5: Discussion

### 5.1 Overview

This thesis work advances our understanding of cell biological mechanisms of cerebral cortex development. We utilized mouse genetic techniques to identify proteins that were not absolutely essential for development, but were necessary for correct cerebral cortex growth. We continued our investigation of one previously identified genetic murine model of microcephaly, and identified a novel murine model that replicates a human phenotype. These two mouse mutants shared in common a role in an understudied process in cortical development; they enabled the completion of cell division at the final stage of cytokinesis, abscission. The investigation of these mouse mutants has revealed the cytokinetic abscission stage of cell division to be a critical decision-making point in neural stem cell divisions, which produce the cells of the cortex. Although we have shown the specific impairments of abscission in these mutants to be unique, they both ultimately have microcephaly in large part due to activation of the p53-apoptotic signaling axis. Interestingly, we found that co-deletion of *p53* could rescue brain size in these mutants to a degree that correlated with the severity of the cellular defects observed. We propose that cytokinetic abscission, as well as the p53 response system to impaired cell division, have evolved to be differentially regulated in the cerebral cortex of mammals to enable the rapid growth of this complex organ.

This discussion brings together the previous chapters and following appendices for an analysis of the conclusions we can take from this work and identification of remaining questions that deserve further investigation. The individual chapter discussions and appendices contain additional specific points for consideration pertaining to the demonstrated findings. The future directions section of this chapter identifies many concrete next steps as well as broader lines of inquiry that may be helpful to future researchers interested in these topics.

### 5.2 p53-dependent and -independent pathways in microcephaly etiology of the *Kif20b* mutant

We have elucidated factors leading to microcephaly in a Kinesin-6 mutant, including important similarities and differences from other described mutants. We discovered that p53 activation is the main driver of microcephaly in the *Kif20b* mutant ((Little & Dwyer, 2019); **Chapter 2**). Total p53 protein was increased in mutant embryonic cortical lysates, and a subset of mutant NSCs showed increased nuclear p53 expression. A slight increase in nuclear p53 was seen in mutant NSCs at the midbody stage, which interestingly increased in later-stage midbodies. Furthermore, bulk mRNA sequencing analysis (**Appendix 2**) showed upregulation of known p53-dependent transcriptional targets in the *Kif20b* mutant, including those involved in cell-cycle arrest (p21) and apoptosis (Eda2r, Puma, Bax). The most conclusive evidence for the role of p53 is the nearly complete rescue of *Kif20b* mutant microcephaly through heterozygous or homozygous p53 deletion, and the complete rescue of cleaved-caspase-3 expression, an indicator of apoptosis.

We have furthered the evidence that *Kif20b* has a cell autonomous role in cytokinesis of NSCs. *Kif20b* mutant NSCs cultured *in vitro* have wider midbodies and increased apoptosis, as was seen *in vivo*. Defects in NSC midbodies, including alterations in shape and alignment to the apical membrane, were not rescued by p53 deletion ((Little & Dwyer, 2019); **Chapter 2**). However, asymmetry of apical endfeet at the midbody stage was p53-dependent, suggesting that p53 activation or the apoptotic process results in membrane shape changes (**Appendix 1**). As cells undergoing cytokinesis *in vitro* have no orientation to an apical membrane, it is therefore more likely that midbody structural changes lead to p53 activation than midbody misalignment. New work from our lab indicates that *Kif20b* mutant NSCs undergo faster abscission (McNeely et al., 2019), and abscise at a width that is wider than normal. This is likely to be p53-independent, as double mutant midbodies with constriction sites, indicating a near-abscission state, are also significantly wider than controls (**Appendix 1**). Taken together, our accumulated data support the hypothesis that p53 activation may occur in *Kif20b* mutant NSCs directly or indirectly due to impaired cytokinetic abscission.

A complementary goal of this work was to determine whether cytokinetic defects in *Kif20b* mutant NSCs led to other consequences for brain development besides p53-dependent apoptosis. We found support for this idea, as despite complete rescue of cortical thickness at E14, brain size in double mutants was incompletely rescued by *p53* deletion at P0 (**Chapter 2**) and P21 (**Appendix 1**). Double mutants occasionally developed hydrocephalus (**Chapter 2**). We hypothesize that this may be due to other observed roles for *Kif20b* in cell fate specification and

neuron polarization and outgrowth. Indeed, premature neurogenesis in the *Kif20b* mutant is not p53-dependent, and could lead to reduced brain size by depleting the progenitor pool (McNeely et al., 2019 and **Appendix 1**). Delayed neuron polarization and neuron morphology defects in *Kif20b* mutants are also p53-independent (**Chapter 4**). The cell density of double mutant neurons in cortical sections is increased at P0, supporting the hypothesis that there may be delayed or defective neuron outgrowth ((Little & Dwyer, 2019); **Chapter 2**).

In the *Kif20b* mutant, we evaluated whether pathways previously shown to activate p53 in the cortex, including mitotic delay, mislocalized progenitors, DNA damage and furrowing failure, were implicated. Progenitors were correctly localized and had normal mitotic index and cell cycle index in both *Kif20b* and *Kif20b;p53* double mutants, suggesting that these pathways for p53 activation are not used. Further analysis of mitotic cells in *Kif20b* mutant progenitor cultures indicated a slight shift to more anaphase/telophase cells, correlating with the increased time to complete cleavage furrowing seen in *Kif20b* knockdown HeLa cells and *Kif20b* mutant NSCs *ex vivo*. However, mitotic delay in other microcephaly mutants was due to delayed prometaphase and was much more severe. Whether a small delay in anaphase/telophase or faster abscission could also activate p53 is not known. Furthermore, there was no observable increase in bright  $\gamma$ H2AX+ cells in *Kif20b* or *Kif20b;p53* mutant cortical sections, as have been observed in other mutants (Houlihan & Feng, 2014). Finally, an analysis of the Hippo pathway, shown to activate p53 in binucleate cultured cells (Ganem et al., 2014), in dissociated NSCs showed an increase in nuclear Yap in *Kif20b* mutants, suggesting downregulation of the Hippo pathway. However, this change in Yap expression was p53-dependent. Therefore, we hypothesize that the mechanism of p53 activation in the *Kif20b* mutant is novel, and is likely to be related to Kif20b's role in cytokinetic abscission.

### **5.3 Comparing and contrasting *Kif20b* and *Cep55* mutant microcephaly**

Kif20b and Cep55 proteins both have roles in cytokinetic abscission, as evidenced through numerous studies in cell lines. Germline mutation in both genes results in severe microcephaly in mice, that is out of proportion to body size defects. Both genes are vertebrate-specific, and as such may have evolved for the precise divisions of NSCs in the mammalian cortex. However, despite these similarities many important differences exist between these two mouse mutants that are informative as to their distinct functions in cortical development (see Table 7).

**Table 7: Comparing and contrasting Kif20b and Cep55 loss in cell lines and mouse mutants**

Phenotype/ Observation	Kif20b kd cell lines (from Janisch et al 2018 or noted)	Kif20b mouse mutant (from Janisch et al 2013 or 2016; Little & Dwyer 2018 or unpublished data)	Cep55 kd cell lines (references in text)	Cep55 mouse mutant (unpublished, Dwyer lab)
<b>Midbody morphology</b>	Thinner with fewer constriction sites	Wider by AurkB in NSCs <i>in vivo</i> and <i>in vitro</i>	Thinner, with loss of dark zone and midbody bulge in subset; ESCRTs do not localize	Thinner by alpha-tubulin in MEFs, shorter by AurkB in NSCs <i>in vivo</i>
<b>Midbody alignment to apical membrane</b>	N/A	Misaligned at E13.5	N/A	Aligned at E14.5
<b>Abscission duration</b>	Overall dysregulation and 15 minute delay	Faster abscission in NSCs at E11.5 and E13.5 <i>in vivo</i>	7+ hr delay after midbody formation	Midbody index is increased at E14.5 suggesting a delay; more work needed
<b>Cytokinesis completion</b>	All cells observed live completed cytokinesis but slight increase in binucleate cells with fixed analysis	All cells observed live completed cytokinesis after midbody formation; flow cytometry analysis indicates DNA content not altered from controls	60-90% failure in completing abscission, usually resulting in regression and formation of a binucleate cell	15-fold increase in numbers of cells with 4N DNA content with flow cytometry; increased binucleates with fixed analyses <i>in vitro</i> (25% of NSCs and 12.5% of neurons); more work needed
<b>Apoptosis</b>	Slight increase	Up to 10-fold increase in apoptosis at E10, E12, E14, E16; majority in VZ/SVZ	Not noted	Up to 200-fold increase in apoptosis at E10 and E14; increased in both VZ/SVZ and CP
<b>Cell fate/cell cycle exit</b>	Not noted	Increased neurogenic divisions <i>in vitro</i> at E11 and E12; increased cell cycle exit <i>in vivo</i> at E12	Reduced proliferation/growth curve	Reduced thickness of upper layer neurons compared to total cortical plate at P0, preliminary evidence suggests increased cell cycle exit at E12 <i>in vivo</i>
<b>p53 activation</b>	Noted with Kif20b knockdown in hepatocellular cancer cells (Liu 2014 and 2018)	Increased total p53 on E12 western blot; Increased p53 N:C ratio seen in cultured NSCs but not <i>in vivo</i> ; increased nuclear p53 in NSCs w/ a midbody	Not noted	Increased p53 N:C ratio seen in cultured NSCs and <i>in vivo</i> ; increased nuclear p53 in binucleate NSCs and binucleate neurons
<b>Gross embryo phenotypes</b>	N/A	Body size 72% of controls at E16.5; microphthalmia, shortened snout	N/A	Body size 90% of controls at P0; normal eye size, flatter head
<b>Survival</b>	N/A	Rarely survive past birth	N/A	Survive to birth at Mendelian ratios; die by weaning
<b>Brain size at E14</b>	N/A	Cortical thickness is approximately 67% of controls	N/A	Cortical thickness is approximately 83% of controls
<b>Brain size at P0</b>	N/A	Cortical length is 83% of controls	N/A	Cortical length is 70% of controls
<b>Neuronal layer thickness</b>	N/A	Decreased thickness of neuronal layer at E14.5	N/A	Decreased thickness of neuronal layer at E14.5
<b>Number of apical and basal progenitors</b>	N/A	Decreased numbers of basal progenitors at E14.5	N/A	Normal numbers of basal progenitors and decreased numbers of apical progenitors at E14.5
<b>p53 deletion ability to rescue apoptosis</b>	N/A	Both heterozygote and homozygous loss of p53 rescues apoptosis at E14	N/A	Homozygous loss of p53 rescues apoptosis at E14
<b>p53 deletion ability to rescue brain size</b>	N/A	Cortical length is rescued from 83% of controls in Kif20b single mutants to 95% of controls in Kif20b;p53 double mutants. Heterozygote and homozygous loss of p53 equally rescue.	N/A	Cortical length is increased from 70% of controls in Cep55 single mutants to 90% of controls in Cep55;p53 double mutants. Only homozygous loss of p53 rescues.
<b>p53 deletion ability to rescue cytokinetic defects</b>	N/A	Wider midbodies, fewer constriction sites, and misalignment are not rescued. Flow cytometry analysis in double mutants is not altered from controls.	N/A	?

## Cell line knockdown phenotypes

Knockdowns of Kif20b and Cep55 in cultured cell lines produce unique phenotypes. Knockdown of Cep55 has been performed primarily in human cancer cells (Fabbro et al., 2005; Zhao, 2006); we also evaluated Cep55 knockdown in immortalized mouse fibroblast (3T3) cells (**Appendix 4**). In HeLa cells, inhibition of Cep55 resulted in abscission failure and formation of binucleate cells at high rates. In one study, 25% of Cep55-depleted HeLa cells were binucleated at 48 hours after transfection compared to < than 10% in controls; this increased to 45% at 96 hrs (Fabbro et al., 2005). Furthermore, live imaging analysis over 18 hours after transfection indicated that Cep55-depleted HeLa cells failed to complete cytokinesis 60% of the time, resulting in midbody regression and formation of a binucleate cell after a prolonged period (up to 7 hours) of abscission delay (Fabbro et al., 2005). Importantly, mononucleate Cep55-depleted cells had normal timing of mitosis and midbody formation, but binucleate cells exhibited errors in the next mitosis. Fixed analyses also showed an increasing midbody index (numbers of midbodies/total cells) over time after transfection, consistent with abscission delay – compared to < 10% in controls, 25% of Cep55-depleted cells were at the midbody stage at 48 hours post-transfection, and this increased to 35% at 96 hours. . Another study of Cep55-depleted HeLa cells reported similar numbers of binucleate cells with fixed analysis, but observed more severe defects with live imaging – over 90% of cells had an abscission delay of > 7 hours and failed to complete cytokinesis before becoming binucleated (Zhao, 2006). Structural defects in Cep55-depleted midbodies were also noted, including loss of the dark zone and Aurora B expression (Zhao, 2006). Cytokinetic defects in Cep55 knockdown cells are thought to be due to an essential role for the protein in recruiting the ESCRT factors that complete abscission (Hyung et al., 2008). Interestingly, knockdown of Cep55 was not reported to cause cell cycle exit or apoptosis in HeLa cells, but did result in increased apoptosis in lung cancer cell lines, and its loss promoted apoptosis in zebrafish (Jeffery et al., 2015; Liu et al., 2016).

In contrast to the severe defects caused by Cep55 knockdown in cell lines, knockdown of Kif20b in HeLa cells causes only subtle defects (Janisch et al., 2018). Midbody maturation defects, including decreased ESCRT recruitment are noted. Kif20b knockdown cells have delayed cleavage furrowing, and dysregulated abscission timing. Our evidence supports a role for Kif20b in microtubule bundling in several cellular processes, but Kif20b's precise molecular cargoes during abscission are not known.

## Gross phenotypes of mouse mutants

Based on the cellular phenotypes observed with knockdown of *Cep55* and *Kif20b* in cell lines, a reasonable hypothesis would be that loss of *Cep55* would be more consequential for embryonic development than loss of *Kif20b*. Surprisingly, we did not find this to be true. *Kif20b* mutants exhibit perinatal lethality, while *Cep55* mutants can live up to several weeks after birth. Thus, it seems likely that the relatively minor defects observed through *Kif20b* knockdown in cell lines may be magnified *in vivo* to explain the embryonic phenotype. Conversely, other proteins may be able to compensate for *Cep55* loss in a germline knockout. Together, these mouse mutants illuminate the limitations of research in cell lines to determine the essentiality of particular proteins for development.

The phenotypes of *Kif20b* mutant and *Cep55* mutant mice are readily differentiable by the embryo appearance. *Kif20b* mutant embryos are noticeably smaller than controls at embryonic ages, while *Cep55* mutants, although slightly smaller when measured at P0, are not. *Kif20b* mutants have a variable appearance including microphthalmia, a shortened snout, and sometimes a protruding brain thought to be due to hydrocephalus. Surprisingly, *Cep55* mutants have normal appearing eyes and snout. However, the top of the head is noticeably flatter due to the much smaller brain, and hydrocephalus was never observed. Despite the overall more severe appearance of the *Kif20b* mutant embryo, the *Cep55* mutant, strikingly, has more severe microcephaly. The overall brain size is smaller: the cortical length at P0 in *Kif20b* mutants is 83% of controls (Janisch et al., 2013), compared to 70% of controls in *Cep55* mutants. Furthermore, neurons in *Cep55* mutant P0 sections are found at decreased density, indicating that the cellular content is even more reduced than appears by the brain size; this defect is not seen in *Kif20b* mutants. Therefore, it appears that *Cep55* is more specifically required for neural tissues compared to other tissues than the *Kif20b* mutant, which is surprising given data from cell lines would suggest it is more essential for normal cell division. However, this is consistent with the phenotype found in human fetuses that inherited homozygous germline *Cep55* mutation: while brain size was severely affected, other organs were not as severe, and some infants could live until shortly after birth (Bondeson et al., 2017; Frosk et al., 2017; Rawlins et al., 2019). *Kif20b* mutation has not yet been discovered in human patients, so it is possible that *Kif20b* loss causes early lethality in human embryos.

## Cellular phenotypes of mouse mutants

We also discovered differences in the cellular and structural defects in *Kif20b* and *Cep55* mutant mouse cortices. *Kif20b* mutants have a noticeable lack of many cellular defects observed in other microcephaly mutants: no abnormalities were noted on analysis of cell cycle indices with flow cytometry, mitotic cell number or location in the cortex, location of progenitors and neurons in the cortex, and S phase indices. Instead, there are abnormalities at the abscission stage of cytokinesis, in midbody number, structure, and abscission timing. In contrast, the *Cep55* mutant has many cellular defects. Cell cycle analysis shows greatly altered DNA content in cortical cells, there are increased numbers of mitotic basal progenitors, and cortical structure is disorganized with mislocalized apical NSCs. Furthermore, there are alterations in the apical membrane, midbody number and structure. These differences likely reflect a greater requirement for *Cep55* in cortical development, including additional secondary consequences when it is lost. We hypothesize, based on studies in cell lines and our own data, that the primary defect induced by both *Kif20b* and *Cep55* loss is impaired cytokinetic abscission. However, *Kif20b* mutant abscission defects are relatively minor and do not result in impairment of downstream division processes. Conversely, *Cep55* abscission defects are severe, resulting in the formation of binucleate NSCs and neurons (approximately 25% of NSCs and 12% of neurons in cortical cultures) which has many downstream consequences for cell division.

## Levels of p53 increase and apoptosis in mouse mutants

Despite differences in cellular phenotypes, both *Kif20b* and *Cep55* loss result in p53 activation and apoptosis in the cortex. However, many more p53+ and apoptotic cells are observed in *Cep55* mutant cortices (apoptosis is increased 50-fold in E14.5 *Cep55* mutant cortices compared to 5-fold in *Kif20b* mutant cortices, both compared to controls). It is possible that some level of p53 activation in both *Cep55* and *Kif20b* mutants comes directly from abscission defects. However, we hypothesize that p53 activation in *Cep55* mutants occurs additionally due to formation of binucleate cells, and subsequent mitotic delay and DNA damage in these cells.

## 5.4 Future Directions

Identifying upstream mediators and downstream effectors of p53 activity in microcephaly mutants

The exact cellular and molecular events that lead to p53 activation in the *Kif20b* and *Cep55* mutants remain to be determined. Despite the absence of cellular abnormalities observed in other mouse mutants, *Kif20b* mutant NSCs exhibit defects at the cytokinetic abscission stage of cell division. Midbodies are wider and misaligned to the apical membrane, and these defects are not rescued by p53 co-deletion. Therefore, it is possible that abnormal midbody formation directly or indirectly results in p53 activation. Additionally, *Kif20b* mutant NSCs have faster abscission in cultured cortical slabs. Knockdown of abscission proteins that normally act during the abscission checkpoint resulted in faster abscission, with not enough time to resolve DNA damage from lagging chromatin in the intercellular bridge (Mathieu et al., 2013; Petsalaki & Zachos, 2016). This could be a mechanism through which faster abscission in the *Kif20b* mutant could result in activation of p53-dependent pathways. We have previously looked for lagging chromatin in intercellular bridges in HeLa cells with Dapi labeling, but another marker such as Lap2b, an inner nuclear envelope marker, may have higher sensitivity. Additionally,  $\gamma$ H2AX expression could be visualized specifically in midbody stage cells and in midbodies (Petsalaki & Zachos, 2016).

Support for the possibility of DNA damage occurring in *Kif20b* mutants comes from subsequent RNA sequencing analysis (**Appendix 2**) of *Kif20b* and *Kif20b;p53* mutant E11.5 cortices. While many classical markers of DNA damage, such as ATM and ATR kinases, were unchanged and may be regulated at the post-translational level, gene ontology analysis did indicate that an enrichment of genes involved in the cellular response to DNA damage, especially DNA repair, were upregulated in both single and double mutants (see **Appendix 2**). These gene expression changes could be validated by RT-PCR or protein expression. These data suggest that there may be low levels of DNA damage that are not readily observable in the *Kif20b* mutant. This is intriguing, as it suggests the mechanism of damage could be distinct from other microcephaly mutants. Alternatively, these upregulated genes may be involved in other cell division processes in addition to the response to damage. As a starting point, it would be worth investigating Smc (structural maintenance of chromosomes) 2 and 4, which were significantly upregulated in RNA sequencing analysis and found to interact with Kif20b by affinity-purification mass spectrometry of transgenic HeLa cell lysates (Maliga et al., 2013). Smc2 and Smc4 form a condensin

heterodimer that promotes chromosome condensation but also have roles in single and double-stranded DNA repair (Wu & Yu, 2012).

In contrast to the *Kif20b* mutant, the *Cep55* mutant exhibits indications of multiple documented avenues for p53 activation, including increased numbers of mitotic cells in the cortex, mislocalized apical and basal progenitors, DNA damage, and binucleate cells. Additional experiments could better differentiate whether these are primary or secondary consequences of *Cep55* loss. If these abnormalities are causative for p53 activation, they should still be observed in *Cep55;p53* double mutants. Our current hypothesis is that cytokinesis failure and formation of binucleate cells is the primary mechanism for p53 activation. This is predicated on our observations of high numbers of binucleate cells in *Cep55* mutants and increased nuclear p53 expression in *Cep55* mutant NSCs *in vivo* and *in vitro*. *In vitro*, this increased nuclear p53 is consistently observed to be in binucleate cells, defined as “paired” nuclei within one cytoplasm, as determined by phalloidin. Mononucleate cells in *Cep55* mutant cultures do not show elevated p53 expression. However, more work is needed to determine whether p53 activation in binucleate *Cep55* mutant cells is a primary or secondary consequence. Addition of BrdU to cell cultures (such as in **Chapter 2**) could differentiate whether cells with high p53 expression recently divided. If only binucleate cells that recently divided have high p53 expression, this would suggest that it is a secondary consequence of impaired cell division in binucleates that activates p53 rather than the binucleate state itself.

The previously discussed pathways for p53 activation evaluated in the *Kif20b* mutant could also be investigated in *Cep55* mutants. The Hippo pathway especially warrants evaluation, as it has been suggested to activate p53 specifically in binucleate cells (Ganem et al., 2014). Furthermore, RNA sequencing of *Cep55* mutant and *Cep55;p53* mutant cortices as we performed for *Kif20b* and *Kif20b;p53* mutants (**Appendix 2**) would be useful to determine p53-dependent and -independent transcriptional pathways that are altered downstream of *Cep55* mutation.

For an unbiased approach to study pathways of p53 activation following *Kif20b* and *Cep55* loss, a CRISPR-Cas9 screen could be used in cultured cells to test candidates for rescue of p53-dependent cell cycle arrest or apoptosis (Wang et al., 2012). A CRISPR screen identified the upstream activators of p53, specifically the USP28-53BP1 pathway, following mitotic delay (Lambrus et al., 2016). HeLa or other cancerous cell lines would not be useful, but a cell line such

as retinal pigment epithelial-1 (RPE-1) with intact p53-status, as were used in the Lambrus et al. study, or a neural cell line, could be advantageous. Cellular consequences of Kif20b loss are likely magnified in the cortical epithelium, but our observation of apoptosis in dissociated NSCs indicates that at least some of the apoptosis is contributed to by cell autonomous mechanisms. Furthermore, p53 activation was noted in hepatocellular cells depleted of Kif20b, indicating that the p53 response is not specific to NSCs (X. Liu et al., 2018). Since p21 was a robust target of upregulation by p53 in *Kif20b* mutant cortices, its activation could be a simpler read out in a CRISPR screen. It would also be interesting to knockdown other cytokinesis proteins and Kif20b family members to see if similar p53-dependent pathways are upregulated.

For both *Kif20b* and *Cep55* mutants, greater temporal and spatial resolution of p53 accumulation in the nucleus, especially in relation to the timing of cytokinesis events, would be valuable. Acute knockdown of Kif20b and Cep55 with siRNAs either in neural cell lines, or in the cortex through electroporation, would allow greater resolution of the time following knockdown at which p53 activation and/or apoptosis occurs. Knockdown in a transgenic p53 reporter and/or apoptosis reporter mouse would allow visualization of p53 activity and/or apoptosis onset *in vivo* (Hamstra et al., 2006; To et al., 2015; Yamaguchi et al., 2011). In a cell line, this could be combined with a live reporter of p53, p21 or caspase activity, as have been previously used (Stewart-Ornstein & Lahav, 2016). A live reporter system would provide significant insights into the timing of p53, p21 or apoptosis activation in relation to abscission and other phases of the cell cycle and cellular events. Furthermore, this system could be used to differentiate whether Kif20b and/or Cep55 mutant cells with cytokinetic defects, such as abscission delay, abnormal midbody structure, or furrow regression, are indeed the cells that ultimately die.

While time-intensive, the definitive results produced from the p53 cross demonstrate the value of mouse mutant crosses to obtain clear answers as to the importance of a particular protein. It could be valuable to cross *Kif20b* and/or *Cep55* mutants to other mouse mutants lacking proteins upstream or downstream of p53 to further delineate the pathway (see Table 8). It would be interesting to see if co-deletion of p21 or PUMA, known downstream effectors of p53 whose RNA expression was increased in the *Kif20b* mutant, could rescue *Kif20b* mutant microcephaly. p21 is thought to mediate p53-dependent cell cycle arrest, while PUMA mediates p53-dependent apoptosis. Therefore, inhibition of p21 and PUMA would allow us to delineate the contributions of those two pathways to the p53-dependent proportion of *Kif20b* mutant microcephaly, and

would be relevant to our understanding of other microcephalies as well. These experiments are doable, as both p21 and PUMA mouse mutants develop normally (Jeffers et al., 2003; Martín-Caballero et al., 2001). Other mouse crosses could elucidate upstream mediators of p53 activity. ATM is a key regulator of the response to DNA double-stranded breaks that is upstream of p53 phosphorylation. There was some indication from RNA sequencing that DNA damage may be happening in the *Kif20b* mutant; if so, crossing to the *ATM* mouse mutant, which develops normally, may be able to rescue microcephaly, as it did in the BRCA1 mutant (Pao et al., 2014). A lack of rescue would be informative in differentiating the *Kif20b* mutant from other DNA damage mutants. There are still other DNA damage pathways that do not involve ATM, such as single-strand break pathways, that could be investigated further if ATM co-deletion provided no rescue. A cross to the USP28 mouse mutant could test for activation of the mitotic delay pathway, while a cross to LATS2 mutant and/or Yap overexpressing mice could test for activation of the tetraploidy pathway (Camargo et al., 2007; Q. Chen et al., 2015; Knobel et al., 2014). Finally, loss of the kinesin-6 family member Kif20a/MKLP2 results in microcephaly with some notable similarities to the *Kif20b* mutant (Geng et al., 2018). Therefore, it would be informative to know whether *p53* deletion can rescue *Kif20a* mutant microcephaly, and if so, to compare RNA sequencing from *Kif20b* and *Kif20a* mutants with and without *p53* loss.

**Table 8: Proposed mouse mutant crosses to identify upstream and downstream-mediators of p53 activation in *Kif20b* and/or *Cep55* mutant microcephaly**

Mouse Mutant Cross	Question Tested	Rationale
p21	Role of p21, a p53-dependent mediator of cell cycle arrest, in <i>Kif20b</i> or <i>Cep55</i> mutant apoptosis and microcephaly	p21 is a known target of p53; Cdkn1a RNA (gene for p21) is significantly upregulated in <i>Kif20b</i> mutant
Puma	Role of Puma, a p53-dependent mediator of apoptosis, in <i>Kif20b</i> or <i>Cep55</i> mutant apoptosis and microcephaly	Puma is a known target of p53; Bbc3 RNA (gene for Puma) is significantly upregulated in <i>Kif20b</i> mutant
ATM	Role of ATM, an upstream regulator of p53 in the DNA damage pathway, in <i>Kif20b</i> or <i>Cep55</i> mutant apoptosis and microcephaly	ATM co-deletion rescued microcephaly in the BRCA1 mutant, but did not rescue in the Cep63 mutant
USP28	Role of USP28, an upstream regulator of p53 in the mitotic delay pathway, in <i>Kif20b</i> or <i>Cep55</i> mutant apoptosis and microcephaly	USP28 activates p53 in response to mitotic delay in cell lines
LATS2 conditional knockout or Yap overexpressing	Role of the Hippo pathway, an upstream regulator of p53 in response to cytokinesis failure, in <i>Kif20b</i> or <i>Cep55</i> mutant apoptosis and microcephaly	The Hippo pathway, which acts through LATS2 to downregulate Yap, activates p53 in tetraploid/binucleate cells in cell lines

#### Examining consequences of apoptosis inhibition in microcephaly mutants

In this thesis work, we have used inhibition of p53 to test the model of microcephaly caused by cytokinetic defects that activate p53-dependent apoptosis (Figure 36, A). In this model, inhibition of p53 should rescue apoptosis and microcephaly, but not rescue cytokinetic defects (Figure 36, B). Inhibition of apoptosis allows us to further determine what cellular defects occur in cells with cytokinetic defects that are prevented from dying (Figure 36, B). It remains highly surprising that *p53* deletion can rescue microcephaly to such a great degree in many microcephaly mutants, including *Kif20b* and *Cep55* mutant microcephaly. While p53's role as a sensor of cellular damage and apoptosis activator is well documented and therefore its role in activating apoptosis in the cortex is not unexpected, it is remarkable that cells prevented from dying through p53 inhibition do not always endure further consequences that are detrimental to brain size. Some

mutants have in fact noted worsened phenotypes; for example, in a centrosome amplification mutant, p53 co-deletion rescued apoptosis but not brain size, and mice died prematurely (Marthiens et al., 2013). More work is needed to determine whether other mouse mutants with partially or completely rescued brain size from p53 co-deletion suffer deleterious consequences at later ages. Mice with rescued brain size may still have structural or lamination abnormalities which could be investigated with antibodies or cell-specific stains or dyes. Alterations in cell fate or identity could be identified with single cell sequencing. Finally, it is possible that even with normal brain size, structure and cell populations, “undead” cells could have defects in cell-cell connectivity or long-range signaling. These could be investigated with behavioral analyses and EEG recordings. Further investigation of the consequences of apoptosis prevention will inform the usefulness of this tool for treatment of human disease.

Apart from treating microcephaly directly, apoptosis inhibition could ultimately be useful for the treatment of other neurological disorders, such as neurodegenerative disorders in which neurons are prematurely eliminated. For example, treatment with a p53 inhibitor improved stroke recovery in rats (Luo et al., 2009). In Alzheimer’s disease, aberrant caspase activity is thought to contribute to Tau pathology and the formation of neurofibrillary tangles (De Calignon et al., 2010). Even reduced neuron function in these conditions may be preferable to complete loss of neuron activity. It would be necessary to target these treatments directly to the intended cell target, and to have temporal control. A more specific target than p53 would be ideal, as p53 inhibition can have secondary consequences for cell proliferation.

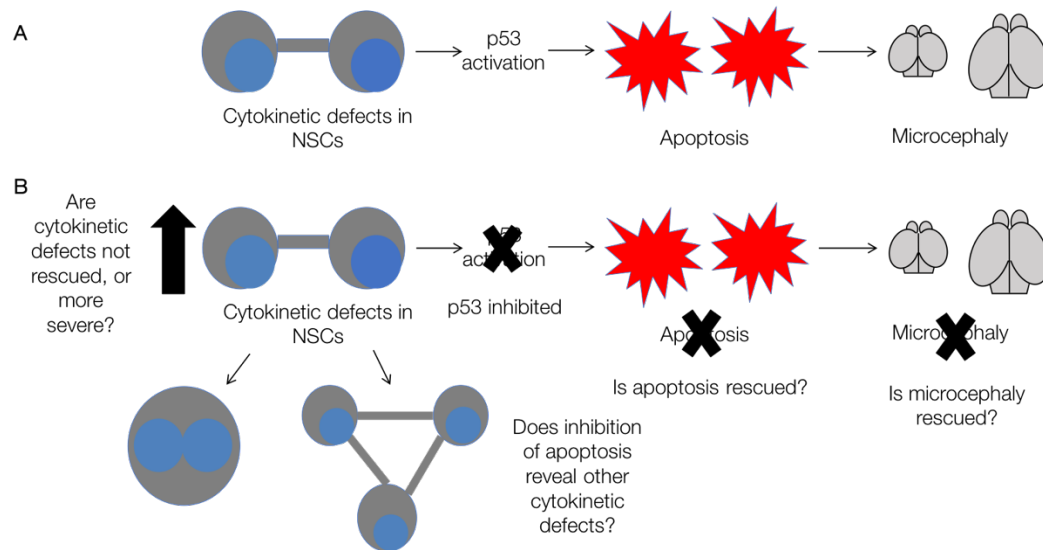


**Figure 37: Model for testing microcephaly etiology through p53 inhibition.**

**A.** Proposed model of microcephaly: Cytokinetic defects activate p53, which causes apoptosis, resulting in small brain size.

**B.** To test this model, we inhibited p53 and asked whether apoptosis and microcephaly were rescued, cytokinetic defects were not. Inhibition of apoptosis allows us to further determine what cellular defects occur in cells with cytokinetic defects that are prevented from dying.

*Addressing the consequences of failed abscission when apoptosis is allowed or prevented*

It is still unclear what defects failed or impaired abscission would result in apart from cell death in the cortex, if cleavage furrow regression did not occur. The dense cellular content of the cortical epithelium can render it difficult to visualize individual cell shapes. We have used electroporation, DiI and Golgi labeling techniques to observe single cells in the cortex (McNeely et al., 2017). These techniques could be utilized to observe shapes of cells prevented from undergoing cell death. A newer technique, mosaic analysis with double markers (MADM), allows genetic mosaic analysis of mutant and wild-type cells within the same embryo (Espinosa et al., 2014). A MADM-19 line has already been created, and could be crossed to Kif20b and Cep55 mutants as both genes are located on chromosome 19. MADM has been used in the cortex to evaluate neuron morphology and cell fates (P. Gao et al., 2014; Hippenmeyer et al., 2010) In addition to using these techniques in Kif20b and/or Cep55; p53 double mutants, it would be informative to acutely knock down Kif20b, Cep55 and/or other abscission proteins in control and p53 mutant cortices. This would enable an understanding of 1) the primary consequences of knockdown, including mitotic or cytokinetic delay, cell morphology changes, epithelium

disruption, migration defects, and/or apoptosis and 2) the direct consequences of cell death inhibition.

*Investigating candidate p53-independent signaling pathways in the Kif20b mutant*

Inhibition of apoptosis has been instrumental in elucidating the primary consequences of *Kif20b* loss, and in the future, will be helpful in differentiating primary versus p53-dependent consequences of *Cep55* loss. In addition to the cytokinetic abscission defects shown to be p53-independent in the *Kif20b* mutant, RNA sequencing analysis revealed several other genes/pathways that are worth investigating in *Kif20b* and/or *Kif20b;p53* double mutants.

*Arl3*: First, expression of the ciliogenesis gene *Arl3* was strongly and very significantly decreased in both *Kif20b* and *Kif20b;p53* double mutants, but was not affected by *p53* mutation itself. *Arl3* is a G-protein that localizes to the cilium and regulates ciliogenesis throughout ciliated organs, including the brain (Hanke-Gogokhia et al., 2016). Better known in the cortical development field, the cilia-specific protein *Arl13b* serves as a guanine exchange factor (GEF) for *Arl3* (Gotthardt et al., 2015). Germline mutation of *Arl3* causes multi-organ ciliopathy and retinal defects in mice and humans (Alkanderi et al., 2018; Schrick et al., 2006). Furthermore, *Arl3* is also expressed in the midbody and knockdown results in cytokinetic defects (Zhou et al., 2006). Interestingly, there are slightly reduced numbers of cilia in *Kif20b* mutant cortices (Janisch & Dwyer, 2016). *Kif20b* mutants display hydrocephalus, a hallmark of ciliopathy, which is not completely rescued by *p53* deletion (approximately 5% of *Kif20b*<sup>-/-</sup>; *p53*<sup>+/-</sup> mutants, less in *Kif20b;p53* double mutants). Therefore, while a mechanism for loss of *Kif20b* resulting in decreased RNA expression of *Arl3* is not obvious, there are many interesting connections between *Kif20b* and *Arl3* pathology that make *Arl3* a worthy target for further investigation. Verification of *Arl3* downregulation with RT-PCR and evaluation of *Arl3* protein expression in *Kif20b* mutant NSCs would be a reasonable place to start.

*Wnt signaling pathways and Atf5*: Wnt pathway genes, including *Wnt3a*, *Wnt7b*, *Wnt9a*, *Fzd9*, and *Rspodins 1,2 and 3* are downregulated in *Kif20b* and *Kif20b;p53* mutants compared to wild-type controls (see **Appendix 2**). The Wnt signaling pathway is known to promote proliferation and inhibit differentiation of neural stem cells (Palenik & Hu, 2009). Overexpression of *B-catenin*, a key downstream effector of the canonical Wnt signaling pathway, increases the progenitor pool leading to forebrain expansion; inhibition reduces brain size (Chenn & Walsh,

2002; Zechner et al., 2003). Therefore, the Wnt signaling pathway is a promising candidate for the p53-independent cell cycle exit and premature neurogenesis displayed in *Kif20b* mutants (**Appendix 1**). Additionally, the transcription factor Atf5 is a strong candidate for cell fate changes in *Kif20b* mutants (**Appendix 2**, Table 12); it normally acts to inhibit neurogenesis, and its expression is significantly reduced by loss of *Kif20b* (Angelastro et al., 2003; Greene et al. 2009).

*The formin mDia2 (Diaph3)*: Finally, RNA sequencing shows that diap3 (gene for protein product mdia2) expression is very significantly increased in *Kif20b;p53* mutants compared to *p53* mutant controls. Mdia2 is a formin that regulates actin remodeling and can also bind microtubules (Watanabe et al., 2008). Furthermore, it binds to Rho during cytokinesis and localizes to the midbody (Watanabe et al., 2008; Watanabe et al., 2010). Loss of diap3 causes microcephaly (Damiani et al., 2016). This target is of high interest, because it was recently shown to co-IP with Kif20b (Isogai et al., 2015). Furthermore, it can bind p53 and increased diap3 expression results in increased p53 activity (Isogai et al., 2015). Excitingly, we found decreased localization of mdia2 to *Kif20b* knockdown HeLa cell midbodies (K. McNeely, unpublished). An attractive hypothesis is that mdia2 may not be able to locate to the midbody without *Kif20b*, but may be increased in expression in the nucleus, since it can shuttle between nuclear and cytoplasmic compartments (Miki et al., 2009). It would be interesting to see whether total mdia2 protein expression and/or mdia2 location is altered in *Kif20b* mutant NSCs. Unfortunately, the antibodies to mDia2 used for immunofluorescence in HeLa cells have not worked in mouse NSC's to date (KM, unpublished).

Investigating the apoptotic process in the cortical epithelium

*Determining the amount of normally-occurring apoptosis in the developing cortex*

It remains surprisingly unclear the extent to which apoptosis and/or other forms of cell death occur in the cortex as a part of normal development. While we and others have observed few apoptotic cells in control cortices using antibodies to cleaved-caspase 3, higher amounts of cell death have been observed in the cortex using other labeling techniques, such as detection of fragmented DNA (Blaschke et al., 1996), and clonal analysis using MADM (Mihalas et al., 2016). Live imaging of cell division with an apoptotic cell marker would be highly informative in

control cortices as well as *Kif20b* and *Cep55* mutant cortices. A transgenic apoptosis reporter mouse would be a useful tool (To et al., 2015; Yamaguchi et al., 2011). Imaging of apoptosis could be done in live cross-section or slab preparations. Undoubtedly, this would require technical troubleshooting to implement, but would be invaluable to our understanding of cell death in the cortical epithelium.

#### *Following the fates of apoptotic cells*

Besides observing whether a cell expressed apoptotic markers, live imaging would also enable visualization of the fate of an apoptotic cell. In epithelia, apoptotic cells can be extruded, involving both actin- and myosin- dependent changes in neighbor cells as well as autonomous changes in the apoptotic cell itself (Gagliardi et al., 2018; Rosenblatt, Raff, & Cramer, 2001). However, it is not well understood whether apoptotic cells are phagocytosed and/or extruded from the apical membrane in the cortical epithelium and the mechanisms by which this occurs. Furthermore, apoptotic cell extrusion has been suggested to occur to maintain cell numbers as apoptotic cells signal for increased proliferation of surviving cells (Eisenhoffer et al., 2012). While there is evidence that neuronal death can stimulate NSC proliferation, the extent to which this occurs *in vivo* is not known (Magavi et al., 2000). The *Cep55* mutant would be an ideal model to study apoptotic cell extrusion, phagocytosis and cell-cell signaling in the cortex. It has also been suggested that some cells that express caspases can “recover” and are not terminally dead (Tang et al., 2012), including neurons overexpressing tau in Alzheimer’s pathology (De Calignon et al., 2010). While unlikely, it would be highly interesting to observe a cell expressing apoptotic cell markers in the cortex stop expressing those markers, polarize and/or divide again.

#### *Elucidating cell- and tissue-type specific apoptotic processes in microcephaly mutants*

A hallmark of primary microcephaly in humans and mouse mutants is the severity of the reduction in brain size in comparison to other body tissues. While an interesting observation, the molecular, cellular and tissue-level mechanisms for this phenomenon have been poorly addressed by the cortical development field. In order to address these mechanisms more directly, it would be advantageous to compare cortical phenotypes to those seen in other epithelia and other cell types, as well as mouse phenotypes to other organisms. Interestingly, centrosome defects caused by loss of *Sas-4*, which are severely consequential in mouse brains due to p53-dependent apoptosis (Insolera et al., 2014) do not cause cell death in fly brains (Basto et al., 2006). This is

proposed to be due to compensation of the spindle assembly checkpoint (SAC) in fly brains to properly complete mitosis, a mechanism which may have been lost in mammalian brains (Poulton et al., 2017). In the *Cep55* mutant, we compared NSC cultures to cultures of mouse embryonic fibroblasts. Interestingly, we saw increased nuclear p53 in *Cep55* mutant NSC cultures but not MEFS, suggesting that the p53 response to cellular defects may be differential between these cell types. This could in part explain why the *Cep55* mutant brain size is so much more severely affected than the rest of the body. Continued work comparing *Cep55* mutant brain phenotypes to other epithelial and non-epithelial tissues *in vivo*, including ESCRT recruitment, formation of binucleate cells or indications of abscission delay, p53 activation and apoptosis would be informative.

Investigating coordination of cytokinetic abscission with multicellular processes in cortical development

There is much more work to be done to understand how processes of abscission are accomplished in the multicellular cortical epithelium. We need a better understanding of how cytokinetic abscission processes are coordinated with A) centrosome segregation and cilia formation, B) new apical junction formation and/or delamination of daughter cells, C) midbody remnant release, and D) adoption of cell fate. We have utilized the fixed cortical slab preparation to visualize the apical membrane of the cortex; immunostaining with Zo-1, aurora B kinase, citron kinase and phospho-histone 3 allows identification of NSC apical endfeet, midbodies, midbody remnants and mitotic cells, respectively. Additionally, we have used live imaging to begin to elucidate the temporal coordination of these events by using a mouse expressing membrane Tomato and membrane GFP (mT/mG) with application of SiR-Tubulin to label microtubules and visualize abscission (McNeely et al., 2019).

Investigation of the above processes in *Cep55* and *Kif20b* mutants and/or with acute knockdown of *Cep55*, *Kif20b* and/or other abscission proteins would be valuable in comparison to controls. In the *Cep55* mutant, disruption of the coordination of multicellular processes could contribute to microcephaly in addition to cell-autonomous impairment of cell division. Live imaging of abscission in a *Cep55* mutant mTmG mouse with SiR-Tubulin as was performed in the *Kif20b* mutant should be highly informative in determining the duration of abscission, completion versus regression of abscission, and coordination of abscission with membrane cleavage.

*A) Centrosome segregation and cilia formation:* The position of midbodies and midbody remnants has a role in multicellular epithelial processes across species. In cultured epithelial cells, the midbody is suggested to play a role in ciliogenesis as well as lumen formation (Bernabé-Rubio et al., 2016; Li et al., 2014). Therefore, it would be interesting to analyze the position of midbodies and midbody remnants in relation to centrosomes (using an antibody to pericentrin, centrin or  $\gamma$ -tubulin) and cilia (using an antibody to Arl13b) in cortical slabs and sections to see if their positions are correlated. Live slab imaging with SiR-Tubulin could be combined with other markers, such as transfection of fluorescently-tagged proteins to centrosome or cilia markers, to visualize coordination of abscission with the processes of new apical centrosome segregation and cilia formation.

*B) New apical junction formation and/or delamination of daughter cells:* We have used Aurora B kinase and Zo-1 to evaluate midbody shape, number and alignment to the apical membrane. Additionally, we analyzed apical endfoot shape changes in relation to midbody maturation, and found that they were significantly correlated (**Appendix 1**). Remodeling of cell-cell junctions in coordination with cytokinesis has been elucidated with fluorescent markers and live imaging in *Xenopus* (Higashi et al., 2016). A comparison of these processes with similar experiments in the mouse cortex would be of great interest. Furthermore, it is not known at what point abscission occurs in relation to nuclear migration away from the apical membrane in daughter cells. Fixed and live analyses in cortical cross-sections with membrane markers (mTmG, p-Vimentin or MPM-2), Dapi or other nuclear markers, and midbody markers (SiR-Tubulin, AurkB, Anillin, or Survivin), could be used to determine the coordination of these events. This question may be better answered by sparse labeling using electroporation or MADM techniques.

Apical endfeet in the *Cep55* mutant appear very disorganized with variability in size and open spaces. These defects could be secondary to apoptotic processes, such as extrusion of apoptotic cells into the ventricle or delamination of dying apical NSCs. Alternatively, binucleate NSCs in *Cep55* mutant cortices may have larger endfeet than mononucleate cells. Finally, it is possible that *Cep55* has a primary role in apical endfeet formation or coordination with cytokinetic processes. These possibilities could be differentiated by 1) analyzing apical endfeet in *Cep55;p53* double mutants, to determine if defects are still present when apoptosis is inhibited, 2) fixed analyses with cleaved-caspase 3, DAPI and Zo-1, to elucidate whether large endfeet contain two

nuclei and/or apoptotic nuclei, and 3) live imaging with a marker for apoptotic cells and/or a live apical junction marker.

C) Midbody remnant release: Recent work in our lab has revealed that abscission is bilateral in the majority of NSC divisions (McNeely et al., 2019). Although we can visualize midbody remnants on the apical membrane with antibodies to Citron kinase, we do not know whether midbody remnants are internalized by daughter cells or simply stuck to the apical membrane. Higher resolution imaging of remnants with membrane and apical junction markers should be able to answer this question. Of particular interest, Cep55 is highly expressed in midbody remnants and a role for Cep55 in midbody remnant signaling has been suggested (Crowell et al., 2014). We did not find a role for Kif20b in midbody remnant release or inheritance, but did find a shift in both control and mutants over developmental time in the association of remnants with daughter cells (McNeely et al., 2019). It would be interesting to determine whether midbody release versus inheritance is shifted in *Cep55* mutants and whether the association of these remnants with specific daughter cell fate is altered. This could be accomplished as done in the *Kif20b* mutant with the pair cell assay and markers for cell type (Nestin, Tuj1) and midbody remnants (Citron kinase).

D) Adoption of cell fate: There are numerous indications from studies in cell lines and epithelia that abscission, and in particular midbody remnant release, is coordinated with cell fate (See this thesis, **Introduction**, and (Dionne et al., 2015). However, this has yet to be clearly shown in cortical cells and in the cortical epithelium. Better temporal resolution is needed to demonstrate clear correlation of these events. Live imaging in dissociated NSCs with a midbody marker, such as SiR-Tubulin, and a marker for cell type could theoretically correlate the timing of abscission, bilaterality of abscission, and inheritance or release of the midbody remnant with cell fate. In particular, mice engineered to fluorescently express doublecortin, a neuronal marker (*Dcx::DsRed* mice; (Wang et al., 2007)) or *Tbr2*, an intermediate progenitor marker (*Tbr2-EGFP* mice; (Arnold et al., 2009)) could be used to identify adoption of neuronal and intermediate progenitor fate in correlation with abscission events. This experimental design was used to show that the length of mitosis in NSCs is correlated with cell fate (Pilaz et al., 2016). However, we have had difficulty imaging abscission in cultured NSCs. *In vivo*, SiR-tubulin or another midbody marker could be used in the *Dcx* or *Tbr2*-expressing mouse to determine fates of cells in

association with abscission events. It may be necessary to image in lateral sections rather than slabs to visualize daughter cell fate.

## Appendix 1: p53-dependent and -independent consequences of *Kif20b* loss in NSCs

The data presented in **Chapter 2** (adapted from (Little & Dwyer, 2019)) indicates that microcephaly in the *Kif20b* mutant is largely p53-dependent, but that there is an additional p53-independent component. Furthermore, we showed midbody morphology and alignment defects were p53-independent. The following experiments identify additional p53-dependent or -independent cellular defects in the *Kif20b* mutant. We also investigated cellular pathways known to activate p53, but did not find evidence to implicate these pathways. Data in Fig. 41A-C was included in a paper (authors McNeely, Little and Dwyer) submitted for publication in January 2019.

The methods used in this appendix include mouse embryo and brain collection, NSC/progenitor culture preparation, flow cytometry, embedding and cryosectioning of whole brains, cortical slab preparation, H&E staining, immunostaining, imaging with Zeiss and DeltaVision fluorescent microscopes and a Leica brightfield microscope, analysis with ImageJ software, and statistical analysis with Excel and GraphPad Prism. These methods are all described in further detail in **Chapters 2 and 3**. Cell fate analysis (Fig. 43A-C) *in vitro* was analyzed using NSC cultures prepared from E12.5 cortices, with the addition of 10  $\mu$ M BrdU added to cultures for the first 6 hours of culturing, followed by wash-out, continued culturing and fixation at 20 hrs. Before immunostaining, antigen retrieval was performed with 0.07M NaOH pH 13 for 2 minutes, followed by permeabilization, in order to visualize BrdU incorporation. Cell cycle exit analysis was analyzed *in vivo* (Fig. 43D-E) by injecting pregnant mothers at E11.5 with 100  $\mu$ M BrdU. Embryos were collected 24 hrs later at E12.5. Antigen retrieval was used for BrdU visualization with sodium citrate buffer as previously described (see **Chapter 2**, methods). Mice collected for p21 analysis (Figure 44) were anesthetized and perfused with PBS, followed by dissection of brains and fixation in 4% PFA for 48 hrs.

We previously showed that *Kif20b* mutant NSCs, when dissociated and cultured for 24 hrs, displayed cell-autonomous defects in midbody structure (**Chapter 2**). *Kif20b* mutant NSC midbodies are wider *in vivo* and *in vitro*, and are less often observed with a constriction site *in vitro*. Reduced constriction site formation is not rescued in midbodies of *Kif20b;p53* mutant NSCs. *Kif20b;p53* mutant NSC midbodies are also wider *in vitro* (Fig. 38A). Interestingly, we found that *Kif20b;p53* mutant midbodies were longer *in vivo*, a defect that was not observed in

*Kif20b* mutant midbodies (**Chapter 2**). *Kif20b;p53* mutant midbodies are also longer *in vitro* (Fig. 38B). New data indicates that *Kif20b* mutant NSCs undergo abscission (defined by microtubule disassembly by SiR-tubulin) faster than control NSCs. Moreover, *Kif20b* mutant NSC midbodies abscise when wider than control NSCs, indicating that Kif20b normally functions to delay abscission until the microtubule-rich midbody structure is appropriately thinned. While we are not currently able to perform live imaging in *Kif20b;p53* double mutants, the aforementioned lack of rescue of structural defects in *Kif20b;p53* mutants indicates that abscission defects are likely p53-independent. Furthermore, *Kif20b;p53* mutant midbodies with a constriction site, signifying a late midbody maturation stage (close to abscission occurring), are wider than controls at the same stage *in vivo* (Fig. 38C), and exhibit a trend to be wider *in vitro* (Fig. 38D). This suggests that faster abscission, occurring when midbodies are wider than controls, is likely p53-independent. These data show that midbody maturation defects in *Kif20b* mutant NSCs are cell autonomous, p53-independent, and are possibly made more severe in *Kif20b;p53* mutants when apoptosis is inhibited.

Midbody maturation and abscission are coordinated in the cortical epithelium with changes in apical junctions between newly-formed daughter cells. We use Zo-1 to visualize the apical endfeet of NSCs at the apical membrane. We noticed that as the midbody matured and became thinner, the apical endfoot of the mother cell pinched in between the two midbody flanks, forming two new daughter cell apical endfeet (Fig. 40A). Thus, midbodies could be described as having open endfeet or closed endfeet. We also noticed that there was variation in apical endfoot shape, including asymmetry between daughter cell endfeet. We wanted to quantify this process to better understand if it was happening in a stereotyped manner and whether it was altered in *Kif20b* mutants. We found that in controls, as midbodies became thinner (later stage), the individual apical endfeet also became smaller (Fig. 39A). Furthermore, as apical endfeet became smaller, the midbodies also became shorter (Fig. 39D). This indicates that normally, as midbody maturation occurs *in vivo*, the distribution of Aurora B becomes thinner and shorter, and apical endfeet become smaller. This process was not disrupted in *Kif20b* mutants, as the same correlations were still seen (Fig. 39B,C,E). However, in *Kif20b;p53* mutants the association between midbody length and apical endfoot size was lost, suggesting some discoordination of this process (Fig. 39F).

In *Kif20b* and *Kif20b;p53* mutants, we observed more midbodies that were at the open endfoot stage, consistent with our observation of wider, early-stage midbodies (Fig. 40B). At this stage, the size of *Kif20b* mutant endfeet was not altered (Fig. 40C). However, we did find that in *Kif20b* mutants and *Kif20b;p53* mutants, the area of closed endfeet in midbody stage cells at the closed endfoot stage was larger (Fig. 40D). This defect appeared to be approximately twice as severe in double mutants. As endfeet become smaller as midbodies become thinner, and *Kif20b* mutant and *Kif20b;p53* mutant midbodies are wider than controls, it is likely that the endfeet are larger at this stage because the midbodies are wider. These data suggest that midbody maturation and apical membrane formation are tightly coupled, and this coupling is not altered by *Kif20b* loss. We also investigated apical endfeet asymmetry. In controls, the ratio of daughter endfeet size (larger endfoot:smaller endfoot) was approximately 2, indicating a high degree of asymmetry (Fig. 40E). In *Kif20b* mutants, this ratio was approximately 50% increased, indicating a higher degree of asymmetry. However, this asymmetry was rescued in *Kif20b;p53* double mutants (Fig. 40E). Further analysis indicated that increased asymmetry in *Kif20b* mutants came from a population of endfeet that were highly asymmetric (ratio >5), which were not observed in *Kif20b;p53* mutants (Fig. 40F). Therefore, the p53-apoptotic process exerts endfeet shape changes in *Kif20b* mutants, perhaps due to apoptotic cells retracting their endfeet. This is interesting as endfeet asymmetry has been noted in other microcephaly mutants and hypothesized to be a cause of cell fate changes; however, our data indicates they are more likely to be secondary to apoptotic processes.

Evidence exists for two pathways for p53 activation in the cortex; the DNA damage pathway and the mitotic delay pathway. Furthermore, there is evidence, albeit controversial, in cell lines that cytokinesis failure resulting in a binucleate or tetraploid cell can activate p53. We attempted to evaluate these pathways in the *Kif20b* mutant. We do not have evidence that *Kif20b* mutation results in mitotic delay before cytokinesis stages (Chapter 2). Furthermore, the mitotic index in E14.5 sections of *Kif20b;p53* double mutants is not significantly different than controls (data not shown). We did not find an increase in the number of  $\gamma$ H2AX+ puncta, the usual indicator of DNA damage, in *Kif20b* mutant cortices (**Chapter 2**). Furthermore, we found no significant difference in nuclear  $\gamma$ H2AX intensity in *Kif20b* mutant or *Kif20b;p53* mutant NSCs compared to controls (Fig. 41A,B). Therefore, we conclude that there is no obvious increase in DNA damage marked by  $\gamma$ H2AX. It is still possible that DNA damage is subtle; it could be occurring in only a portion of cells or only at a certain point of the cell cycle. Furthermore, damage can occur that is not marked by  $\gamma$ H2AX, such as single-stranded breaks. RNA sequencing analysis (**Appendix 2**)

suggests that there is activation of DNA repair genes in *Kif20b* and *Kif20b;p53* double mutants. However, if DNA damage is occurring it is likely to be a different pathway than that demonstrated in other microcephaly mutants, such as the *Nde1* mouse mutant, which have obviously increased  $\gamma$ H2AX+ puncta.

The Hippo pathway stabilizes p53 in binucleate or tetraploid cells in some cell lines (Ganem et al., 2014). This is thought to be due to sensing of the increased size of binucleate cells. We investigated Hippo pathway activation by looking at Yap expression in *Kif20b* mutant NSC cultures. Activation of the Hippo pathway results in inhibition of Yap by sequestering it in the cytoplasm. Surprisingly, we found increased nuclear Yap expression in *Kif20b* mutant NSCs (Fig. 41C-E). Therefore, the Hippo pathway is likely not active and may be inhibited. In *Kif20b;p53* mutants, this defect was rescued and no difference in Yap expression compared to controls was observed (Fig. 41F). Surprisingly, this indicates that p53 activation results in increased nuclear Yap in *Kif20b* mutant NSCs. We find no evidence of Hippo pathway activation that could be upstream of p53. However, it would be more ideal to test for activation of this pathway *in vivo*. To test whether *Kif20b* loss resulted in increased binucleate NSCs, as it did in HeLa cells, we used NSC cultures and flow cytometry. In NSC cultures, we did find a slight increase in binucleate cells, which was primarily due to an increase of binucleate neurons (Fig. 42A,B). However, we found that *p53* deletion itself was the main contributor to this phenotype; *Kif20b*<sup>+/-</sup>; *p53*<sup>-/-</sup> NSC cultures had increased numbers of binucleate cells, and specifically binucleate neurons, compared to double heterozygote controls (Fig. 42B). To further evaluate the existence of binucleate or tetraploid cells *in vivo*, we performed flow cytometric analysis of E14.5 cortices to assess DNA content. We found no significant difference in DNA content (and thus, cell cycle parameters) in *Kif20b;p53* double mutants (Fig. 42C-E). We found no evidence to support a role for *Kif20b* in prevention of binucleation. However, our finding of an increase in binucleate cells in *p53* mutant cultures suggests that p53 may normally act to eliminate small numbers of naturally occurring binucleate cortical cells, consistent with our hypothesis of a role for p53 in eliminating binucleate cells in the *Cep55* mutant.

*Kif20b* mutation results in a premature increase in neurogenic divisions as opposed to proliferative divisions (McNeely et al., 2019). To determine whether this was a consequence of p53 loss or a p53-dependent effect, we cultured NSCs from *Kif20b;p53* mutants with BrdU to identify dividing cells (Fig. 43A). We found that *Kif20b;p53* mutant NSCs still underwent

increased numbers of symmetric neurogenic divisions compared to controls (Fig. 43B). This shift was not due to *p53* mutation itself as NSCs from *p53* mutants had normal fates. We also determined the number of NSCs that had exited the cell cycle during the culture period by calculating the number of BrdU+ cells that were positive for neuronal markers out of the total BrdU+ cells. We found increased cell cycle exit in *Kif20b;p53* mutant cultures (Fig. 43C). To investigate whether cell fate changes occurred *in vivo* as well as *in vitro*, we injected E11.5 pregnant mothers with BrdU and collected pups 24 hours later. At E12.5, the neuronal layer is a greater proportion of the total cortical thickness in *Kif20b* mutants with wild-type *p53*, indicating increased early neurogenesis (Fig. 43D). This phenotype was not as robust in *Kif20b;p53* double mutants, but a trend was still observed. In calculating cell cycle exit, however, we found that *Kif20b;p53* double mutants did have increased cell cycle exit (Fig. 43E). Taken together, these data indicate increased cell cycle exit in the *Kif20b* mutant is *p53*-independent.

Finally, we wanted to investigate whether cell fate changes resulted in a permanent reduction in brain growth, and whether this altered brain functioning. Alternatively, the smaller brain size seen in *Kif20b;p53* mutants at P0 could be due to delayed brain growth that would eventually catch up to controls. To address this, we collected brains from *Kif20b;p53* mutants at age P21 (Fig. 44A,B). We found the cortical length in *Kif20b;p53* mutants was still decreased (approximately 5%) and the cortical thickness was still significantly reduced in rostral and middle sections, compared to controls and *p53* single mutants. (Fig. 44C,D). Therefore, brain size in *Kif20b;p53* mutants is permanently reduced.

To determine whether reduced brain size had any effect on functioning, we performed EEG recordings to monitor for spontaneous seizures in *Kif20b<sup>-/-</sup>;p53<sup>+/-</sup>* mice in collaboration with Dr. Howard Goodkin. Two male and two female adult *Kif20b<sup>+/-</sup>;p53<sup>+/-</sup>* mice (control group), three male and two female adult *Kif20b<sup>-/-</sup>; p53<sup>+/-</sup>* mice, one female adult *Kif20b<sup>-/-</sup>;p53<sup>+/+</sup>* mouse, and one female adult *Kif20b<sup>-/-</sup>;p53<sup>-/-</sup>* mouse were recorded continuously for approximately two weeks. Mice were between P60 and P150 at the time of recording. The following methodological information was provided from Pravin Wagley from Dr. Goodkin's laboratory: Animals were stereotaxically implanted with bipolar insulated stainless-steel electrodes in the left hippocampus (3mm AP, 3mm ML, 3 mm DV), bilateral parietal cortical electrodes, and a cerebellar reference electrode (see (Lewczuk et al., 2018) for electrode coordinates). To obtain EEG recordings, a special cable (op-amp cable, see (Zanelli et al., 2014)) made with a unity gain impedance

matching head stage (TLC2274 Quad Low-Noise Rail-to Rail Operational Amplifier, Texas Instruments, Dallas Tx) was used. Animals were connected to a video-EEG monitoring system (Grass AURA LTM64 using Twin software) via a flexible cable connected to the amplifier through an electrical swivel. Animals were monitored continuously with video-EEG system. EEG recordings were reviewed by Dr. Howard Goodkin. No spontaneous seizures were observed in *Kif20b*<sup>-/-</sup>;*p53*<sup>+/-</sup> mice and no obvious differences were observed from control recordings (data not shown). This analysis cannot completely rule out the presence of abnormal discharges.

## Figures

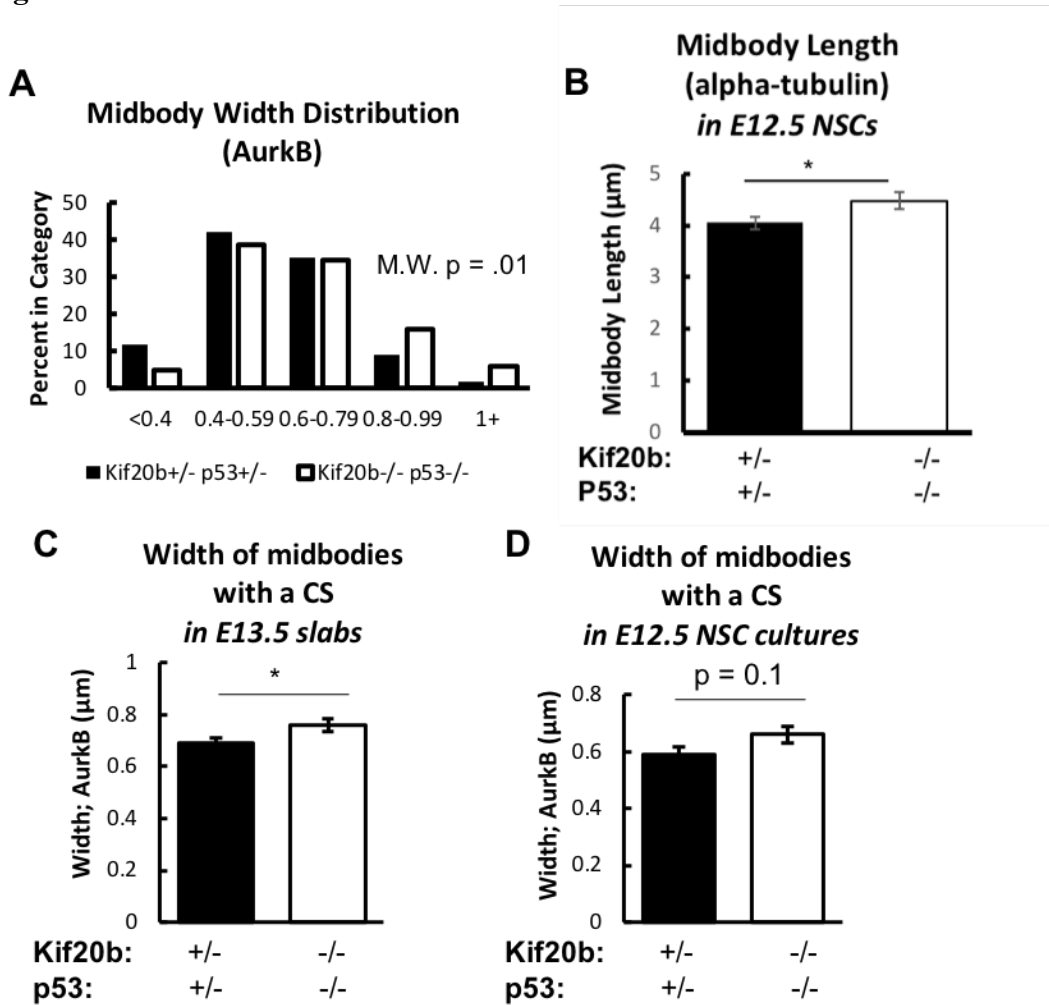


**Figure 38.** *Kif20b;p53* mutant midbodies are wider and longer than control midbodies.

(A) Early-stage MBs are wider with no constriction sites, while late-stage MBs are thinner and have one or two constriction sites (see **Chapter 2**, Fig. 8A-C). *Kif20b;p53* mutant midbodies in NSCs cultured from E12.5 cortices for 24 hrs *in vitro* (white bars) have a significantly shifted width distribution, with more wide midbodies compared to double heterozygote controls (black bars). Medians (width defined by AurkB signal): *Kif20b*<sup>+/-</sup>;*p53*<sup>+/-</sup>, 0.58 μm; *Kif20b*<sup>-/-</sup>;*p53*<sup>-/-</sup>, 0.63 μm (B) *Kif20b;p53* mutant midbodies are significantly longer than controls as defined by alpha-tubulin immunostaining in E12.5 NSC cultures at 24 hrs. (C) *Kif20b;p53* mutant midbodies (defined by AurkB) in E13.5 cortical slabs are wider than controls at the constriction site stage. n = 63 control and 36 double mutant midbodies. (D) *Kif20b;p53* mutant midbodies (defined by AurkB) in E12.5 NSC cultures at 24 hrs trend but are not significantly wider than controls. n = 41 control and 28 double mutant midbodies. n for A,B = 111 *Kif20b*<sup>+/-</sup>;*p53*<sup>+/-</sup> and 101 *Kif20b*<sup>-/-</sup>;*p53*<sup>-/-</sup> midbodies from 3 coverslips and embryos each. Mann-Whitney test for A; student's t-test for B-D. \*, p < 0.05.

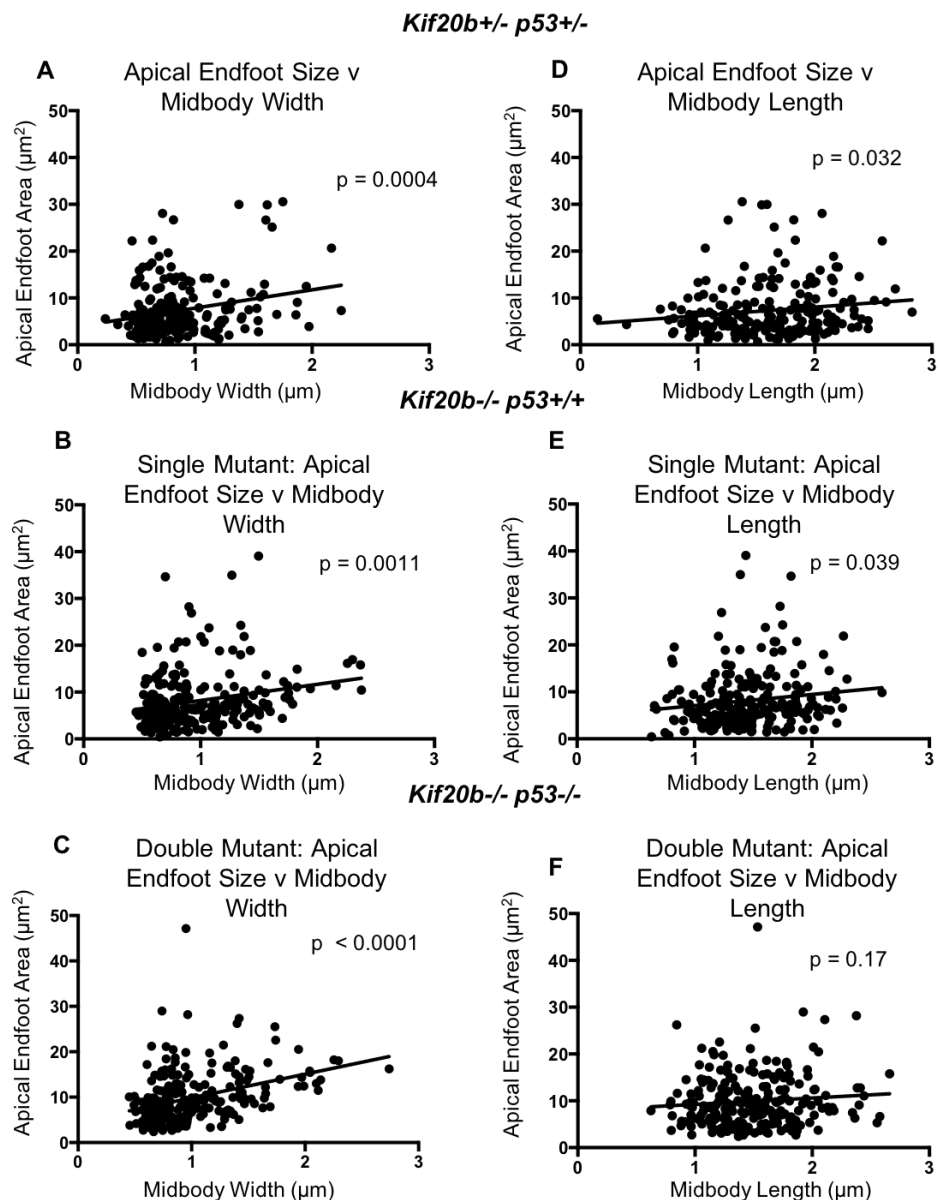


**Figure 39.** Midbody maturation is coordinated with NSC apical endfeet morphological changes. (A) Midbodies are wide after cleavage furrowing and become thinner before abscission occurs. There is a significant correlation between midbody width and NSC apical endfoot size in control (*Kif20b*<sup>+/-</sup>;*p53*<sup>+/-</sup>) cells; wider midbodies are associated with larger endfeet. As the midbody thins, the endfoot becomes smaller. (B-C) *Kif20b* mutation, with or without *p53* co-deletion, does not impair coordination of midbody thinning with reduction in apical endfoot size. (D) Midbody length is also significantly correlated with apical endfoot size in control cells; longer midbodies are associated with larger endfeet, and shorter midbodies are associated with smaller endfeet. (E-F) *Kif20b* mutation does not impair coordination of midbody length with apical endfoot size (E). However, *Kif20b*;*p53* mutants do not have a significant coordination between midbody length and apical endfoot size, suggesting a dysregulation of this process (F). All analysis completed on E13.5 cortical slabs; midbodies were defined by AurkB and apical endfeet were defined by Zo-1 immunolabeling. N = 218 *Kif20b*<sup>+/-</sup>;*p53*<sup>+/-</sup>, 219 *Kif20b*<sup>-/-</sup>;*p53*<sup>+/-</sup> and 231 *Kif20b*<sup>-/-</sup>;*p53*<sup>-/-</sup> midbodies/endfeet. Correlation analysis conducted with GraphPad Prism software.

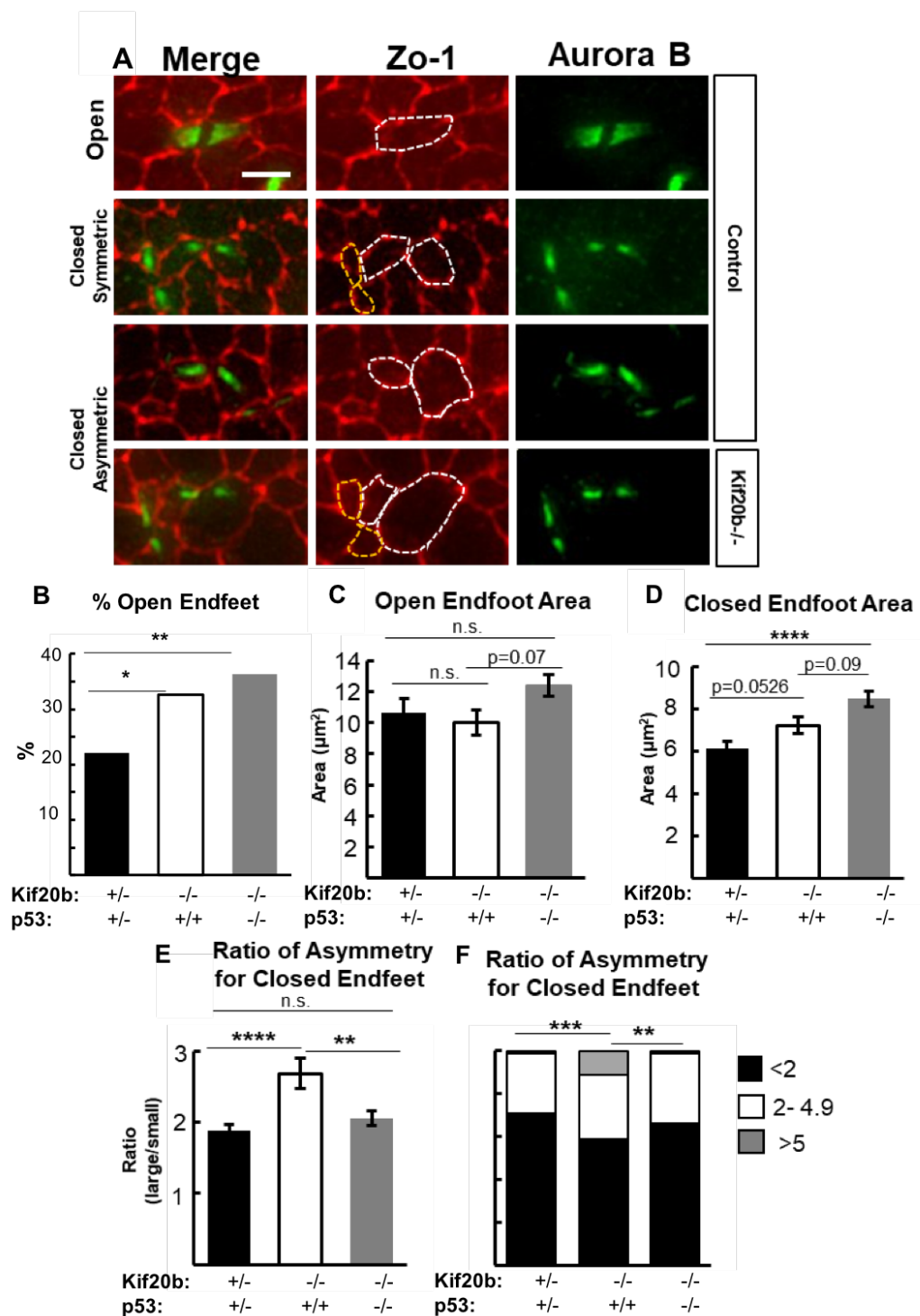


**Figure 40.** *Kif20b* mutants exhibit p53-dependent and p53-independent changes in NSC endfeet morphology. (continued on next page)

**Figure 40.** Kif20b mutants exhibit p53-dependent and p53-independent changes in NSC endfeet morphology.

**(A)** Max projection images of apical endfeet (Zo-1) and midbodies (AurkB) immunolabeling on E13.5 cortical slabs. Midbody maturation is coordinated in changes with NSC apical endfeet morphology. At the end of furrowing, the midbody is wide, and the mother NSC has one open endfoot surrounding the midbody (Control, open). As the midbody thins, two new daughter cell endfeet are formed by pinching in of the mother cell open endfoot (Control, closed). The new daughter cell endfeet may be symmetric (Control, closed symmetric) or asymmetric (Control, closed asymmetric). We evaluated the size of endfeet and degree of asymmetry in Kif20b mutant NSCs (*Kif20b*<sup>-/-</sup>, closed asymmetric). **(B)** The % of midbody-stage NSCs with open endfeet is increased in *Kif20b*<sup>-/-</sup> and *Kif20b*<sup>-/-</sup>;*p53*<sup>-/-</sup> brains. Fishers exact test. n = 181 *Kif20b*<sup>+/-</sup>;*p53*<sup>+/-</sup>, 178 *Kif20b*<sup>-/-</sup>;*p53*<sup>+/+</sup>, 231 *Kif20b*<sup>-/-</sup>;*p53*<sup>-/-</sup> midbody stage NSCs. Kif20b mutant NSCs have normal apical endfoot area at the midbody-open endfoot stage. **(C)** In midbodies associated with closed apical endfeet, Kif20b mutant apical endfoot area is significantly larger than controls. This is not rescued by p53 co-deletion and in fact is more significant. **(D)** In midbody-stage cells associated with closed endfeet, Kif20b mutant NSCs exhibit increased asymmetry of daughter cell endfeet, defined as a ratio of the larger endfoot to the smaller endfoot. However, this is rescued by p53 co-deletion. **(E)** Increased asymmetry of Kif20b mutant endfeet at the closed-midbody stage is due to an increase in cells with asymmetric ratios of > 5, which is rescued by p53 co-deletion. All analysis completed on E13.5 cortical slabs; at least 4 for each genotype. n for B: 40 *Kif20b*<sup>+/-</sup>;*p53*<sup>+/-</sup>, 58 *Kif20b*<sup>-/-</sup>;*p53*<sup>+/+</sup> and 84 *Kif20b*<sup>-/-</sup>;*p53*<sup>-/-</sup> endfeet. n for C-E: 168 *Kif20b*<sup>+/-</sup>;*p53*<sup>+/-</sup>, 143 *Kif20b*<sup>-/-</sup>;*p53*<sup>+/+</sup>, 147 *Kif20b*<sup>-/-</sup>;*p53*<sup>-/-</sup> endfeet pairs. B-D, one-way ANOVA; E, Chi square analysis. Scale bar: 5  $\mu$ m. \*p < 0.05, \*\* p < 0.01, \*\*\* p < 0.001, \*\*\*\* p < 0.0001.

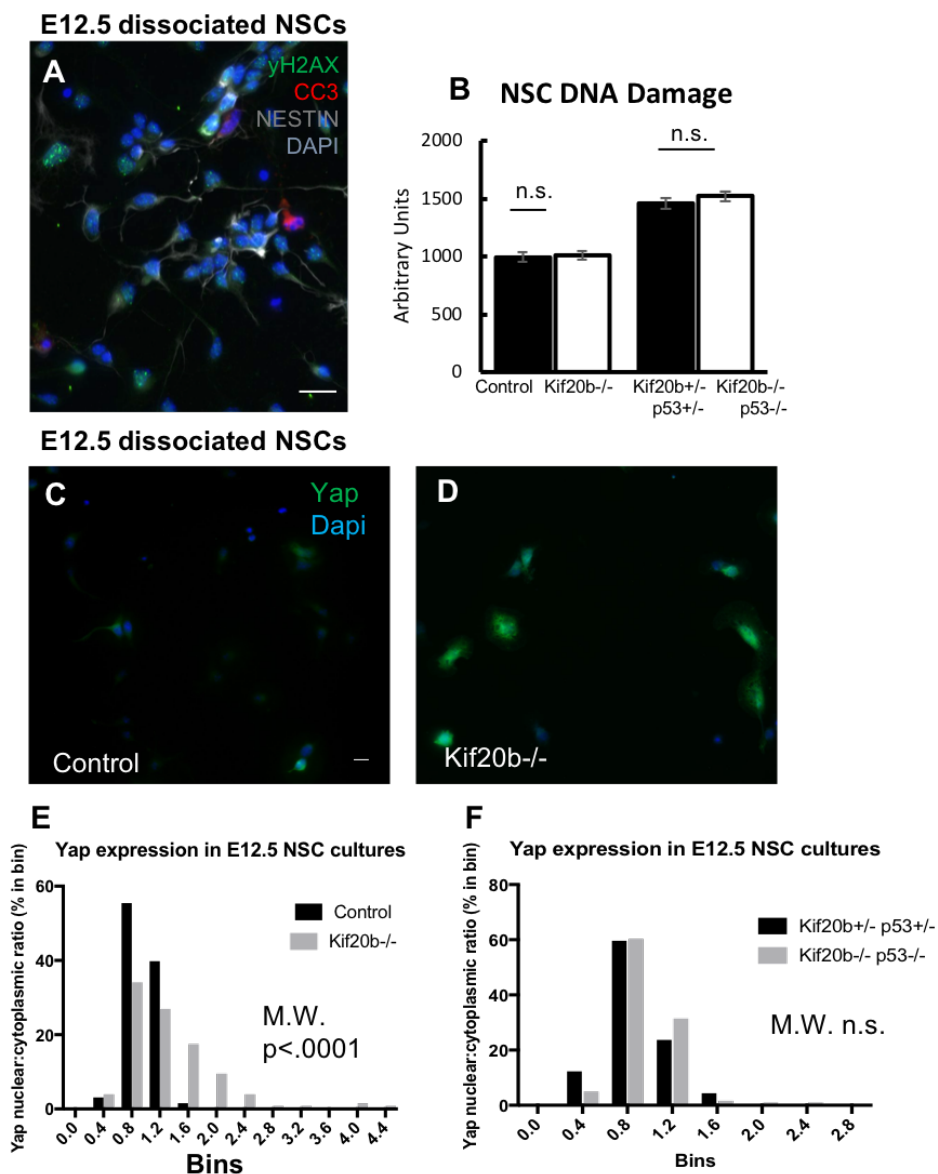


**Figure 41.** Evaluation of DNA damage and Hippo pathways in *Kif20b* mutants *in vitro*. (A) E12.5 NSCs cultured for 24 hrs and labeled with antibodies to yH2AX (green) to mark sites of DNA damage, cleaved-caspase 3 (red) to mark apoptotic cells, Nestin (gray) to identify NSCs and Dapi to identify nuclei. (B) *Kif20b* mutant and *Kif20b*;p53 double mutant NSCs have no significant difference in nuclear yH2AX intensity. t-test.  $n = 284$  *Kif20b*<sup>+/+; +/-</sup> and 448 *Kif20b*<sup>-/-</sup> NSCs; 140 *Kif20b*<sup>+/+; p53+/-</sup> and 113 *Kif20b*;p53 mutant NSCs. Cells were from at least 3 coverslips from at least 3 embryos each. (C,D) E12.5 NSCs cultured for 24 hrs and labeled with antibodies to Yap (green) and Dapi in Control (C) and *Kif20b* mutant (D) cultures. (E) The distribution of the nuclear:cytoplasmic ratio of Yap in NSCs is significantly altered in *Kif20b* mutant NSC cultures.  $N = 128$  *Kif20b*<sup>+/+; +/-</sup> and 126 *Kif20b*<sup>-/-</sup> NSCs. Medians: Control, 0.93; Mutant, 1.12. (F) Altered Yap expression in *Kif20b* mutant cultures is p53-dependent. The distribution of nuclear:cytoplasmic ratio of Yap in *Kif20b*;p53 mutant NSCs is not different from double heterozygote controls.  $N = 114$  *Kif20b*<sup>+/+; p53+/-</sup>, 121 *Kif20b*<sup>-/-; p53-/-</sup> NSCs. M.W. = Mann-Whitney test; n.s. = not significant.

## E12.5 dissociated NSCs

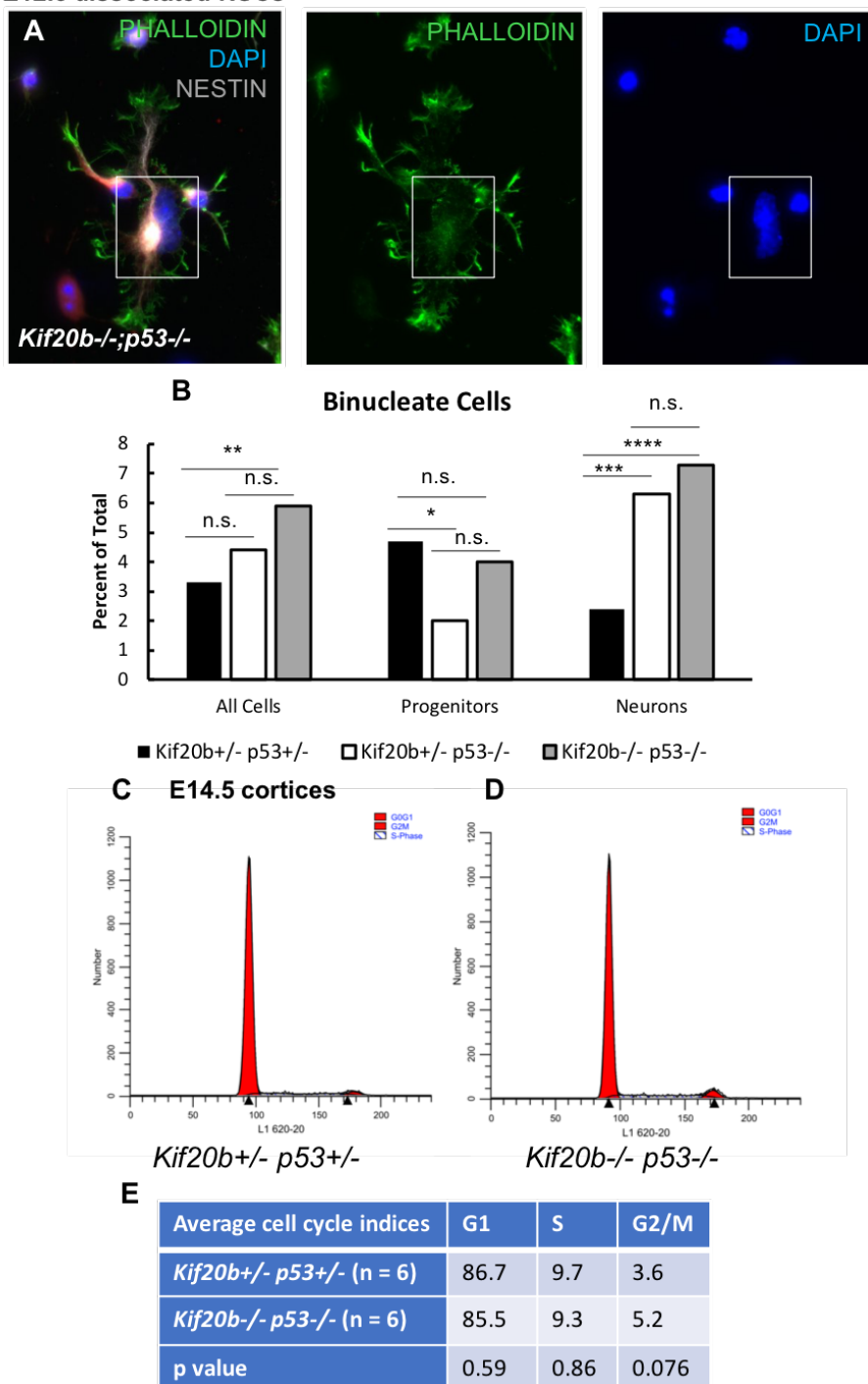


**Figure 42.** *p53* but not *Kif20b* mutation increases binucleate neuron number *in vitro*. (continued on next page)

**Figure 42.** p53 but not Kif20b mutation increases binucleate neuron number *in vitro*.

**(A)** Binucleate cells in E12.5 NSC cultures at 24 hrs can be identified with antibodies to Nestin (gray) to identify NSCs and Dapi to identify nuclei and the actin dye Phalloidin (green). Example, white box. **(B)** There is an approximately two-fold increase in binucleate cells in Kif20b;p53 mutant NSC cultures. Further analysis reveals that there is no significant increase in binucleate progenitors, but there is a 3-fold increase in binucleate neurons. However, a similar increase in binucleate neurons is also seen in p53 mutant cultures, and no significant difference between p53 mutant and Kif20b;p53 mutant cultures is observed. Therefore, increased binucleate neurons in Kif20b;p53 mutant cultures is due to p53 mutation. Fischer's exact test. n (*Kif20b*<sup>+/-</sup>;*p53*<sup>+/-</sup>) = 428 progenitors and 659 neurons; (*Kif20b*<sup>+/-</sup>;*p53*<sup>-/-</sup>) = 400 progenitors and 508 neurons; (*Kif20b*<sup>-/-</sup>;*p53*<sup>-/-</sup>) = 550 progenitors and 576 neurons. Cells were counted from at least 3 coverslips and at least 3 brains for each genotype. **(C,D)** Flow cytometric analysis of cell cycle indices was performed with propidium iodide (PI) on dissociated cells from E14.5 *Kif20b*<sup>+/-</sup>;*p53*<sup>+/-</sup> (C) and *Kif20b*<sup>-/-</sup>;*p53*<sup>-/-</sup> (D) cortices. **(E)** No significant differences in DNA content (represented as cell cycle indices) were noted between the genotypes. n = 6 *Kif20b*<sup>+/-</sup>;*p53*<sup>+/-</sup> and 6 *Kif20b*<sup>-/-</sup>;*p53*<sup>-/-</sup> cortices. t-tests. n.s. = not significant, \*p < 0.05, \*\* p < 0.01, \*\*\* p < 0.001, \*\*\*\* p < 0.0001.

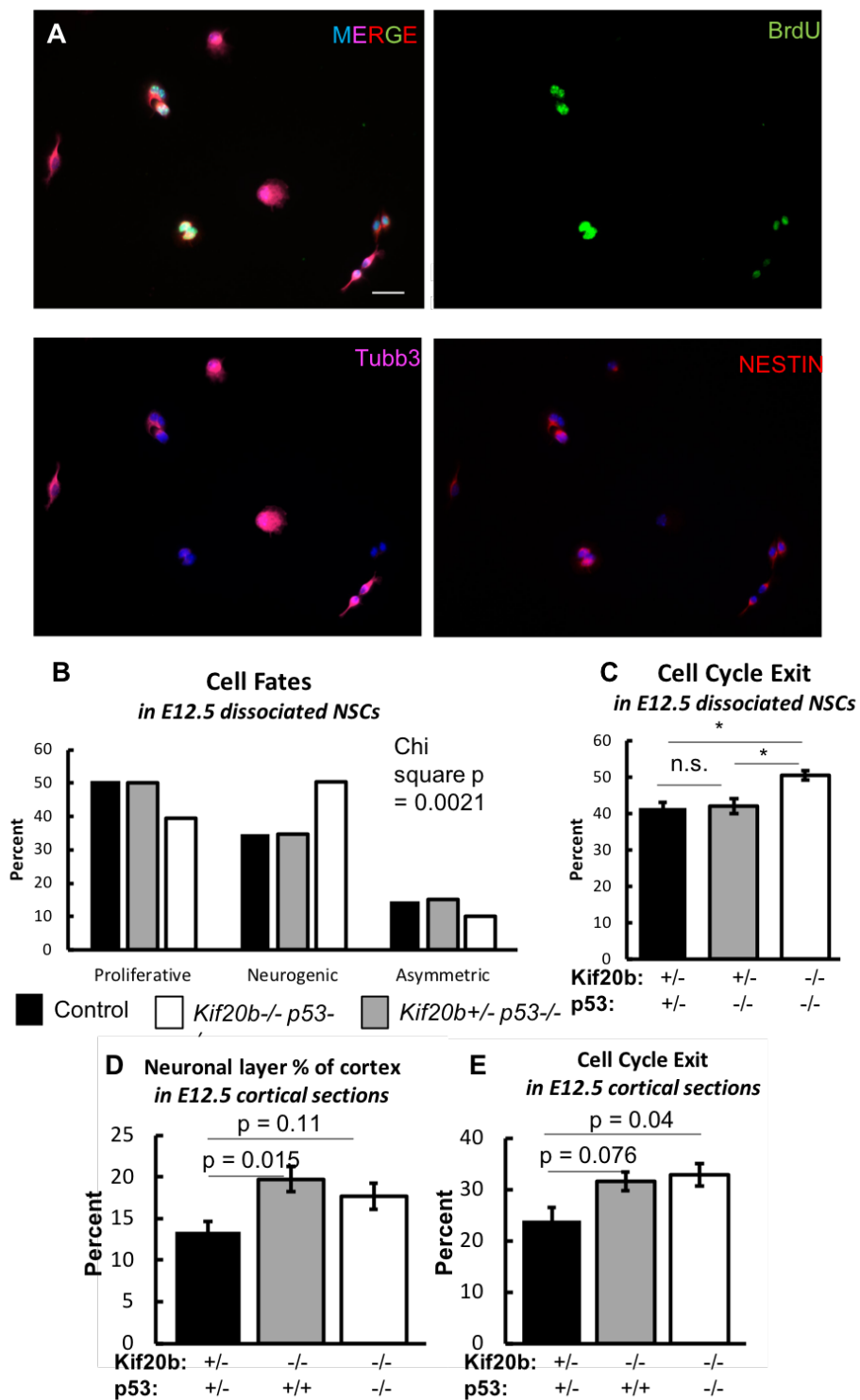


**Figure 43.** *Kif20b* mutant NSCs have p53-independent alterations in cell fate. (continued on next page)

**Figure 43.** Kif20b mutant NSCs have p53-independent alterations in cell fate

**(A)** Dissociated NSC cultures from E12.5 cortices were treated with Bromodeoxy-Uridine (BrdU, green) when plated for 6 hrs, followed by wash out and fixation at 20 hrs to identify NSC divisions. BrdU+ daughter pairs were classified as one of the three different division types using Nestin (red) and Tubb3 (magenta). **(B)** The increased proportion of neurogenic symmetric divisions was still observed when the Kif20b mutant was combined with p53 knockout (Kif20b<sup>-/-</sup>; p53<sup>-/-</sup>), but was not seen in controls: double heterozygotes (Kif20b<sup>+/-</sup>; p53<sup>+/-</sup>) or p53 single mutants (Kif20b<sup>+/-</sup>; p53<sup>-/-</sup>). N=276 control (Kif20b<sup>+/-</sup>; p53<sup>+/-</sup>) division pairs (3 brains), 228 p53 single mutant (Kif20b<sup>+/-</sup>; p53<sup>-/-</sup>) division pairs (3 brains), and 270 double mutant (Kif20b<sup>-/-</sup>; p53<sup>-/-</sup>) division pairs (5 brains). **(C)** Cell cycle exit among the daughters of NSC division pairs was scored as daughters that were BrdU<sup>+</sup>, Tubb3<sup>+</sup>. The increased cell cycle exit in Kif20b<sup>-/-</sup> daughters is not dependent on p53 function. n= 613 control (Kif20b<sup>+/-</sup>; p53<sup>+/-</sup>) daughter cells; 689 p53 single mutant daughters (Kif20b<sup>+/-</sup>; p53<sup>-/-</sup>); and 593 double mutant daughter cells (Kif20b<sup>-/-</sup>; p53<sup>-/-</sup>). **(D)** Pregnant mothers were injected with BrdU at E11.5 and embryo brains were collected 24 hrs later at E12.5 to evaluate cell cycle exit *in vivo*. Kif20b mutants with wild-type p53 status have increased early neurogenesis, as evidenced by the thicker neuronal layer as a proportion of the total cortical thickness. In Kif20b;p53 mutants, there is a trend for a thicker neuronal layer as a proportion of the total thickness. **(E)** To evaluate cell cycle exit, we counted the number of BrdU<sup>+</sup> cells that were Tubb3<sup>+</sup> out of the total BrdU<sup>+</sup> cells. Cell cycle exit is increased in Kif20b;p53 mutant cortices compared to controls, and there is a trend for an increase in Kif20b single mutants. n = multiple images from 4 brains of each genotype. B, Chi-square; C-E, one-way ANOVA. Scale bar: 20  $\mu$ m. \*p < 0.05.

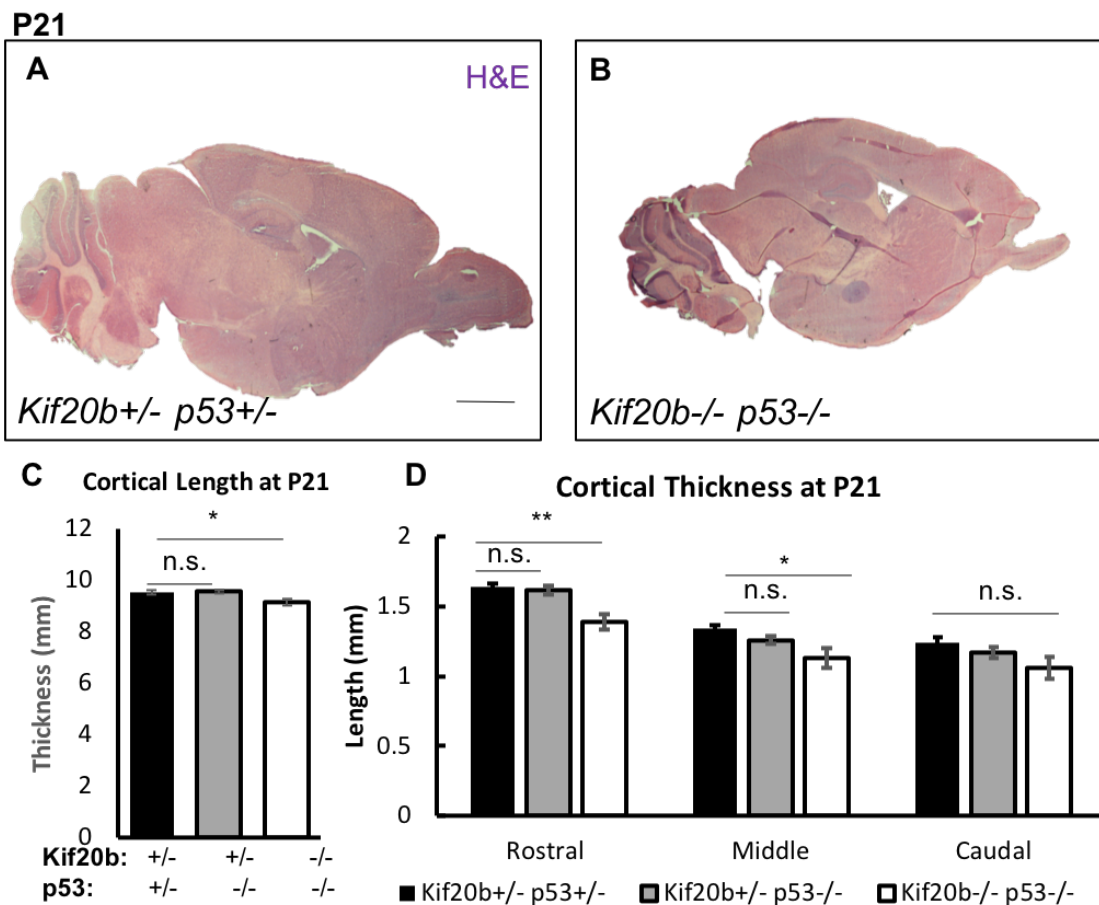


**Figure 44.** *Kif20b*;p53 mutant brains are smaller than controls postnatally.

(A,B) Sagittal sections of P21 brains stained with hematoxylin and eosin (H&E). (C) *Kif20b*;p53 mutants have approximately 5% reduced cortical length at P21, and this is not due to p53 mutation. (D) Cortical thickness in *Kif20b*;p53 mutants is decreased by approximately 15% in rostral and middle level sections compared to double heterozygote controls, but is not reduced in caudal level sections. p53 mutation does not prevent normal brain size. n for C = 6 *Kif20b+/-;p53+/-*, 5 *Kif20b+/-;p53-/-* and 5 *Kif20b-/-;p53-/-*; for D = multiple images from 4 brains of each genotype C,D one-way ANOVA. Scale bar: 1.5 mm. n.s. = not significant; \* $p < 0.05$ . \*\* $p < 0.01$ .

## Appendix 2: RNA sequencing of *Kif20b* and *Kif20b;p53* mutant cortices

To take an unbiased approach towards answering some of our outstanding questions, we performed RNA sequencing of E11.5 cortices of wild-type (*Kif20b*<sup>+/+</sup>; *p53*<sup>+/+</sup>), *Kif20b* mutant (*Kif20b*<sup>-/-</sup> *p53*<sup>+/+</sup>), *p53* mutant (*Kif20b*<sup>+/+</sup> *p53*<sup>-/-</sup>) and *Kif20b;p53* double mutant (*Kif20b*<sup>-/-</sup>; *p53*<sup>-/-</sup>) cortices. Only cortices were collected for RNA extraction, but at this age it was not possible to separate meninges from cortical tissue, so meningeal cells were present in the analysis. Embryos were dissected from pregnant mothers and placed in PBS on ice. Tails were collected for genotyping, the primitive skull was removed, and cortices were quickly dissected out. Cortices were placed into 1.5 ml Eppendorf tubes and immediately submerged in dry ice with an ethanol bath. Flash-frozen cortices were placed in a -80 freezer. RNA was extracted from frozen samples using the Qiagen RNeasy Mini kit. RNA concentration and quality were assessed using a NanoDrop. Further quality analysis was done at the UVA Genome Analysis and Technology Core; all samples were of high quality. Library preparation and sequencing was performed by the Core (Katia Sol-Church and Alyson Prorock). 3 samples of each genotype were analyzed for a total of 12 samples. Statistical analysis was done using DESeq software by the Core (Yongde Bao) with further gene ontology analysis obtained using the PANTHER classification system software ([www.geneontology.org](http://www.geneontology.org)). For gene ontology analysis, we varied the statistically significant threshold used (from  $\text{padj} < 0.05$  to  $p < 0.05$ ) as needed in order to include enough genes to observe trends.  $\text{Padj}$  (P adjusted) indicates that a Benjamini-Hochberg correction was performed on the p value to account for multiple tests.

**Chapter 4**, Tables 2-6 show gene expression changes observed in *p53* mutants compared to wild-type controls. *p53* does exert functions at the gene expression level during cortical development, which are important to keep in mind when evaluating changes in *Kif20b* and *Kif20b;p53* mutants.

### Gene expression changes in *Kif20b* mutants compared to wild-type controls

These genes were significantly altered in *Kif20b* mutant E11.5 cortices compared to wild-type controls at the strictest standard of significance ( $\text{padj} < 0.05$  or  $p < 0.0001$ ). “Needs further analysis” indicates genes that were not as significantly downregulated in *Kif20b;p53* mutants compared to wild-type controls as in *Kif20b* mutants compared to wild-type controls (i.e. not  $\text{padj} < 0.05$ , but still  $p < 0.05$ ).

**Table 9:** Upregulated genes in *Kif20b*<sup>-/-</sup>; *p53*<sup>+/+</sup> E11.5 cortices compared to wild-type samples (padj < 0.05)

	log2FoldChange	fold change	pvalue	padj	notes	p53-dependent?
Npm3-ps1	3.858411546	14.50432796	1.23E-26	8.77E-23		<b>no</b>
Eda2r	2.455111861	5.483556377	1.56E-10	5.55E-07		yes
Adamts3	0.832758715	1.781087896	5.77E-09	1.36E-05		yes
Ccng1	1.375642902	2.594835177	2.20E-08	4.47E-05	cyclin g1	yes
Sall4	1.288635451	2.442968821	7.59E-08	0.00013464		yes
Nfxl1	0.345784993	1.27084228	8.03E-07	0.00087683		yes
Zmat3	0.813687929	1.757698871	1.15E-06	0.00116724		yes
Zfp365	0.983242079	1.976902992	1.24E-06	0.00117427		yes
Psrc1	0.436925777	1.353716632	1.96E-06	0.0015489		yes
Got1	0.303253921	1.233924327	2.78E-06	0.00197305		yes
Gtse1	0.298307489	1.229700932	3.01E-06	0.00203597		yes
Ano3	1.521128123	2.870153951	3.17E-06	0.00204721		yes
Pvt1	1.234508679	2.353012001	4.27E-06	0.00242344		yes
Senp1	0.300338475	1.23143329	9.65E-06	0.00456764		yes
Usp2	0.749273261	1.680945862	1.20E-05	0.00503316		yes
Phlda3	1.398961539	2.637116925	1.23E-05	0.00503316		yes
Dmbx1	2.488701983	5.612727365	1.46E-05	0.00576807		yes
Rrm2	0.255286815	1.193573008	1.63E-05	0.00616424		yes
Fndc3c1	0.878581531	1.838566719	1.65E-05	0.00616424		yes
Elf3	2.450142835	5.464702037	3.09E-05	0.01014733		yes
Pax2	3.008868569	8.049329252	4.36E-05	0.01375898		yes
Ak1	0.767340904	1.702129619	4.78E-05	0.01444927		yes
Cdkn1a	1.08852374	2.126563213	5.55E-05	0.01527537	p21	yes
Vars	0.504870892	1.418996363	5.60E-05	0.01527537		yes
Tcf7l1	0.454963002	1.370747652	7.05E-05	0.01787453		needs further analysis
Rps18	0.527494856	1.441424084	8.45E-05	0.02033264		yes
Ddit4l	0.92656277	1.900742067	0.00010205	0.02374843		yes
Scube1	0.810847265	1.75424137	0.00010561	0.02407001		yes
Dna2	0.212328231	1.158556362	0.00011387	0.02456237		yes
4632434i11R	0.389953716	1.310351365	0.00011593	0.02456237		yes
Nek2	0.197395518	1.146626493	0.00012033	0.02509024		needs further analysis
2810417H13	0.335541167	1.261850651	0.00012444	0.02512871		yes
B230120H23	0.57631322	1.491034066	0.0001563	0.02881521		yes
Ly75	0.866581448	1.823337271	0.00016141	0.02909087		yes
Slc19a2	0.522534751	1.436476858	0.00016189	0.02909087		yes
Pmel	2.883261953	7.37816449	0.00016863	0.02944337		yes
Nphp1	0.412475303	1.330967463	0.00017215	0.02944337		yes
Alg13	0.253929747	1.192450804	0.00018529	0.03023461		yes
Me1	0.741125238	1.67147901	0.00019602	0.03078166		needs further analysis
Mastl	0.228678952	1.171761498	0.00024522	0.03700514		needs further analysis
Got2	0.166601489	1.122411339	0.00024764	0.03700514		yes
Ckap2	0.241214795	1.181987514	0.000266	0.03845232		yes
Sars2	0.242368777	1.182933339	0.00027022	0.03845232		yes
9230114K14l	0.843718589	1.79467	0.00027358	0.03845232		yes
Fam149a	0.473586444	1.388557042	0.00029045	0.04042347		yes
Wdhd1	0.247079822	1.18680246	0.00031424	0.04110547		yes
Thap6	0.772967504	1.708780992	0.00032141	0.04110547		yes
Sesn2	0.775359029	1.711615951	0.00034744	0.04326476		yes
Sdad1	0.312382778	1.241756913	0.00037332	0.04453435		yes
Ctnnal1	0.453116838	1.368994678	0.00039152	0.04593444		yes
Cs	0.161847424	1.118718782	0.00039492	0.04595299		yes
5930403L14f	0.538427886	1.452388977	0.00041852	0.04728455		needs further analysis
Nup160	0.270681061	1.206377194	0.00041969	0.04728455		yes
Mthfd1l	0.418656269	1.336681985	0.00043311	0.04803475		yes
Abcf1	0.237530761	1.178973067	0.00043694	0.04803715		yes
Rhobtb3	0.306529093	1.236728735	0.000443	0.04803715		needs further analysis
Dars	0.202566434	1.150743612	0.00044536	0.04803715		yes
Sgpp2	2.03636316	4.102101416	0.00044943	0.04803715		yes
Dcxr	0.575653406	1.490352301	0.00045009	0.04803715		yes
Shc4	0.931902694	1.907790421	0.00045344	0.04803715		needs further analysis
Tbx3	3.11828396	8.683543955	0.00053299	0.05331082		yes
Cdh6	0.580716131	1.495591452	0.00055561	0.05406618		yes

*Gene Ontology Analysis of Upregulated Genes in Kif20b mutants compared to WT controls – comparison of possible p53-dependent (genes upregulated in Kif20b mutant compared to WT but not Kif20b;p53 mutants compared to WT) and -independent effects (genes upregulated in Kif20b mutant and Kif20b;p53 mutants compared to WT)*

Biological process

*Likely p53-dependent*

mitotic cell cycle process: Lsrc1, Kifc1, Trim71, Ccng1, Cdkn1a, Ckap2, Fgf10, Zfp365, DnaI  
intrinsic apoptotic signaling pathway by p53-class mediator: Eda2r, Puma, Bax, Cdkn1a, Aen

signal transduction by p53 class mediator

cellular response to DNA damage stimulus

DNA metabolic process

regulation of mitotic cell cycle/phase transition: Ccng1, Cdc25a, Ercc3, Plk1, Ccnb1, Ccnl1, Cdkn1a

negative regulation of gene expression

RNA metabolic process

cellular biosynthetic process

negative regulation of nucleobase containing compound metabolic process

DNA duplex unwinding

neural tube closure

DNA replication

rRNA processing

negative regulation of cellular metabolic process

regulation of RNA metabolic process

*Possibly p53-independent*

DNA repair

organelle organization

ribosome biogenesis

**Table 10:** Downregulated genes in *Kif20b*<sup>-/-</sup>;*p53*<sup>+/+</sup> E11.5 cortices compared to wild-type samples (padj < 0.05)

	log2FoldChange	fold change	pvalue	padj	notes	p53-dependent?
Kif20b	-1.23	-2.34	4.00E-35	5.69E-31	expected	no
Arl3	-0.62	-1.54	6.94E-16	3.28E-12	cilia gene	no
Nanos1	-0.75	-1.68	3.93E-10	1.12E-06		needs further analysis
Lyve1	-2.34	-5.06	8.93E-08	0.00014093		needs further analysis
Pink1	-0.41	-1.33	1.60E-07	0.00022643		yes
Dctn3	-0.48	-1.39	5.25E-07	0.00067735		needs further analysis
Klhdc8b	-0.47	-1.39	6.62E-07	0.00078273		needs further analysis
C1qtnf4	-0.92	-1.89	1.42E-06	0.00120141		yes
Cspg5	-1.10	-2.14	1.44E-06	0.00120141		needs further analysis
Sparcl1	-0.74	-1.67	2.41E-06	0.00179726		yes
Cuedc2	-0.29	-1.23	3.61E-06	0.00218723		needs further analysis
Atp1b2	-0.70	-1.63	3.70E-06	0.00218723		yes
Pcp4l1	-1.11	-2.15	6.32E-06	0.00340056		needs further analysis
Rgs2	-0.58	-1.49	6.47E-06	0.00340056		yes
Adamts1	-1.19	-2.28	8.51E-06	0.00431303		yes
Gareml	-0.97	-1.96	9.27E-06	0.00453705		yes
Txndc15	-0.28	-1.22	1.08E-05	0.00494226		needs further analysis
Adcy5	-0.61	-1.52	1.13E-05	0.00499778		yes
Pdcd4	-0.76	-1.69	1.24E-05	0.00503316		needs further analysis
Foxj1	-1.00	-2.00	2.30E-05	0.00838415		needs further analysis
Tmem180	-0.52	-1.44	2.38E-05	0.00844548		no
Wnt3a	-1.08	-2.11	2.48E-05	0.00858206		needs further analysis
Gp1bb	-0.89	-1.86	2.73E-05	0.00921336		yes
Atp1a2	-1.59	-3.02	3.15E-05	0.01014733		yes
Tmcc2	-0.38	-1.30	4.78E-05	0.01444927		yes
F13a1	-1.49	-2.80	5.00E-05	0.0147936		needs further analysis
Il18	-0.87	-1.82	5.52E-05	0.01527537		yes
Rhcg	-1.00	-1.99	5.56E-05	0.01527537		yes
Lmo2	-1.20	-2.30	6.09E-05	0.01615683		yes
Lrrtm3	-1.21	-2.31	6.15E-05	0.01615683		yes
Zfp949	-0.63	-1.54	6.44E-05	0.01661721		yes
Edil3	-0.73	-1.66	7.50E-05	0.01868957		yes
Dkk3	-0.82	-1.77	7.83E-05	0.0191576		needs further analysis
Grcc10	-0.35	-1.28	0.00010203	0.02374843		needs further analysis
Chsy3	-1.02	-2.02	0.00010682	0.02407001		needs further analysis
Luzp2	-1.12	-2.18	0.00011492	0.02456237		yes
Ogn	-1.63	-3.09	0.0001154	0.02456237		yes
Man1b1	-0.16	-1.12	0.00012195	0.02509024		needs further analysis
Adra2a	-1.74	-3.34	0.00012713	0.02512871		yes
Gfod2	-0.28	-1.21	0.00012745	0.02512871		yes
Sfr1	-0.19	-1.14	0.00013029	0.0253371		needs further analysis
Pcdhb17	-0.84	-1.79	0.0001329	0.02549545		yes
Galnt14	-1.46	-2.76	0.00013867	0.0262469		yes

Rdm1	-0.60	-1.52	0.00014173	0.0264738	yes
Purg	-0.39	-1.31	0.0001687	0.02944337	yes
Camk2n1	-0.68	-1.60	0.00017209	0.02944337	yes
Efnb3	-0.29	-1.23	0.00017819	0.03011352	yes
Khdrbs2	-0.82	-1.77	0.00018166	0.03023461	yes
Clu	-0.65	-1.56	0.00018354	0.03023461	needs further analysis
Gdf5	-1.06	-2.09	0.00019214	0.03078166	needs further analysis
Tpbp	-0.58	-1.49	0.00019586	0.03078166	needs further analysis
Kcnk2	-0.51	-1.42	0.00019732	0.03078166	yes
Dmp1	-1.64	-3.12	0.000211	0.03255832	yes
Gabra2	-1.36	-2.56	0.00021556	0.03290408	yes
Tex264	-0.63	-1.54	0.00026583	0.03845232	needs further analysis
Mrc1	-1.40	-2.64	0.0002683	0.03845232	yes
Ypel5	-0.47	-1.39	0.00027166	0.03845232	yes
Eltd1	-0.71	-1.64	0.00030352	0.04110547	yes
Mmd2	-1.10	-2.14	0.00030596	0.04110547	yes
Larp6	-1.12	-2.18	0.00031046	0.04110547	yes
Mmp15	-0.30	-1.23	0.00031054	0.04110547	yes
Cd99l2	-0.40	-1.32	0.00031519	0.04110547	yes
Mpzl1	-0.27	-1.21	0.00031742	0.04110547	yes
3110082J24F	-1.22	-2.34	0.00032025	0.04110547	yes
Ly6h	-0.62	-1.53	0.00034379	0.04326476	needs further analysis
Coro1a	-0.24	-1.18	0.00034537	0.04326476	needs further analysis
Sst	-2.39	-5.25	0.0003573	0.04408673	yes
Lrp1b	-1.73	-3.31	0.00036344	0.04408673	yes
Hist3h2ba	-0.72	-1.65	0.00036559	0.04408673	yes
Golga7b	-1.20	-2.29	0.00036646	0.04408673	yes
Pthlh	-1.11	-2.15	0.00038659	0.04573361	yes
Hdac11	-0.31	-1.24	0.00039821	0.04595946	needs further analysis
Atp9a	-0.72	-1.65	0.00041561	0.04728455	yes
Cenpv	-0.28	-1.21	0.00042438	0.04743661	yes
Btrc	-0.30	-1.23	0.00046617	0.04902068	needs further analysis
Slc39a3	-0.41	-1.33	0.00047093	0.04915668	yes
Qsox1	-0.26	-1.20	0.00048291	0.05003957	needs further analysis
Arhgef6	-0.88	-1.84	0.0004978	0.05120834	yes
Maf1	-0.20	-1.15	0.00050346	0.05136837	yes
H2-K1	-0.88	-1.84	0.00050659	0.05136837	needs further analysis
Wfikkn2	-1.07	-2.10	0.00053326	0.05331082	needs further analysis
Abi3bp	-2.69	-6.44	0.00053832	0.05343038	yes
Adamts5	-0.68	-1.61	0.00054198	0.05343038	yes
Ccdc85a	-0.86	-1.82	0.0005602	0.05406618	yes
Sgk1	-0.70	-1.62	0.00056665	0.05406618	yes
Emx2os	-1.15	-2.22	0.00056701	0.05406618	needs further analysis
H2-T24	-2.59	-6.03	0.00056747	0.05406618	yes

*Gene Ontology Analysis of Downregulated Genes in Kif20b mutants compared to WT controls – comparison of possible p53-dependent (genes downregulated in Kif20b mutant compared to WT but not Kif20b;p53 mutants compared to WT) and -independent effects (genes downregulated in Kif20b mutant and Kif20b;p53 mutants compared to WT)*

Biological process

*Likely p53-dependent*

biological quality  
development response to endogenous stimulus  
development  
negative regulation of developmental process  
locomotion  
regulation of glutamate receptor signaling pathway  
pathway  
positive regulation of synapse assembly  
axonogenesis  
pathway  
angiogenesis  
stimulus  
cell adhesion  
chemical synaptic transmission  
ion transmembrane transport  
cell-cell/second messenger mediated signaling  
cell migration  
negative regulation of signal transduction  
cell metabolism  
cell development/proliferation  
system development/process

*Possibly p53-independent*

multicellular organism  
nervous system  
  
cell component organization  
cell component disassembly  
regulation of Wnt signaling  
  
ECM organization  
cell surface receptor signaling  
  
response to growth factor

**p53-independent gene expression changes**

*Gene Ontology Analysis of Genes Upregulated in both Kif20b and Kif20b;p53 mutants compared to wild-type controls*

Biological Process (p < 0.05)

- 1) **Cellular response to DNA damage stimulus:** Smc2, Rad50, Rps6ka6, Mms22l, Cul4b, Rnf138, Atad5, Traf6, Parg, Gen1, Bard1, Cep63, Recql, Fancl, Pold3, Tlk1, Nucks1
- 2) DNA metabolic process

Molecular Process (p < 0.05)

- 1) **ATP binding:** Prkci, Kif5b, Ddx52, Nek2, Nmnat3, Acsl4, Hells, Ppip5ks, Mastl, Abcb7, Papd4, Rhobtb3, Lars, Ddx46, Grk5, Vps4b, Ube2q2, Chuk
- 2) RNA binding
- 3) Catalytic activity

Cellular Component (p < 0.05)

- 1) **Nucleoplasm:** Gtf2a1, Tcf7l1, Hnrnpab, Nop58, Hnrnpa2b1, Mtdh, Taf2, Haus6, Hnrnpd, Dut, Col4a3bp, Opa1, Ibtik, Hmg5, Mastl, Did, Orc3, Belaf1, Affl
- 2) **Intracellular non-membrane-bounded organelle:** Cenpk, Ppp1r7, Rnf138, Eif2a, Acsl4, Pls3, Eri1, Shcbp1
- 3) Cytosol
- 4) Protein-containing complex

*Gene Ontology Analysis of Genes Downregulated in both Kif20b and Kif20b;p53 mutants compared to wild-type controls*

Biological Process (p < 0.05)

- 1) **Regulation of canonical Wnt signaling pathway:** Wnt3a, Folr1, Axin2, Nphp3, Fzd9, Rspo1, Rspo2, Rspo3, Lmx1a, Nkd1, Ddit3, Aes, Dkk3, Btrc
- 2) **Wnt signaling pathway:** Wnt7b, Wnt9a
- 3) **Regulation of developmental process:** Mmp14, Ankrd54, H2-K1, Rxrb, Rac3, Zkscan3, Gdf4, Rhoc, Gas2l1, Clu, Rac3, Slc39a12, Bmp6, Mmp11, Kif20b, Clic1, Foxj1, Tpbp, Akt1, Gdpd2

Molecular Function (p < 0.05)

- 1) Frizzled binding

Cellular component (p < 0.05)

- 1) Endomembrane system
- 2) Cytoplasm

\*Note: Because p53 mutation itself does exert gene expression changes, it can be difficult to differentiate whether changes in *Kif20b;p53* mutants are due to *Kif20b* mutation, *p53* mutation or both. We also compared *Kif20b;p53* mutants to *p53* mutants so that only *Kif20b* mutation status was changing and *p53* status was staying constant. I found these gave some very good candidates for processes we are interested in investigating (see below).

**Table 11:** Genes Upregulated in *Kif20b;p53* mutant E11.5 cortices compared to *p53* mutants (*Kif20b*<sup>+/+</sup>;*p53*<sup>-/-</sup>) (*padj* < 0.05)

	log2FoldChange	Fold Change	pvalue	padj	
<b>Diap3</b>	0.402761842	1.32203635	6.16E-08	0.00018769	Kif20b and p53 interactor; actin remodeling, cytokinesis
Igsf10	0.551819283	1.46593312	1.04E-05	0.00955704	Immunoglobulin superfamily member 10; migration of GnRH-expressing neurons
Slc20a1	0.186204895	1.1377668	1.05E-05	0.00955704	phosphate transport
Fam111a	0.280621541	1.2147181	2.51E-05	0.01763623	promotes S phase entry and DNA synthesis
Golim4	0.315742191	1.2446518	4.00E-05	0.02434719	Golgi integral membrane protein 4
Rps2	0.631539961	1.54921778	6.59E-05	0.02869309	Ribosomal protein S2
<b>Smc2</b>	0.224577041	1.16843465	0.00011989	0.04058931	Candidate Kif20b interactor; Structural maintenance of chromosome 2; condensin complex;DNA repair
<b>Foxp1</b>	0.310628783	1.24024813	0.00013525	0.04415304	transcription factor; cortical neuron subtype specific expression
<b>Smc4</b>	0.250408399	1.1895438	0.0001817	0.05190337	Candidate Kif20b interactor; Structural maintenance of chromosome 4; condensin complex;DNA repair

**Gene Ontology Analysis of Genes Upregulated in Kif20b;p53 mutants compared to p53 mutant controls**

Biological Process

*P* < 0.0001

1) **Kinetechore organization**: Smc2, Smc4, Cenpe

2) DNA metabolic process

*P* < 0.005

1) **DNA repair**: Cul4b, Wdhd1, Clspn, Fancl, Dclre1a

2) **Nuclear DNA replication**: Atad5, Orc3, Brca2, Pola1

3) **DNA recombination**: Brip1, Rad50, Foxp1, Msh3, Recql, Nucks1

4) **Cell division**: Tpr, Lrrcc1, Casc5, Anln, Kif11, Hells, Mastl, Ect2

5) Mitotic cell cycle process

6) Chromosome organization

Additional: regulation of RNA metabolic process, positive regulation of nitrogen compound metabolic process, regulation of gene expression, positive regulation of macromolecule metabolic process

**Table 12:** Genes Downregulated in *Kif20b;p53* mutant E11.5 cortices compared to *p53* mutants (*Kif20b*<sup>+/+</sup>;*p53*<sup>-/-</sup>) (padj < 0.05).

	log2FoldChange	Fold Change	pvalue	padj	notes
<b>Kif20b</b>	-1.29948852	-2.461416024	1.17E-39	1.07E-35	expected
<b>Arl3</b>	-0.656321549	-1.576059006	7.48E-18	3.42E-14	cilia-genesis
<b>Dctn3</b>	-0.497335953	-1.411604518	1.32E-07	0.00030266	dynactin subunit 3
<b>Atf5</b>	-0.407331638	-1.326230591	1.30E-06	0.00218829	transcription factor; promotes proliferation and inhibits cell cycle exit in the cerebral cortex
<b>Sfr1</b>	-0.234266175	-1.176308257	1.44E-06	0.00218829	homologous recombination
<b>Dnalc4</b>	-0.298886553	-1.230194604	2.97E-06	0.00387411	Dynein axonemal light chain 4; force generating protein of cilia
<b>Pea15a</b>	-0.426261737	-1.343747189	9.74E-06	0.00955704	apoptosis and insulin modulator
<b>Al846148</b>	-0.211399074	-1.157810443	2.16E-05	0.01763623	aka SPINDOC
<b>Pdcd4</b>	-0.72890235	-1.657377624	2.34E-05	0.01763623	tumor repressor; mTOR signaling
<b>Abhd8</b>	-0.222893473	-1.167071923	3.03E-05	0.01980292	
<b>Aes</b>	-0.27287784	-1.208215534	4.39E-05	0.02496328	transcriptional corepressor; Wnt pathway
<b>Tesk1</b>	-0.2187094	-1.16369211	4.64E-05	0.02496328	testis associated actin remodeling kinase 1
<b>Ptms</b>	-0.349065329	-1.273735152	5.56E-05	0.02825663	parathymosin; immune modulator
<b>Eri3</b>	-0.207684931	-1.154833554	6.26E-05	0.02869309	
<b>Cuedc2</b>	-0.251758557	-1.19065757	6.34E-05	0.02869309	toll-like signaling
<b>Rnf187</b>	-0.178281127	-1.131534935	7.01E-05	0.02912206	
<b>Chmp1a</b>	-0.172867693	-1.127297025	7.40E-05	0.02940102	ESCRT factor; multivesicular body formation, abscission
<b>Tmsb10</b>	-0.38086315	-1.302120668	8.60E-05	0.03276918	inhibits actin polymerization
<b>Nkain1</b>	-0.174150553	-1.128299875	9.64E-05	0.03524064	Na, K ATPase
<b>Fbxo46</b>	-0.304343291	-1.234856407	0.00010484	0.03685756	E3 ubiquitin ligase
<b>Ap1s1</b>	-0.224191566	-1.168122492	0.00014387	0.04534852	clathrin coat assembly complex
<b>Snapc2</b>	-0.239836807	-1.180859079	0.00015659	0.04771173	subunit of snRNA-activating protein complex
<b>Mlf2</b>	-0.150412915	-1.109887088	0.00017518	0.05165491	myeloid leukemia factor 2
<b>Rn45s</b>	-2.275323871	-4.841063006	0.00019971	0.05252371	pre-ribosomal RNA
<b>Lars2</b>	-2.543598747	-5.830415691	0.00020063	0.05252371	mitochondrial leucyl-tRNA synthetase
<b>Cfl1</b>	-0.189994381	-1.140759273	0.00020111	0.05252371	Cofilin-1; actin polymerization

## Gene Ontology Analysis of Genes Downregulated in *Kif20b*;p53 mutants compared to p53 mutant controls

### Biological Process

$P < 0.005$

#### 1) Establishment of protein localization to organelle

Summary – takeaways for further consideration (see **Chapter 5** for additional comments)

- 1) Most genes changes in the *Kif20b* mutant are p53-dependent. Notably we can see upregulation of p21, Puma, Bax, cyclin G1, cyclin B1, cyclin E1 and Cdc25a, p53-dependent effectors of apoptosis and cell-cycle arrest. p53 activation in the *Kif20b* mutant also leads to down regulation of neurogenesis, proliferation, cell-cell adhesion, and cell migration-related genes.
- 2) Candidates for p53 activation: Npm3-ps1 (a pseudogene with no characterization), Smc2, Smc4, Ibk and Diap3 (candidate interactors of *Kif20b* that were upregulated), and DNA damage pathways.
- 3) DNA repair genes were upregulated in single and double mutants.
- 4) Two abscission related genes that were upregulated in both *Kif20b* single and *Kif20b*;p53 double mutants are Vps4b and anillin. Chmp1a is upregulated in *Kif20b*;p53 mutants compared to p53 mutants.
- 5) Nucleoplasm and chromosome organization were significant terms. Smc2 and Smc4 are candidate *Kif20b* interactors and have roles in both chromosome organization and DNA damage response, so would be worth investigating.
- 6) Possible candidates for cell fate changes include Wnt signaling pathways, which were downregulated (Wnt3a, Wnt7b, Wnt9a, Rspo1, Rspo2, Rspo3, Fzd9 among others). The transcription factor Atf5, which has a demonstrated role in inhibiting neurogenesis, was also very significantly downregulated in *Kif20b*;p53 mutants compared to p53 mutants.
- 7) Arl3, a cilia gene, was very significantly downregulated ( $\text{padj} < 0.05$ ) in both *Kif20b* and *Kif20b*;p53 mutants. Dnalc4, a dynein localized to cilia was also significantly downregulated. Several actin-related genes including Dctn3 are downregulated.
- 8) diaph3/mdia2 is down regulated in the p53 mutant, but is significantly upregulated in the *Kif20b*;p53 mutant compared to wildtype and very significant when comparing *Kif20b*;p53 mutant to p53 single mutant. This is a demonstrated interactor of *Kif20b*.

- 9) The *p53* mutant itself does have a role in normal development. Developmental genes were down regulated, but the only upregulated genes were involved in neuron outgrowth, synapse development, and vesicle trafficking (see **Chapter 4**).

### Appendix 3: Postnatal consequences of *Cep55* loss

At birth, *Cep55* mutants exhibit a reduction in brain size that is disproportional to body size. However, body length is reduced by approximately 10%. In the data presented in this appendix, we further investigated the postnatal consequences of *Cep55* loss for murine development. The methods used in this appendix include mouse dissection and brain collection, embedding and cryosectioning of whole brains, H&E staining, immunostaining, imaging with Zeiss fluorescent microscopes and Leica brightfield microscope, analysis with ImageJ software, and statistical analysis with Excel and GraphPad Prism. These methods are all described in further detail in **Chapters 2 and 3**. Survival endpoints (Fig. 45C) were either death or requested euthanizing by mouse handlers due to severe failure to thrive. The righting reflex (Fig. 45E) was determined by placing mouse pups on their backs on a flat surface and recording the time expired before the mouse righted itself with all four paws on the ground. Mice collected for analyses at P8 (Fig. 46) were perfused with PBS and then fixed in 4% PFA for two days before sectioning. H&E staining was performed by the UVA Research Histology Core.

*Cep55* mutants were rarely found dead on the day of birth. Most were alive, and had milk present in their bellies, indicating some ability to feed. At P0, *Cep55* mutant bladders were fluid-filled, and intestines contained waste (data not shown). Surprisingly, *Cep55* mutant kidneys appeared similar in size, morphology and texture to controls at P0 (Fig. 45A). By P8 however, *Cep55* mutants were noticeably smaller than controls (Fig. 45B). Approximately 30% of mutants died before 15 days of age, but the majority lived until P20 (Fig. 45C). After P20, *Cep55* mutants exhibited a dramatic reduction in survival, and none survived beyond 26 days. Pups were kept with their littermates and mothers until death occurred; none were weaned. Reduction in body weight of *Cep55* mutants was evident at P6 (Fig. 45D). Controls gained weight from P6 to P10, but *Cep55* mutants failed to gain any weight. In addition to noticeably smaller size, *Cep55* mutants exhibited abnormal movements. Jerking, hopping and spasmodic movements were noted in *Cep55* mutants that were not observed in controls at any age. When placed on their backs, mouse pups reflexively right themselves by a few days of age; this is known as the righting reflex. *Cep55* mutants took much longer to right themselves than controls, and in some mutants, could not right themselves before 30 seconds expired (Fig. 45E). Attempts to right themselves were observed, but *Cep55* mutants exhibited abnormal movements, including clasping of arms and legs. With the noted apoptosis occurring in the spinal cord as early as embryonic day 10 in *Cep55* mutants (**Chapter 3**), it is likely that spinal cord defects contribute to these phenotypes.

To investigate the consequence of *Cep55* loss for brain development postnatally, we collected brains from mice at postnatal day 8. Consistent with the large reduction in brain size at P0, *Cep55* mutant brains were markedly reduced at P8 (Fig. 46A,B). However, the previously noted caudal thinning appeared to have progressed to caudal-lateral tissue degeneration. This was further confirmed with tissue sectioning and staining with hematoxylin and eosin (H&E) (Fig. 46C,D). Compared to controls, all *Cep55* mutant brain regions were smaller. In the lateral striatum, tissue degeneration had occurred, with large spaces connected only by a thin layer of tissue (Fig. 46D). Large spaces consistent with tissue degeneration were also observed in the midline. Therefore, it seems likely that a secondary degenerative process is occurring postnatally that may be different mechanistically from the initial impaired brain growth. Perhaps this process is also contributing to failure to thrive and reduction in body size postnatally.

To begin to address what could be contributing to postnatal defects in brain growth, we investigated whether apoptosis and p53 activation, which were widespread embryonically, also occurred after birth. Indeed, we found that apoptosis was still elevated in the proliferating zones of *Cep55* mutant cortices at P0 (Fig. 47A,B). However, fewer apoptotic cells were observed than were seen in embryonic tissues (Fig. 47C; 10-fold increase compared to 50+ fold increase before birth). P53+ cells were also seen in *Cep55* mutant cortical proliferative zones at P0 (Fig. 47D,E). We wondered whether the degeneration could also be a delayed response to DNA damage in the cortex, as DNA damage has been shown to occur in cells that failed cytokinesis. Using  $\gamma$ H2AX to visualize sites of DNA damage, we did observe many damaged cells in E14.5 *Cep55* mutant cortices, compared to very few in controls (Fig. 47F,G). However, more work is needed to determine whether this damage is a cause and/or consequence of apoptosis.

Because we observed greatly increased numbers of p53+ and apoptotic cells in *Cep55* mutant cortices, we wondered whether the apoptosis was p53-dependent, and if so, whether inhibition of p53 could restore brain size, as was observed in the *Kif20b* mutant. To test this, we crossed *Cep55*<sup>+/-</sup> mice to *p53*<sup>+/-</sup> mice in order to create progeny homozygous for both *Cep55* and p53. As expected, *Cep55* mutant mice with wild-type p53 status exhibited microcephaly (Fig. 48A,B). We detected no difference in brain size with partial deletion of p53 (Fig. 48C). However, complete deletion of p53 partially rescued brain size (Fig. 48D). Quantification showed that *Cep55*;*p53* mutant cortical length was 21% longer than *Cep55* mutants, but still 10% shorter than

wild-type controls (Fig. 48E). Furthermore, cortical area was 32% larger than *Cep55* mutants, but still 19% smaller than wild-type controls (Fig. 48F). Next, we evaluated whether deletion of p53 rescued microcephaly due to inhibition of apoptosis. Indeed, we found that apoptosis in *Cep55* mutants was p53-dependent (Fig. 48G,H). Therefore, preventing apoptosis improves brain size in *Cep55* mutants, but not to wild-type levels. Cells prevented from dying may obtain additional errors that impair brain growth.

## Figures

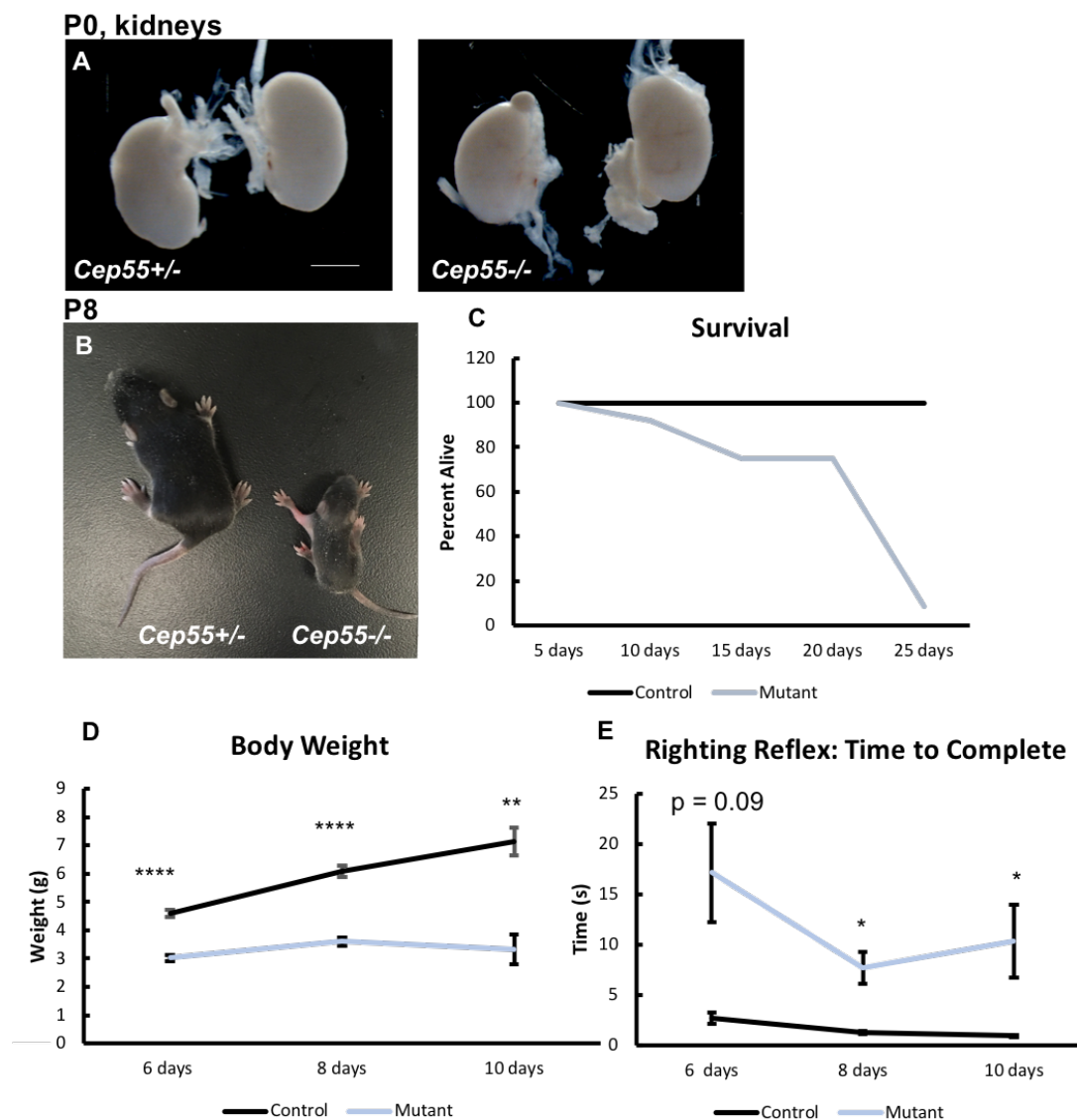


**Figure 45.** *Cep55* mutants exhibit failure to thrive and pre-weaning lethality.

(A) *Cep55* mutant kidneys (right) are not differentiable from controls (left) in shape or appearance at P0. (B) *Cep55* mutants (right) are noticeably smaller than controls (left) by P8. (C) *Cep55* mutants exhibit pre-weaning lethality; the majority die after 20 days.  $n =$  many controls, 12 *Cep55* mutants. (D) *Cep55* mutants have reduced body weight compared to controls at 6, 8 and 10 days old. While controls gain weight over time, *Cep55* mutants fail to gain weight over time.  $n$ , days: 6 = 13 controls and 6 mutants; 8 = 26 controls and 13 mutants, 10 = 11 controls and 4 mutants. (E) When placed on their backs, mouse pups reflexively right themselves. The time it took to perform this reflex was recorded. *Cep55* mutants have highly variable righting reflex times, and were significantly, approximately 10-fold slower at 8 and 10 days old. Some *Cep55* mutants failed to right, which was recorded as a max time of 30 seconds.  $n$ , days: 6 = 13 controls and 6 mutants; 8 = 17 controls and 9 mutants; 10 = 20 controls and 8 mutants. D,E: t-tests. Scale bars: A, 1 mm; B, 1 cm. \* $p < 0.05$ , \*\* $p < 0.01$ , \*\*\*\* $p < 0.0001$ .

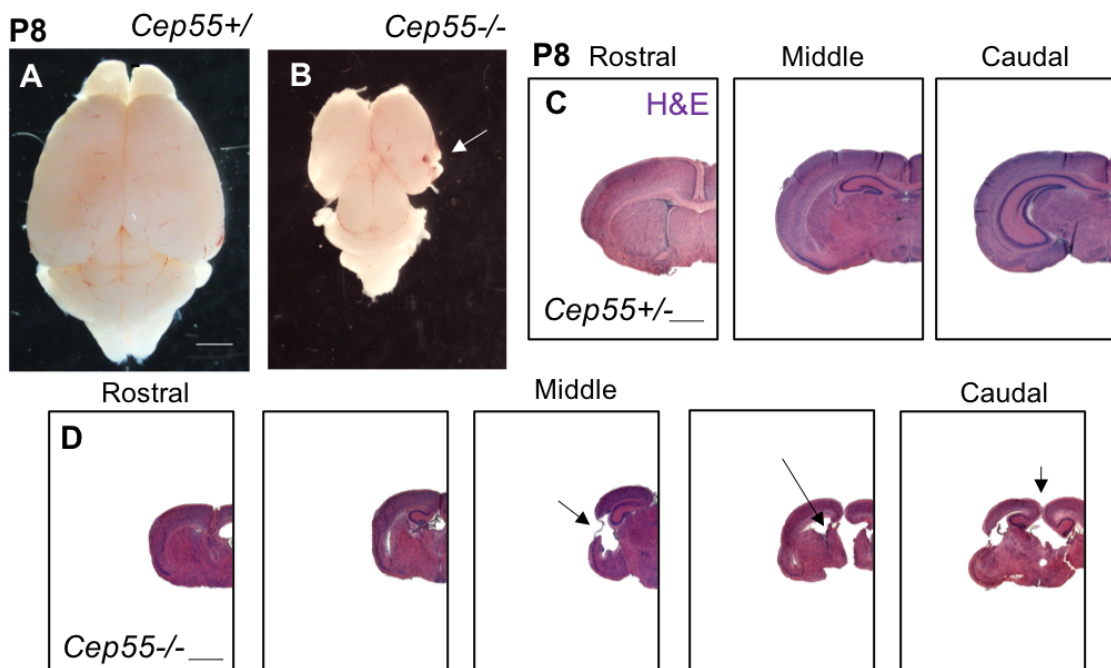


**Figure 46.** *Cep55* mutants exhibit degeneration of forebrain structures postnatally.

(A,B) *Cep55* mutant brains at postnatal day 8 (P8) (B) are markedly reduced in size compared to heterozygote controls (A). *Cep55* mutant lateral cortices show tissue degeneration not seen at P0 (arrow).  $n = 3$  *Cep55*<sup>+/-</sup> and 3 *Cep55*<sup>-/-</sup> brains. (C) Coronal sections of heterozygote control brains at P8 stained with hematoxylin and eosin (H&E) at rostral, middle and caudal levels. (D) Coronal sections of *Cep55* mutant brains at P8 stained with H&E at rostral, middle and caudal levels. All brain structures are dramatically reduced in size. Many structural abnormalities are noted, including lateral-stratial tissue degeneration, enlarged ventricles, and midline defects (shown in arrows from left to right, respectively).  $n = 3$  *Cep55*<sup>+/-</sup> and 3 *Cep55*<sup>-/-</sup> brains. Scale bars: A, 2 mm; C,D 1 mm.

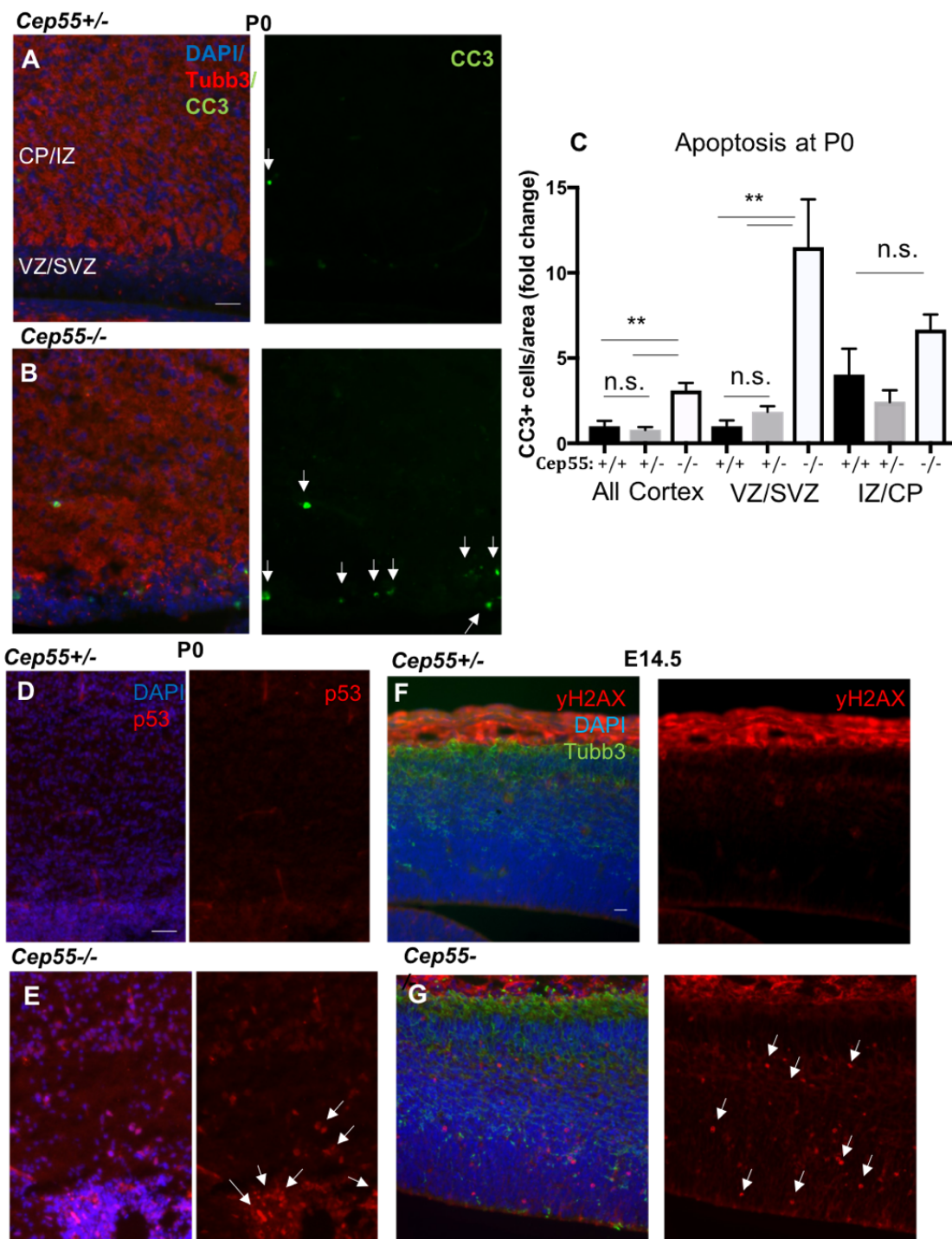


**Figure 47.** *Cep55* mutants have continued apoptosis and p53 activation postnatally and DNA damage prenatally.  
(continued on next page)

**Figure 47.** Cep55 mutants have continued apoptosis and p53 activation postnatally and DNA damage prenatally.

**(A,B)** Cep55 heterozygote (A) and mutant (B) P0 sections labeled with antibodies to cleaved-caspase 3 (CC3, green) and Tubb3 (red), show increased numbers of apoptotic cells in the proliferating zones (vz/svz (ventricular zone/subventricular zone; Tubb3-) of Cep55 mutant cortices (arrows). **(C)** Quantification shows that apoptotic cells are increased in Cep55 mutant proliferating zones (vz/svz) but not in the iz/cp (intermediate zone/cortical plate). n = 3 *Cep55*<sup>+/+</sup>, 4 *Cep55*<sup>-/-</sup> and 3 *Cep55*<sup>-/-</sup> brains. one-way ANOVA. **(D,E)** In addition to apoptosis, P0 Cep55 mutant cortices (E) show highly increased numbers of p53<sup>+</sup> nuclei (red) compared to controls (D). These nuclei are concentrated in proliferating zones (arrows). n = 2 *Cep55*<sup>+/-</sup> and 2 *Cep55*<sup>-/-</sup> brains. **(F,G)** In E14.5 sections,  $\gamma$ H2AX<sup>+</sup> nuclei, denoting DNA damage (green), are rarely observed in controls (F) but are easily noted in Cep55 mutants (G, arrows).  $\gamma$ H2AX<sup>+</sup> puncta are not in both proliferating and non-proliferating (Tubb3<sup>+</sup>, green) zones. n = 2 *Cep55*<sup>+/-</sup> and 2 *Cep55*<sup>-/-</sup> brains. Scale bars: A,D, 50  $\mu$ m; F, 20  $\mu$ m. n.s. = not significant; \*\*p < 0.01.

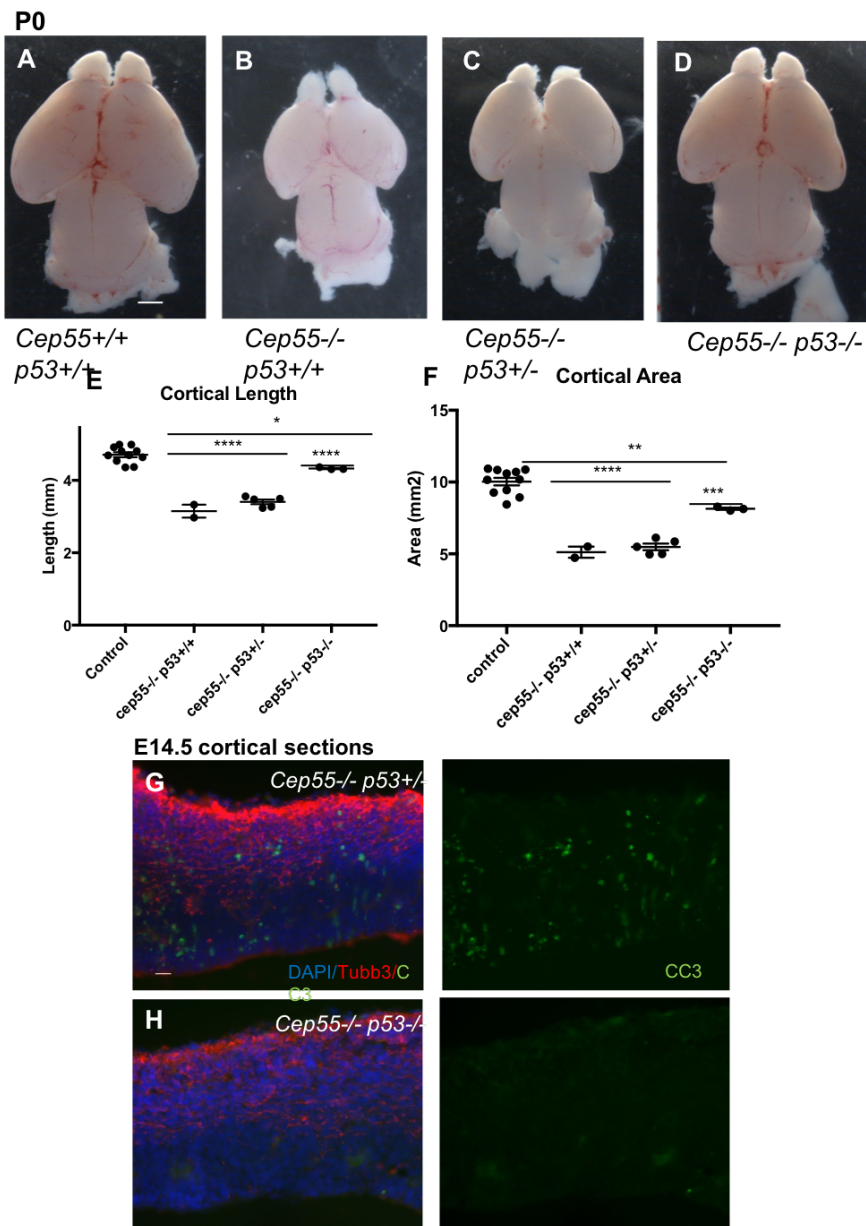


**Figure 48.** *Cep55* mutant microcephaly is partially dependent on p53.

(A,B) *Cep55* mutants with wild-type p53 expression (B) exhibit decreased brain size at P0 compared to wild-type controls (A). (C) Loss of one p53 allele does not appreciably improve *Cep55* mutant brain size. (D) Complete loss of p53 improves *Cep55* mutant brain size. (E) Quantification of cortical length at P0 shows a 21% improvement of cortical length in *Cep55*;*p53* mutants compared to *Cep55*<sup>-/-</sup>;*p53*<sup>+/-</sup> cortices; however, *Cep55*;*p53* mutant cortices are still 10% shorter than wild-type controls. (F) Quantification of cortical area at P0 shows a 32% improvement of cortical area in *Cep55*;*p53* mutants compared to *Cep55*<sup>-/-</sup>;*p53*<sup>+/-</sup> cortices; however, *Cep55*;*p53* mutant cortices are still 19% smaller than wild-type controls. n = 11 control (*Cep55*<sup>+/+</sup>;*p53*<sup>+/+</sup> and *p53*<sup>+/+</sup>;*p53*<sup>+/-</sup>), 5 *Cep55*<sup>-/-</sup> *p53*<sup>+/+</sup> and 3 *Cep55*<sup>-/-</sup> *p53*<sup>-/-</sup> brains for E and F. (G,H) At E14.5, apoptotic (cleaved-caspase 3<sup>+</sup>, green) cells are readily observed in both proliferating and neuronal (Tubb3<sup>+</sup>, red) zones of *Cep55*<sup>-/-</sup> *p53*<sup>+/+</sup> cortices (G). However, CC3<sup>+</sup> cells are greatly reduced in *Cep55*;*p53* mutant cortices (H). n = 2 *Cep55*<sup>-/-</sup>;*p53*<sup>+/+</sup> and 2 *Cep55*<sup>-/-</sup>;*p53*<sup>-/-</sup> brains. E-F one-way ANOVA. Scale bars: A, 1 mm; G, 20  $\mu$ m. \*p < 0.05, \*\*p < 0.01, \*\*\*p < 0.001, \*\*\*\*p < 0.0001.

## Appendix 4: Primary consequences of Cep55 loss in NIH 3T3 cells

In the experiments presented in this appendix, we tested siRNAs for use in knockdown of Cep55 for analysis in cell lines and for future use *in vivo*. NIH 3T3 cells were purchased from ATCC (ref: CRL-1658) and were not used past passage 10. OnTarget Plus Cep55 siRNAs were purchased from Dharmacon (ref: J-044799-09-0002 and J-044799-10-0002) as well as a non-targeting siRNA used as a control (ref: D-001810-01-05) and used at 40 nM. Transfection was performed as previously described (Kerstin M. Janisch et al., 2017). Fixation was performed at 24 or 48 hrs with either an equal volume of 8% PFA added for 10 minutes, or removal of media followed by addition of cold methanol for 10 minutes. Immunostaining, imaging and analysis was performed as described in **Chapters 2 and 3**.

In HeLa cells, Cep55 is localized to the midbody ring at the center of the midbody flank. We found that a mouse embryonic fibroblast cell line (3T3) exhibited a similar pattern of Cep55 localization (Fig. 49A). Independent use of two siRNAs at a concentration of 40 nM showed a 90% reduction of Cep55 localization to the midbody at 24 hrs post-transfection and 75% reduction at 48 hrs (Fig. 49B-E).

Previous studies in HeLa cells indicated that knockdown of Cep55 resulted in increasing numbers of midbody-stage cells; live imaging showed this was due to abscission delay. Furthermore, knockdown of Cep55 resulted in midbody regression, as evidenced by live imaging and fixed analyses showing high numbers of binucleate cells. We investigated whether these defects occurred with Cep55 knockdown in 3T3 cells. At 24 hrs post-transfection, we found a trend for increased numbers of midbodies per cells with one siRNA and a significant, approximately 2-fold increase with the other (Fig. 50A,B). We further normalized this to the number of cells that were in the cell cycle (proliferating cells) by immunostaining with Ki67. We saw an approximately 2-fold increase in the number of midbodies per proliferating cells with both siRNAs (Fig. 50C). At 48 hrs post-transfection, the midbody index was still increased, especially when normalized to the number of proliferating cells (Fig. 50D,E). We did observe a slight increase in binucleate cells at 24 hrs post-transfection, but by 48 hrs there was no significant difference (Fig. 51D,E). Therefore, the most consistent phenotype we observed was an increase in midbody-stage cells, indicating abscission delay.

We next wondered whether abscission delay in 3T3 cells due to reduction of Cep55 had any consequences for cell proliferation or survival. We observed a normal amount of proliferating (Ki67+) cells in siCep55 cultures at 24 hrs post-transfection (Fig. 51F), but by 48 hrs there was a significant reduction in proliferation (Fig. 49A-C,G). These data suggests that Cep55 loss may result in cell-cycle exit or G1 arrest. To evaluate apoptosis, we used antibodies to cleaved-caspase 3 (CC3). We observed a slight increase in apoptosis with siCep55 #2 at 24 hrs post-transfection (Fig. 52A). By 48 hrs, there was no difference in apoptosis (Fig. 52B). Finally, we observed no difference in the nuclear:cytoplasmic ratio of p53 expression in siCep55 cultures (Fig. 52C). This suggests that 3T3 cells lacking Cep55 are more likely to exit the cell cycle than undergo apoptosis. Surprisingly, this cell cycle exit does not appear to be obviously p53-dependent.

Finally, we investigated whether Cep55 loss impaired mitosis in 3T3 cells. As predicted, we found no difference in the number of mitotic cells in siCep55 cultures, suggesting that although abscission is delayed, mitosis is not affected (Fig. 52D).

These siRNAs could be used in the future to knock down Cep55 in the cortex and determine the acute consequences of loss. This could be done using electroporation. We have electroporated pCAG-GFP plasmids into control cortices at E14.5, followed by either slab preparation or vibratome sectioning, and overnight culture. Slab preparation allows visualization of the apical membrane, by combining electroporation of GFP with antibody labeling of apical membrane and mitotic markers. This could also be used with antibodies to midbody proteins. Alternatively, slice preparation allows visualization of lateral cortical sections. With just electroporated GFP and DAPI, cell shapes can be visualized. Culturing for different amounts of time would allow evaluation of neuron migration into the cortex. Electroporation of GFP could be combined with Cep55 siRNAs to evaluate these parameters with Cep55 loss. First, confirmation of Cep55 knockdown by electroporation and dissociation of NSCs, followed by immunostaining for Cep55, would be needed. It is possible the concentration may have to be adjusted compared to that used in 3T3 cells.

## Figures

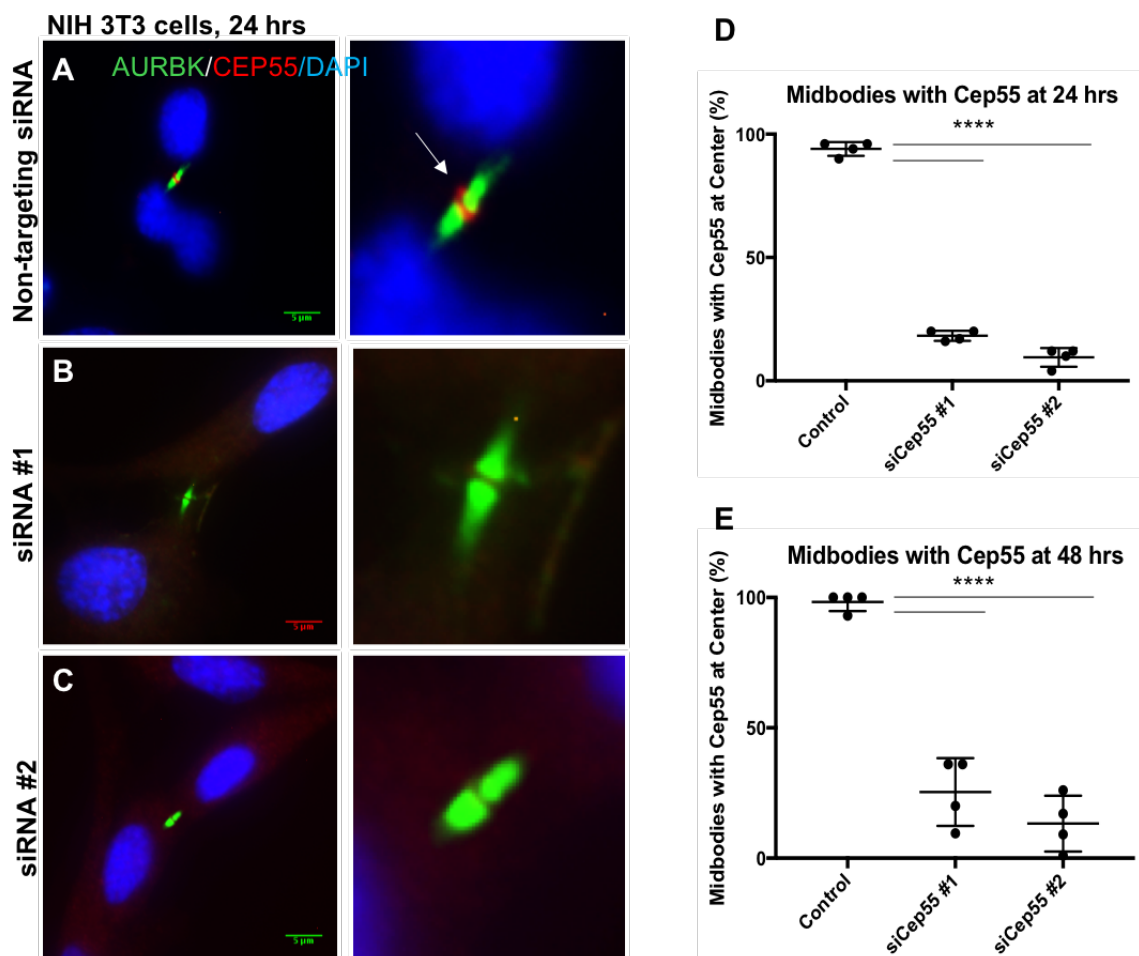


**Figure 49.** siRNAs to *Cep55* decrease *Cep55* midbody expression in 3T3 cells.

(A) *Cep55* (red) is localized to the center (arrow) of post-furrowing midbodies (AurbK+, green) in 3T3 cells. (B,C) Two independent siRNAs to *Cep55* sequence decrease the number of midbodies with detectable *Cep55* expression. (D) The number of midbodies with detectable *Cep55* is decreased to <10% with both siRNAs at 24 hrs post-transfection. (E) The number of midbodies with detectable *Cep55* is decreased to <25% with both siRNAs at 48 hrs post-transfection.  $n = 50$  midbodies from 3 coverslips each from 3 independent experiments. D,E: one-way ANOVA. Scale bars: 5  $\mu\text{m}$ . \*\*\*\* $p < 0.0001$ .

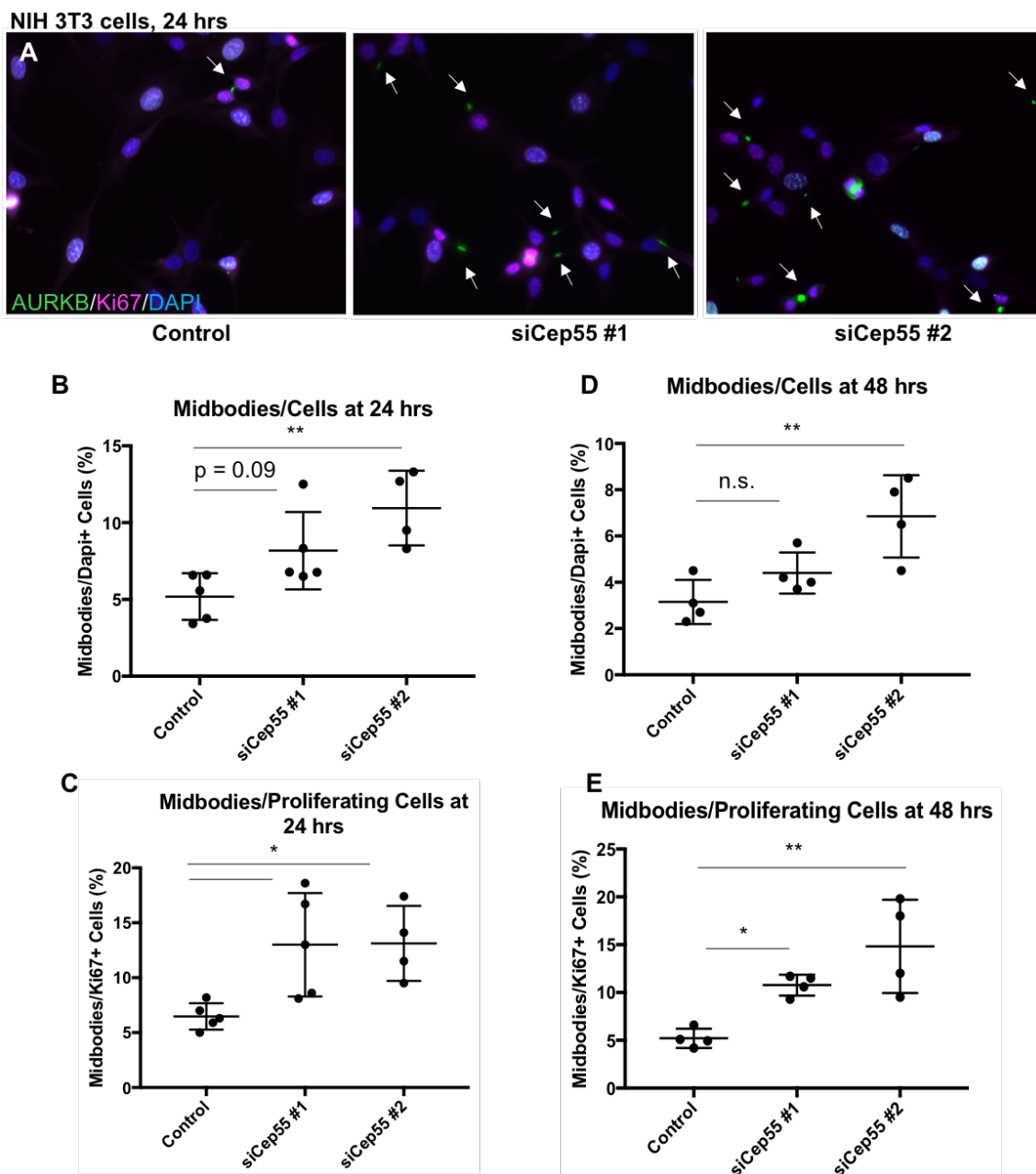


**Figure 50.** *Cep55* depletion increases midbody-stage cells in 3T3 cultures.

(A) 3T3 cells with midbodies are identified with AurKb (green) and proliferating cells are identified with Ki67 (magenta). Midbodies are denoted with arrows. (B) At 24 hrs after transfection, increased numbers of midbodies per Dapi+ cells are observed with siCep55#2. (C) The number of midbodies out of the total number of proliferating cells at 24 hrs is increased with both siRNAs (D) At 48 hrs after transfection, increased numbers of midbodies per Dapi+ cells are observed with siCep55 #2. (E) The number of midbodies out of the total number of proliferating cells at 48 hrs is increased with both siRNAs. n (B,C) = 5 control, 5 siCep55 #1 and 4 siCep55 #2 coverslips; (D,E) = 4 coverslips for each condition. All from 3 independent experiments. All: one-way ANOVA. n.s., not significant; \* $p < .05$ , \*\* $p < 0.01$ .

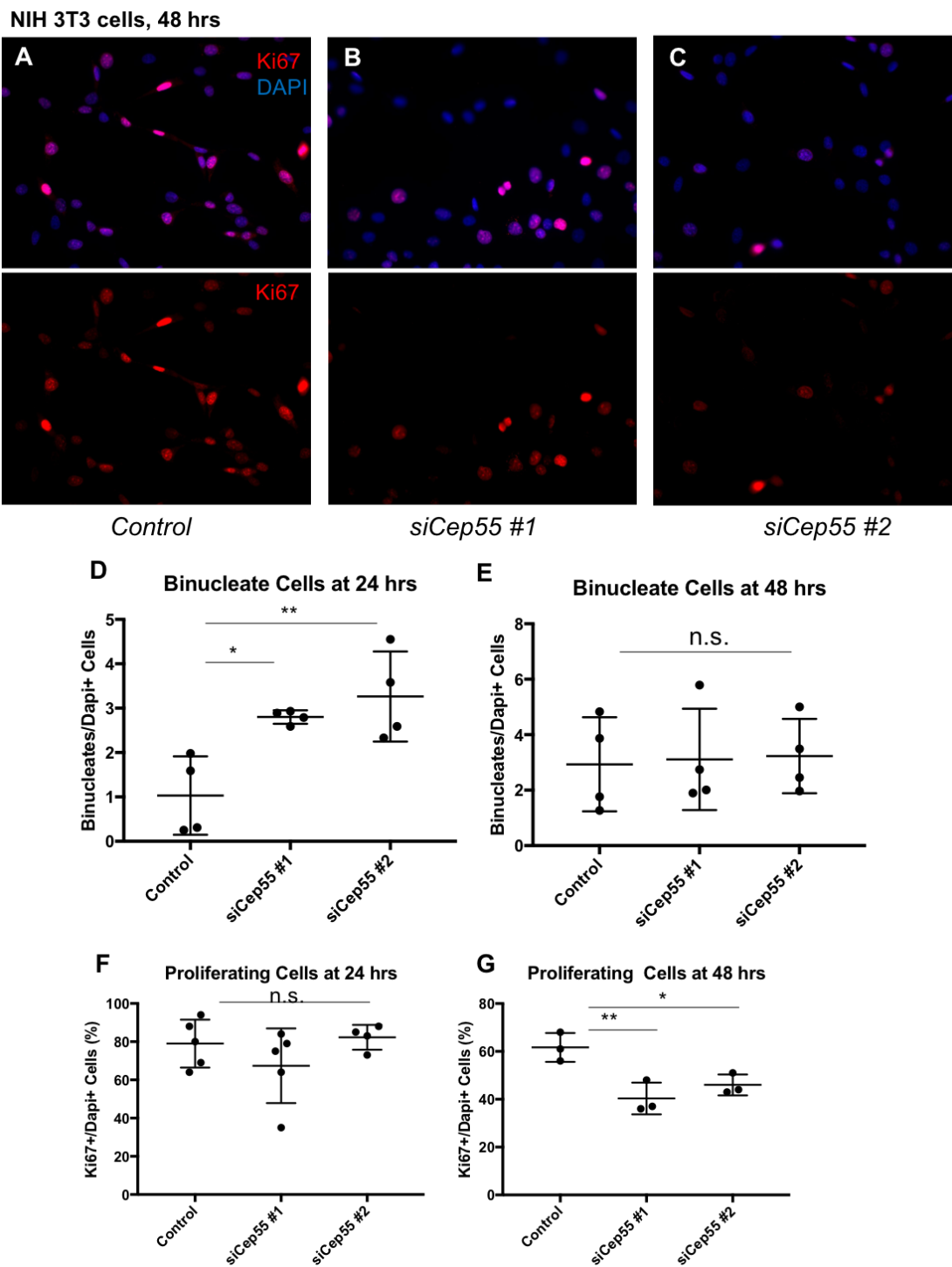


**Figure 51.** Cep55 depletion decreases 3T3 cell proliferation.  
(continued on next page)

**Figure 51. Cep55 depletion decreases 3T3 cell proliferation**

**(A)** Proliferating 3T3 cells are identified with an antibody to Ki67 (red), a nuclear marker of proliferation. **(B,C)** Decreased numbers of proliferating cells are observed in siCep55 #1 and #2 cultures. **(D,E)** Increased numbers of binucleate cells are observed in siCep55 #1 and #2 cultures at 24 but not 48 hrs after transfection. **(F,G)** The number of proliferating (Ki67+) cells in siCep55 #1 and #2 cultures is normal at 24 hrs, but is decreased at 48 hrs after transfection. n (D,F) = 5 control, 5 siCep55 #1 and 4 siCep55 #2 coverslips; (E) = 3 coverslips for each condition; (G) = 4 coverslips for each condition. All from 3 independent experiments. All: one-way ANOVA. n.s., not significant; \* $p < .05$ , \*\* $p < 0.01$ .

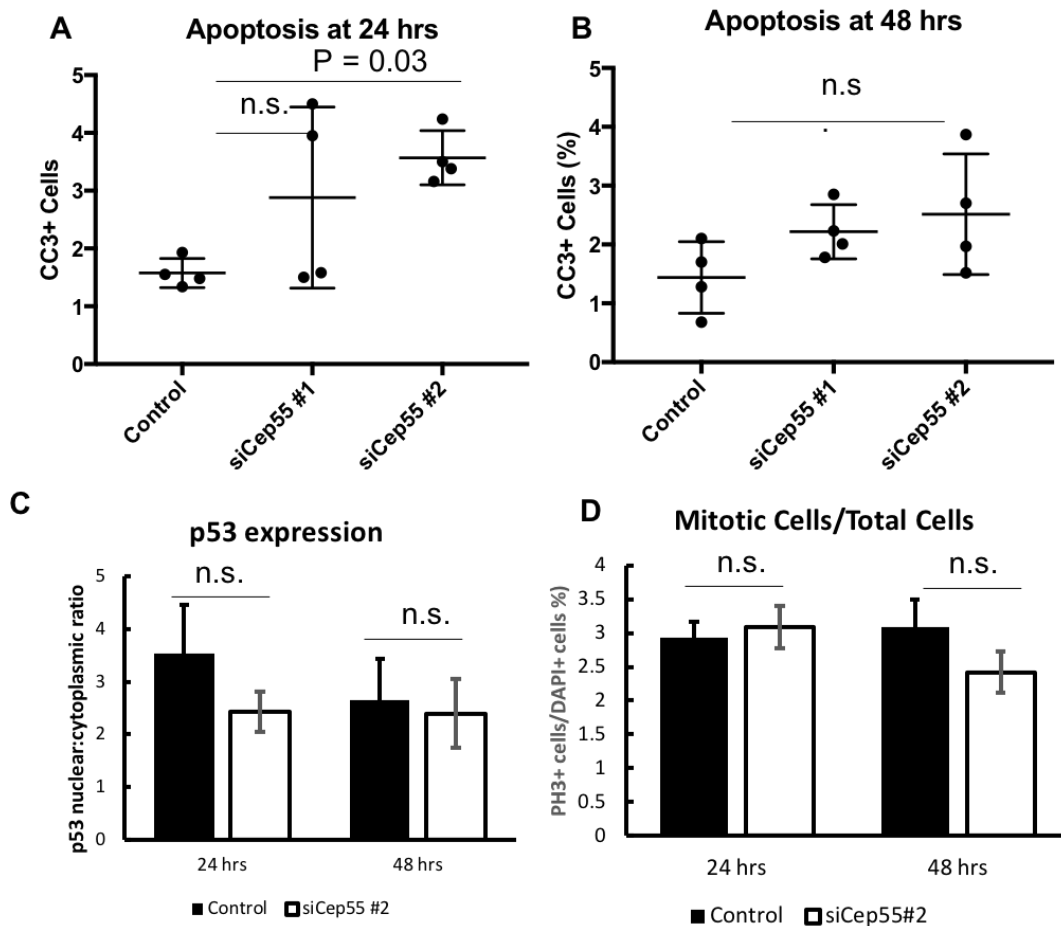


**Figure 52.** *Cep55* depletion in 3T3 cells does not alter apoptosis, p53 expression or mitosis. **(A)** Apoptosis, defined as the number of cleaved-caspase 3 (CC3)+ cells per total Dapi+ cells, is increased at 24 hrs after transfection with siCep55 #2 in 3T3 cells. **(B)** Apoptosis is not increased with either Cep55 siRNA at 48 hrs. **(C)** The nuclear:cytoplasmic ratio of p53 is not altered in siCep55 #2 3T3 cell cultures at 24 or 48 hrs. **(D)** The number of mitotic cells, defined as phospho-histone 3 (PH3)+, per total Dapi+ 3T3 cells is not significantly different in siCep55 #2 cultures at 24 or 48 hrs. n (A) = 5 control, 5 siCep55 #1 and 4 siCep55 #2 coverslips; (B) = 4 coverslips for each condition; (C,D) = 4 coverslips for each condition at 24 hrs and 3 coverslips for each condition at 48 hrs. All from 3 independent experiments. A,B: one-way ANOVA; C,D: t-test. n.s., not significant.

## References

- Aaku-Saraste, E., Hellwig, A., & Huttner, W. B. (1996). Loss of occludin and functional tight junctions, but not ZO-1, during neural tube closure - Remodeling of the neuroepithelium prior to neurogenesis. *Developmental Biology*, *180*(2), 664–679.  
<https://doi.org/10.1006/dbio.1996.0336>
- Abaza, A., Soleilhac, J., Westendorf, J., Piel, M., Crevel, I., Pirollet, F., & Cell, J. M. M. B. (2003). M Phase Phosphoprotein 1 Is a Human Plus-end-directed Kinesin-related Protein Required for Cytokinesis \* teins specifically phosphorylated at the G 2 / M transition. *Biochemistry*, *278*(30), 27844–27852. <https://doi.org/10.1074/jbc.M304522200>
- Abuelo, D. (2007). Microcephaly Syndromes. *Seminars in Pediatric Neurology*, *14*(3), 118–127.  
<https://doi.org/10.1016/j.spen.2007.07.003>
- Alkanderi, S., Molinari, E., Shaheen, R., Elmaghloob, Y., Stephen, L. A., Sammut, V., ... Sayer, J. A. (2018). ARL3 Mutations Cause Joubert Syndrome by Disrupting Ciliary Protein Composition. *American Journal of Human Genetics*, *103*(4), 612–620.  
<https://doi.org/10.1016/j.ajhg.2018.08.015>
- Amini, R., Goupil, E., Labella, S., Zetka, M., Maddox, A. S., Labbé, J. C., & Chartier, N. T. (2014). C. Elegans Anillin proteins regulate intercellular bridge stability and germline syncytial organization. *Journal of Cell Biology*, *206*(1), 129–143.  
<https://doi.org/10.1083/jcb.201310117>
- Andersen, E. F., & Halloran, M. C. (2012). Centrosome movements in vivo correlate with specific neurite formation downstream of LIM homeodomain transcription factor activity. *Journal of Cell Science*, *125*(19), e1–e1. <https://doi.org/10.1242/jcs.122424>
- Angelastro, J. M., Ignatova, T. N., Kukekov, V. G., Steindler, D. A., Stengren, G. B., Mendelsohn, C., & Greene, L. A. (2003). Regulated expression of ATF5 is required for the progression of neural progenitor cells to neurons. *The Journal of Neuroscience: The Official Journal of the Society for Neuroscience*, *23*(11), 4590–4600. Retrieved from <http://www.ncbi.nlm.nih.gov/pubmed/12805299>
- Angevine, J. B., & Sidman, R. L. (1961). Autoradiographic study of cell migration during histogenesis of cerebral cortex in the mouse. *Nature*, *192*(4804), 766–768.  
<https://doi.org/10.1038/192766b0>
- Arai, Y., Pulvers, J. N., Haffner, C., Schilling, B., Nüsslein, I., Calegari, F., & Huttner, W. B. (2011). Neural stem and progenitor cells shorten S-phase on commitment to neuron

- production. *Nature Communications*, 2(1). <https://doi.org/10.1038/ncomms1155>
- Arai, Y., Sampaio, J. L., Wilsch-Bräuninger, M., Ettinger, A. W., Haffner, C., & Huttner, W. B. (2015). Lipidome of midbody released from neural stem and progenitor cells during mammalian cortical neurogenesis. *Frontiers in Cellular Neuroscience*, 9. <https://doi.org/10.3389/fncel.2015.00325>
- Arakawa, H. (2005). P53, Apoptosis and Axon-Guidance Molecules. *Cell Death and Differentiation*. <https://doi.org/10.1038/sj.cdd.4401601>
- Arnold, S. J., Sugnaseelan, J., Groszer, M., Srinivas, S., & Robertson, E. J. (2009). Generation and analysis of a mouse line harboring GFP in the Eomes/Tbr2 locus. *Genesis*, 47(11), 775–781. <https://doi.org/10.1002/dvg.20562>
- Arquint, C., & Nigg, E. A. (2014). STIL microcephaly mutations interfere with APC/C-mediated degradation and cause centriole amplification. *Current Biology*, 24(4), 351–360. <https://doi.org/10.1016/j.cub.2013.12.016>
- Arya, R., & White, K. (2015). Cell death in development: Signaling pathways and core mechanisms. *Seminars in Cell and Developmental Biology*. <https://doi.org/10.1016/j.semcdb.2015.02.001>
- Asami, M., Pilz, G. A., Ninkovic, J., Godinho, L., Schroeder, T., Huttner, W. B., & Gotz, M. (2011). The role of Pax6 in regulating the orientation and mode of cell division of progenitors in the mouse cerebral cortex. *Journal of Cell Science*, 124(23), e1–e1. <https://doi.org/10.1242/jcs.103960>
- Atilla-Gokcumen, G. E., Muro, E., Relat-Goberna, J., Sasse, S., Bedigian, A., Coughlin, M. L., ... Eggert, U. S. (2014). Dividing cells regulate their lipid composition and localization. *Cell*, 156(3), 428–439. <https://doi.org/10.1016/j.cell.2013.12.015>
- Barnes, A. P., & Polleux, F. (2009). Establishment of Axon-Dendrite Polarity in Developing Neurons. *Annual Review of Neuroscience*, 32(1), 347–381. <https://doi.org/10.1146/annurev.neuro.31.060407.125536>
- Basto, R., Brunk, K., Vinadogrova, T., Peel, N., Franz, A., Khodjakov, A., & Raff, J. W. (2008). Centrosome Amplification Can Initiate Tumorigenesis in Flies. *Cell*, 133(6), 1032–1042. <https://doi.org/10.1016/j.cell.2008.05.039>
- Basto, R., Lau, J., Vinogradova, T., Gardiol, A., Woods, C. G., Khodjakov, A., & Raff, J. W. (2006). Flies without Centrioles. *Cell*, 125(7), 1375–1386. <https://doi.org/10.1016/j.cell.2006.05.025>
- Bastos, R. N., & Barr, F. A. (2010). Plk1 negatively regulates Cep55 recruitment to the midbody

- to ensure orderly abscission. *Journal of Cell Biology*, 191(4), 751–760.  
<https://doi.org/10.1083/jcb.201008108>
- Baudoin, J. P., Viou, L., Launay, P. S., Luccardini, C., Espeso Gil, S., Kiyasova, V., ... Métin, C. (2012). Tangentially Migrating Neurons Assemble a Primary Cilium that Promotes Their Reorientation to the Cortical Plate. *Neuron*, 76(6), 1108–1122.  
<https://doi.org/10.1016/j.neuron.2012.10.027>
- Bazzi, H., & Anderson, K. V. (2014). Acentriolar mitosis activates a p53-dependent apoptosis pathway in the mouse embryo. *Proceedings of the National Academy of Sciences*, 111(15), E1491–E1500. <https://doi.org/10.1073/pnas.1400568111>
- Bernabé-Rubio, M., Andrés, G., Casares-Arias, J., Fernández-Barrera, J., Rangel, L., Reglero-Real, N., ... Alonso, M. A. (2016). Novel role for the midbody in primary ciliogenesis by polarized epithelial cells. *Journal of Cell Biology*, 214(3), 259–273.  
<https://doi.org/10.1083/jcb.201601020>
- Bianchi, F. T., Tocco, C., Pallavicini, G., Liu, Y., Verni, F., Merigliano, C., ... Di Cunto, F. (2017). Citron Kinase Deficiency Leads to Chromosomal Instability and TP53-Sensitive Microcephaly. *Cell Reports*, 18(7), 1674–1686. <https://doi.org/10.1016/j.celrep.2017.01.054>
- Bizzotto, S., & Francis, F. (2015). Morphological and functional aspects of progenitors perturbed in cortical malformations. *Frontiers in Cellular Neuroscience*, 9.  
<https://doi.org/10.3389/fncel.2015.00030>
- Blaschke, A. J., Staley, K., & Chun, J. (1996). Widespread programmed cell death in proliferative and postmitotic regions of the fetal cerebral cortex. *Development (Cambridge, England)*, 122(4), 1165–1174. Retrieved from <http://www.ncbi.nlm.nih.gov/pubmed/8620843>
- Bondeson, M. L., Ericson, K., Gudmundsson, S., Ameer, A., Pontén, F., Wesström, J., ... Wilbe, M. (2017). A nonsense mutation in CEP55 defines a new locus for a Meckel-like syndrome, an autosomal recessive lethal fetal ciliopathy. *Clinical Genetics*, 92(5), 510–516.  
<https://doi.org/10.1111/cge.13012>
- Bradke, F., & Dotti, C. G. (1997). Neuronal polarity: Vectorial cytoplasmic flow precedes axon formation. *Neuron*, 19(6), 1175–1186. [https://doi.org/10.1016/S0896-6273\(00\)80410-9](https://doi.org/10.1016/S0896-6273(00)80410-9)
- Breuss, M., Fritz, T., Gstrein, T., Chan, K., Ushakova, L., Yu, N., ... Keays, D. A. (2016). Mutations in the murine homologue of TUBB5 cause microcephaly by perturbing cell cycle progression and inducing p53-associated apoptosis. *Journal of Cell Science*, 129(8), e1.1-e1.1. <https://doi.org/10.1242/jcs.190165>
- Breuss, M., Heng, J. I. T., Poirier, K., Tian, G., Jaglin, X. H., Qu, Z., ... Keays, D. A. (2012).

- Mutations in the  $\beta$ -Tubulin Gene TUBB5 Cause Microcephaly with Structural Brain Abnormalities. *Cell Reports*, 2(6), 1554–1562. <https://doi.org/10.1016/j.celrep.2012.11.017>
- Breuss, M. W., Hansen, A. H., Landler, L., & Keays, D. A. (2017). Brain-specific knockin of the pathogenic Tubb5 E401K allele causes defects in motor coordination and prepulse inhibition. *Behavioural Brain Research*, 323, 47–55. <https://doi.org/10.1016/j.bbr.2017.01.029>
- Bultje, R. S., Castaneda-Castellanos, D. R., Jan, L. Y., Jan, Y. N., Kriegstein, A. R., & Shi, S. H. (2009). Mammalian Par3 Regulates Progenitor Cell Asymmetric Division via Notch Signaling in the Developing Neocortex. *Neuron*, 63(2), 189–202. <https://doi.org/10.1016/j.neuron.2009.07.004>
- Camargo, F. D., Gokhale, S., Johnnidis, J. B., Fu, D., Bell, G. W., Jaenisch, R., & Brummelkamp, T. R. (2007). YAP1 Increases Organ Size and Expands Undifferentiated Progenitor Cells. *Current Biology*, 17(23), 2054–2060. <https://doi.org/10.1016/j.cub.2007.10.039>
- Capalbo, L., Montembault, E., Takeda, T., Bassi, Z. I., Glover, D. M., & D'Avino, P. P. (2012). The chromosomal passenger complex controls the function of endosomal sorting complex required for transport-III Snf7 proteins during cytokinesis. *Open Biology*, 2(MAY). <https://doi.org/10.1098/rsob.120070>
- Carlton, J. G., Agromayor, M., & Martin-Serrano, J. (2008). Differential requirements for Alix and ESCRT-III in cytokinesis and HIV-1 release. *Proceedings of the National Academy of Sciences*, 105(30), 10541–10546. <https://doi.org/10.1073/pnas.0802008105>
- Carlton, J. G., Caballe, A., Agromayor, M., Kloc, M., & Martin-Serrano, J. (2012). ESCRT-III governs the Aurora B-mediated abscission checkpoint through CHMP4C. *Science*, 336(6078), 220–225. <https://doi.org/10.1126/science.1217180>
- Carlton, J. G., & Martin-Serrano, J. (2007). Parallels between cytokinesis and retroviral budding: A role for the ESCRT machinery. *Science*, 316(5833), 1908–1912. <https://doi.org/10.1126/science.1143422>
- Chai, Y., Tian, D., Yang, Y., Feng, G., Cheng, Z., Li, W., & Ou, G. (2012). Apoptotic regulators promote cytokinetic midbody degradation in *C. Elegans*. *Journal of Cell Biology*, 199(7), 1047–1055. <https://doi.org/10.1083/jcb.201209050>
- Chen, C. T., & Doxsey, S. (2009). A Last-Minute Rescue of Trapped Chromatin. *Cell*, 136(3), 397–399. <https://doi.org/10.1016/j.cell.2009.01.028>
- Chen, C. T., Ettinger, A. W., Huttner, W. B., & Doxsey, S. J. (2013). Resurrecting remnants: The lives of post-mitotic midbodies. *Trends in Cell Biology*.

<https://doi.org/10.1016/j.tcb.2012.10.012>

- Chen, J. F., Zhang, Y., Wilde, J., Hansen, K. C., Lai, F., & Niswander, L. (2014). Microcephaly disease gene *Wdr62* regulates mitotic progression of embryonic neural stem cells and brain size. *Nature Communications*, *5*. <https://doi.org/10.1038/ncomms4885>
- Chen, Q., Zhang, N., Xie, R., Wang, W., Cai, J., Choi, K. S., ... Pan, D. (2015). Homeostatic control of Hippo signaling activity revealed by an endogenous activating mutation in YAP. *Genes and Development*, *29*(12), 1285–1297. <https://doi.org/10.1101/gad.264234.115>
- Chenn, A., & McConnell, S. K. (1995). Cleavage orientation and the asymmetric inheritance of *notchl* immunoreactivity in mammalian neurogenesis. *Cell*, *82*(4), 631–641. [https://doi.org/10.1016/0092-8674\(95\)90035-7](https://doi.org/10.1016/0092-8674(95)90035-7)
- Chenn, A., & Walsh, C. A. (2002). Regulation of cerebral cortical size by control of cell cycle exit in neural precursors. *Science*, *297*(5580), 365–369. <https://doi.org/10.1126/science.1074192>
- Christ, L., Wenzel, E. M., Liestøl, K., Raiborg, C., Campsteijn, C., & Stenmark, H. (2016). ALIX and ESC RT-I/II function as parallel ESC RT-III recruiters in cytokinetic abscission. *Journal of Cell Biology*, *212*(5), 499–513. <https://doi.org/10.1083/jcb.201507009>
- Chu, J., & Anderson, S. A. (2015). Development of cortical interneurons. *Neuropsychopharmacology*. <https://doi.org/10.1038/npp.2014.171>
- Conduit, P. T., Wainman, A., & Raff, J. W. (2015). Centrosome function and assembly in animal cells. *Nature Reviews Molecular Cell Biology*, *16*(10), 611–624. <https://doi.org/10.1038/nrm4062>
- Connell, J. W., Lindon, C., Luzio, J. P., & Reid, E. (2009). Spastin couples microtubule severing to membrane traffic in completion of cytokinesis and secretion. *Traffic*, *10*(1), 42–56. <https://doi.org/10.1111/j.1600-0854.2008.00847.x>
- Contreras, E. G., Sierralta, J., & Glavic, A. (2018). P53 is required for brain growth but is dispensable for resistance to nutrient restriction during *Drosophila* larval development. *PLoS ONE*, *13*(4). <https://doi.org/10.1371/journal.pone.0194344>
- Couture, O., Lombardi, E., Davis, K., Hays, E., & Chandar, N. (2013). Gene expression profiles resulting from stable loss of p53 mirrors its role in tissue differentiation. *PLoS ONE*, *8*(11). <https://doi.org/10.1371/journal.pone.0082494>
- Crowell, E. F., Gaffuri, A.-L., Gayraud-Morel, B., Tajbakhsh, S., & Echard, A. (2014). Engulfment of the midbody remnant after cytokinesis in mammalian cells. *Journal of Cell Science*, *127*(17), 3840–3851. <https://doi.org/10.1242/jcs.154732>

- D'Arcangelo, G. D., Nakajima, K., Miyata, T., Ogawa, M., Mikoshiba, K., & Curran, T. (1997). Reelin is a secreted glycoprotein recognized by the CR-50 monoclonal antibody. *The Journal of Neuroscience*. <https://doi.org/10.1523/jneurosci.2934-08.2009>
- D'Arcangelo, G., Miao, G. G., Chen, S. C., Scares, H. D., Morgan, J. I., & Curran, T. (1995). A protein related to extracellular matrix proteins deleted in the mouse mutant reeler. *Nature*, *374*(6524), 719–723. <https://doi.org/10.1038/374719a0>
- Dambournet, D., MacHicoane, M., Chesneau, L., Sachse, M., Rocancourt, M., El Marjou, A., ... Echard, A. (2011). Rab35 GTPase and OCRL phosphatase remodel lipids and F-actin for successful cytokinesis. *Nature Cell Biology*, *13*(8), 981–988. <https://doi.org/10.1038/ncb2279>
- Damiani, D., Goffinet, A. M., Alberts, A., & Tissir, F. (2016). Lack of Diaph3 relaxes the spindle checkpoint causing the loss of neural progenitors. *Nature Communications*, *7*. <https://doi.org/10.1038/ncomms13509>
- Dang, J., Tiwari, S. K., Lichinchi, G., Qin, Y., Patil, V. S., Eroshkin, A. M., & Rana, T. M. (2016). Zika Virus Depletes Neural Progenitors in Human Cerebral Organoids through Activation of the Innate Immune Receptor TLR3. *Cell Stem Cell*, *19*(2), 258–265. <https://doi.org/10.1016/j.stem.2016.04.014>
- de Anda, F. C., Meletis, K., Ge, X., Rei, D., & Tsai, L.-H. (2010). Centrosome Motility Is Essential for Initial Axon Formation in the Neocortex. *Journal of Neuroscience*, *30*(31), 10391–10406. <https://doi.org/10.1523/jneurosci.0381-10.2010>
- De Anda, F. C., Pollarolo, G., Da Silva, J. S., Camoletto, P. G., Feiguin, F., & Dotti, C. G. (2005). Centrosome localization determines neuronal polarity. *Nature*, *436*(7051), 704–708. <https://doi.org/10.1038/nature03811>
- De Calignon, A., Fox, L. M., Pitstick, R., Carlson, G. A., Bacskai, B. J., Spires-Jones, T. L., & Hyman, B. T. (2010). Caspase activation precedes and leads to tangles. *Nature*, *464*(7292), 1201–1204. <https://doi.org/10.1038/nature08890>
- Dehay, C., Kennedy, H., & Kosik, K. S. (2015). The Outer Subventricular Zone and Primate-Specific Cortical Complexification. *Neuron*. <https://doi.org/10.1016/j.neuron.2014.12.060>
- Di Cunto, F., Imarisio, S., Hirsch, E., Broccoli, V., Bulfone, A., Migheli, A., ... Altruda, F. (2000). Defective neurogenesis in citron kinase knockout mice by altered cytokinesis and massive apoptosis. *Neuron*, *28*(1), 115–127. [https://doi.org/10.1016/S0896-6273\(00\)00090-8](https://doi.org/10.1016/S0896-6273(00)00090-8)
- Di Giovanni, S., Knights, C. D., Rao, M., Yakovlev, A., Beers, J., Catania, J., ... Faden, A. I.

- (2006). The tumor suppressor protein p53 is required for neurite outgrowth and axon regeneration. *EMBO Journal*, 25(17), 4084–4096. <https://doi.org/10.1038/sj.emboj.7601292>
- Di Giovanni, S., & Rathore, K. (2012). P53-Dependent Pathways in Neurite Outgrowth and Axonal Regeneration. *Cell and Tissue Research*. <https://doi.org/10.1007/s00441-011-1292-5>
- Dionne, L. K., Wang, X. J., & Prekeris, R. (2015). Midbody: From cellular junk to regulator of cell polarity and cell fate. *Current Opinion in Cell Biology*. <https://doi.org/10.1016/j.ceb.2015.04.010>
- Donehower, L. A., Harvey, M., Slagle, B. L., McArthur, M. J., Montgomery, C. A., Butel, J. S., & Bradley, A. (1992). Mice deficient for p53 are developmentally normal but susceptible to spontaneous tumours. *Nature*, 356(6366), 215–221. <https://doi.org/10.1038/356215a0>
- Dotti, C. G., & Banker, G. A. (1987). Experimentally induced alteration in the polarity of developing neurons. *Nature*, 330(6145), 254–256. <https://doi.org/10.1038/330254a0>
- Dotti, C. G., Sullivan, C. A., & Banker, G. A. (1988). The establishment of polarity by hippocampal neurons in culture. *The Journal of Neuroscience : The Official Journal of the Society for Neuroscience*, 8(4), 1454–1468. <https://doi.org/10.1523/JNEUROSCI.08-04-01454.1988>
- Dubreuil, V., Marzesco, A. M., Corbeil, D., Huttner, W. B., & Wilsch-Bräuninger, M. (2007). Midbody and primary cilium of neural progenitors release extracellular membrane particles enriched in the stem cell marker prominin-1. *Journal of Cell Biology*, 176(4), 483–495. <https://doi.org/10.1083/jcb.200608137>
- Duerinckx, S., & Abramowicz, M. (2018). The genetics of congenitally small brains. *Seminars in Cell and Developmental Biology*. <https://doi.org/10.1016/j.semcdb.2017.09.015>
- Dwyer, N. D., Chen, B., Chou, S.-J., Hippenmeyer, S., Nguyen, L., & Ghashghaei, H. T. (2016). Neural Stem Cells to Cerebral Cortex: Emerging Mechanisms Regulating Progenitor Behavior and Productivity. *The Journal of Neuroscience*, 36(45), 11394–11401. <https://doi.org/10.1523/jneurosci.2359-16.2016>
- Dwyer, N. D., Manning, D. K., Moran, J. L., Mudbhary, R., Fleming, M. S., Favero, C. B., ... Beier, D. R. (2011). A forward genetic screen with a thalamocortical axon reporter mouse yields novel neurodevelopment mutants and a distinct *emx2* mutant phenotype. *Neural Development*, 6(1). <https://doi.org/10.1186/1749-8104-6-3>
- Eisenhoffer, G. T., Loftus, P. D., Yoshigi, M., Otsuna, H., Chien, C. Bin, Morcos, P. A., & Rosenblatt, J. (2012). Crowding induces live cell extrusion to maintain homeostatic cell numbers in epithelia. *Nature*, 484(7395), 546–549. <https://doi.org/10.1038/nature10999>

- El Ghouzzi, V., Bianchi, F. T., Molineris, I., Mounce, B. C., Berto, G. E., Rak, M., ... Di Cunto, F. (2016). ZIKA virus elicits P53 activation and genotoxic stress in human neural progenitors similar to mutations involved in severe forms of genetic microcephaly and p53. *Cell Death and Disease*, 7(10). <https://doi.org/10.1038/cddis.2016.266>
- Elia, N., Sougrat, R., Spurlin, T. A., Hurley, J. H., & Lippincott-Schwartz, J. (2011). Dynamics of endosomal sorting complex required for transport (ESCRT) machinery during cytokinesis and its role in abscission. *Proceedings of the National Academy of Sciences*, 108(12), 4846–4851. <https://doi.org/10.1073/pnas.1102714108>
- Espinosa, J. S., Tea, J. S., & Luo, L. (2014). Mosaic analysis with double markers (MADM) in mice. *Cold Spring Harbor Protocols*, 2014(2), 182–189. <https://doi.org/10.1101/pdb.prot080366>
- Ettinger, A. W., Wilsch-Bräuninger, M., Marzesco, A. M., Bickle, M., Lohmann, A., Maliga, Z., ... Huttner, W. B. (2011). Proliferating versus differentiating stem and cancer cells exhibit distinct midbody-release behaviour. *Nature Communications*, 2(1). <https://doi.org/10.1038/ncomms1511>
- Evsyukova, I., Plestant, C., & Anton, E. S. (2013). Integrative Mechanisms of Oriented Neuronal Migration in the Developing Brain. *Annual Review of Cell and Developmental Biology*, 29(1), 299–353. <https://doi.org/10.1146/annurev-cellbio-101512-122400>
- Fabbro, M., Zhou, B. B., Takahashi, M., Sarcevic, B., Lal, P., Graham, M. E., ... Khanna, K. K. (2005). Cdk1/Erk2- and Plk1-dependent phosphorylation of a centrosome protein, Cep55, is required for its recruitment to midbody and cytokinesis. *Developmental Cell*, 9(4), 477–488. <https://doi.org/10.1016/j.devcel.2005.09.003>
- Faheem, M., Naseer, M. I. mra., Rasool, M., Chaudhary, A. G., Kumosani, T. A., Ilyas, A. M. uhamma., ... Saleh Jamal, H. (2015). Molecular genetics of human primary microcephaly: an overview. *BMC Medical Genomics*. <https://doi.org/10.1186/1755-8794-8-S1-S4>
- Fazeli, G., Trinkwalder, M., Irmisch, L., & Wehman, A. M. (2016). C. elegans midbodies are released, phagocytosed and undergo LC3-dependent degradation independent of macroautophagy. *Journal of Cell Science*, 129(20), 3721–3731. <https://doi.org/10.1242/jcs.190223>
- Feng, Y., & Walsh, C. A. (2004). Mitotic spindle regulation by Nde1 controls cerebral cortical size. *Neuron*, 44(2), 279–293. <https://doi.org/10.1016/j.neuron.2004.09.023>
- Ferreira, a, & Kosik, K. S. (1996). Accelerated neuronal differentiation induced by p53 suppression. *Journal of Cell Science*, 109 ( Pt 6, 1509–1516.

- Florindo, C., Perdigo, J., Fesquet, D., Schiebel, E., Pines, J., & Tavares, Á. A. (2012). Human Mob1 proteins are required for cytokinesis by controlling microtubule stability. *Journal of Cell Science*, *125*(13), 3085–3090. <https://doi.org/10.1242/jcs.097147>
- Florio, M., & Huttner, W. B. (2014). Neural progenitors, neurogenesis and the evolution of the neocortex. *Development*, *141*(11), 2182–2194. <https://doi.org/10.1242/dev.090571>
- Frosk, P., Arts, H. H., Philippe, J., Gunn, C. S., Brown, E. L., Chodirker, B., ... Davis, E. E. (2017). A truncating mutation in CEP55 is the likely cause of MARCH, a novel syndrome affecting neuronal mitosis. *Journal of Medical Genetics*, *54*(7), 490–501. <https://doi.org/10.1136/jmedgenet-2016-104296>
- Gagliardi, P. A., Somale, D., Puliafito, A., Chiaverina, G., di Blasio, L., Oneto, M., ... Primo, L. (2018). MRCK $\alpha$  is activated by caspase cleavage to assemble an apical actin ring for epithelial cell extrusion. *Journal of Cell Biology*, *217*(1), 231–249. <https://doi.org/10.1083/jcb.201703044>
- Gallo, V., & Deneen, B. (2014). Glial development: The crossroads of regeneration and repair in the CNS. *Neuron*. <https://doi.org/10.1016/j.neuron.2014.06.010>
- Ganem, N. J., Cornils, H., Chiu, S. Y., O'Rourke, K. P., Arnaud, J., Yimlamai, D., ... Pellman, D. (2014). Cytokinesis failure triggers hippo tumor suppressor pathway activation. *Cell*, *158*(4), 833–848. <https://doi.org/10.1016/j.cell.2014.06.029>
- Gao, P., Postiglione, M. P., Krieger, T. G., Hernandez, L., Wang, C., Han, Z., ... Shi, S. H. (2014). Deterministic progenitor behavior and unitary production of neurons in the neocortex. *Cell*, *159*(4), 775–788. <https://doi.org/10.1016/j.cell.2014.10.027>
- Gao, Y., Liu, X., Tang, B., Li, C., Kou, Z., Li, L., ... Gao, S. (2017). Protein Expression Landscape of Mouse Embryos during Pre-implantation Development. *Cell Reports*, *21*(13), 3957–3969. <https://doi.org/10.1016/j.celrep.2017.11.111>
- Garcez, P. P., Loiola, E. C., Da Costa, R. M., Higa, L. M., Trindade, P., Delvecchio, R., ... Rehen, S. K. (2016). Zika virus: Zika virus impairs growth in human neurospheres and brain organoids. *Science*, *352*(6287), 816–818. <https://doi.org/10.1126/science.aaf6116>
- Gärtner, A., Fornasiero, E. F., Munck, S., Vennekens, K., Seuntjens, E., Huttner, W. B., ... Dotti, C. G. (2012). N-cadherin specifies first asymmetry in developing neurons. *EMBO Journal*, *31*(8), 1893–1903. <https://doi.org/10.1038/emboj.2012.41>
- Gaspard, N., Bouschet, T., Hourez, R., Dimidschstein, J., Naeije, G., Van Den Ameele, J., ... Vanderhaeghen, P. (2008). An intrinsic mechanism of corticogenesis from embryonic stem cells. *Nature*, *455*(7211), 351–357. <https://doi.org/10.1038/nature07287>

- Geng, A., Qiu, R., Murai, K., Liu, J., Wu, X., Zhang, H., ... Lu, Q. (2018). KIF20A/MKLP2 regulates the division modes of neural progenitor cells during cortical development. *Nature Communications*, 9(1). <https://doi.org/10.1038/s41467-018-05152-1>
- Gershony, O., Péér, T., Noach-Hirsh, M., Elia, N., & Tzur, A. (2014). Cytokinetic abscission is an acute G1 event. *Cell Cycle*, 13(21), 3436–3441. <https://doi.org/10.4161/15384101.2014.956486>
- Giannakakou, P., Nakano, M., Nicolaou, K. C., O’Brate, A., Yu, J., Blagosklonny, M. V., ... Fojo, T. (2002). Enhanced microtubule-dependent trafficking and p53 nuclear accumulation by suppression of microtubule dynamics. *Proceedings of the National Academy of Sciences*, 99(16), 10855–10860. <https://doi.org/10.1073/pnas.132275599>
- Giannakakou, P., Sackett, D. L., Ward, Y., Webster, K. R., Blagosklonny, M. V., & Fojo, T. (2000). P53 Is Associated With Cellular Microtubules and Is Transported To the Nucleus By Dynein. *Nature Cell Biology*, 2(10), 709–717. <https://doi.org/10.1038/35036335>
- Gilmore, E. C., & Walsh, C. A. (2013). Genetic causes of microcephaly and lessons for neuronal development. *Wiley Interdisciplinary Reviews: Developmental Biology*. <https://doi.org/10.1002/wdev.89>
- Giunta, S., Belotserkovskaya, R., & Jackson, S. P. (2010). DNA damage signaling in response to double-strand breaks during mitosis. *Journal of Cell Biology*, 190(2), 197–207. <https://doi.org/10.1083/jcb.200911156>
- Golas, P. L., Tsarevsky, N. V., Sumerlin, B. S., Walker, L. M., & Matyjaszewski, K. (2007). Multisegmented block copolymers by click coupling of polymers prepared by ATRP. *Australian Journal of Chemistry*, 60(6), 400–404. <https://doi.org/10.1071/CH07073>
- Gotthardt, K., Lokaj, M., Koerner, C., Falk, N., Giebl, A., & Wittinghofer, A. (2015). A G-protein activation cascade from Arl13B to Arl3 and implications for ciliary targeting of lipidated proteins. *ELife*, 4(NOVEMBER2015). <https://doi.org/10.7554/eLife.11859.001>
- Green, R. A., Mayers, J. R., Wang, S., Lewellyn, L., Desai, A., Audhya, A., & Oegema, K. (2013). The midbody ring scaffolds the abscission machinery in the absence of midbody microtubules. *Journal of Cell Biology*, 203(3), 505–520. <https://doi.org/10.1083/jcb.201306036>
- Greenbaum, M. P., Iwamori, T., Buchold, G. M., & Matzuk, M. M. (2011). Germ cell intercellular bridges. *Cold Spring Harbor Perspectives in Biology*, 3(8), 1–18. <https://doi.org/10.1101/cshperspect.a005850>
- Greene, L. A., Lee, H. Y., & Angelastro, J. M. (2009). The transcription factor ATF5: Role in

- neurodevelopment and neural tumors. *Journal of Neurochemistry*.  
<https://doi.org/10.1111/j.1471-4159.2008.05749.x>
- Gromley, A., Jurczyk, A., Sillibourne, J., Halilovic, E., Mogensen, M., Groisman, I., ... Doxsey, S. (2003). A novel human protein of the maternal centriole is required for the final stages of cytokinesis and entry into S phase. *Journal of Cell Biology*, *161*(3), 535–545.  
<https://doi.org/10.1083/jcb.200301105>
- Guizetti, J., Schermelleh, L., M??ntler, J., Maar, S., Poser, I., Leonhardt, H., ... Gerlich, D. W. (2011). Cortical constriction during abscission involves helices of ESCRT-III-dependent filaments. *Science*, *331*(6024), 1616–1620. <https://doi.org/10.1126/science.1201847>
- Gupta, D. K., Du, J., Kamranvar, S. A., & Johansson, S. (2018). Tension-induced cytokinetic abscission in human fibroblasts. *Oncotarget*, *9*(10).  
<https://doi.org/10.18632/oncotarget.24016>
- Hamstra, D. A., Bhojani, M. S., Griffin, L. B., Laxman, B., Ross, B. D., & Rehemtulla, A. (2006). Real-time evaluation of p53 oscillatory behavior in vivo using bioluminescent imaging. *Cancer Research*, *66*(15), 7482–7489. <https://doi.org/10.1158/0008-5472.CAN-06-1405>
- Hanke-Gogokhia, C., Wu, Z., Gerstner, C. D., Frederick, J. M., Zhang, H., & Baehr, W. (2016). Arf-like protein 3 (ARL3) regulates protein trafficking and ciliogenesis in mouse photoreceptors. *Journal of Biological Chemistry*, *291*(13), 7142–7155.  
<https://doi.org/10.1074/jbc.M115.710954>
- Harding, B. N., Moccia, A., Drunat, S., Soukarieh, O., Tubeuf, H., Chitty, L. S., ... Bielas, S. L. (2016). Mutations in Citron Kinase Cause Recessive Microlissencephaly with Multinucleated Neurons. *American Journal of Human Genetics*, *99*(2), 511–520.  
<https://doi.org/10.1016/j.ajhg.2016.07.003>
- Hatanaka, Y., & Yamauchi, K. (2013). Excitatory cortical neurons with multipolar shape establish neuronal polarity by forming a tangentially oriented axon in the intermediate zone. *Cerebral Cortex*, *23*(1), 105–113. <https://doi.org/10.1093/cercor/bhr383>
- Hatanaka, Y., Yamauchi, K., & Murakami, F. (2012). Formation of Axon-dendrite polarity in situ: Initiation of axons from polarized and non-polarized cells. *Development Growth and Differentiation*. <https://doi.org/10.1111/j.1440-169X.2012.01344.x>
- Haubensak, W., Attardo, A., Denk, W., & Huttner, W. B. (2004). From The Cover: Neurons arise in the basal neuroepithelium of the early mammalian telencephalon: A major site of neurogenesis. *Proceedings of the National Academy of Sciences*, *101*(9), 3196–3201.

- <https://doi.org/10.1073/pnas.0308600100>
- Haydar, T. F., Kuan, C. Y., Flavell, R. A., & Rakic, P. (1999). The role of cell death in regulating the size and shape of the mammalian forebrain. *Cerebral Cortex*, *9*(6), 621–626.  
<https://doi.org/10.1093/cercor/9.6.621>
- Herszterg, S., Pinheiro, D., & Bellaïche, Y. (2014). A multicellular view of cytokinesis in epithelial tissue. *Trends in Cell Biology*. <https://doi.org/10.1016/j.tcb.2013.11.009>
- Higashi, T., Arnold, T. R., Stephenson, R. E., Dinshaw, K. M., & Miller, A. L. (2016). Maintenance of the Epithelial Barrier and Remodeling of Cell-Cell Junctions during Cytokinesis. *Current Biology*, *26*(14), 1829–1842. <https://doi.org/10.1016/j.cub.2016.05.036>
- Hippenmeyer, S., Youn, Y. H., Moon, H. M., Miyamichi, K., Zong, H., Wynshaw-Boris, A., & Luo, L. (2010). Genetic mosaic dissection of *Lis1* and *Ndel1* in neuronal migration. *Neuron*, *68*(4), 695–709. <https://doi.org/10.1016/j.neuron.2010.09.027>
- Hochreiter-Hufford, A., & Ravichandran, K. S. (2013). Clearing the dead: Apoptotic cell sensing, recognition, engulfment, and digestion. *Cold Spring Harbor Perspectives in Biology*, *5*(1). <https://doi.org/10.1101/cshperspect.a008748>
- Houlihan, S. L., & Feng, Y. (2014). The scaffold protein *Nde1* safeguards the brain genome during S phase of early neural progenitor differentiation. *ELife*, *3*.  
<https://doi.org/10.7554/elife.03297>
- Hyung, H. L., Elia, N., Ghirlando, R., Lippincott-Schwartz, J., & Hurley, J. H. (2008). Midbody targeting of the ESCRT machinery by a noncanonical coiled coil in CEP55. *Science*, *322*(5901), 576–580. <https://doi.org/10.1126/science.1162042>
- Insolera, R., Bazzi, H., Shao, W., Anderson, K. V., & Shi, S. H. (2014). Cortical neurogenesis in the absence of centrioles. *Nature Neuroscience*, *17*(11), 1528–1535.  
<https://doi.org/10.1038/nn.3831>
- Isogai, T., van der Kammen, R., Goerdal, S. S., Heck, A. J. R., Altelaar, A. F. M., & Innocenti, M. (2015). Proteomic Analyses Uncover a New Function and Mode of Action for Mouse Homolog of Diaphanous 2 (*mDia2*). *Molecular & Cellular Proteomics*, *14*(4), 1064–1078.  
<https://doi.org/10.1074/mcp.m114.043885>
- Iwamori, T., Iwamori, N., Ma, L., Edson, M. A., Greenbaum, M. P., & Matzuk, M. M. (2010). TEX14 Interacts with CEP55 To Block Cell Abscission. *Molecular and Cellular Biology*, *30*(9), 2280–2292. <https://doi.org/10.1128/mcb.01392-09>
- Jacks, T., Remington, L., Williams, B. O., Schmitt, E. M., Halachmi, S., Bronson, R. T., & Weinberg, R. A. (1994). Tumor spectrum analysis in p53-mutant mice. *Current Biology*,

- 4(1), 1–7. [https://doi.org/10.1016/S0960-9822\(00\)00002-6](https://doi.org/10.1016/S0960-9822(00)00002-6)
- Jain, A. K., & Barton, M. C. (2018). P53: Emerging Roles in Stem Cells, Development and Beyond. *Development*, 145(8), dev158360. <https://doi.org/10.1242/dev.158360>
- Janisch, K. M., & Dwyer, N. D. (2016). Imaging and quantitative analysis of cytokinesis in developing brains of Kinesin-6 mutant mice. In *Methods in Cell Biology* (Vol. 131, pp. 233–252). <https://doi.org/10.1016/bs.mcb.2015.06.008>
- Janisch, K. M., McNeely, K. C., Dardick, J. M., Lim, S. H., & Dwyer, N. D. (2017). Kinesin-6 KIF20B is required for efficient cytokinetic furrowing and timely abscission in human cells. *Molecular Biology of the Cell*, 29(2), 166–179. <https://doi.org/10.1091/mbc.e17-08-0495>
- Janisch, K. M., Vock, V. M., Fleming, M. S., Shrestha, A., Grimsley-Myers, C. M., Rasoul, B. A., ... Dwyer, N. D. (2013). The vertebrate-specific Kinesin-6, Kif20b, is required for normal cytokinesis of polarized cortical stem cells and cerebral cortex size. *Development*, 140(23), 4672–4682. <https://doi.org/10.1242/dev.093286>
- Jeffers, J. R., Parganas, E., Lee, Y., Yang, C., Wang, J. L., Brennan, J., ... Zambetti, G. P. (2003). Puma is an essential mediator of p53-dependent and -independent apoptotic pathways. *Cancer Cell*, 4(4), 321–328. [https://doi.org/10.1016/S1535-6108\(03\)00244-7](https://doi.org/10.1016/S1535-6108(03)00244-7)
- Jeffery, J., Neyt, C., Moore, W., Paterson, S., Bower, N. I., Chenevix-Trench, G., ... Khanna, K. K. (2015). Cep55 regulates embryonic growth and development by promoting Akt stability in zebrafish. *FASEB Journal*, 29(5), 1999–2009. <https://doi.org/10.1096/fj.14-265090>
- Jongsma, M. L. M., Berlin, I., & Neefjes, J. (2015). On the move: Organelle dynamics during mitosis. *Trends in Cell Biology*. <https://doi.org/10.1016/j.tcb.2014.10.005>
- Joshi, S., Braithwaite, A. W., Robinson, P. J., & Chircop, M. (2011). Dynamin inhibitors induce caspase-mediated apoptosis following cytokinesis failure in human cancer cells and this is blocked by Bcl-2 overexpression. *Molecular Cancer*, 10. <https://doi.org/10.1186/1476-4598-10-78>
- Kamimoto, T., Zama, T., Aoki, R., Muro, Y., & Hagiwara, M. (2001). Identification of a Novel Kinesin-related Protein, KRMP1, as a Target for Mitotic Peptidyl-prolyl Isomerase Pin1. *Journal of Biological Chemistry*, 276(40), 37520–37528. <https://doi.org/10.1074/jbc.M106207200>
- Kanehira, M., Katagiri, T., Shimo, A., Takata, R., Shuin, T., Miki, T., ... Nakamura, Y. (2007). Oncogenic role of MPHOSPH1, a cancer-testis antigen specific to human bladder cancer. *Cancer Research*, 67(7), 3276–3285. <https://doi.org/10.1158/0008-5472.CAN-06-3748>
- Kastan, M. B., Onyekwere, O., Sidransky, D., Vogelstein, B., & Craig, R. W. (1991).

- Participation of p53 Protein in the Cellular Response to DNA Damage. *Cancer Research*, 51, 6304–6311. <https://doi.org/10.1158/0008-5472.CAN-16-1560>
- Kasthuber, E. R., & Lowe, S. W. (2017). Putting p53 in Context. *Cell*. <https://doi.org/10.1016/j.cell.2017.08.028>
- Kim, H. J., Yoon, J., Matsuura, A., Na, J.-H., Lee, W.-K., Kim, H., ... Lee, H. H. (2015). Structural and biochemical insights into the role of testis-expressed gene 14 (TEX14) in forming the stable intercellular bridges of germ cells. *Proceedings of the National Academy of Sciences*, 112(40), 12372–12377. <https://doi.org/10.1073/pnas.1418606112>
- Knobel, P. A., Belotserkovskaya, R., Galanty, Y., Schmidt, C. K., Jackson, S. P., & Stracker, T. H. (2014). USP28 Is Recruited to Sites of DNA Damage by the Tandem BRCT Domains of 53BP1 but Plays a Minor Role in Double-Strand Break Metabolism. *Molecular and Cellular Biology*. <https://doi.org/10.1128/MCB.00197-14>
- Knowles, J. T., & Leitner, M. (2007). Visual representations of the spatial relationship between Bermuda High strengths and hurricane tracks. *Cartographic Perspectives*, (56), 37–51. <https://doi.org/10.14714/CP56.316>
- Knudson, C. M., Tung, K. S. K., Tourtellotte, W. G., Brown, G. A. J., & Korsmeyer, S. J. (1995). Bax-deficient mice with lymphoid hyperplasia and male germ cell death. *Science*, 270(5233), 96–99. <https://doi.org/10.1126/science.270.5233.96>
- Konno, D., Shioi, G., Shitamukai, A., Mori, A., Kiyonari, H., Miyata, T., & Matsuzaki, F. (2008). Neuroepithelial progenitors undergo LGN-dependent planar divisions to maintain self-renewability during mammalian neurogenesis. *Nature Cell Biology*, 10(1), 93–101. <https://doi.org/10.1038/ncb1673>
- Konstantinidis, D. G., Giger, K. M., Risinger, M., Pushkaran, S., Zhou, P., Dexheimer, P., ... Kalfa, T. A. (2015). Cytokinesis failure in RhoA-deficient mouse erythroblasts involves actomyosin and midbody dysregulation and triggers p53 activation. *Blood*, 126(12), 1473–1482. <https://doi.org/10.1182/blood-2014-12-616169>
- Kosodo, Y., Röper, K., Haubensak, W., Marzesco, A. M., Corbeil, D., & Huttner, W. B. (2004). Asymmetric distribution of the apical plasma membrane during neurogenic divisions of mammalian neuroepithelial cells. *EMBO Journal*, 23(11), 2314–2324. <https://doi.org/10.1038/sj.emboj.7600223>
- Kosodo, Y., Toida, K., Dubreuil, V., Alexandre, P., Schenk, J., Kiyokage, E., ... Huttner, W. B. (2008). Cytokinesis of neuroepithelial cells can divide their basal process before anaphase. *EMBO Journal*, 27(23), 3151–3163. <https://doi.org/10.1038/emboj.2008.227>

- Kriegstein, A. R., & Götz, M. (2003). Radial glia diversity: A matter of cell fate. *Glia*, *43*(1), 37–43. <https://doi.org/10.1002/glia.10250>
- Kuida, K., Haydar, T. F., Kuan, C. Y., Gu, Y., Taya, C., Karasuyama, H., ... Flavell, R. A. (1998). Reduced apoptosis and cytochrome C-mediated caspase activation in mice lacking Caspase 9. *Cell*, *94*(3), 325–337. [https://doi.org/10.1016/S0092-8674\(00\)81476-2](https://doi.org/10.1016/S0092-8674(00)81476-2)
- Kulda, K., Zheng, T. S., Na, S., Kuan, C. Y., Yang, D., Karasuyama, H., ... Flavell, R. A. (1996). Decreased apoptosis in the brain and premature lethality in CPP32- deficient mice. *Nature*, *384*(6607), 368–372. <https://doi.org/10.1038/384368a0>
- Kumar, A., Girimaji, S. C., Duvvari, M. R., & Blanton, S. H. (2008). Mutations in STIL, encoding a pericentriolar and centrosomal protein, cause primary microcephaly. *American Journal of Human Genetics*, *84*(2), 286–290. <https://doi.org/10.1016/j.ajhg.2009.01.017>
- Kuo, T. C., Chen, C. T., Baron, D., Onder, T. T., Loewer, S., Almeida, S., ... Doxsey, S. (2011). Midbody accumulation through evasion of autophagy contributes to cellular reprogramming and tumorigenicity. *Nature Cell Biology*, *13*(10), 1214–1223. <https://doi.org/10.1038/ncb2332>
- Lafaurie-Janvore, J., Maiuri, P., Wang, I., Pinot, M., Manneville, J. B., Betz, T., ... Piel, M. (2013). ESCRT-III assembly and cytokinetic abscission are induced by tension release in the intercellular bridge. *Science*, *340*(6127), 1625–1629. <https://doi.org/10.1126/science.1233866>
- Lambrus, B. G., Daggubati, V., Uetake, Y., Scott, P. M., Clutario, K. M., Sluder, G., & Holland, A. J. (2016). A USP28-53BP1-p53-p21 signaling axis arrests growth after centrosome loss or prolonged mitosis. *Journal of Cell Biology*, *214*(2), 143–153. <https://doi.org/10.1083/jcb.201604054>
- Lenhart, K. F., & DiNardo, S. (2015). Somatic Cell Encystment Promotes Abscission in Germline Stem Cells following a Regulated Block in Cytokinesis. *Developmental Cell*, *34*(2), 192–205. <https://doi.org/10.1016/j.devcel.2015.05.003>
- Lewczuk, E., Joshi, S., Williamson, J., Penmetsa, M., Shan, S., & Kapur, J. (2018). Electroencephalography and behavior patterns during experimental status epilepticus. *Epilepsia*, *59*(2), 369–380. <https://doi.org/10.1111/epi.13972>
- Li, B., Qing, T., Zhu, J., Wen, Z., Yu, Y., Fukumura, R., ... Shi, L. (2017). A Comprehensive Mouse Transcriptomic BodyMap across 17 Tissues by RNA-seq. *Scientific Reports*, *7*(1). <https://doi.org/10.1038/s41598-017-04520-z>
- Li, C., Xu, D., Ye, Q., Hong, S., Jiang, Y., Liu, X., ... Xu, Z. (2016). Zika Virus Disrupts Neural

- Progenitor Development and Leads to Microcephaly in Mice. *Cell Stem Cell*, 19(1), 120–126. <https://doi.org/10.1016/j.stem.2016.04.017>
- Li, D., Mangan, A., Cicchini, L., Margolis, B., & Prekeris, R. (2014). FIP5 phosphorylation during mitosis regulates apical trafficking and lumenogenesis. *EMBO Reports*, 15(4), 428–437. <https://doi.org/10.1002/embr.201338128>
- Li, H., Bielas, S. L., Zaki, M. S., Ismail, S., Farfara, D., Um, K., ... Gleeson, J. G. (2016). Biallelic Mutations in Citron Kinase Link Mitotic Cytokinesis to Human Primary Microcephaly. *American Journal of Human Genetics*, 99(2), 501–510. <https://doi.org/10.1016/j.ajhg.2016.07.004>
- Li, H., Saucedo-Cuevas, L., Yuan, L., Ross, D., Johansen, A., Sands, D., ... Gleeson, J. G. (2019). Zika Virus Protease Cleavage of Host Protein Septin-2 Mediates Mitotic Defects in Neural Progenitors. *Neuron*. <https://doi.org/10.1016/j.neuron.2019.01.010>
- Lindsten, T., Ross, A. J., King, A., Zong, W. X., Rathmell, J. C., Shiels, H. A., ... Thompson, C. B. (2000). The combined functions of proapoptotic Bcl-2 family members Bak and Bax are essential for normal development of multiple tissues. *Molecular Cell*, 6(6), 1389–1399. [https://doi.org/10.1016/S1097-2765\(00\)00136-2](https://doi.org/10.1016/S1097-2765(00)00136-2)
- Little, J. N., & Dwyer, N. D. (2019). P53 Deletion Rescues Lethal Microcephaly in a Mouse Model With Neural Stem Cell Abscission Defects. *Human Molecular Genetics*, 28(3), 434–447. <https://doi.org/10.1093/hmg/ddy350>
- Liu, L., Mei, Q., Zhao, J., Dai, Y., & Fu, Q. (2016). Suppression of CEP55 reduces cell viability and induces apoptosis in human lung cancer. *Oncology Reports*, 36(4), 1939–1945. <https://doi.org/10.3892/or.2016.5059>
- Liu, W. A., Chen, S., Li, Z., Lee, C. H., Mirzaa, G., Dobyns, W. B., ... Shi, S. H. (2018). PARD3 dysfunction in conjunction with dynamic HIPPO signaling drives cortical enlargement with massive heterotopia. *Genes and Development*, 32(11–12), 763–780. <https://doi.org/10.1101/gad.313171.118>
- Liu, X., Li, Y., Zhang, X., Liu, X. Y., Peng, A., Chen, Y., ... Huang, K. (2018). Inhibition of kinesin family member 20B sensitizes hepatocellular carcinoma cell to microtubule-targeting agents by blocking cytokinesis. *Cancer Science*. <https://doi.org/10.1111/cas.13794>
- Liu, X., Zhou, Y., Liu, X., Peng, A., Gong, H., Huang, L., ... Huang, K. (2014). MPHOSPH1: A potential therapeutic target for hepatocellular carcinoma. *Cancer Research*, 74(22), 6623–6634. <https://doi.org/10.1158/0008-5472.CAN-14-1279>
- Loo, L., Simon, J. M., Xing, L., McCoy, E. S., Niehaus, J. K., Guo, J., ... Zylka, M. J. (2019).

- Single-cell transcriptomic analysis of mouse neocortical development. *Nature Communications*, 10(1). <https://doi.org/10.1038/s41467-018-08079-9>
- Lowery, L. A., & Vactor, D. Van. (2009). The trip of the tip: Understanding the growth cone machinery. *Nature Reviews Molecular Cell Biology*. <https://doi.org/10.1038/nrm2679>
- Luo, Y., Kuo, C. C., Shen, H., Chou, J., Greig, N. H., Hoffer, B. J., & Wang, Y. (2009). Delayed treatment with a p53 inhibitor enhances recovery in stroke brain. *Annals of Neurology*, 65(5), 520–530. <https://doi.org/10.1002/ana.21592>
- Mackay, D. R., Makise, M., & Ullman, K. S. (2010). Defects in nuclear pore assembly lead to activation of an Aurora B-mediated abscission checkpoint. *Journal of Cell Biology*, 191(5), 923–931. <https://doi.org/10.1083/jcb.201007124>
- Magavi, S. S., Leavitt, B. R., & Macklis, J. D. (2000). Induction of neurogenesis in the neocortex of adult mice. *Nature*, 405(6789), 951–955. <https://doi.org/10.1038/35016083>
- Makrythanasis, P., Maroofian, R., Stray-Pedersen, A., Musaev, D., Zaki, M. S., Mahmoud, I. G., ... Antonarakis, S. E. (2018). Biallelic variants in KIF14 cause intellectual disability with microcephaly. *European Journal of Human Genetics*, 26(3), 330–339. <https://doi.org/10.1038/s41431-017-0088-9>
- Maliga, Z., Junqueira, M., Toyoda, Y., Ettinger, A., Mora-Bermúdez, F., Klemm, R. W., ... Hyman, A. A. (2013). A genomic toolkit to investigate kinesin and myosin motor function in cells. *Nature Cell Biology*, 15(3), 325–334. <https://doi.org/10.1038/ncb2689>
- Manabe, N., Hirai, S. I., Imai, F., Nakanishi, H., Takai, Y., & Ohno, S. (2002). Association of ASIP/mPAR-3 with adherens junctions of mouse neuroepithelial cells. *Developmental Dynamics*, 225(1), 61–69. <https://doi.org/10.1002/dvdy.10139>
- Mao, H., McMahon, J. J., Tsai, Y. H., Wang, Z., & Silver, D. L. (2016). Haploinsufficiency for Core Exon Junction Complex Components Disrupts Embryonic Neurogenesis and Causes p53-Mediated Microcephaly. *PLoS Genetics*, 12(9). <https://doi.org/10.1371/journal.pgen.1006282>
- Maréchal, A., & Zou, L. (2013). DNA damage sensing by the ATM and ATR kinases. *Cold Spring Harbor Perspectives in Biology*, 5(9). <https://doi.org/10.1101/cshperspect.a012716>
- Margall-Ducos, G., Celton-Morizur, S., Couton, D., Bregerie, O., & Desdouets, C. (2007). Liver tetraploidization is controlled by a new process of incomplete cytokinesis. *Journal of Cell Science*. <https://doi.org/10.1016/j.sna.2005.02.001>
- Marjanović, M., Sánchez-Huertas, C., Terré, B., Gómez, R., Scheel, J. F., Pacheco, S., ... Stracker, T. H. (2015). CEP63 deficiency promotes p53-dependent microcephaly and

- reveals a role for the centrosome in meiotic recombination. *Nature Communications*, 6.  
<https://doi.org/10.1038/ncomms8676>
- Marthiens, V., & French-Constant, C. (2009). Adherens junction domains are split by asymmetric division of embryonic neural stem cells. *EMBO Reports*, 10(5), 515–520.  
<https://doi.org/10.1038/embor.2009.36>
- Marthiens, V., Piel, M., & Basto, R. (2012). Never tear us apart - the importance of centrosome clustering. *Journal of Cell Science*, 125(14), 3281–3292. <https://doi.org/10.1242/jcs.094797>
- Marthiens, V., Rujano, M. A., Penetier, C., Tessier, S., Paul-Gilloteaux, P., & Basto, R. (2013). Centrosome amplification causes microcephaly. *Nature Cell Biology*, 15(7), 731–740.  
<https://doi.org/10.1038/ncb2746>
- Martín-Caballero, J., Serrano, M., Flores, J. M., & García-Palencia, P. (2001). Tumor susceptibility of p21waf1/cip1-deficient mice. *Cancer Research*.
- Mathieu, J., Cauvin, C., Moch, C., Radford, S. J., Sampaio, P., Perdigoto, C. N., ... Huynh, J. R. (2013). Aurora B and Cyclin B have opposite effects on the timing of cytokinesis abscission in drosophila germ cells and in vertebrate somatic cells. *Developmental Cell*, 26(3), 250–265. <https://doi.org/10.1016/j.devcel.2013.07.005>
- McKinley, K. L., & Cheeseman, I. M. (2017). Large-Scale Analysis of CRISPR/Cas9 Cell-Cycle Knockouts Reveals the Diversity of p53-Dependent Responses to Cell-Cycle Defects. *Developmental Cell*, 40(4), 405–420.e2. <https://doi.org/10.1016/j.devcel.2017.01.012>
- McNeely, K. C., Cupp, T. D., Little, J. N., Janisch, K. M., Shrestha, A., & Dwyer, N. D. (2017). Mutation of Kinesin-6 Kif20b causes defects in cortical neuron polarization and morphogenesis. *Neural Development*, 12(1). <https://doi.org/10.1186/s13064-017-0082-5>
- McNeely, K.C., Little, J.N. & Dwyer, N.D. (2019). Cytokinetic furrowing and abscission dynamics during brain development revealed by live imaging. bioRxiv: doi: <https://doi.org/10.1101/529164>. *Journal of Cell Biology*, in revision.
- Meitinger, F., Anzola, J. V., Kaulich, M., Richardson, A., Stender, J. D., Benner, C., ... Oegema, K. (2016). 53BP1 and USP28 mediate p53 activation and G1 arrest after centrosome loss or extended mitotic duration. *Journal of Cell Biology*, 214(2), 155–166.  
<https://doi.org/10.1083/jcb.201604081>
- Mierzwa, B., & Gerlich, D. W. (2014). Cytokinetic Abscission: Molecular Mechanisms and Temporal Control. *Developmental Cell*. <https://doi.org/10.1016/j.devcel.2014.11.006>
- Mihalas, A. B., Elsen, G. E., Bedogni, F., Daza, R. A. M., Ramos-Laguna, K. A., Arnold, S. J., & Hevner, R. F. (2016). Intermediate Progenitor Cohorts Differentially Generate Cortical

- Layers and Require Tbr2 for Timely Acquisition of Neuronal Subtype Identity. *Cell Reports*, 16(1), 92–105. <https://doi.org/10.1016/j.celrep.2016.05.072>
- Miki, T., Okawa, K., Sekimoto, T., Yoneda, Y., Watanabe, S., Ishizaki, T., & Narumiya, S. (2009). mDia2 shuttles between the nucleus and the cytoplasm through the importin- $\alpha/\beta$ - and CRM1-mediated nuclear transport mechanism. *Journal of Biological Chemistry*, 284(9), 5753–5762. <https://doi.org/10.1074/jbc.M806191200>
- Mishima, M., Kaitna, S., & Glotzer, M. (2002). Central spindle assembly and cytokinesis require a kinesin-like protein/RhoGAP complex with microtubule bundling activity. *Developmental Cell*, 2(1), 41–54. [https://doi.org/10.1016/S1534-5807\(01\)00110-1](https://doi.org/10.1016/S1534-5807(01)00110-1)
- Misra, S., & Oommen, B. J. (2005). New algorithms for maintaining All-Pairs Shortest Paths. *Proceedings - IEEE Symposium on Computers and Communications*, 116–121. <https://doi.org/10.1109/ISCC.2005.107>
- Miyata, T., Kawaguchi, A., Okano, H., & Ogawa, M. (2001). Asymmetric inheritance of radial glial fibers by cortical neurons. *Neuron*, 31(5), 727–741. [https://doi.org/10.1016/S0896-6273\(01\)00420-2](https://doi.org/10.1016/S0896-6273(01)00420-2)
- Miyata, T., Kawaguchi, A., Saito, K., Kawano, M., Muto, T., & Ogawa, M. (2004). Asymmetric production of surface-dividing and non-surface-dividing cortical progenitor cells. *Development (Cambridge, England)*, 131(13), 3133–3145. <https://doi.org/10.1242/dev.01173>
- Moawia, A., Shaheen, R., Rasool, S., Waseem, S. S., Ewida, N., Budde, B., ... Hussain, M. S. (2017). Mutations of KIF14 cause primary microcephaly by impairing cytokinesis. *Annals of Neurology*, 82(4), 562–577. <https://doi.org/10.1002/ana.25044>
- Morita, E., Sandrin, V., Chung, H. Y., Morham, S. G., Gygi, S. P., Rodesch, C. K., & Sundquist, W. I. (2007). Human ESCRT and ALIX proteins interact with proteins of the midbody and function in cytokinesis. *EMBO Journal*, 26(19), 4215–4227. <https://doi.org/10.1038/sj.emboj.7601850>
- Murga, M., Bunting, S., Montãa, M. F., Soria, R., Mulero, F., Cãamero, M., ... Fernandez-Capetillo, O. (2009). A mouse model of ATR-Seckel shows embryonic replicative stress and accelerated aging. *Nature Genetics*, 41(8), 891–898. <https://doi.org/10.1038/ng.420>
- Ngo, L., Haas, M., Qu, Z., Li, S. S. ha., Zenker, J., Teng, K. S. u. L., ... Heng, J. I. k. T. (2014). TUBB5 and its disease-associated mutations influence the terminal differentiation and dendritic spine densities of cerebral cortical neurons. *Human Molecular Genetics*, 23(19), 5147–5158. <https://doi.org/10.1093/hmg/ddu238>

- Noctor, S. C., Flint, A. C., Weissman, T. A., Wong, W. S., Clinton, B. K., & Kriegstein, A. R. (2002). Dividing precursor cells of the embryonic cortical ventricular zone have morphological and molecular characteristics of radial glia. *The Journal of Neuroscience : The Official Journal of the Society for Neuroscience*, 22(8), 3161–3173. <https://doi.org/20026299>
- Noctor, S. C., Martínez-Cerdeño, V., Ivic, L., & Kriegstein, A. R. (2004). Cortical neurons arise in symmetric and asymmetric division zones and migrate through specific phases. *Nature Neuroscience*, 7(2), 136–144. <https://doi.org/10.1038/nn1172>
- Noctor, S. C., Martínez-Cerdeño, V., & Kriegstein, A. R. (2008). Distinct behaviors of neural stem and progenitor cells underlie cortical neurogenesis. *Journal of Comparative Neurology*, 508(1), 28–44. <https://doi.org/10.1002/cne.21669>
- Nonomura, K., Yamaguchi, Y., Hamachi, M., Koike, M., Uchiyama, Y., Nakazato, K., ... Miura, M. (2013). Local apoptosis modulates early mammalian brain development through the elimination of morphogen-producing cells. *Developmental Cell*, 27(6), 621–634. <https://doi.org/10.1016/j.devcel.2013.11.015>
- Norden, C., Mendoza, M., Dobbelaere, J., Kotwaliwale, C. V., Biggins, S., & Barral, Y. (2006). The NoCut Pathway Links Completion of Cytokinesis to Spindle Midzone Function to Prevent Chromosome Breakage. *Cell*, 125(1), 85–98. <https://doi.org/10.1016/j.cell.2006.01.045>
- Normand, G., & King, R. W. (2010). Understanding cytokinesis failure. *Advances in Experimental Medicine and Biology*, 675, 27–55. [https://doi.org/10.1007/978-1-4419-6199-0\\_3](https://doi.org/10.1007/978-1-4419-6199-0_3)
- Olivier, M., Hollstein, M., & Hainaut, P. (2010). TP53 mutations in human cancers: origins, consequences, and clinical use. *Cold Spring Harbor Perspectives in Biology*. <https://doi.org/10.1101/cshperspect.a001008>
- Ou, G., Stuurman, N., D'Ambrosio, M., & Vale, R. D. (2010). Polarized myosin produces unequal-size daughters during asymmetric cell division. *Science*, 330(6004), 677–680. <https://doi.org/10.1126/science.1196112>
- Palenik, G. J., & Hu, S. Z. (2009). Assignment of oxidation states in metal complexes. Cerium(III) or cerium(IV) and other questions. *Inorganica Chimica Acta*, 362(13), 4740–4743. <https://doi.org/10.1016/j.ica.2009.06.052>
- Pancarci, S. M., Jordan, E. R., Risco, C. A., Schouten, M. J., Lopes, F. L., Moreira, F., & Thatcher, W. W. (2010). Use of Estradiol Cypionate in a Presynchronized Timed Artificial

- Insemination Program for Lactating Dairy Cattle. *Journal of Dairy Science*, 85(1), 122–131.  
[https://doi.org/10.3168/jds.s0022-0302\(02\)74060-5](https://doi.org/10.3168/jds.s0022-0302(02)74060-5)
- Pao, G. M., Zhu, Q., Perez-Garcia, C. G., Chou, S.-J., Suh, H., Gage, F. H., ... Verma, I. M. (2014). Role of BRCA1 in brain development. *Proceedings of the National Academy of Sciences*, 111(13), E1240–E1248. <https://doi.org/10.1073/pnas.1400783111>
- Paolini, A., Duchemin, A.-L., Albadri, S., Patzel, E., Bornhorst, D., Gonzalez Avalos, P., ... Poggi, L. (2015). Asymmetric inheritance of the apical domain and self-renewal of retinal ganglion cell progenitors depend on Anillin function. *Development*, 142(5), 832–839.  
<https://doi.org/10.1242/dev.118612>
- Papari, E., Bastami, M., Farhadi, A., Abedini, S., Hosseini, M., Bahman, I., ... Najmabadi, H. (2013). Investigation of primary microcephaly in Bushehr province of Iran: Novel STIL and ASPM mutations. *Clinical Genetics*. <https://doi.org/10.1111/j.1399-0004.2012.01949.x>
- Paradis, A. N., Gay, M. S., & Zhang, L. (2014). Binucleation of cardiomyocytes: The transition from a proliferative to a terminally differentiated state. *Drug Discovery Today*.  
<https://doi.org/10.1016/j.drudis.2013.10.019>
- Paridaen, J. T. M. L., Wilsch-Bräuninger, M., & Huttner, W. B. (2013). XAsymmetric inheritance of centrosome-associated primary cilium membrane directs ciliogenesis after cell division. *Cell*, 155(2), 333. <https://doi.org/10.1016/j.cell.2013.08.060>
- Petsalaki, E., & Zachos, G. (2016). Clks 1, 2 and 4 prevent chromatin breakage by regulating the Aurora B-dependent abscission checkpoint. *Nature Communications*, 7.  
<https://doi.org/10.1038/ncomms11451>
- Pilaz, L.-J., Patti, D., Marcy, G., Ollier, E., Pfister, S., Douglas, R. J., ... Dehay, C. (2009). Forced G1-phase reduction alters mode of division, neuron number, and laminar phenotype in the cerebral cortex. *Proceedings of the National Academy of Sciences*, 106(51), 21924–21929. <https://doi.org/10.1073/pnas.0909894106>
- Pilaz, L. J., McMahon, J. J., Miller, E. E., Lennox, A. L., Suzuki, A., Salmon, E., & Silver, D. L. (2016). Prolonged Mitosis of Neural Progenitors Alters Cell Fate in the Developing Brain. *Neuron*, 89(1), 83–99. <https://doi.org/10.1016/j.neuron.2015.12.007>
- Pohl, C., & Jentsch, S. (2009). Midbody ring disposal by autophagy is a post-abscission event of cytokinesis. *Nature Cell Biology*, 11(1), 65–70. <https://doi.org/10.1038/ncb1813>
- Pollarolo, G., Schulz, J. G., Munck, S., & Dotti, C. G. (2011). Cytokinesis remnants define first neuronal asymmetry in vivo. *Nature Neuroscience*, 14(12), 1525–1533.  
<https://doi.org/10.1038/nn.2976>

- Poon, I. K. H., Lucas, C. D., Rossi, A. G., & Ravichandran, K. S. (2014). Apoptotic cell clearance: Basic biology and therapeutic potential. *Nature Reviews Immunology*.  
<https://doi.org/10.1038/nri3607>
- Postiglione, M. P., Jüschke, C., Xie, Y., Haas, G. A., Charalambous, C., & Knoblich, J. A. (2011). Mouse inscuteable induces apical-basal spindle orientation to facilitate intermediate progenitor generation in the developing neocortex. *Neuron*, *72*(2), 269–284.  
<https://doi.org/10.1016/j.neuron.2011.09.022>
- Poulton, J. S., Cuningham, J. C., & Peifer, M. (2017). Centrosome and spindle assembly checkpoint loss leads to neural apoptosis and reduced brain size. *Journal of Cell Biology*, *216*(5), 1255–1265. <https://doi.org/10.1083/jcb.201607022>
- Pulvers, J. N., Bryk, J., Fish, J. L., Wilsch-Bräuninger, M., Arai, Y., Schreier, D., ... Huttner, W. B. (2010). Mutations in mouse *Aspm* (abnormal spindle-like microcephaly associated) cause not only microcephaly but also major defects in the germline. *Proceedings of the National Academy of Sciences of the United States of America*, *107*(38), 16595–16600.  
<https://doi.org/10.1073/pnas.1010494107>
- Qian, X., Goderie, S. K., Shen, Q., Stern, J. H., & Temple, S. (1998). Intrinsic programs of patterned cell lineages in isolated vertebrate CNS ventricular zone cells. *Development*.  
<https://doi.org/10.1145/2248371.2248401>
- Qian, X., Nguyen, H. N., Song, M. M., Hadiono, C., Ogden, S. C., Hammack, C., ... Ming, G. L. (2016). Brain-Region-Specific Organoids Using Mini-bioreactors for Modeling ZIKV Exposure. *Cell*, *165*(5), 1238–1254. <https://doi.org/10.1016/j.cell.2016.04.032>
- Qin, Q., Baudry, M., Liao, G., Noniyev, A., Galeano, J., & Bi, X. (2009). A Novel Function for p53: Regulation of Growth Cone Motility through Interaction with Rho Kinase. *Journal of Neuroscience*, *29*(16), 5183–5192. <https://doi.org/10.1523/jneurosci.0420-09.2009>
- Rakic, P. (1972). Mode of cell migration to the superficial layers of fetal monkey neocortex. *Journal of Comparative Neurology*, *145*(1), 61–83. <https://doi.org/10.1002/cne.901450105>
- Rakic, P. (1995). A small step for the cell, a giant leap for mankind: a hypothesis of neocortical expansion during evolution. *Trends in Neurosciences*, *18*(9), 383–388.  
[https://doi.org/10.1016/0166-2236\(95\)93934-P](https://doi.org/10.1016/0166-2236(95)93934-P)
- Rawlins, L. E., Jones, H., Wenger, O., Aye, M., Fasham, J., Harlalka, G. V., ... Baple, E. L. (2019). An Amish founder variant consolidates disruption of CEP55 as a cause of hydranencephaly and renal dysplasia. *European Journal of Human Genetics*.  
<https://doi.org/10.1038/s41431-018-0306-0>

- Reinhardt, H. C., & Schumacher, B. (2012). The p53 network: Cellular and systemic DNA damage responses in aging and cancer. *Trends in Genetics*.  
<https://doi.org/10.1016/j.tig.2011.12.002>
- Ren, H. P., & Russell, L. D. (1991). Clonal development of interconnected germ cells in the rat and its relationship to the segmental and subsegmental organization of spermatogenesis. *American Journal of Anatomy*, 192(2), 121–128. <https://doi.org/10.1002/aja.1001920203>
- Rhyu, M. S., Jan, L. Y., & Jan, Y. N. (1994). Asymmetric distribution of numb protein during division of the sensory organ precursor cell confers distinct fates to daughter cells. *Cell*, 76(3), 477–491. [https://doi.org/10.1016/0092-8674\(94\)90112-0](https://doi.org/10.1016/0092-8674(94)90112-0)
- Robert, A., Desdouets, C., Brechot, C., Guidotti, J.-E., Debey, P., & Brégerie, O. (2003). Liver Cell Polyploidization: A Pivotal Role for Binuclear Hepatocytes. *Journal of Biological Chemistry*, 278(21), 19095–19101. <https://doi.org/10.1074/jbc.m300982200>
- Rosenblatt, J., Raff, M. C., & Cramer, L. P. (2001). An epithelial cell destined for apoptosis signals its neighbors to extrude it by an actin- and myosin-dependent mechanism. *Current Biology*, 11(23), 1847–1857. [https://doi.org/10.1016/S0960-9822\(01\)00587-5](https://doi.org/10.1016/S0960-9822(01)00587-5)
- Sah, V. P., Attardi, L. D., Mulligan, G. J., Williams, B. O., Bronson, R. T., & Jacks, T. (1995). A subset of p53-deficient embryos exhibit exencephaly. *Nature Genetics*.  
<https://doi.org/10.1038/ng0695-175>
- Sakakibara, A., Sato, T., Ando, R., Noguchi, N., Masaoka, M., & Miyata, T. (2014). Dynamics of centrosome translocation and microtubule organization in neocortical neurons during distinct modes of polarization. *Cerebral Cortex*, 24(5), 1301–1310.  
<https://doi.org/10.1093/cercor/bhs411>
- Salzmann, V., Chen, C., Chiang, C.-Y. A., Tiyaboonchai, A., Mayer, M., & Yamashita, Y. M. (2013). Centrosome-dependent asymmetric inheritance of the midbody ring in *Drosophila* germline stem cell division. *Molecular Biology of the Cell*, 25(2), 267–275.  
<https://doi.org/10.1091/mbc.e13-09-0541>
- Samson, R. Y., Obita, T., Freund, S. M., Williams, R. L., & Bell, S. D. (2008). A role for the ESCRT system in cell division in archaea. *Science*, 322(5908), 1710–1713.  
<https://doi.org/10.1126/science.1165322>
- Santaguida, S., Richardson, A., Iyer, D. R., M'Saad, O., Zasadil, L., Knouse, K. A., ... Amon, A. (2017). Chromosome Mis-segregation Generates Cell-Cycle-Arrested Cells with Complex Karyotypes that Are Eliminated by the Immune System. *Developmental Cell*, 41(6), 638–651.e5. <https://doi.org/10.1016/j.devcel.2017.05.022>

- Sarkisian, M. R., Li, W., Di Cunto, F., D’Mello, S. R., & LoTurco, J. J. (2018). Citron-Kinase, A Protein Essential to Cytokinesis in Neuronal Progenitors, Is Deleted in the Flathead Mutant Rat. *The Journal of Neuroscience*, *22*(8), RC217-RC217.  
<https://doi.org/10.1523/jneurosci.22-08-j0001.2002>
- Schiel, J. A., Simon, G. C., Zaharris, C., Weisz, J., Castle, D., Wu, C. C., & Prekeris, R. (2012). FIP3-endosome-dependent formation of the secondary ingression mediates ESCRT-III recruitment during cytokinesis. *Nature Cell Biology*, *14*(10), 1068–1078.  
<https://doi.org/10.1038/ncb2577>
- Schmid, P., Lorenz, A., Hameister, H., & Montenarh, M. (1991). Expression of p53 during mouse embryogenesis. *Development*.
- Schrick, J. J., Vogel, P., Abuin, A., Hampton, B., & Rice, D. S. (2006). ADP-ribosylation factor-like 3 is involved in kidney and photoreceptor development. *American Journal of Pathology*, *168*(4), 1288–1298. <https://doi.org/10.2353/ajpath.2006.050941>
- Sessa, A., Mao, C. an, Hadjantonakis, A. K., Klein, W. H., & Broccoli, V. (2008). Tbr2 Directs Conversion of Radial Glia into Basal Precursors and Guides Neuronal Amplification by Indirect Neurogenesis in the Developing Neocortex. *Neuron*, *60*(1), 56–69.  
<https://doi.org/10.1016/j.neuron.2008.09.028>
- Shen, Q., Wang, Y., Dimos, J. T., Fasano, C. A., Phoenix, T. N., Lemischka, I. R., ... Temple, S. (2006). The timing of cortical neurogenesis is encoded within lineages of individual progenitor cells. *Nature Neuroscience*, *9*(6), 743–751. <https://doi.org/10.1038/nn1694>
- Silver, D. L., Watkins-Chow, D. E., Schreck, K. C., Pierfelice, T. J., Larson, D. M., Burnett, A. J., ... Pavan, W. J. (2010). The exon junction complex component Magoh controls brain size by regulating neural stem cell division. *Nature Neuroscience*, *13*(5), 551–558.  
<https://doi.org/10.1038/nn.2527>
- Singh, D., & Pohl, C. (2014). Coupling of Rotational Cortical Flow, Asymmetric Midbody Positioning, and Spindle Rotation Mediates Dorsoventral Axis Formation in *C. elegans*. *Developmental Cell*, *28*(3), 253–267. <https://doi.org/10.1016/j.devcel.2014.01.002>
- Sinha, D., Kalimutho, M., Bowles, J., Chan, A. L., Jo Merriner, D., Bain, A. L., ... Khanna, K. K. (2018). Cep55 overexpression causes male-specific sterility in mice by suppressing Foxo1 nuclear retention through sustained activation of PI3K/Akt signaling. *FASEB Journal*, *32*(9), 4984–4999. <https://doi.org/10.1096/fj.201701096RR>
- Skop, A. R., Liu, H., Yates, J., Meyer, B. J., & Heald, R. (2004). Dissection of the mammalian midbody proteome reveals conserved cytokinesis mechanisms. *Science*, *305*(5680), 61–66.

- <https://doi.org/10.1126/science.1097931>
- Steigemann, P., Wurzenberger, C., Schmitz, M. H. A., Held, M., Guizetti, J., Maar, S., & Gerlich, D. W. (2009). Aurora B-Mediated Abscission Checkpoint Protects against Tetraploidization. *Cell*, *136*(3), 473–484. <https://doi.org/10.1016/j.cell.2008.12.020>
- Stewart-Ornstein, J., & Lahav, G. (2016). Dynamics of CDKN1A in Single Cells Defined by an Endogenous Fluorescent Tagging Toolkit. *Cell Reports*, *14*(7), 1800–1811. <https://doi.org/10.1016/j.celrep.2016.01.045>
- Storchova, Z., & Kuffer, C. (2008). The consequences of tetraploidy and aneuploidy. *Journal of Cell Science*, *121*(23), 3859–3866. <https://doi.org/10.1242/jcs.039537>
- Stottmann, R. W., Donlin, M., Hafner, A., Bernard, A., Sinclair, D. A., & Beier, D. R. (2013). Amutation in *tubb2b*, a human polymicrogyria gene, leads to lethality and abnormal cortical development in the mouse. *Human Molecular Genetics*, *22*(20), 4053–4063. <https://doi.org/10.1093/hmg/ddt255>
- Stukenberg, P. T. (2004). Triggering p53 after cytokinesis failure. *Journal of Cell Biology*. <https://doi.org/10.1083/jcb.200405089>
- Swart, S. J., van der Heide, A., Brinkkemper, T., van Zuylen, L., Perez, R., & Rietjens, J. (2012). Continuous palliative sedation until death: practice after introduction of the Dutch national guideline. *BMJ Supportive & Palliative Care*, *2*(3), 256–263. <https://doi.org/10.1136/bmjspcare-2011-000063>
- Tabata, H., & Nakajima, K. (2018). Multipolar Migration: The Third Mode of Radial Neuronal Migration in the Developing Cerebral Cortex. *The Journal of Neuroscience*, *23*(31), 9996–10001. <https://doi.org/10.1523/jneurosci.23-31-09996.2003>
- Tang, H., Hammack, C., Ogden, S. C., Wen, Z., Qian, X., Li, Y., ... Ming, G. L. (2016). Zika virus infects human cortical neural progenitors and attenuates their growth. *Cell Stem Cell*, *18*(5), 587–590. <https://doi.org/10.1016/j.stem.2016.02.016>
- Tang, H. L., Tang, H. M., Mak, K. H., Hu, S., Wang, S. S., Wong, K. M., ... Fung, M. C. (2012). Cell survival, DNA damage, and oncogenic transformation after a transient and reversible apoptotic response. *Molecular Biology of the Cell*, *23*(12), 2240–2252. <https://doi.org/10.1091/mbc.e11-11-0926>
- Tanikawa, C., Matsuda, K., Fukuda, S., Nakamura, Y., & Arakawa, H. (2003). p53RDL1 regulates p53-dependent apoptosis. *Nature Cell Biology*, *5*(3), 216–223. <https://doi.org/10.1038/ncb943>
- Tedeschi, A., & Di Giovanni, S. (2009). The non-apoptotic role of p53 in neuronal biology:

- Enlightening the dark side of the moon. *EMBO Reports*.  
<https://doi.org/10.1038/embor.2009.89>
- To, T.-L., Piggott, B. J., Makhijani, K., Yu, D., Jan, Y. N., & Shu, X. (2015). Rationally designed fluorogenic protease reporter visualizes spatiotemporal dynamics of apoptosis in vivo. *Proceedings of the National Academy of Sciences*, *112*(11), 3338–3343.  
<https://doi.org/10.1073/pnas.1502857112>
- Tsunekawa, Y., Britto, J. M., Takahashi, M., Polleux, F., Tan, S. S., & Osumi, N. (2012). Cyclin D2 in the basal process of neural progenitors is linked to non-equivalent cell fates. *EMBO Journal*, *31*(8), 1879–1892. <https://doi.org/10.1038/emboj.2012.43>
- Tyler, W. A., Medalla, M., Guillamon-Vivancos, T., Luebke, J. I., & Haydar, T. F. (2015). Neural Precursor Lineages Specify Distinct Neocortical Pyramidal Neuron Types. *The Journal of Neuroscience*, *35*(15), 6142–6152. <https://doi.org/10.1523/JNEUROSCI.0335-15.2015>
- Uetake, Y., & Sluder, G. (2004). Cell cycle progression after cleavage failure: Mammalian somatic cells do not possess a “tetraploidy checkpoint.” *Journal of Cell Biology*, *165*(5), 609–615. <https://doi.org/10.1083/jcb.200403014>
- Van de Putte, T., Zwijsen, A., Lonnoy, O., Rybin, V., Cozijnsen, M., Francis, A., ... Huylebroeck, D. (2001). Mice with a homozygous gene trap vector insertion in mgcRacGAP die during pre-implantation development. *Mechanisms of Development*, *102*(1–2), 33–44. [https://doi.org/10.1016/S0925-4773\(01\)00279-9](https://doi.org/10.1016/S0925-4773(01)00279-9)
- Van Lookeren Campagne, M., & Gill, R. (1998). Tumor-suppressor p53 is expressed in proliferating and newly formed neurons of the embryonic and postnatal rat brain: Comparison with expression of the cell cycle regulators p21(Waf1/Cip1), p27(Kip1), p57(Kip2), p16(Ink4a), cyclin G1, and the proto-oncogene. *Journal of Comparative Neurology*, *397*(2), 181–198. [https://doi.org/10.1002/\(SICI\)1096-9861\(19980727\)397:2<181::AID-CNE3>3.0.CO;2-X](https://doi.org/10.1002/(SICI)1096-9861(19980727)397:2<181::AID-CNE3>3.0.CO;2-X)
- Visel, A. (2003). GenePaint.org: an atlas of gene expression patterns in the mouse embryo. *Nucleic Acids Research*, *32*(90001), 552D–556. <https://doi.org/10.1093/nar/gkh029>
- W.-F., L., X.-L., L., S.-W., F., L., Y., C.-T., T., Y.-J., G., ... Z.-Z., G. (2018). Pseudopod-associated protein KIF20B promotes Gli1-induced epithelial-mesenchymal transition modulated by pseudopodial actin dynamic in human colorectal cancer. *Molecular Carcinogenesis*, *57*(7), 911–925.
- Wang, X., Qiu, R., Tsark, W., & Lu, Q. (2007). Rapid promoter analysis in developing mouse brain and genetic labeling of young neurons by doublecortin-DsRed-express. *Journal of*

- Neuroscience Research*, 85(16), 3567–3573. <https://doi.org/10.1002/jnr.21440>
- Wang, X., Tsai, J. W., Imai, J. H., Lian, W. N., Vallee, R. B., & Shi, S. H. (2009). Asymmetric centrosome inheritance maintains neural progenitors in the neocortex. *Nature*, 461(7266), 947–955. <https://doi.org/10.1038/nature08435>
- Watanabe, S., Ando, Y., Yasuda, S., Hosoya, H., Watanabe, N., Ishizaki, T., & Narumiya, S. (2008). mDia2 Induces the Actin Scaffold for the Contractile Ring and Stabilizes Its Position during Cytokinesis in NIH 3T3 Cells. *Molecular Biology of the Cell*, 19(5), 2328–2338. <https://doi.org/10.1091/mbc.e07-10-1086>
- Watanabe, S., Okawa, K., Miki, T., Sakamoto, S., Morinaga, T., Segawa, K., ... Narumiya, S. (2010). Rho and Anillin-dependent Control of mDia2 Localization and Function in Cytokinesis. *Molecular Biology of the Cell*, 21(18), 3193–3204. <https://doi.org/10.1091/mbc.e10-04-0324>
- Weiderhold, K. N., Fadri-Moskwik, M., Pan, J., Nishino, M., Chuang, C., Deeraksa, A., ... Yu-Lee, L. Y. (2016). Dynamic Phosphorylation of NudC by Aurora B in Cytokinesis. *PLoS ONE*, 11(4). <https://doi.org/10.1371/journal.pone.0153455>
- Westendorf, J. M., Rao, P. N., & Gerace, L. (2006). Cloning of cDNAs for M-phase phosphoproteins recognized by the MPM2 monoclonal antibody and determination of the phosphorylated epitope. *Proceedings of the National Academy of Sciences*, 91(2), 714–718. <https://doi.org/10.1073/pnas.91.2.714>
- Westphal, D., Dewson, G., Czabotar, P. E., & Kluck, R. M. (2011). Molecular biology of Bax and Bak activation and action. *Biochimica et Biophysica Acta - Molecular Cell Research*. <https://doi.org/10.1016/j.bbamcr.2010.12.019>
- Williams, A. B., & Schumacher, B. (2016). p53 in the DNA-damage-repair process. *Cold Spring Harbor Perspectives in Medicine*, 6(5). <https://doi.org/10.1101/cshperspect.a026070>
- Witte, H., & Bradke, F. (2008). The role of the cytoskeleton during neuronal polarization. *Current Opinion in Neurobiology*. <https://doi.org/10.1016/j.conb.2008.09.019>
- Wong, C., & Stearns, T. (2005). Mammalian cells lack checkpoints for tetraploidy, aberrant centrosome number, and cytokinesis failure. *BMC Cell Biology*, 6. <https://doi.org/10.1186/1471-2121-6-6>
- Wu, N., & Yu, H. (2012). The Smc complexes in DNA damage response. *Cell and Bioscience*. <https://doi.org/10.1186/2045-3701-2-5>
- Xu, X., Qiao, W., Linke, S. P., Cao, L., Li, W. M., Furth, P. A., ... Deng, C. X. (2001). Genetic interactions between tumor suppressors Brcal and p53 in apoptosis, cell cycle and

- tumorigenesis. *Nature Genetics*, 28(3), 266–271. <https://doi.org/10.1038/90108>
- Yamaguchi, Y., Shinotsuka, N., Nonomura, K., Takemoto, K., Kuida, K., Yosida, H., & Miura, M. (2011). Live imaging of apoptosis in a novel transgenic mouse highlights its role in neural tube closure. *Journal of Cell Biology*, 195(6), 1047–1060. <https://doi.org/doi/10.1083/jcb.201104057>
- Yamashita, Y. M., & Fuller, M. T. (2008). Asymmetric centrosome behavior and the mechanisms of stem cell division. *Journal of Cell Biology*. <https://doi.org/10.1083/jcb.200707083>
- Yang, D., Rismanchi, N., Renvoisé, B., Lippincott-Schwartz, J., Blackstone, C., & Hurley, J. H. (2008). Structural basis for midbody targeting of spastin by the ESCRT-III protein CHMP1B. *Nature Structural and Molecular Biology*, 15(12), 1278–1286. <https://doi.org/10.1038/nsmb.1512>
- Yang, H. W., Chung, M., Kudo, T., & Meyer, T. (2017). Competing memories of mitogen and p53 signalling control cell-cycle entry. *Nature*, 549(7672), 404–408. <https://doi.org/10.1038/nature23880>
- Yingling, J., Youn, Y. H., Darling, D., Toyo-oka, K., Pramparo, T., Hirotsune, S., & Wynshaw-Boris, A. (2008). Neuroepithelial Stem Cell Proliferation Requires LIS1 for Precise Spindle Orientation and Symmetric Division. *Cell*, 132(3), 474–486. <https://doi.org/10.1016/j.cell.2008.01.026>
- Zanelli, S., Goodkin, H. P., Kowalski, S., & Kapur, J. (2014). Impact of transient acute hypoxia on the developing mouse EEG. *Neurobiology of Disease*. <https://doi.org/10.1016/j.nbd.2014.03.005>
- Zechner, D., Fujita, Y., Hülsken, J., Müller, T., Walther, I., Taketo, M. M., ... Birchmeier, C. (2003).  $\beta$ -Catenin signals regulate cell growth and the balance between progenitor cell expansion and differentiation in the nervous system. *Developmental Biology*, 258(2), 406–418. [https://doi.org/10.1016/S0012-1606\(03\)00123-4](https://doi.org/10.1016/S0012-1606(03)00123-4)
- Zhang, B., Rotelli, M., Dixon, M., & Calvi, B. R. (2015). The function of *Drosophila* p53 isoforms in apoptosis. *Cell Death and Differentiation*, 22(12), 2058–2067. <https://doi.org/10.1038/cdd.2015.40>
- Zhao, W. -m. (2006). Cep55, a Microtubule-bundling Protein, Associates with Centralspindlin to Control the Midbody Integrity and Cell Abcission during Cytokinesis. *Molecular Biology of the Cell*, 17(9), 3881–3896. <https://doi.org/10.1091/mbc.e06-01-0015>
- Zhou, C. (2006). Arl2 and Arl3 Regulate Different Microtubule-dependent Processes. *Molecular Biology of the Cell*, 17(5), 2476–2487. <https://doi.org/10.1091/mbc.e05-10-0929>

